THE UNIVERSITY
of EDINBURGH

Targeting hydrogen sulfide breakdown for regulation of myocardial injury and repair

Barry Emerson

PhD – the University of Edinburgh - 2015

Declaration

I hereby declare that the work described here in this thesis was performed entirely by myself, except for procedures acknowledged in the text. This work contains no material that has been accepted for the award of any other degree or diploma in any university or tertiary institution and to the best of my knowledge contains no material previously published or written by any other person, except where stated in the text.

Barry Emerson

Acknowledgements

Firstly, I would like to thank my primary supervisor, Dr. Gillian Gray for training me to think not only logically but also laterally, which has lead my research to areas I never expected. You gave me the freedom to pursue my scientific curiosity without constraints, allowing me to enjoy the science all the more. Your encouragement and support has helped me through the entirety of my research and for that, I will always be grateful. Thank you to my second supervisor, Prof. Nik Morton, for giving me the opportunity of working on a novel area full of twists and turns and always being on hand to lend an enthusiastic ear to newfound data and rightly pushing me (often reluctantly) towards that infamous 'Figure 1'. I would like to thank all the people who have helped me with generating data for this thesis, Katie, Xiaofeng, Kieran, Rod, Matt and Martin and other members of the Morton group, Dr. Chris Kenyon, Emma & Christina and the Notre Dame team, thank you. I would also like to thank Dr. Matt Bailey and Dr. Dawn Livingston for allowing me to use your metabolic cage equipment without hesitation.

I would like to thank the British Heart Foundation for funding this work and my stipend. I would also like to thank the BHF Exchange grant and the BHF CORE Grant, both received from the QMRI for funding costs to visit Prof. Olson's laboratory, University of Notre Dame for technical training and for funding equipment for my work.

To my thesis writing pals Charlotte and Catherine, thanks for making thesis writing a happier place. Lets be honest, it was grim but the tunes, the coffee and the banter kept my head above water. Thanks to all the other students in my year, Cristina & Rachel and to students from other PhD years for the fun times and support throughout our time in the QMRI.

To my parents, brothers (and sisters), you're support was always felt and your (bad) jokes & banter kept me sane in times of lab crises…there were many (bad jokes).

To my second family, the Deacons, your support during my PhD writing especially has been unwavering and your stress busting gift packs and words of encouragement have been brilliant, and not forgotten.

Above all, I would like to thank my partner Cora. You've been wonderful and without you, truly, this thesis wouldn't have materialised. You've been with me every step of the way on this journey, through the highs and the lows and I wouldn't ever want to travel it with anyone else.

A French mans apt proverb kept me motivated in the final writing days and goes something like this; 'Craque pas à deux mètres du bol de sangria'. Thanks Rapha, made me laugh.

Abstract

Hydrogen sulfide (H_2S) is an endogenous gasotransmitter that regulates vascular function and blood pressure, and also protects the heart from injury associated with myocardial infarction (MI). The mitochondrial enzyme thiosulfate sulfurtransferase (TST) has a putative role in the breakdown of H_2S but its role in the cardiovascular system is unknown. I hypothesised that TST reduces cardiovascular H_2S availability and that inhibiting TST activity may therefore ameliorate cardiovascular pathology.

In the heart, TST was expressed by cardiomyocytes and vascular smooth muscle cells. *Tst*$^{-/-}$ mice all survived to adulthood and had normal cardiac structure and function. Cardiac and hepatic H_2S breakdown rates were reduced and H_2S levels were higher in the blood of *Tst*$^{-/-}$ mice. However, in heart tissue, protein levels for the H_2S-activated Nrf2 downstream targets, thioredoxin (Trx1) and heme oxygenase-1 (HO-1) were comparable. In contrast, protein levels for the cardiac specific H_2S-synthetic enzyme, cystathionine gamma lyase (CSE) was reduced, suggesting a homeostatic negative feedback mechanism to maintain H_2S at non-toxic levels. Respiration, measured using an oxygen-sensing electrode was normal in isolated mitochondria from whole *Tst*$^{-/-}$ compared to control C57BL6 hearts. Endothelial nitric oxide synthase (eNOS) protein expression was lower in *Tst*$^{-/-}$ hearts, highlighting potential cross talk between H_2S and nitric oxide (NO) signalling.

TST was expressed in whole aorta homogenates and in isolated endothelial cells from aorta and small intramuscular vessels of the hindlimb from C57BL/6N control mice. Myography and western blotting revealed a greater influence of NO in aorta from *Tst*$^{-/-}$ mice that was associated with increased phosphorylation of the activating serine1177 residue of eNOS (P-eNOS^{Ser1177}). NO plays a lesser role in resistance arteries, but in comparison to control vessels, small mesenteric vessels from *Tst*$^{-/-}$ mice was more reliant on small and intermediate calcium activated potassium channels for relaxation.

Tst$^{-/-}$ mice were normotensive, despite this alteration in the regulation of vascular tone. However, metabolic cage experiments identified that *Tst*$^{-/-}$ mice presented with diuresis, polydipsia, and increased urinary electrolyte excretion of sodium, potassium and chloride, possibly to compensate for increased vascular tone in order to maintain stable blood pressure.

To investigate the role of TST in regulating the response to pathological challenge, MI was induced by coronary artery ligation (CAL). In control mice, gene expression of CSE was downregulated by 2 days after CAL, but TST expression was 12-fold increased, suggesting regulation of H_2S bioavailability during the acute MI-healing phase. *Tst*$^{-/-}$ male mice had a 40% greater incidence of cardiac rupture during infarct healing and surviving *Tst*$^{-/-}$ mice had greater left ventricular dilatation and impaired function compared to controls. *Ex vivo*, isolated perfused hearts from *Tst*$^{-/-}$ mice were more susceptible to ischaemia/ reperfusion injury, suggesting an additional role of TST in determining cardiomyocyte susceptibility to injury.

In conclusion, these data indicate that cardiovascular H_2S bioavailability is regulated through degradation by TST. The data presented here provide evidence for significant tissue specific crosstalk between H_2S synthetic and degradative mechanisms and between H_2S and other local regulatory mechanisms, including ion channels and NOS. We infer TST has a physiological role in the kidney where its loss leads to changes in renal electrolyte and water handling, although other compensatory mechanisms prevent a change in blood pressure. Under conditions of pathological challenge following MI, loss of TST is detrimental, illustrating its key role in removal of H_2S. The data refute the original hypothesis that TST inhibition would be protective against cardiovascular pathology. Further studies in mice with tissue specific deletion of TST are now required to more fully reveal the cardiovascular role of TST.

Publications and Presentations

Barry Emerson, Emma Batchen, Katie J Mylonas, Nik M Morton & Gillian A Gray, (2014) "Myocardial ischaemic injury is unexpectedly increased in mice lacking the H_2S metabolising enzyme thiosulfate sulfurtransferase." Poster presentation at the 3rd International Conference for Hydrogen Sulfide Biology, Kyoto, Japan.

Barry Emerson, Roderick Carter, Nik M Morton, Gillian A Gray, (2013) "Cardiovascular phenotyping in mice with thiosulfate sulfurtransferase gene knockout." Poster presentation at the 2nd European Conference for Hydrogen Sulfide biology, Exeter.

Barry Emerson, Roderick Carter, Nik M Morton, Gillian A Gray, (2013) "Mitochondrial sulfurtransferase deficiency provokes alteration of blood pressure regulatory mechanisms." Poster presentation at British Heart Foundation Fellows Meeting, Cambridge.

Barry Emerson, Ian Dransfield, Nik M Morton, Gillian A Gray, (2013) "Expression & localisation of H_2S metabolising enzymes in the murine myocardium and liver." Poster presentation at the Scottish Cardiovascular Forum, Glasgow.

Barry Emerson, Ian Dransfield, Nik M Morton, Gillian A Gray, (2012) "Identification of synthetic and degradation pathways of H_2S in the murine myocardium." Oral presentation at the 2nd International Conference for Hydrogen Sulfide Biology, Atlanta, USA.

Barry Emerson, Ian Dransfield, Nik M Morton, Gillian A Gray, (2012) "Identification of synthetic and degradation pathways of H_2S in the murine myocardium." Oral presentation at the Edinburgh & Glasgow Universities British Heart Foundation meeting, Edinburgh.

Publications

Stephen, J., **Emerson, B.,** Fox, K.A.A. &, Dransfield, I., "The uncoupling of monocyte-platelet interactions from the induction of proinflammatory signalling in monocytes." *J Immunol.* **191:** 5677-5683 (2013).

Publications In Preparation

Emerson, B., Mylonas, KJ., Zhao, X., Batchen, E., Barios-Lelerena, M., Madhani, M., DeLeon, E., Olson, K., Morton, NM & Gray, GA., "Mitochondrial thiosulfate sulfurtransferase regulates injury and repair following myocardial infarction." In preparation for *Circulation Research.*

Emerson, B., Gibbins, M., Kenyon, C., Bailey, M., Morton, NM. & Gray, GA., "A novel role for thiosulfate sulfurtransferase in blood pressure maintenance through kidney electrolyte handling and vascular endothelial function." In preparation for *Hypertension.*

Non-standard Abbreviations and Acronyms

α-tubulin; alpha tubulin

ACh; acetylcholine

APA; apamin

β-actin; beta actin

CAL; coronary artery ligation

cGMP; cyclic guanosine monophosphate

CSE; cystathionine gamma-lyase

CBS; cystathionine beta-synthase

CHx; charybdotoxin

COX; cyclooxygenase

DAB; 3-3'-diaminobenzidine

DAPI; 4', 6-diamidino-2-phenylindole

DBP; diastolic blood pressure

DCT; distal convoluted tubule

DHLA; dihydrolipoic acid

DSS; dextran sulfate sodium

DTT; dithiothreitol

EAC; endocardial area change

ECFV; extracellular fluid volume

EF; ejection fraction

eNOS; endothelial nitric oxide synthase

ET; ejection time

ETHE1; ethylmanonic sulfur dioxygenase

FS; fractional shortening

GAPDH; glyceraldehyde 3-phosphate dehydrogenase

HO-1; hemeoxygenase 1

H_2S; hydrogen sulfide

IBD; inflammatory bowel disease

INDO; indomethacin

iNOS; inducible nitric oxide synthase

IVCT; isovolumetric contraction time

IRI; ischaemia reperfusion injury

IVRT; isovolumetric relaxation time

$IK_{Ca;}$ intermediate calcium activated potassium channel

kDa; kilo Daltons

LNAME; N(G)-nitro-L-arginine methyl ester

LVEDA; left ventricular end diastolic area

LVESA; left ventricular end systolic area

MABP; mean arterial blood pressure

MBB; monobromobimane

MI; myocardial infarction

MLC; myosin light chain

MPI; myocardial performance index

MPST/ 3MST; mercaptopyruvate sulfurtransferase

mRNA; messenger ribosomal nucleic acid

NA; noradrenaline

nNOS; neuronal nitric oxide synthase

Nrf2; nuclear-receptor factor E2-related factor

PBS; phosphate buffered saline

PCT; proximal convoluted tubule

PE; phenylephrine

PKG; protein kinase G

PN; pressure natriuresis

qRT-PCR; quantitative reverse transcription polymerase chain reaction

RAP; renal arterial pressure

SBP; systolic blood pressure

SK_{Ca}; small calcium activated potassium channel

SNP; sodium nitroprusside

SQR; sulfide quinone oxidoreductase

SUOX; sulfide oxidase

TAC; transaortic constriction

TALH; thick ascending limb of Henle

TBP; tata binding protein

Trx1; thioredoxin

TST; thiosulfate sulfurtransferase

VEGF; vascular endothelial growth factor

WT; wild type

5HD; 5-hydroxydecanoate

Table of Contents

List of Figures

List of Tables

1 Background

1.1 Hydrogen sulfide

Hydrogen sulfide (H_2S) is a gaseous signalling molecule and the latest member to join the gasotransmitter family alongside nitric oxide (NO) and carbon monoxide (CO). Historically, H_2S was characterised as a toxic gas, capable of fatally inhibiting mitochondrial respiration via cytochrome c (Szabó, 2007). However, H_2S has since been shown to be biologically relevant molecule, endogenously produced and capable of modulating a variety of biological functions including neuromodulation in the brain (Abe *et al.*, 1995), vascular function and blood pressure management (Elsey *et al.*, 2010; Geng *et al.*, 2004; Ishigami *et al.*, 2009; Mikami *et al.*, 2011; Zhao *et al.*, 2001) and stimulation of angiogenesis (Papapetropoulos *et al.*, 2009). Numerous pharmacological studies have shown the therapeutic potential of H_2S-donors in a variety of disease models such as hypertension, inflammatory disorders and most notably, ischaemic injury in the heart (Elrod *et al.*, 2007; Johansen *et al.*, 2006), which will be discussed in detail later (section 1.1.6.2).

In water, H_2S dissociates to HS^- (hydrosulfide anion) and S^{2-} (sulfide anion) (Whiteman *et al.*, 2011). Under physiological pH and temperatures, ≈80% of total sulfide exists as HS^-, ≈20% as free H_2S gas and only negligible amounts as S^{2-}, making it unlikely that S^{2-} plays any significant role in H_2S' effects (Kevil, 2012). The term hydrogen sulfide refers to the sum of these sulfide species with free H_2S considered the most biologically relevant species (Whiteman *et al.*, 2011).

1.1.1 Enzymatic H_2S production

Hydrogen sulfide is not only a therapeutic molecule but is endogenously synthesised within most major tissues by cytosolic and mitochondrial bound enzymes. The sulfur-containing amino acid methionine is initially converted to homocysteine by methionine adenosyltransferase (MAT) and glycine N-methyltransferase (GNMT) (Figure 1-1). Homocysteine is broken down to L-cysteine and used as substrate by the cytosolic pyridoxal-5-phosphate dependent enzymes, cystathionine-β-synthase (CBS) and cystathionine-γ-lyase (CSE) to produce H_2S (Figure 1-1) (Elsey *et al.*, 2010). Cysteine aminotransferase (CAT) converts L-cysteine to 3-mercaptopyruvate (3-MP), which is used as substrate by the cytosolic and mitochondrial bound enzyme, 3-mercaptopyruvate sulfurtransferase (3MST) to produce H_2S in the presence of thioredoxin (Figure 1-1) (Mikami *et al.*, 2011). Administration of L-cysteine or 3-MP dose dependently increases H_2S production in brain homogenates (Ishigami *et al.*, 2009) and isolated rat liver mitochondria

respectively (Modis *et al.*, 2013b). CBS, CSE and 3MST are expressed in a variety of tissues within the body but exhibit a tissue specific expression pattern.

CBS is highly expressed in the brain, liver and kidneys (Szabó, 2007) where it is involved in the transsulfuration pathway, converting homocysteine to cystathionine and L-cysteine to H_2S (Figure 1-1). CBS expression and its contribution to H_2S production within the cardiovascular system remains controversial (Elsey *et al.*, 2010; Sen *et al.*, 2008). However, human umbilical vein endothelial cells (HUVEC) express CBS and knockdown of CBS with lentiviral shRNA reduces cell proliferation and induces premature senescence that is exacerbated by homocysteine (Albertini, 2012). In humans, genetic deficiency of CBS causes hyperhomocysteinemia, which increases the risk of hypertension and cardiovascular events (Maron & Loscalzo, 2009). These data identify a role for CBS in endothelial function and cardiovascular health but it remains unclear if these outcomes are H_2S related or secondary effects of homocysteine-induced damage.

CSE is considered the chief H_2S synthetic enzyme within the cardiovascular system with high expression observed in the heart, vascular endothelium and smooth muscle (Fu *et al.*, 2012b; Zhao *et al.*, 2001). CSE converts cystathionine to L-cysteine and L-cysteine to H_2S (Figure 1-1). It has been reported that CSE activity is regulated by calcium-calmodulin but these conclusions remain controversial. *In vitro* studies have shown that administration of calcium and calmodulin to recombinant CSE increases CSE activity (Yang *et al.*, 2008). Furthermore, administration of the calcium ionophore, A23187 or the muscarinic receptor agonist, methacholine to HUVECs or bovine aortic endothelial cells (BAECs) increases H_2S production (Yang *et al.*, 2008). H_2S production can be attenuated by the calcium chelators, EGTA, the calmodulin antagonist W7 or by silencing of CSE with siRNA (Yang *et al.*, 2008). However, high concentrations of calcium were used in these studies (1-2mM), relative to intracellular calcium concentrations achieved under steady state conditions (100nM) or following cell stimulation (3μM) (Kimura, 2014). Mikami and colleagues 2013 showed that H_2S production in purified rat liver CSE is stimulated at low concentrations of calcium (<100nM) but that H_2S production is inhibited when calcium concentrations exceed 300nM. Furthermore, calmodulin had no effect on H_2S production in purified rat liver CSE in the presence of calcium (Mikami *et al.*, 2013). Improved understanding of the mechanisms that regulate CSE-activation holds great therapeutic potential given the positive role that CSE plays in cardioprotection and blood pressure regulation.

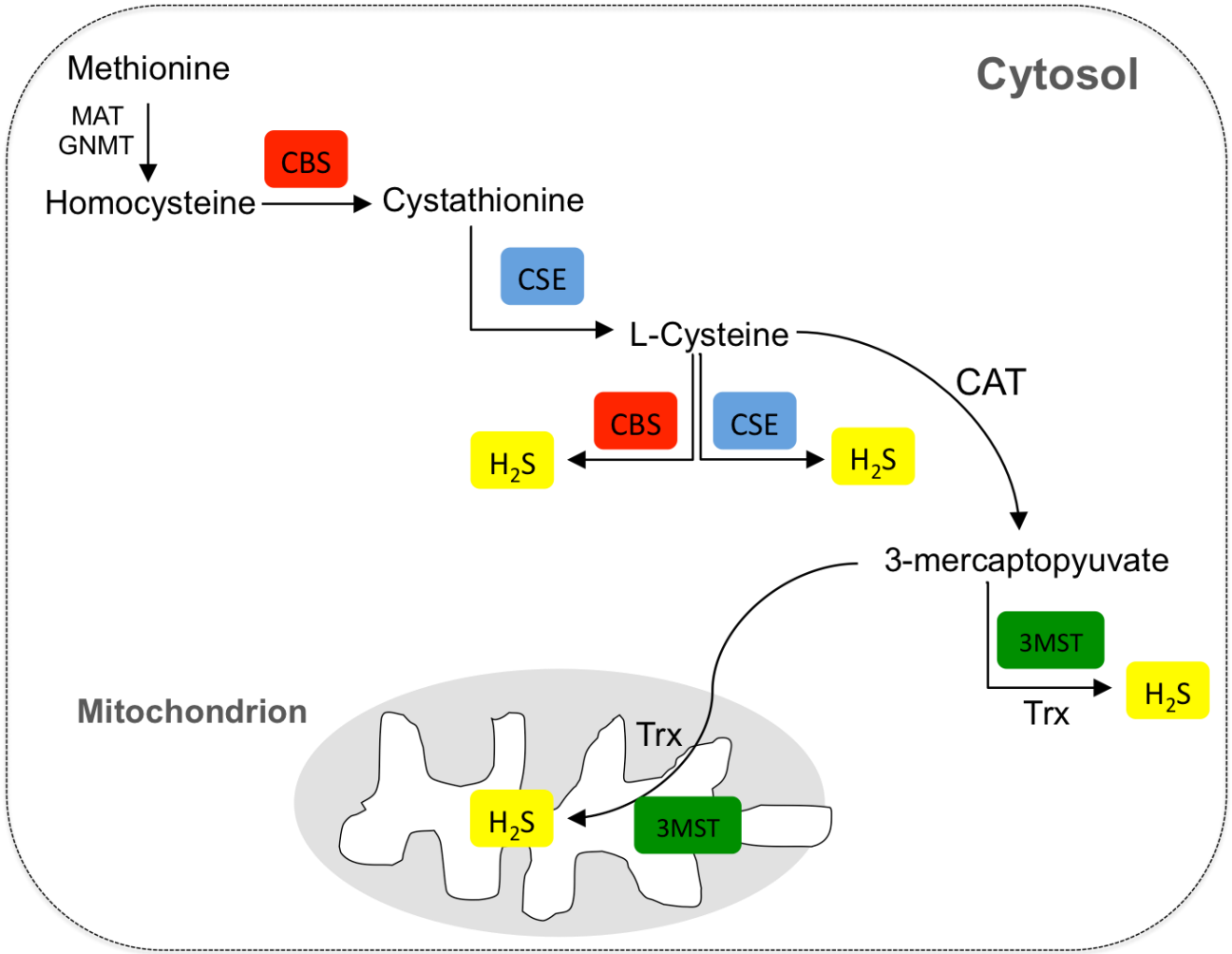

Figure 1-1 Enzymatic H_2S production pathway in tissues

CBS is involved in the transsulfuration pathway converting homocysteine to cystathionine. CSE catalyses a β-disulfide elimination reaction of cystathionine forming L-cysteine which is used as a substrate by cytosolic enzymes, CBS and CSE to produce H_2S. L-cysteine is converted to mercaptopyruvate by cysteine aminotransferase (CAT), which is used as a substrate by mercaptopyruvate sulfurtransferase (MPST) to produce H_2S in the presence of thioredoxin (Trx). Diagram adapted from (Szabo *et al.*, 2014)

3MST is highly expressed in the brain, liver and kidney tissues and has been localised to aortic endothelial cells (Nagahara *et al.*, 1998; Shibuya *et al.*, 2009). The sulfur from L-cysteine (Figure 1-1) is transferred to α-ketoglutarate by cysteine aminotransferase (CAT), forming 3-mercaptopyruvate (3-MP). 3-MP is used as substrate by 3-mercaptopyruvate sulfurtransferase (3MST) to form a persulfide thiol (RSSH), which releases H_2S in the presence of an endogenous or exogenous reducing agent such as thioredoxin (Trx) or dithiothreitol (DTT) respectively (Mikami *et al.*, 2011). There is evidence that 3MST is redox sensitive as H_2S production in the presence of 3MP is enhanced or reduced by Trx1 (Mikami *et al.*, 2011) or hydrogen peroxide (Modis *et al.*, 2013) respectively. Cysteine aminotransferase (CAT) and 3MST are present in the cytosol and in mitochondrial fractions, where cysteine concentrations are high (Fu *et al.*, 2012). Inhibition of CAT with aspartate in isolated rat liver mitochondria inhibits H_2S production stimulated by L-cysteine and α-ketoglutarate (Szabó *et al.*, 2014).

Although characterised as an H_2S synthesising enzyme, 3MST is evolutionarily comparable to the mitochondrial H_2S and cyanide breakdown enzyme, thiosulfate sulfurtransferase (TST). 3MST is located immediately adjacent to TST on chromosome 15 and both enzymes share considerable structural and sequence homology (Spallarossa 2004, Cipollone *et al.*, 2007). However, 3MST and TST differ in their active site loop residues and their substrates, 3-MP and sulfite respectively (Cipollone *et al.*, 2007; Hildebrandt & Grieshaber, 2008; Spallarossa *et al.*, 2004). The similarities between these two enzymes suggest that 3MST may also have a role in H_2S removal under certain conditions.

1.1.2 H_2S Breakdown

Endogenous levels of H_2S are likely regulated not only by its synthesis but also by its breakdown. Given the ability of H_2S to inhibit mitochondrial respiration, H_2S bioavailability is tightly regulated to avoid such harmful effects. The mitochondrial H_2S breakdown enzymes have a high affinity for H_2S and it is believed that free H_2S is rapidly removed (within seconds-minutes) under basal conditions. H_2S is rapidly oxidised within the mitochondria by the sulfide quinone oxidoreductase (SQR), persulfide dioxygenase (ETHE1), thiosulfate sulfurtransferase (TST) and sulfide oxidase to form persulfide, sulfite, thiosulfate and sulfate respectively (Figure 1-2) (Kabil *et al.*, 2014). The mitochondrial H_2S breakdown enzymes are believed to be ubiquitously expressed in most tissues, with high expression observed in liver (Modis *et al.*, 2013a; Modis *et al.*, 2013b). However, it remains unclear if the breakdown enzymes are co-expressed in the same cell types as the H_2S synthetic enzymes to enable rapid H_2S breakdown, warranting further investigation.

The SQR, situated in the inner mitochondrial membrane, initiates oxidation of H_2S and converts it to two persulfide groups (SSH), resulting in a 2-electron donation to coenzyme Q in the respiratory chain via ubiquinone, which are used to generate ATP (Kabil *et al.*, 2014). According to the widely accepted H_2S breakdown pathway mechanism described by Hildebrandt and Grieshaber (Hildebrandt *et al.*, 2008), SQR-produced persulfides are transferred to a mobile acceptor, which is yet to be fully identified. The sulfur dioxygenase ETHE1 oxidises one of the persulfide groups, forming sulfite (SO_3^{2-}), consuming oxygen and water in the process. TST utilises the second persulfide group, transferring sulfur to sulfite, forming thiosulfate ($S_2O_3^{2-}$), a stable non-harmful metabolite that can be excreted in urine (Hildebrandt *et al.*, 2008). Alternatively, SO in the mitochondrial intermembrane space transfers an atom of oxygen from water to sulfite, forming sulfate (SO_4^{2-}), which is excreted in urine.

Currently, no selective inhibitors are available to inhibit any of the enzymes in the H_2S breakdown pathway and as a result, research into their functional roles in mammalian tissues has been relatively scant. Silencing of SQR with siRNA in murine Hepa1c1c7 hepatoma cells reduces SQR protein expression and impairs basal respiration (Modis *et al.*, 2013b). SQR siRNA significantly attenuates stimulation of mitochondrial respiration by 3MST in the presence of 3-MP (Modis *et al.*, 2013b). Together these observations suggest that impaired H_2S breakdown leads to H_2S accumulation and consequently to inhibition of mitochondrial respiration. ETHE1 deficient mice also have markedly elevated tissue H_2S levels and mitochondrial dysfunction associated with retarded growth and they die from sulfide toxicity by 40 days of age (Tiranti *et al.*, 2009).

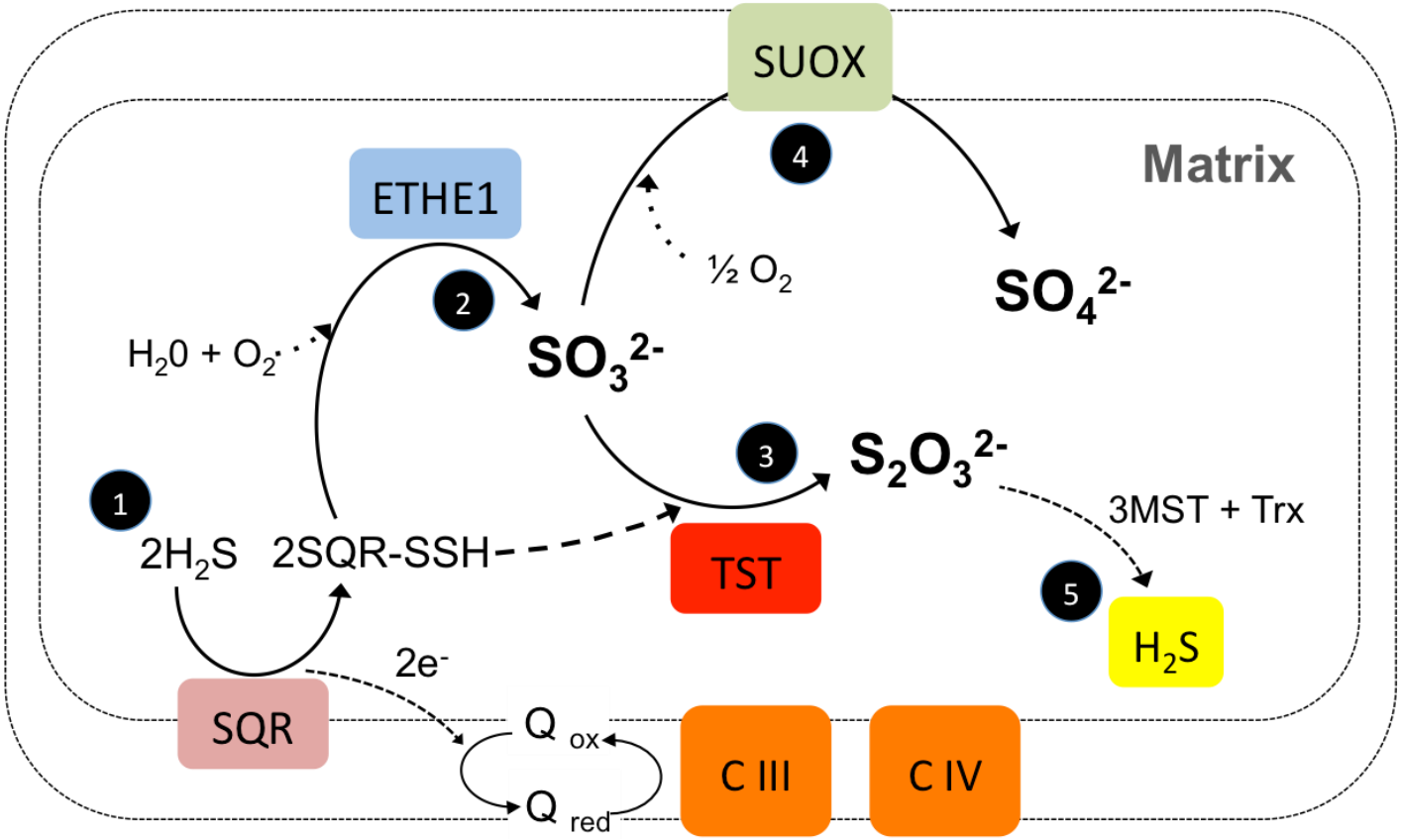

Figure 1-2 Mitochondrial H_2S breakdown pathway

(1) Two H_2S molecules are converted to persulfide groups (SSH) by the SQR, donating 2 electrons to quinone oxidoreductase and used by complex III and IV in the electron transport chain to form ATP. (2) One SQR-persulfide is converted to sulfite (SO_3^{2-}) by ETHE1 in an oxygen and water dependent reaction. (3) TST uses the second SQR persulfide group to convert sulfite (SO_3^{2-}) to thiosulfate ($S_2O_3^{2-}$), which can be excreted in urine. (4) Alternatively, sulfite oxidase converts sulfite (SO_3^{2-}) to sulfate (SO_4^{2-}), in an oxygen dependent reaction, which can be excreted in urine. (5) Thiosulfate can be recycled to H_2S by 3MST and the endogenous reducing agent, thioredoxin (Trx).

1.1.2.1 TST and its involvement in H_2S breakdown

TST, previously referred to as rhodanese, is a mitochondrial bound enzyme that has been highly conserved throughout evolution and is widely expressed in prokaryotes and eukaryotes (Billaut-Laden *et al.*, 2012; Nagahara *et al.*, 1998). In mice, TST is highly expressed in the liver, kidney and lung tissues, specifically in hepatocytes in close proximity to hepatic blood supply within the renal proximal tubule and in epithelial cells surrounding the lungs bronchioles (Cipollone *et al.*, 2007; Nagahara *et al.*, 1998). The mitochondrial bovine TST, commonly known as Rhobov, is the most well characterised TST and it is regularly used as a reference structure for other species (Cipollone *et al.*, 2007). The TST sequence varies between species but its 3D structure is highly conserved, for example TST in *Pseudomonas aeruginosa* shows only 22% sequence identity with Rhobov but their 3D structures are remarkably similar (Cipollone *et al.*, 2007). TST is commonly thought to utilise thiosulfate as a natural substrate for its reaction. Indeed, patients suffering from cyanide poisoning receive sodium thiosulfate as treatment. TST transfers sulfur from thiosulfate to cyanide, forming the stable thiocyanate, which can then be excreted in urine (Figure 1-3) (Hildebrandt *et al.*, 2008). However, purified TST from rat and lugworm show low substrate affinity for thiosulfate and the Km (mM range) is low compared to that of sulfite and persulfides (μM range), supporting the view that these may preferentially act as natural substrates *in vivo* (Hildebrandt *et al.*, 2008).

TST has also been implicated in sulfide clearance, especially in the colon where bacterial flora produce large amounts of H_2S. TST is highly expressed in the colon where it may modulate local H_2S bioavailability. Sulfate reducing bacteria in the colon produce large amounts of H_2S and are widely believed to be involved in the aetiology of ulcerative colitis (Rowan *et al.*, 2009; Taniguchi *et al.*, 2009). Reduced TST expression has been reported in mice following experimentally induced ulcerative colitis using dextran sulfate sodium (DSS) in drinking water (Taniguchi *et al.*, 2009), supporting a role for TST in H_2S removal. At days 3-6 of DSS treatment, TST activity and protein content were reduced in colonic tissues corresponding with time dependent features of ulcerative colitis such as diarrhoea and hematochezia (Taniguchi *et al.*, 2009). Currently, no selective inhibitors for TST are available and no transgenic models have yet been published on this enzyme to help elucidate its impact upon H_2S breakdown.

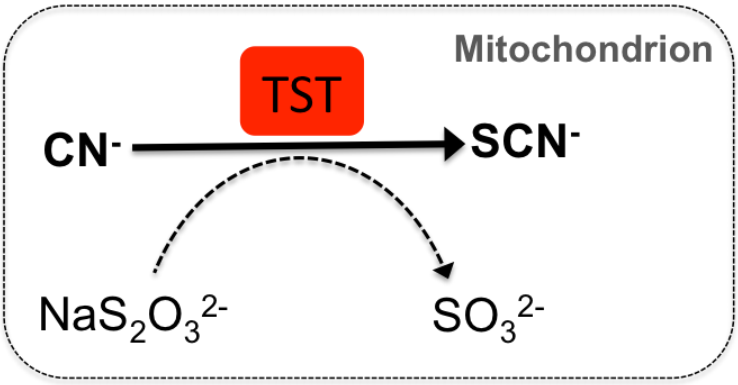

Figure 1-3 Cyanide detoxification reaction catalysed by TST

Mitochondrial TST transfers sulfur from sodium thiosulfate ($NaS_2O_3^{2-}$) to cyanide (CN^-), forming thiocyanate (SCN^-) and sulfite (SO_3^{2-}). Diagram modified from (Billaut-Laden et al., 2012).

1.1.3 Intracellular H_2S stores

Sulfide can be stored in the cell in either acid-labile sulfide stores or as bound sulfane sulfur and released as H_2S in response to acidic and reducing conditions respectively (Ogasawara *et al.*, 1994; Shen *et al.*, 2012). It is becoming clear that these pools are important in regulating bioavailable sulfur and may serve as emergency sources of H_2S under pathophysiological conditions. Acid-labile sulfur stores consist of sulfur atoms present in iron-sulfur cluster proteins found in a variety of mitochondrial proteins such as aconitase and succinate dehydrogenase (Shen *et al.*, 2012). Rat hearts contain markedly higher acid-labile sulfur stores compared to liver, kidney and brain tissues (Ogasawara *et al.*, 1994) and release H_2S in acidic conditions (Ishigami *et al.*, 2009). As pH is tightly regulated under steady state conditions, acid-labile sulfur stores may only release H_2S under pathophysiological conditions such as ischemia, perhaps when lactic acid accumulation promotes an intracellular acidic environment (Kimura, 2010).

Bound sulfane sulfur exists when sulfur covalently binds to another sulfur atom, such as thiosulfate ($S_2O_3^{2-}$), persulfides (R-S-S-H) or polysulfides (R-S_n-R) (Shen 2012). Bound sulfane sulfur releases H_2S under reducing conditions and can be liberated with exogenous or endogenous reducing agents such as dithiothreitol (DTT) or dihydrolipoic acid (DHLA) respectively (Ishigami *et al.*, 2009; Olson *et al.*, 2013). The kidney, liver and brain contain high bound sulfane sulfur stores whilst heart shows relatively low levels (Ogasawara *et al.*, 1994). By 30 minutes after administration of the H_2S-donor Na_2S, H_2S is absorbed into bound sulfane sulfur stores in brain homogenates (Ishigami *et al.*, 2009). Administration of DTT liberated 45% more H_2S from Na_2S pre-treated brain homogenates compared to non

pre-treated homogenates supporting the concept that intracellular sulfide storage regulates free H_2S bioavailability (Ishigami *et al.*,2009).

However, the action of release and the precise endogenous conditions in which these stores liberate H_2S are poorly understood, requiring further investigation (Kolluru *et al.*, 2013). Currently, no data supports that stored sulfane sulfur is used instead of free H_2S for signalling within the cell (Kabil *et al.*, 2014).

1.1.4 Cellular mechanisms of H_2S

Given its ability to diffuse through cell and organelle membranes, H_2S exerts effects in multiple cell types and within intracellular organelles, namely the mitochondria. H_2S has been reported to act upon several molecular targets including; ion channels (section 1.1.5.5), protein modification by S-sulfhydration (section 1.1.5.5) and upregulation of the antioxidant and anti-apoptotic signalling (section 1.1.6.3). H_2S-mediated signalling and cytoprotection will be discussed in relation to its contribution to cardiovascular function under health and pathophysiological states in the following sections.

1.1.4.1 The mitochondria are an important target of H_2S under stress conditions

High concentrations of H_2S are toxic, capable of inhibiting cytochrome c in the mitochondrial respiratory chain, which can be fatal (Tiranti *et al.*, 2009). In recent years it has become clear that H_2S donor compounds exert a biphasic effect with low doses ($<1\mu M$) shown to stimulate mitochondrial respiration and ATP production whilst higher doses ($>10\mu M$) inhibit these effects (Elrod *et al.*, 2007; Modis *et al.*, 2013b). Administration of low doses of the H_2S donor, Na_2S (50μg/kg body weight) to mouse hearts at the time of reperfusion preserves mitochondrial function at 24 hours after ischaemia reperfusion injury (IRI) (Elrod *et al.*, 2007). H_2S-donors are believed to mediate these protective effects, in part by acting as an emergency mitochondrial energy source during low oxygen conditions by donating electrons to the mitochondrial respiratory chain via the sulfide quinone oxidoreductase (SQR) enzyme at Complex II, to help generate ATP (Szabo *et al.*, 2014).

Recent evidence now shows that the endogenous H_2S synthetic enzymes can also contribute to mitochondrial respiration and ATP production under certain conditions. In isolated rat liver mitochondria, administration of the H_2S-synthetic enzyme substrates, L-cysteine or 3-MP increases H_2S production, mitochondrial respiration and ATP generation in a dose

dependent fashion, but these substrates become inhibitory at higher concentrations (Modis *et al.*, 2013b; Szabo *et al.*, 2014). Furthermore, the cytosolic H_2S synthetic enzymes can translocate to the mitochondria and produce H_2S under stress conditions. Mitochondria contain high concentrations of cysteine, facilitating enzymatic H_2S production (Fu *et al.*, 2012b). Following hepatic ischaemic injury *in vivo*, CBS translocates to the hepatic mitochondria in a time dependent manner, peaking at 60 minutes of ischaemia (Teng *et al.*, 2013). At this time mitochondrial H_2S levels were increased compared to shams and this could be prevented by the CBS inhibitor aminooxyacetic acid (AOAA). CSE was not found to translocate to liver mitochondria during ischaemia. Interestingly, H_2S production was not different in whole liver homogenates between sham and 60 minutes ischaemic liver tissues (Teng *et al.*, 2013) indicating that CBS translocation does not increase whole tissue H_2S production, but diverts its release to the mitochondria. Following hepatic ischaemia, reintroduction of oxygen rapidly degraded CBS enzyme, likely a mechanism to avoid sustained mitochondrial H_2S delivery and induced cytotoxicity (Teng *et al.*, 2013).

Translocation of CSE has been reported in vascular smooth muscle cells following administration of the calcium ionophore A23187. Translocation occurs via the mitochondrial membrane transporter Tom-20 and results in H_2S production and ATP generation (Fu *et al.*, 2012a). Silencing of Tom-20 with siRNA, or administration of calcium chelators, reduces CSE translocation, H_2S production and ATP synthesis (Fu *et al.*, 2012a). These data indicate that in conditions associated with ischaemia reperfusion injury (IRI) such as ischaemia and calcium overload, H_2S enzymes have the potential to translocate and energise the mitochondrion, protecting it from injury. Moreover, under reducing conditions (such as ischaemia), thiosulfate can be converted to H_2S by 3MST and endogenous reducing agents, such as Trx1 or DHLA (Mikami *et al.*, 2011). Olson and colleagues propose that during hypoxia, when the mitochondrial matrix becomes reduced, thiosulfate is rapidly recycled and used as a readily available source of H_2S to conserve thiols (Olson *et al.*, 2013). Currently, it is unclear if H_2S enzyme translocation occurs in cardiomyocytes following coronary artery ligation (CAL)-induced ischaemia to help generate ATP and this warrants further investigation.

Currently, there is little data regarding the behaviour of mitochondrial H_2S breakdown enzymes during ischaemia, although this is likely to have a significant impact on H_2S bioavailability. ETHE1 and SO are oxygen dependent and therefore H_2S breakdown is likely to be reduced in ischaemic conditions, which may lead to H_2S accumulation.

1.1.4.2 H_2S-Nitric oxide crosstalk

Nitric oxide (NO) is endogenously produced by neuronal, inducible and endothelial nitric oxide synthase (NOS1, NOS2, NOS3 respectively), which produce NO from L-arginine (Yuan *et al.*, 2015). NO is produced in many tissues in the body and critical in mediating cardiac and vascular physiology as well as the response to injury (Scherrer-Crosbie *et al.*, 2001; Elrod *et al.*, 2006). NO activates cyclic guanosine monophosphate and protein kinase G (PKG), which have been shown to alter calcium handling by the sarcoplasmic reticulum, and thereby modulating vasodilatation in vascular smooth muscle cells and limiting injury following IRI (Elrod *et al.*, 2006, King *et al.*, 2014). PKG phosphorylates vasodilator-stimulated phosphoprotein (Vasp) at the serine residue 239 (P-Vasp^{239}) and so, P-Vasp^{239} can serve as a surrogate biomarker of NO bioavailability and PKG activation (Chen *et al.*, 2004). In the heart, eNOS and nNOS are constitutively expressed in the coronary vascular endothelium and cardiomyocytes respectively (Danson *et al.*, 2005), whilst iNOS is induced in leukocytes recruited to the heart following injury or infection (Yuan *et al.*, 2015). Cardiomyocyte specific eNOS overexpressing mice subjected to myocardial IRI have reduced MI size and preserved cardiac function by 72 hours of reperfusion (Elrod *et al.*, 2006), supporting a role for NO in cardioprotection.

It is becoming increasingly clear that H_2S and NO interact to regulate biological effects *in vivo*. In isolated aortic rings, low doses of the NO donors, sodium nitroprusside (SNP, 10nM) or morpholinosydnonimine (30nM) enhance the relaxant effect of NaHS (H_2S donor, see Table 1-1) (Hosoki *et al.*,1997). Conversely, pre-treatment with the NO synthase inhibitor L-NAME reduces H_2S-mediated vasorelaxation in isolated rat aorta rings (Zhao *et al.*, 2001). While these outcomes suggest interaction at target level there is also evidence for crosstalk at the level of synthesis. Incubation of cultured aortic smooth muscle cells with the NO donor, S-nitroso-N-acetyl-D, L-penicillamine (SNAP) for 6 hours increases CSE transcription and administration of SNP increased H_2S production in a dose dependent fashion (Zhao *et al.*, 2001).

Recently, H_2S donors have been shown to increase NO availability via phosphorylation of the eNOS activation site at the serine1177 residue (P-eNOS^{Ser1177}) (Kondo *et al.*, 2013). Daily administration of the H_2S donor, SG1002 to mice for 6 weeks following transaortic constriction (TAC) surgery increased P-eNOS^{Ser1177} and myocardial nitrite levels, but had no influence on myocardial iNOS or nNOS (Kondo *et al.*, 2013). Furthermore, CSE deficient (*Cse*$^{-/-}$) mice produce less H_2S and have reduced myocardial P-eNOS^{Ser1177} and increased

myocardial phosphorylation of the eNOS inhibitory site at threonine495 (P-eNOS^{T495}) (King *et al.*, 2014). As a result *Cse*$^{-/-}$ mice have reduced levels of nitrite, nitrosothiols and other nitroso species in the heart, supporting the existence of gasotransmitter crosstalk occurs *in vivo* (King *et al.*, 2014).

Furthermore, it has been reported that H_2S and NO can also react to form several potent intermediates including nitrosothiol (HSNO) or nitropersulfide (SSNO-). Feelisch and colleagues argue that the S-N bonds in nitrosothiol are too strong and do not readily release NO (Cortese-Krott *et al.*, 2014; Kimura, 2014). Conversely, nitropersulfide has been reported to be more stable than nitrosothiol but release NO and polysulfides more efficiently, resulting in activation of soluble guanylyl cyclase and relaxation of vascular smooth muscle (Kimura, 2014). However, the significance of these H_2S-NO intermediate molecules in biological signalling and functional relevance is far from clear at this stage.

Compound	Action
Sodium sulfide (Na_2S)	H_2S donor - Fast release
Sodium hydrosulfide (NaHS)	H_2S donor - Fast release
SG1002 (garlic derived)	H_2S donor - Slow release
GYY4137	H_2S donor - Slow release
AP39	H_2S donor - Slow release
Propargylglycine (PAG)	CSE enzyme inhibitor
β-cyano-l-alanine (BCA)	CSE enzyme inhibitor
L-aminoethoxyvinylglycine (AOAA)	CBS enzyme inhibitor

Table 1-1 Summary of H_2S donors and enzymatic inhibitors of H_2S generation

1.1.5 H_2S and Cardiovascular Physiology

1.1.5.1 Regulation of blood pressure

Blood pressure is maintained within the body by renal electrolyte-fluid handling, vascular resistance and by endocrine pathways, such as the renin-angiotensin system. Kidney electrolyte fluid handling is the predominant regulator of long-term blood pressure maintenance (Guyton, 1987; Mullins *et al.*, 2006). Increased peripheral resistance in small resistance arteries increases the resistance the heart must pump against with each beat, causing blood pressure to rise. Additionally, over-activation of the renin angiotensin aldosterone system (RAAS) increases sodium and water reabsorption and causes vasoconstriction, raising blood pressure. Hypertension is clinically diagnosed when systolic blood pressure is >140mmHg or diastolic pressure is >90mmHg. The majority of hypertensive patients suffer with primary or essential hypertension meaning no clear mechanism or secondary causes such as renal disease has been identified (Mullins *et al.*, 2006).

Blood pressure is predominantly determined by extracellular fluid volume (ECFV) homeostasis, which is in turn determined by renal sodium handling (Mullins *et al.*, 2006). The kidney maintains sodium balance and ECFV by matching sodium intake with urinary sodium excretion via a series of ion pumps and exchangers throughout the renal tubules. The kidney acutely modulates sodium excretion in response to changes in blood pressure, a critical mechanism named 'pressure natriuresis' (Guyton, 1987; Mullins *et al.*, 2006). Paracrine signalling is involved in the pressure natriuresis response and contributes to modulation of tubular sodium transport. Impaired pressure natriuresis responsiveness and tubular function are therefore considered as initiating forces in the development of hypertension. All antihypertensive treatments influence renal sodium handling by direct inhibition of tubular sodium transport proteins or indirectly via modulation of endocrine pathways or cardiovascular function (Ivy *et al.*, 2014).

1.1.5.2 H_2S, renal function and contribution to blood pressure control

H_2S has long been characterised for its abilities to reduce blood pressure, via relaxation of blood vessels (Yang *et al.*, 2008; Zhao *et al.*, 2001) and will be covered in detail in section 1.1.5.5. Intravenous administration of NaHS to rats (Zhao *et al.*, 2001) or mice (Yang *et al.*, 2008; Zhao *et al.*, 2001) dose dependently reduces blood pressure but this effect is transitory, likely due to acute changes in neurohormonal pathways to maintain normotension via renal tubular sodium handling. H_2S synthetic enzymes are present in the kidney and recent

evidence suggests that H_2S donors can modify salt handling transporters in the renal nephron, intensifying interest in its role in the kidney (Nagahara *et al.*, 1998; Yamamoto *et al.*, 2012).

1.1.5.3 Salt handling in the kidney

The human kidneys filter approximately 180L of water at the glomerulus daily, with over 99% of the water reabsorbed with sodium and other electrolytes in the renal nephron (Castrop *et al.*, 2014). Sodium and water homeostasis is tightly regulated by complex neurohormonal systems that keep sodium water balance neutral and maintain plasma osmolality. The filtrate concentrating ability of the nephron allows plasma osmolality to remain constant while tubular filtrate can become hypo-osmotic or hyperosmotic depending on water intake. Dehydration increases tubular sodium reabsorption and water retention to maintain plasma osmolality and ECFV, resulting in excretion of small volumes of highly concentrated urine (Mullins *et al.*, 2006). Conversely, high water intake reduces sodium reabsorption and water retention along the nephron, resulting in large volumes of dilute urine, preventing dilution of plasma and volume expansion. The renal nephron is composed of different tubular segments (Figure 1-4), which are responsible for electrolyte and water reabsorption to different degrees.

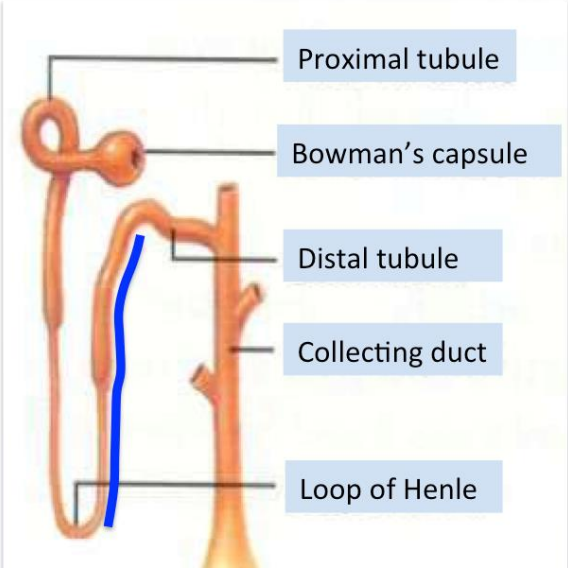

Figure 1-4 The renal nephron reabsorbs electrolyte and water from the filtrate

Blue highlighted area delineates the thick ascending limb of Henle. Diagram modified from www.kidneystreament.com

Filtrate from the glomerulus initially enters the proximal convoluted tubule (PCT) where the majority of sodium and potassium (≈67%), phosphate (≈80-90%) and calcium (≈60%) cations are reabsorbed (Amirlak *et al.*, 2000), by sodium-coupled exchangers or by paracellular transport. In the PCT, large amounts of water (60-70%) are reabsorbed via aquaporin channels 1 and 7 in response to Na^+ reabsorption to maintain plasma osmolality (Figure 1-5). Sodium is reabsorbed from the filtrate via several sodium-coupled exchangers such as the sodium- phosphate co-transporter but mainly by the apical sodium-hydrogen exchanger (NHE3) where sodium is reabsorbed in exchange for hydrogen (Amemiya *et al.*, 1995; Mullins *et al.*, 2006). Other cations such as potassium and calcium are reabsorbed from filtrate in the PCT by passive paracellular reabsorption. The active movement of sodium and passive movement of other electrolytes into the cell is driven by the electrochemical gradient produced by the basolateral membrane bound Na^+/ K^+-ATPase pump (Figure 1-5) (Amirlak *et al.*, 2000). The Na^+/ K^+-ATPase pump is present in the PCT, thick ascending limb of Henle (TALH) and the distal convoluted tubule (DCT) (Wang *et al.*, 2009). At the basolateral membrane, the Na^+/ K^+-ATPase uses ATP generated by nearby mitochondria to actively pump intracellular sodium out of the cell and into the interstitium and then the blood (Amirlak *et al.*, 2000; Wang *et al.*, 2009).

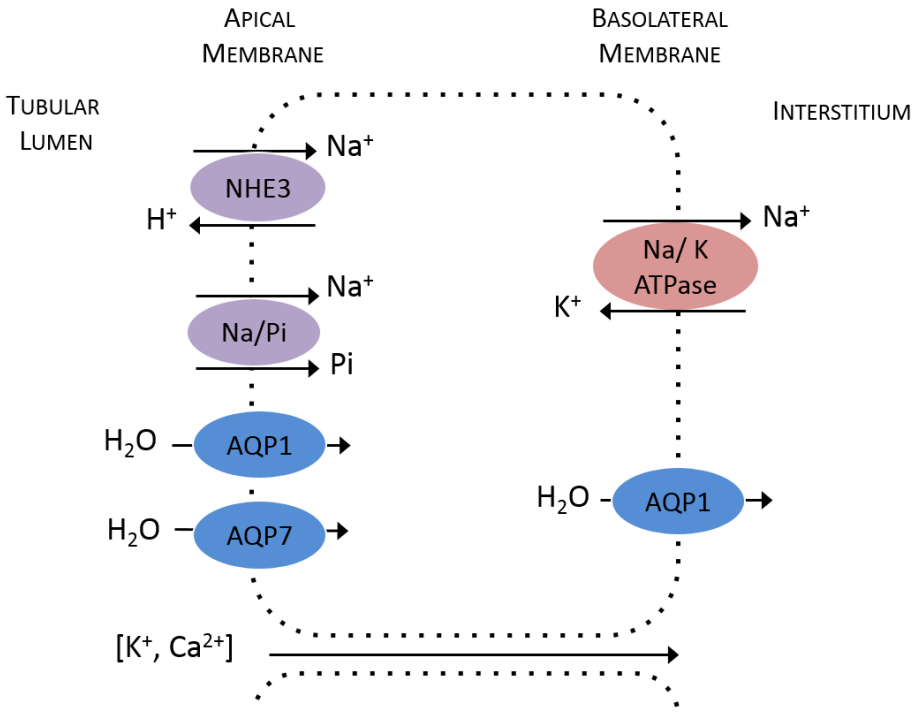

Figure 1-5 Electrolyte and water transport in a proximal tubular cell

NHE3; sodium hydrogen exchanger isoform 3, Na/ Pi; sodium phosphate co-transporter, AQP1/ 7; aquaporin 1/ 7, Na/ K ATP-ase; sodium potassium ATPase pump.

TST and the H_2S synthetic enzymes are highly expressed in the kidney have been localised to the proximal convoluted tubule (PCT) (Nagahara *et al.*, 1998; Sylvester *et al.*, 1990; Yamamoto *et al.*, 2012), and may play a role in PCT sodium reabsorption.

Following PCT reabsorption, the thick ascending limb of Henle (TALH) is responsible for 20-25% of tubular NaCl and 20% of potassium reabsorption from the filtrate (Mullins *et al.*, 2006). Water is not reabsorbed in the TALH. Within the TALH, sodium, potassium and chloride reabsorption is mediated by the apical membrane bound Na-K-2Cl cotransporter (NKCC2) and renal outer medulla potassium (ROMK) channel and by the basolateral membrane bound chloride (ClC-Kb) channel (Figure 1-6). The apical ROMK channels recycle intracellular potassium back into the lumen and enable the NKCC2 to passively co-transport luminal sodium, potassium and chloride into the cell (Bhat, *et al.*, 2012; Castrop *et al.*, 2014). The NKCC2 plays a critical role in the handling of sodium, potassium and chloride within the TALH and is driven by the electrochemical gradient produced by the basolateral membrane bound Na^+/ K^+-ATPase pump (Amirlak *et al.*, 2000). Large amounts of calcium and magnesium are passively reabsorbed in the TALH, which are coupled with sodium reabsorption (Figure 1-6) (Amirlak *et al.*, 2000).

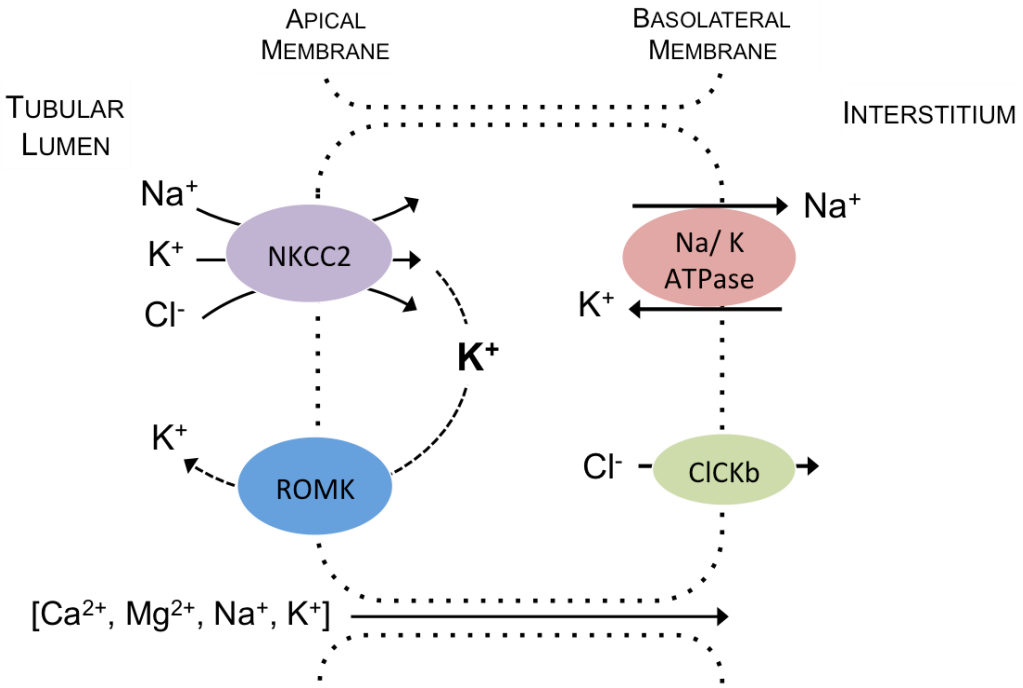

Figure 1-6 Electrolyte transport in the thick ascending limb of Henle

NKCC2; sodium-potassium-chloride co-transporter, ROMK; renal outer medulla potassium channel, Na/ K ATP-ase; sodium potassium ATPase pump, ClCKb; basolateral chloride channel.

1.1.5.4 H_2S donor effects on kidney function

Relatively few studies have investigated H_2S' effect on renal sodium handling. Administration of NaHS to the renal artery of rats increases urinary flow rate and excretion of sodium, highlighting a potential role of endogenous H_2S in electrolyte-fluid homeostasis (Xia *et al.*, 2009). *In vitro* studies performed on isolated renal basolateral membranes from rats showed that NaHS dose dependently reduced Na^+/ K^+-ATPase activity caused by internalisation of the Na^+/ K^+-ATPase pump from the basolateral membrane to the cytosol (Ge *et al.*, 2014; Xia *et al.*, 2009). As renal basolateral membranes were isolated from whole kidneys in this study rather than from individual regions of the nephron, it remains unclear where H_2S acts along the nephron. However, as the Na^+/ K^+-ATPase pump is present in the PCT, TALH and DCT and significant sodium and water losses are observed following NaHS infusion, it seems plausible that H_2S inhibits Na^+/ K^+-ATPase activity at each of these regions. CSE, CBS, 3MST and TST are all expressed in the PCT and may play a role in tubular sodium handling via inhibition of the Na^+/ K^+-ATPase pump. NaHS has also been reported to reduce Na^+/ K^+-ATPase currents and sodium absorption in the human bronchiolar epithelial cell line H441 and in tracheal tissues of pigs and mice (Althaus *et al.*, 2012). Patients with chronic exposure to H_2S gas have pulmonary oedema, potentially because of impaired transepithelial sodium reabsorption.

1.1.5.5 Regulation of vascular function by H_2S

Several rodent studies have shown that the H_2S-donors, NaHS and Na_2S dose dependently relax blood vessels and reduce blood pressure (Hosoki *et al.*, 1997; Mustafa *et al.*, 2011; Yang *et al.*, 2008; Zhao *et al.*, 2001). Importantly, H_2S is endogenously produced in the vasculature, predominantly by CSE, which is localised within murine endothelium and vascular smooth muscle (Fu *et al.*, 2012a; King *et al.*, 2011; Li *et al.*, 2011; Zhao *et al.*, 2001). CSE deficient ($Cse^{-/-}$) mice produce less H_2S and suffer from endothelial dysfunction in mesenteric arteries and associated age-dependent hypertension, confirming that H_2S acts as an endogenous vasodilator and blood pressure regulator (Mustafa *et al.*, 2011; Paul *et al.*, 2012; Yang *et al.*, 2008). Vasorelaxation within the rat aorta is largely NO and cyclooxygenase dependent, with H_2S mediating <25% of total relaxation (Hosoki *et al.*, 1997; Mustafa *et al.*, 2011). Conversely, vasorelaxation within the small resistance arteries is largely H_2S dependent with NO playing a relatively minor role (Mustafa *et al.*, 2011).

In mesenteric arteries, cholinergic stimulation with acetylcholine (ACh) releases calcium from the endoplasmic reticulum causing activation of calmodulin and resultantly activates

CSE, producing H_2S (Paul *et al.*, 2012; Shibuya *et al.*, 2009). Endothelial generated H_2S activates small and intermediate calcium activated potassium (SK_{Ca} and IK_{Ca}) channels in the endothelium and via diffusion, activates K_{ATP} channels in smooth muscle cells (Figure 1-7). Activation of SK_{Ca} and IK_{Ca} channels causes endothelial hyperpolarisation via potassium extrusion, which is then transmitted to the smooth muscle through open K_{ATP} channels to cause whole vessel relaxation (Figure 1-7) (Albertini, 2012; Paul *et al.*, 2012). SK_{Ca} and IK_{Ca} channels only mediate part of the vasodilator capacity of H_2S (10-20% of total). The majority of its effects are exerted by activation of ATP-sensitive potassium (K_{ATP}) channels in the vascular smooth muscle. Inhibition of K_{ATP} channels with glibenclamide or 5-hydroxydecanoate (5-HD) abolishes H_2S-donor mediated vasorelaxation in aortic and mesenteric arteries and attenuates H_2S-mediated blood pressure reduction (Maron *et al.*, 2009; Mustafa *et al.*, 2011; Ovechkin *et al.*, 2006; Zhao *et al.*, 2001).

H_2S activates K_{ATP} channels by causing post-translational modification of one of its subunits in a process termed S-sulfhydration. S-sulfhydration adds a sulfur to thiols groups of cysteine residues, producing a hydropersulfide (-SSH) moiety (King *et al.*, 2011; Li *et al.*, 2011; Sutton *et al.*, 2000) with increased biological activity. Under basal conditions, the K_{ATP} channels found in vascular smooth muscle cells are bound to ATP, and remain closed (Figure 1-7). Following cholinergic stimulation, CSE-derived H_2S diffuses to smooth muscle from the endothelium, and sulfhydrates the K_{ATP} channels Kir6.1 subunit at the cysteine 43 (Cys43) residue. This promotes Kir6.1 binding to phosphatidylinositol-4, 5-biphosphate (PIP2) and reduces the binding affinity of ATP, leading to K_{ATP} channel opening, potassium influx and vasodilatation (Figure 1-7) (Mustafa *et al.*, 2011; Paul *et al.*, 2012; Sutton *et al.*, 2000). Administration of the K_{ATP} channel blocker glibenclamide or mutation of the Kir6.1-Cys43 residue in HEK293 cells attenuates NaHS- mediated hyperpolarisation via reduced Kir6.1-Cys43 sulfhydration, reduced PIP2 binding and enhanced ATP-binding, keeping the channel closed (Hausenloy *et al.*, 2013; Mustafa *et al.*, 2011). *Cse*$^{-/-}$ mice produce less H_2S and have reduced sulfhydration of Cys43 at Kir6.1, accounting for vascular dysfunction and hypertension in this model (Mustafa *et al.*, 2011).

3MST is expressed in aortic endothelium and smooth muscle (Koivumaki *et al.*, 2009; Shibuya *et al.*, 2009; Yellon *et al.*, 2007) but as no selective 3MST inhibitors are currently available, 3MST's influence on vascular function remains unclear. CBS has also been localised to the aortic endothelium but its expression is considered to be low and its contribution to vascular H_2S synthesis has been largely dismissed. As mentioned previously, CBS is expressed in HUVECs and CBS knockdown with shRNA reduces cellular

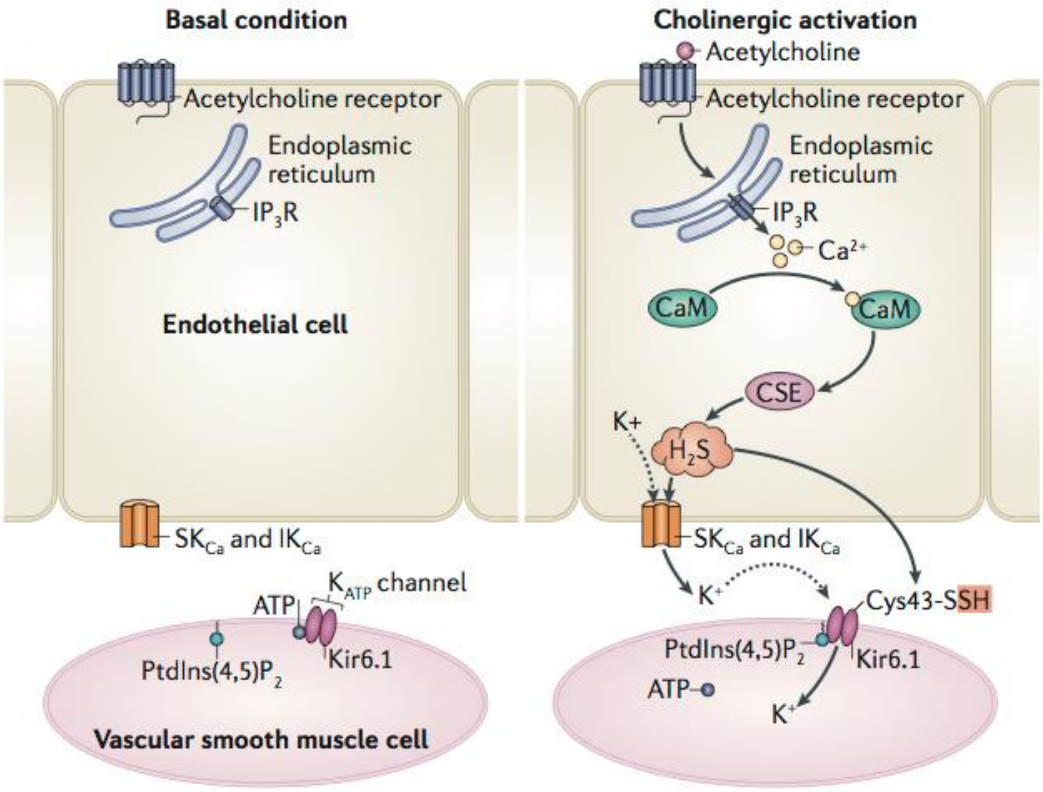

Figure 1-7 Mechanisms of H_2S-mediated vasodilatation

Diagram from Paul *et al.* 2012. *Abbreviations;* CaM; calmodulin, Cys43; Cysteine43, IP_3R; inositol triphosphate receptors, PtdIns(4,5)P_2 / PIP2; phosphatidylinositol-4, 5-biphosphate.

proliferation and induces premature senescence, which is enhanced by homocysteine administration (Albertini, 2012; Hausenloy *et al.*, 2013). CBS deficient (*Cbs*$^{-/-}$) mice suffer from hyperhomocysteinemia, endothelial dysfunction and hypertension, mimicking the human disorder, but the levels of H_2S in *Cbs*$^{-/-}$ mice are currently unknown making it difficult to interpret if their dysfunction is due to reduced H_2S availability or a secondary effect of high homocysteine concentrations (Maron *et al.*, 2009; Ovechkin *et al.*, 2006; Yellon *et al.*, 2007). Therefore, it is clear that CBS plays a vital role in endothelial health and function, likely via homocysteine breakdown. It remains unclear if TST is present in the vasculature and if it plays any role in the regulation of vascular function, via H_2S availability.

1.1.6 Cardiovascular pathophysiology and H_2S mediated cardioprotection

1.1.6.1 Myocardial Infarction & reperfusion Injury

Cardiovascular disease is responsible for 160,000 deaths each year in the United Kingdom (British Heart Foundation 2015). Cardiovascular disease encompasses a host of morbidities such as myocardial infarction, stroke, coronary heart disease and angina.

Myocardial infarction (MI) occurs when a coronary vessel is occluded by thrombus formation on a ruptured atherosclerotic plaque. Tissue downstream of the occlusion is deprived of oxygen, preventing aerobic respiration and causing cardiomyocyte cell death through necrosis and apoptosis. As the heart is unable to regenerate, the damaged tissue is replaced by scar tissue. The remaining myocardium undergoes structural and functional remodelling in an attempt to maintain cardiac output (Sutton *et al.*, 2000; van der Horst *et al.*, 2007). Over time, reduced pumping efficiency of the heart reduces blood supply to organs and tissues and increases and risk of developing chronic heart failure (Sutton *et al.*, 2000). With increasing rates of intervention now clinically performed to restore blood supply to the heart after MI, the number of individuals surviving MI, but subsequently going on to develop heart failure is increasing.

Infarct size is a key determinant of long-term outcome post MI. Experimental and clinical studies have shown that this can be reduced by early reperfusion. However, reperfusion still results in irreversible 'reperfusion injury' to the myocardium (Hausenloy *et al.*, 2013). Reperfusion injury itself can generate large amounts of reactive oxygen species (ROS) and cause calcium overload, which can irreversibly damage the cells mitochondria, propagating cardiomyocyte death (Hausenloy *et al.*, 2013). Oxidative stress causes dysfunction of the sarcoplasmic reticulum, releasing high concentrations of calcium into the cytosol causing further mitochondrial damage, cardiomyocyte hypercontracture and cell death (Koivumaki *et al.*, 2009; Yellon *et al.*, 2007). Therefore, therapies aimed at reducing reperfusion injury are key in reducing the likelihood of developing of heart failure (Hausenloy *et al.*, 2013). Brief periods of ischaemia administered either immediately before (pre-conditioning) or immediately after (post-conditioning) reperfusion reduces reperfusion injury and patient outcome (Yellon *et al.*, 2007). β-blockers, ACE inhibitors and diuretics are currently used to reduce the likelihood of cardiac remodelling and the development of heart failure following injury (van der Horst *et al.*, 2007). H_2S has shown great promise in animal studies by reducing infarct size when given before, during or shortly after myocardial ischaemia and

reperfusion (Polhemus *et al.*, 2014). However the H_2S-donor compounds release H_2S quickly in an uncontrolled manner, which may not be a safe approach given the toxic capabilities of H_2S at high concentrations.

1.1.6.2 H_2S mediated cardioprotection in acute models of myocardial infarction

Several *in vivo* studies have shown the therapeutic potential of administering H_2S donors before, during or after IRI (Calvert *et al.*, 2010; Elrod *et al.*, 2007; Sodha *et al.*, 2009; Zhu *et al.*, 2006). *Ex vivo* IRI studies show that administration of the H_2S donor NaHS prior to and during ischaemia until shortly after reperfusion, dose dependently reduces MI size in isolated perfused rat hearts (Johansen *et al.*, 2006). Johansen and colleagues showed that 0.1μM - 1μM of NaHS dose dependently reduced MI size but at 10μM NaHS, these effects were lost showing a narrow therapeutic window of action (Johansen *et al.*, 2006). The biphasic concentration dependent effect of H_2S on MI size was confirmed in *in vivo* IRI studies with protection being lost at higher concentrations (Elrod *et al.*, 2007). Administration of low doses of Na_2S ($\leq$50μg/kg body weight) directly into the left ventricular lumen of mice at the time of reperfusion significantly reduced 24 hour serum cardiac troponin-I, MI size, left ventricular dilatation and preserved-ventricular contractility compared to vehicle treated controls (Elrod *et al.*, 2007). Higher concentrations of Na_2S (100μg/kg body weight) were less effective at reducing MI size whilst maximal concentrations of Na_2S (500μg/kg body weight) had no effect on MI size whatsoever.

Conversely, pharmacological CSE inhibitor studies and transgenic mouse models of altered CSE expression have shown how important endogenous H_2S production is in the hearts response to MI. Administration of the CSE inhibitor propargylglycine (PAG) to rats for 7 days prior to permanent coronary artery ligation (CAL) increases infarct size and mortality compared to vehicle treated controls (Zhu *et al.*, 2006). Furthermore, $Cse^{-/-}$ mice have reduced levels of L-cysteine and H_2S and are more susceptible to IRI (King *et al.*, 2014; Yang *et al.*, 2008). Conversely, cardiac specific CSE over-expressing (αMHC-CGL-Tg) mice have increased CSE expression and myocardial H_2S availability and are protected from IRI (Elrod *et al.*, 2007), highlighting the therapeutic potential of increasing myocardial CSE expression following IRI. Given the low expression of CBS in the heart, it is not currently a major area of interest. 3MST is highly expressed in the heart and due to the recent generation of the 3MST knockout mouse (Nagahara *et al.*, 2013), there is much anticipation within the field to investigate its response to MI.

1.1.6.3 H_2S mediated mechanisms of cardioprotection

Hydrogen sulfide exerts its cardiovascular protection via several mechanisms including mitochondrial protection (section 1.1.4.1), H_2S-NO crosstalk (section 1.1.4.2), upregulation of antioxidant genes, anti-apoptotic cell signalling and ion channel activation.

As discussed in section 1.1.4.1, exogenous H_2S has been shown to preserve cardiac mitochondrial function in *in vitro* and *in vivo* IRI studies (Elrod *et al.*, 2007). The H_2S synthetic enzymes have been reported to translocate to the mitochondria in liver and smooth muscle cells under ischaemic and high calcium conditions to produce H_2S and stimulate mitochondrial respiration and ATP formation (section 1.1.4.1) (Fu *et al.*, 2012a; Teng *et al.*, 2013). These data indicate that the heart may also possess this ability under conditions associated with IRI and may underlie H_2S ability to limit cardiac injury, but this remains to be confirmed.

As discussed in section 1.1.4.2, H_2S-NO crosstalk plays a major role in mediating H_2S-related cellular mechanisms. *Cse*$^{-/-}$ mice produce less H_2S and have reduced eNOS activity and NO availability in the heart (King *et al.*, 2014). Resultantly, *Cse*$^{-/-}$ mice have an increased susceptibility to myocardial IRI (King *et al.*, 2014). Administration of Na_2S to *Cse*$^{-/-}$ mice increases myocardial P-eNOS^{Ser1177}, normalises myocardial P-eNOS^{T495} and increases cardiac nitrite and RXNO levels resulting in reduced infarct size at 24 hours following IRI (King *et al.*, 2014). However, Na_2S failed to reduce infarct size in eNOS knockout mice or in mice with mutated eNOS^{Ser1177} indicating that H_2S-mediated cytoprotection is eNOS and NO dependent. This is the most compelling *in vivo* data thus far showing that H_2S-NO crosstalk is vital in mediating cardioprotection. However it is currently unclear how H_2S phosphorylates eNOS^{Ser1177} and dephosphorylates eNOS^{Thr495}, warranting further investigation.

Several groups have reported the ability of H_2S to act as an antioxidant and reduce apoptosis. Administration of Na_2S to mice at 24 hours before myocardial IRI reduces injury induced-oxidative stress and apoptosis (Calvert *et al.*, 2009). Na_2S pre-treatment maintains myocardial redox potential (reduced glutathione oxidation) and reduces lipid hydroperoxide levels following 45minutes of ischaemia and 1 hour, 4 hours or 24 hours reperfusion injury (Calvert *et al.*, 2009). Following 4 hours reperfusion, Na_2S pre-treated mice had reduced myocardial expression of cleaved caspase 3, reduced cytochrome c release and reduced number of TUNEL positive nuclei (Calvert *et al.*, 2009). The ability of H_2S to reduce

oxidative stress is mediated via the upregulation of antioxidant enzymes. H_2S initiates translocation of the antioxidant transcription factor, nuclear factor E2 related factor (Nrf2) to the nucleus where it is involved in transcription of several anti-oxidant enzymes such as thioredoxin (Trx1) and hemeoxygenase 1 (HO-1). Hearts isolated from uninjured mice at 30 or 120 minutes following intravenous Na_2S treatment show that Nrf2 time dependently translocates from the cytosol to the nucleus (Calvert *et al.*, 2009) and by 24 hours, protein expression of Trx1 and HO-1 are significantly increased in the heart (Calvert *et al.*, 2009). In Nrf2 deficient (*Nrf2*$^{-/-}$) mice treated with Na_2S, upregulation of Trx1 is significantly stunted whilst HO-1 protein expression is unchanged after 24 hours (Calvert *et al.*, 2009). Furthermore, *Nrf2*$^{-/-}$ mice have increased susceptibility to myocardial IRI and cannot be rescued with Na_2S (Calvert *et al.*, 2009). Moreover, αMHC-CGL-Tg mice, which produce more H_2S in the heart and are protected from IRI 6, have increased myocardial Nrf2, Trx1 and HO-1 under basal conditions (Calvert *et al.*, 2009). These data support that 1) H_2S exerts its cardioprotective effects via Nrf2 antioxidant signalling and 2) Trx1 and HO-1 are largely regulated by the H_2S-sensitive Nrf2.

H_2S reduces apoptosis via phosphorylation of the anti-apoptotic pathways, extracellular signal-regulated kinase (ERK1/2) and phosphatidylinositol 3-kinase PI3K/Akt (Hu *et al.*, 2007). Inhibition of CSE with PAG or β-cyano-l-alanine (BCA) attenuated H_2S-mediated phosphorylation of ERK ½ in rat cardiomyocytes (Hu *et al.*, 2007). Moreover, pharmacological inhibition of ERK1/2 with PD98059 and PI3K/Akt with LY-294002 and Akt III attenuated H_2S mediated protection of rat cardiomyocytes undergoing *in vitro* IRI (Hu *et al.*, 2007) supporting that anti-apoptotic signalling plays a role in H_2S-mediated cardioprotection. Furthermore, administration of Na_2S to mice increases expression of the anti-apoptogens Bcl-2 and Bcl-xL in the heart by 24 hours, corresponding to reduced TUNEL staining (Calvert *et al.*, 2009).

H_2S-induced activation of ion channels has also been shown to play a role in cardioprotection (Bian, 2005; Johansen *et al.*, 2006; Sivarajah *et al.*, 2006; Sun *et al.*, 2008). As detailed previously, H_2S activates K_{ATP} channels via sulfhydration of the K_{ATP} channels Kir6.1 subunit at the cysteine 43 (Cys43) causing vasorelaxation (Mustafa *et al.*, 2011). *Ex vivo* isolated perfused hearts exposed to NaHS show a dose dependent reduction of MI size, which was attenuated with the K_{ATP} channel inhibitors, glibenclamide or 5-hydroxydecanoate (5HD) (Johansen *et al.*, 2006). Coronary flow rate was not significantly altered in isolated hearts by NaHS or by K_{ATP} channel inhibition at any timepoint during the

IRI protocol indicating that H_2S does not protect hearts via increased tissue perfusion (Johansen *et al.*, 2006). Sarcolemmal and putative mitochondrial K_{ATP} channels play a role in protection from IRI (Garlid *et al.*, 2012). However, due to a lack of selective subcellular K_{ATP} channel inhibitors, it remains unclear which of these channels is acted upon by H_2S, requiring further investigation with a more selective approach. Additionally, H_2S dose dependently inhibits opening of cardiac L-type calcium channels in isolated rat cardiomyocytes (Dewald *et al.*, 2005; Sun *et al.*, 2008; Zhang *et al.*, 2012), which may also help to prevent Ca^{2+} overload upon reperfusion injury.

1.1.6.4 Infarct healing

Ischaemia and cell death initiates a strong inflammatory response, facilitated by activation of toll-like receptors and the complement cascade, which upregulate chemoattractant and cell-adhesion molecules, directing neutrophils and monocytes towards the necrotic site (Frangogiannis *et al.*, 2002; Ghigo *et al.*, 2014). Enhanced neutrophil infiltration can exacerbate cardiomyocyte death by vascular plugging, degradative enzyme release and reactive oxygen species (ROS) production (Carden *et al.*, 2000; Gao *et al.*, 2005; Yellon *et al.*, 2007).

Although leukocyte infiltration is considered harmful in IRI, it is critical for effective infarct healing and scar formation in models of permanent coronary artery ligation (CAL). In CAL, post-infarct healing is orchestrated by infiltrating inflammatory cells, which remove dead cardiomyocytes and stimulate collagen deposition by myofibroblasts, forming a scar in place of damaged myocardium and stabilising the structural integrity of the heart (Frangogiannis, 2012; McSweeney *et al.*, 2010). In mouse models of permanent ligation, the stages of leukocyte infiltration are well defined (Frangogiannis *et al.*, 2002). Neutrophils and monocytes infiltrate the infarcted myocardium facilitated by chemoattractant and adhesion molecules in the hours- days after MI. The neutrophil content of the heart peaks at 1-2 days after injury. Thereafter, monocyte subsets and the macrophages derived from them dominate and accumulate in a biphasic pattern, responding to different chemokine signals released from the injured myocardium during the early and late healing phases (Elrod *et al.*, 2007; Nahrendorf *et al.*, 2010; Sodha *et al.*, 2009; Zhang *et al.*, 2014). Pro-inflammatory $Ly6C^{high}$ monocytes and macrophages predominate until 3-4 days after injury, attracted by the potent chemoattractant MCP-1. These release pro-inflammatory cytokines and their primary function is to ensure the removal of apoptotic and necrotic tissue. Impaired or excessive early neutrophil and monocyte recruitment can destabilise the reparative process and lead to

cardiac rupture (Gao *et al.*, 2005; Sodha *et al.*, 2009). By 24 hours post-MI, MCP-1 deficient mice have reduced macrophage recruitment and by day 3 post-MI, the removal of necrotic myocardium and replacement with granulation tissue is delayed compared to wild type controls (Dewald *et al.*, 2005; Zanardo *et al.*, 2006).

From day 3-4 post-MI the monocytes/macrophages population becomes a more predominantly anti-inflammatory, pro-repair phenotype ($Ly6C^{low}$), under the influence of cytokines e.g. IL-4 and IL-13, generated in the healing myocardium by other cells, including fibroblasts and T cells. These release growth factors including TGF-β, which stimulate angiogenesis and fibroblast to myofibroblast differentiation, necessary for collagen synthesis and deposition for scar formation (Frangogiannis *et al.*, 2002; Zanardo *et al.*, 2006). Poor infarct healing and impaired resolution of inflammation limits removal of dead cells and delayed scar formation with a reduced tensile strength resulting in increased dilatation of the left ventricle and an increased risk of cardiac rupture (Gao *et al.*, 2005; Zhang *et al.*, 2008). Administration of clodronate-loaded liposomes to mice immediately following CAL or at day 3 post CAL depletes $Ly6C^{high}$ and $Ly6C^{low}$ monocytes respectively resulting in reduced scavenging of necrotic tissue, impaired collagen deposition and reduced microvessel formation (Nahrendorf 2007). Conversely, promotion of pro-repair macrophages leads to increased angiogenesis reduced infarct expansion and improved retention of cardiac function (McSweeney *et al.*, 2010; Zhang *et al.*, 2014).

1.1.6.5 H_2S and post-infarct inflammation, wound healing and development of heart failure

The anti-inflammatory actions of H_2S have been reported in various models of inflammation and injury, including CAL and IRI models of MI (Elrod *et al.*, 2007; Sheng *et al.*, 2013; Sodha *et al.*, 2009; Zhang *et al.*, 2014). Yorkshire pigs pre-treated with Na_2S prior to IRI have markedly reduced leukocyte infiltration and IL-6, IL-8 and TNF-α cytokine levels (Cai *et al.*, 2007; Sodha *et al.*, 2009), but it is unclear if this effect is mediated by reduced MI size. Intravital microscopy experiments show that H_2S dose-dependently inhibits aspirin-induced leukocyte adherence in mesenteric arteries of rats and that was attenuated with the K_{ATP} channel inhibitor glibenclamide (Papapetropoulos *et al.*, 2009; Zanardo *et al.*, 2006). Furthermore, in models of carrageenan induced air pouch inflammation, H_2S treatment reduces leukocyte infiltration, which is abrogated in rats pre-treated with the CSE or K_{ATP} channel inhibitors, BCA and glibenclamide respectively (Papapetropoulos *et al.*, 2009; Zanardo *et al.*, 2006). Together these data suggest that H_2S derived from endothelial bound

CSE prevents acute leukocyte attachment via activation of K_{ATP} channels. Conversely, high concentrations of H_2S can evoke a pro-inflammatory response, again highlighting the important relationship between H_2S concentration and outcome. Zhang and colleagues showed that in mice subjected to cecal ligation and puncture-induced sepsis, NaHS increases TNF-α, IL-1β IL-6 and MCP-1 expression but that could be rescued with the CSE inhibitor PAG (Polhemus *et al.*, 2014; Zhang *et al.*, 2008). However, as this study administered high concentrations of Na_2S (10mg/ kg), it is likely that H_2S caused a toxic effect, propagating inflammation.

Following permanent ligation, neutrophil recruitment to the heart at 24 hours post CAL is abrogated by NaHS treatment (Calvert *et al.*, 2010; Zhang *et al.*, 2014). As described previously (section 1.1.8), a timely inflammatory response is required in permanent ligation models to replace dead cardiomyocytes with collagen rich scar tissue to preserve the structural integrity of the heart. Inhibition of inflammation by H_2S would potentially impair this process. Whilst the Zhang 2014 study shows a similar H_2S-mediated inflammatory suppression response as seen in other studies, it did not assess the effects of H_2S on scar formation or cardiac function at later timepoints. *In vitro* studies have shown that H_2S can inhibit the differentiation of fibroblasts to myofibroblasts, which would limit scar formation and increase the risk of cardiac rupture in permanent coronary artery ligation models (Calvert *et al.*, 2010; Sheng *et al.*, 2013). Although the anti-inflammatory effects of H_2S are protective in models of IRI, it is currently unclear what effect increased H_2S availability has on early infarct healing in models of permanent ligation.

H_2S treatment is also beneficial following injury by promoting angiogenesis. Cai and colleagues showed that low doses of NaHS increased cell migration in scratch wound assays and increased tube-like structure formation in matrigel experiments performed on RF/6A endothelial cells (Cai *et al.*, 2007; Kondo *et al.*, 2013). In *in vivo* Matrigel plug assay in mice, 7-day NaHS treatment significantly increased cellular infiltration, neovascularisation and haemoglobin content, compared to vehicle treated mice. Paradoxically, higher concentrations (200μM) of H_2S do not produce any pro-angiogenic effects (Cai 2007) highlighting the importance of dose in determining the effects of H_2S. H_2S promotes angiogenic branching and complexity of vascular networks in chicken chorioallantoic membranes, which are attenuated by CSE inhibitors, PAG and BCA (Papapetropoulos *et al.*, 2009). *In vitro* aortic ring angiogenesis assays show that aortas from $Cse^{-/-}$ mice have significantly reduced microvessel formation compared to wild type controls

(Papapetropoulos *et al.*, 2009), confirming that endogenous H_2S production mitigates the angiogenic response.

1.1.6.6 H_2S and heart failure

Heart failure patients have markedly reduced levels of circulating H_2S compared to age matched controls (Polhemus *et al.*, 2014). Calvert and colleagues show that daily H_2S-treatment for the first 7 days following IRI prevented left ventricular end systolic dilatation and preserved ejection fraction by 4 weeks after IRI (Calvert *et al.*, 2010). Interestingly this was not reproduced by single dose Na_2S treatment immediately following IRI, suggesting the improved outcomes are not accounted for simply by reduction of infarct size (Calvert *et al.*, 2010). Furthermore, αMHC-CGL-Tg mice, which produce more H_2S, have markedly reduced cardiac dilatation and preserved cardiac function compared to wild type controls at 4 weeks post IRI suggesting that chronic elevation of H_2S may have long-term benefits in preventing the development of heart failure.

In a model of pressure overload-induced heart failure, mice subjected to transaortic constriction (TAC) surgery had reduced H_2S levels in the heart and blood by 6 weeks (Kondo *et al.*, 2013). Mice placed on the garlic derived H_2S-donor SG1002-containing chow 1 week before TAC and then continuously for 6 weeks after TAC had increased circulating and tissue H_2S levels. This was associated with reduced left ventricular dilatation, cardiac fibrosis and lung weight and preserved ejection fraction compared to vehicle treated controls. αMHC-CGL-Tg mice also had reduced left ventricular end systolic diameters and preserved ejection fraction by 12 weeks following TAC compared to wild type controls. Conversely, *Cse*$^{-/-}$ mice had greater left ventricular dilatation, heavier hearts and lungs and reduced ejection fraction by 12 weeks post TAC, which could be rescued when *Cse*$^{-/-}$ mice were maintained on SG1002-containing chow. These two separate models of heart failure show that elevated H_2S is capable of preventing heart failure when administered chronically.

Although SG1002 increases H_2S levels, it also increases NO availability as discussed previously (1.1.4.2) and this may have contributed to improved outcomes. Following 6 week of TAC, eNOS$^{-/-}$ mice develop heart failure but cannot be rescued with SG1002-containing chow highlighting the key importance of H_2S-NO crosstalk in the beneficial effects of H_2S in heart failure. Previously found to be non-toxic to humans, SG1002 is currently in the phase 1 of a heart failure clinical trial.

1.2 Hypothesis

The distribution of the H_2S synthetic enzymes in the cardiovascular system is well defined. However, it is unclear if TST is localised in the same tissues and cell types and may be responsible for regulating local H_2S availability and cardiovascular function.

The first hypothesis of this thesis is that TST is present in the heart and vasculature where it regulates local H_2S availability by efficient breakdown.

The second hypothesis of this thesis is that lack of TST would lead to increased H_2S availability resulting in

(i) reduced blood pressure associated with increased vasodilation

(ii) protection of the heart from injury associated with myocardial ischaemia

1.2.1 The specific aims were to:

- Establish the expression and localisation of TST and the H_2S synthetic enzymes in the healthy heart and vasculature

- Quantify the expression profile of the H_2S synthetic and breakdown enzymes in the heart during the early and late phases of infarct healing following coronary artery ligation

- Using the novel TST knockout mouse, investigate if TST deletion impacts upon;
    i. Whole body H_2S availability, H_2S-NO crosstalk, and the regulation of the H_2S synthetic enzymes in the heart
    ii. Cardiac function and mitochondrial respiration under basal conditions
    iii. Blood pressure and sodium-fluid homeostasis in the kidney
    iv. Vascular function in isolated large and small conductance arteries
    v. Mortality, infarct healing, leukocyte recruitment and cardiac function following *in vivo* coronary artery ligation
    vi. MI size in isolated perfused hearts following *ex vivo* IRI and mitochondrial function following *in vitro* IRI

2 Materials and Methods

2.1 Animals

All experimental protocols were approved by the University of Edinburgh Preclinical Ethical Review Committee and by the UK Home Office (GA Gray, PPL 60/4247). Mice were fed standard chow, had free access to food and water and maintained on a 12hour light: dark cycle.

A global *Tst* -deficient (*Tst*$^{-/-}$) mouse was generated by Velocigene (Regeneron Pharmaceuticals, USA) using KOMP technology to ablate the entire TST gene to achieve a definitive null allele. A LacZ neomycin resistant gene cassette with homology arms that flank the 5′ 3′ regions of the entire *Tst* gene was inserted into blastocyst cells by homologous recombination. Cells incorporating the gene cassette were positively selected following neomycin treatment, expanded and microinjected into blastocysts and placed back into a pseudopregnant surrogate mother on a C57BL/6N background. The *Tst* knockout allele went germline and *Tst* heterozygous sperm from male offspring was sent to Edinburgh and used for *in vitro* fertilization onto a C57BL/6N background, performed in-house by a local transgenic facility (GIST; Dr Matthew Sharp). F1 progeny that were heterozygous for *Tst* deficiency mice were identified by genotyping (Transnetyx, USA). The initial colony was maintained through het x het breeding with 1:4 mice in the progeny obtained as *Tst* knockout (*Tst* $^{-/-}$). From generation 4 of backcross to C57BL/6N, *Tst*$^{-/-}$ and littermate C57BL/6N mice were bred as separate colonies. Age matched C57BL/6N wild type littermates were bred as controls. Male mice aged 11-20 weeks were used for experiments.

Professor Nik Morton acquired the *Tst*$^{-/-}$ sperm from Velocigene and subsequently set up initial breeding colonies to select for *Tst*$^{-/-}$ offspring that were then bred to obtain *Tst*$^{-/-}$ litters.

2.2 *In vivo* work

2.2.1 Intra-carotid blood pressure

Blood pressure was measured using a pressure transducer tipped Millar catheter (1.4F cannula, Millar). Prior to blood pressure measurement, the Millar catheter was equilibrated in warmed 0.9% saline for 20 minutes. The Millar catheter was connected to a PCU-2000 Pressure Control unit (Millar), which was connected to AD Instruments Powerlab 8/30 for real time data acquisition and signal was recorded using LabChart 7 software (AD Instruments). The catheter was calibrated using the PCU-2000 unit and LabChart7 software to set the range of voltages that corresponded to 0, 25, 100 and 125 mmHg.

Mice were anaesthetised with ketamine (50mg/kg)/ medatomidine (0.5mg/kg) administered intraperitoneally. Depth of anaesthesia was established by a lack of the pedal pain withdrawal reflex. Mice were shaved from the lower jaw to rib cage and placed on a heat mat. A 1.5cm incision was made from the lower jaw and the salivary gland manoeuvred to allow visualisation of the right carotid artery. Ligatures were tied distally to stop blood flow to the head and the tie clamped to stretch the carotid. The right carotid was clamped proximately and an incision was made into the carotid artery. The Millar catheter was inserted into the carotid artery, tied into place around the artery and the proximal clamp removed to return blood flow. Blood pressure was recorded in real time using LabChart 7. Blood pressure was allowed to equilibrate for 30 minutes before basal blood pressure was measured. Blood pressure traces that did not remain steady throughout 30 minutes of baseline were excluded from analysis (Figure 2-1).

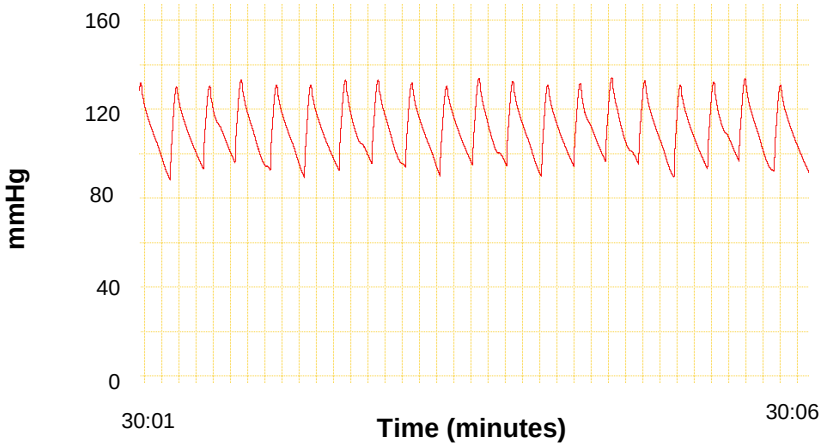

Figure 2-1 Typical steady blood pressure trace recorded from the carotid artery of anaesthetised mice

The waveform displays arterial pressure in mmHg. Peak pressure corresponds to systolic pressure and minimum pressure corresponds to diastolic pressure.

2.2.2 Echocardiography

Echocardiography scanning was performed by Adrian Thomson. *Tst*$^{-/-}$ mice and wild-type controls underwent high frequency ultrasound (Visualsonics Vevo 770) and trans-mitral doppler ultrasound at 6 & 10 weeks of age and at 7days following coronary artery ligation surgery (section 1.2.3). Mice were lightly anaesthetised with isofluorane (1%) delivered via a nose cone. Hair was removed from the thoracic scanning area to improve image acquisition. Anaesthetised mice were laid supine on a platform and their legs secured to electrocardiogram electrodes to measure heart rate. Body temperature was maintained at 37-38^{0}C using a heat pad and lamp and continuously monitored with a rectal thermometer. Gel was applied to the chest and a 15-45MHz real time micro visualization scanhead transducer was placed in contact with the gel to acquire a real time cardiac image. The platform the mice were attached to was manoeuvred to obtain a long axis view of the left ventricle (LV) as well as a short axis view of the whole heart. The M-mode short axis view provided information on tissue motion during systole and diastole, which was used to calculate fractional shortening. The B-mode long axis view allowed collection of ventricular dimensions at end-systole and end-diastole for calculation of structural and functional parameters (Table 2-1). Following echocardiograms, gel was cleaned from the chest and the mice were allowed to recover from anaesthesia. Naïve mice were placed back into allocated animal house rooms and 7 day post MI mice transferred to the *ex vivo* room for perfusion fixation as described below. Echocardiograms were analysed in a single blind manner using Vevo770-Image Analysis Software (Visualsonics) to measure cardiac size, function and performance parameters from the B-mode, M-mode and pulse waved Doppler ultrasound respectively. Table 2-1 lists the formulae used to calculate cardiac size and functional measurements.

Parameter	Method of Acquisition	Formula
LV end systolic area (mm^2)	B-mode	*Area at end systole*
LV end diastolic area (mm^2)	B-mode	*Area at end diastole*
LV end systolic volume	B-mode	*4/3 *(LV Major; s/ 2) * LV Area; s/ (LV Major; s/2)^2*
LV end diastolic volume	B-mode	*4/3 *(LV Major; d/ 2) * LV Area; d/ (LV Major; d/2)^2*
Ejection Fraction (%)	B-mode	*(SV/ LV Vol; d) * 100*
Stroke Volume (µL)	B-mode	*LV vol; d – LV vol; s*
Cardiac Output (mL/ min)	B-mode	*HR * SV*
Endocardial area change (mm^2)	B-mode	*Endocardial Area; d – Endocardial Area; s*
Fractional area change (%)	B-mode	*(LV Area; d – LV Area; s/ LV Area; d) * 100*
Fractional Shortening (%)	M-mode	*(LV dimension; d – LV dimension;n s/ LV dimension; d) * 100*
Myocardial Performance Index (MPI)	Doppler	*(IVCT + IVRT)/ ET*

Table 2-1 Echocardiography parameters

Formula used to calculate Ultrasound Doppler parameters from different image modes.

2.2.3 Coronary artery ligation surgery

Male *Tst*$^{-/-}$ and controls (10-12weeks old) underwent coronary artery ligation (performed by Dr. Katie Mylonas and Xiaofeng Zhao). Mice were anaesthetised with 3% isoflurane and maintained under anaesthesia with 1% isoflurane with oxygen for the duration of the surgery. Mice were intubated and their ventilation maintained mechanically (120 strokes/min, 200ul stroke volume, HSE-Harvard MiniVent Ventilator). Mice were injected with analgesic subcutaneously (buprenorphine 0.05mg/kg) prior to surgery. An initial incision was made in the left upper thorax, the superficial pectoralis muscles were then blunt-dissected and chest opened at the fourth intercostal space. Rib retractors were inserted to maintain an open chest. The pericardium surrounding the heart was removed and a 6-0 prolene suture (Ethicon) was placed around the left anterior descending (LAD) artery and tied. Ligation of the LAD was confirmed by apical cyanosis. Rib retractors were removed and the chest sewn shut using 5-0 mersilk suture (Ethicon), ensuring that no air remained in the chest cavity to avoid pneumothorax. The skin was stapled shut using 9mm autoclips (Harvard Apparatus) and 1.5ml 0.9% saline was administered subcutaneously to maintain hydration. Mice were placed in cages on top of 37^{0}C heat pad overnight and subsequently moved to a quiet room to limit noise-related stress to aid recovery. Mice were checked daily and any deaths following CAL were recorded and subsequently investigated by post-mortem analysis to determine the cause. Briefly, post-mortem analysis identified cardiac rupture as the cause of death when the chest cavity was filled with blood. Acute heart failure was identified as cause of death in the absence of blood within the chest cavity. Surviving mice were culled at 4hours, 2days or 7days following CAL surgery by perfusion (section 1.4.2) and hearts excised for western blotting (section 1.5.6), flow cytometry (section 1.5.8) or histology (section 1.4.5).

2.2.4 Tail blood venesection

Blood was withdrawn from conscious mice at 24 and 48hours after CAL surgery via the tail vein to detect circulating leukocyte numbers by flow cytometry (as detailed below). Briefly, mice were lightly restrained, a small cut was made from the tip of the tail and using a milking action, blood (30µl) was withdrawn into an Eppendorff tube, containing 3.2mM sodium citrate solution (30µl) to avoid coagulation. Blood samples were kept on ice at all times. Analgesia (0.05mg/kg buprenorphine) was administered subcutaneously following venesection.

2.2.5 Metabolic cages

Metabolic cage sample collections were performed in collaboration with Matthew Gibbins. C57BL/6N wild type and *Tst* $^{-/-}$ mice aged 10-12weeks were acclimatised to single housed metabolic cages for 4-6days prior to data acquisition. Data was not recorded during the acclimatisation periods. Mice were fed a standard ground RM1 diet (0.25% salt content) and given free access to water. 12hr light: dark cycles were maintained in ambient 21^{0}C heated rooms to control for lack of bedding in single housing. Daily measurements of body weight, water & food intake (weighing water and food hoppers), urine & faecal output (weighing urine and faecal collecting containers) were taken at the same time of day for the duration of the study. Measurements were displayed as mean readings to reduce natural daily fluctuations of water and food intake and excretion. Electrolyte measurements were performed on urine samples as detailed below. Electrolyte intake was calculated as food intake * (g) sodium/ potassium/ chloride in RM1 diet. Fluid and electrolyte balances (Intake – excretion) were displayed as cumulative values.

2.2.6 Urinary & plasma electrolyte measurement

Sodium and potassium levels in urine samples from metabolic cage studies (as described in chapter 2.2.5) and plasma from naïve *Tst*$^{-/-}$ and C57BL6 mice were measured using the Roche 9180 Electrolyte analyser. Prior to measurements, quality control samples were measured to confirm that the Na, K and Cl electrodes were all operating within the correct parameters. Urine samples were spun at 13,000rpm for 5 minutes to pellet food particulates and the debris-free urine used for sampling. Urine samples were diluted 1:5 and 1:50 with 120mM NaCl for sodium and potassium readings respectively. Plasma samples were diluted 1:5 in distilled water (MilliQ) for potassium measurements. Urinary electrolyte values were multiplied by total urinary weight in a 24hr period to calculate total electrolyte excretion and then corrected to body weight.

Urinary calcium and phosphate measurements were performed by Forbes Howie in the Clinical Analysis Core Services at the University of Edinburgh using commercially available colorimetric assays (Alpha Laboratories Ltd., Eastleigh, UK).

2.3 *Ex vivo* work

2.3.1 Langendorff model of ischaemia reperfusion injury

Ex vivo myocardial infarction was performed on isolated perfused hearts using the Langendorff technique (performed by Emma Batchen). Mice were injected with heparin (1000U/mL) i.p. 10 minutes prior to tissue extraction to avoid thrombus formation within the coronary vasculature. Mice were anaesthetised with 2% isoflurane and the hearts rapidly dissected and immediately placed in ice cold Krebs-Henseleit buffer containing (mM; NaCl 118, $NaHCO_3$ 25, Glucose 11, KCl 4.7, $MgS0_4$ 1.22, KH_2PO_4 1.21, $CaCl_2$ 1.84) for preservation. In a petri dish filled with cold Krebs buffer, the ascending aorta was tied onto the Langendorff cannula (AD Instruments), which was primed with Krebs buffer to avoid bubbles entering the heart. The cannula was held under the flowing Langendorff for a few seconds to remove air bubbles before placing onto the apparatus (Figure 2-2) and perfusing the heart at a rate of 3ml/min with 95% O_2/ 5%CO_2 aerated Krebs-Henseleit buffer, at 37^0C for the duration of the experiment. The heated (37^0C) water-jacketed organ chamber was placed around the heart to provide a warm atmosphere. All hearts were cannulated and perfused by approximately 3-4 minutes from the time the chest was opened. Coronary perfusion pressure was measured with a pressure transducer connected to AD Instruments Powerlab 8/30 and signal was recorded in real time using LabChart 5 software (AD Instruments). The pressure transducer used to detect coronary perfusion pressure was calibrated daily using a manual sphygmomanometer and LabChart5 software to relate pressure (mmHg) to voltage change. Coronary perfusion pressure of 80-110mmHg was considered acceptable whilst pressures above or below these parameters were omitted from the study. Hearts were allowed to stabilize for 15 minutes before ischaemia was induced. Ischaemia was performed by passing a 5-0 suture (11mm round bodied, Interfocus Ltd, England) around the left anterior descending artery (LAD), threading it through a plastic tube and clamping it against the heart with an alligator clip forming a snare and occluding the artery. Following 30 minutes of ischaemia, the clip was removed, loosening the snare allowing reperfusion for 2hours. At the end of the 2hours reperfusion, the suture was re-tied and Evans blue (1% w/v in phosphate buffered saline (PBS), Sigma) was injected into the aortic cannula to differentiate between ischaemic (area at risk; AAR, red) and perfused non-ischaemic heart tissue (blue). The heart was rapidly rinsed in PBS, the myocardium above the ligature cut away and remaining tissue was stored at -20^0C until analysis.

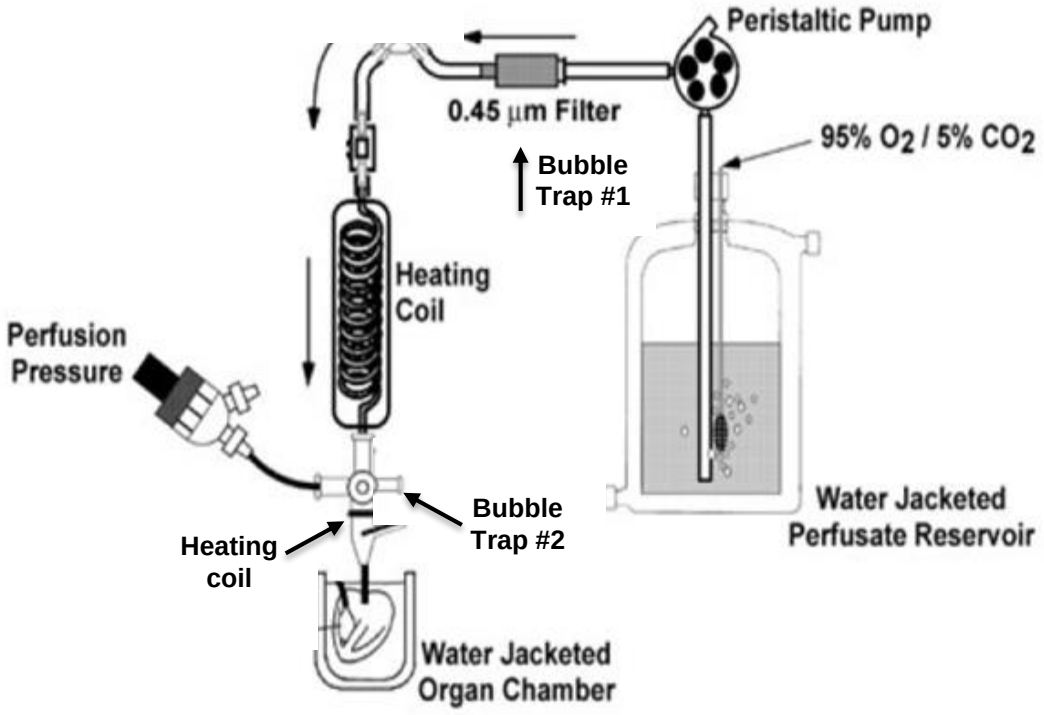

Figure 2-2 Schematic diagram of the Langendorff apparatus

Hearts are attached to the Langendorff apparatus via the cannula and perfused with warmed Krebs solution at a constant rate by the peristaltic pump. Bubble traps at 2 points along the system prevent bubbles from entering the heart. Coronary perfusion pressure is monitored from a side port in the junction block above the heart. Figure adapted from (Reichelt, Willems, Hack, Peart, & Headrick, 2008).

2.3.2 Infarct size assessment – 2, 3, 5 triphenyltetrozolium Chloride (TTC) staining

Infarct tissue was visualised using 2, 3, 5 triphenyltetrozolium chloride (TTC) staining (Jeanes, Tabor, Black, Ederveen, & Gray, 2008). TTC staining allows further definition of the AAR (identified as Evans blue negatively stained myocardium) into viable (ischaemic but viable tissue) and infarcted (non-viable ischaemic tissue) myocardium (Figure 2-3). Frozen infarcted hearts were cut transversely into 1mm slices using a blade and tissue slicer matrix (Alto), the right ventricle was discarded and the remaining myocardium was immersed in 1% w/v TTC in 0.9% saline and incubated at 37^0C for 30 minutes. TTC is enzymatically reduced to triphenylformazan in the presence of various dehydrogenases present in viable tissues forming a brick red colour. Infarcted necrotic myocardium remains white as the tissues dehydrogenases are denatured or degraded. Photographs were taken of each heart slice (Leica MZFLIII microscope) and analysed using Image J software. Areas of the left ventricle (LV) and blue, red and white zones were analysed on Image J. The AAR (red and white zones) was expressed as percentage of LV and the infarct size (white zone) expressed as percentage of AAR.

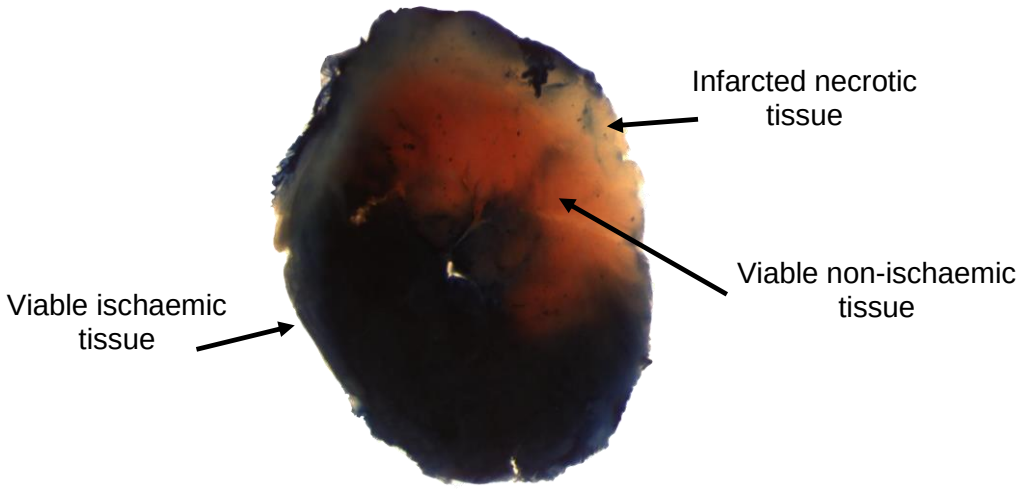

Figure 2-3 Representative TTC stained heart section following *ex vivo* MI

Representative image of a murine heart section following Evans blue and TTC staining. Tissue stained by Evans blue represents perfused non-ischaemic tissue. Red tissue and white tissue stained by TTC represent viable ischaemic and infarcted necrotic myocardium respectively.

2.3.3 Cardiomyocyte Isolation

Cardiomyocytes were isolated from whole mouse hearts using collagenase digestion mixture perfused through the heart using the Langendorff apparatus and then placed into lysis buffer for protein extraction. Mice were injected with heparin (1000U/mL) i.p. 10 minutes prior to tissue extraction to avoid thrombus formation within the coronary vasculature. Mice were killed by cervical dislocation and the heart rapidly removed and arrested in ice-cold calcium free solution containing (mM; NaCl 134, Glucose 11, KCl 4, $MgSO_4$ 1.2, $Na_2H_2PO_4$ 1.2, HEPES 10, pH 7.34). In a petri dish filled with cold calcium free solution, the ascending aorta was pulled and tied onto the Langendorff cannula, which was primed with buffer to avoid bubbles entering the heart. The cannula was held under the flowing Langendorff for a few seconds to remove air bubbles before placing onto the apparatus and perfusing the heart at a rate of 5ml/min with calcium free buffer at 37^0C for 5 minutes. The heart was then perfused for 8 minutes with 0.075mg/ml protease (Sigma, Type XIV, 3.5U/ mg) and 0.6mg/ml collagenase type 2 (Worthington, 320U/ mg) dissolved in calcium free solution at 37^0C. Hearts were then perfused for 8 minutes with a taurine (Sigma) containing low calcium buffer containing (mM; NaCl 108, Glucose 11, KCl 4, $MgSO_4$ 1.2, $Na_2H_2PO_4$ 1.2, HEPES 10, Taurine 50, $CaCl_2$ 50nM, pH 7.34) to wash off enzymes and preserve cardiomyocyte survival. Heart digests were considered effective when the heart turned pale during the collagenase/ protease step. Hearts were cut below the atria, the ventricles transferred to a 7ml bijout with warmed taurine containing solution and minced with a scissors. The tissue was allowed to sediment in the bottom of the bijout before the solution was tipped out and replaced with fresh warmed taurine solution before the mincing process was repeated. This process was repeated 5 times before the myocardial tissue was transferred to a sterile eppendorff containing protein lysis buffer (as detailed in section 1.5.4) and homogenised. Protein content was quantified using Bradford assays (sections 1.5.5) and Western blots performed as detailed in sections 1.5.6.

2.3.4 Endothelial cell isolation

Isolated CD31+ endothelial cells from thoracic aorta and intramuscular vessels of the hindlimb of C57BL/6J mice, were kindly donated by Dr. Andrea Caporali and Lorraine Rose. Endothelial cell (EC) isolation from thoracic aorta was performed by Lorraine Rose. The thoracic aorta from C57BL/6J mice were isolated and then flushed with heparinised endothelial growth basal medium (EBM2) media (20U/ ml heparin) containing 1mM aurintricarboxylic acid. Following this, the lumen of the aorta was flushed with collagenase type II containing EBM2 media (2mg/ ml collagenase type II) and then aorta was incubated

in 0.5ml of collagenase solution for 30 minutes at 37^0C with agitation. EBM2 media containing 1mM aurintricarboxylic acid was added to the aorta to block collagenase activity and then the endothelium was carefully removed by slowly flushing PBS through the lumen and collected in a 15ml corning tube. Cells were centrifuged for 10 minutes x 300g, immunomagnetically labelled with commercially available CD31 microbeads (Miltneyi), isolated using MACS columns in magnetic fields and sorted as per kit instructions (CD31 micobead kit, Miltneyi). The CD31 antibody reacts with the cell surface protein CD31, which is present on mature endothelial cells (Woodfin, Voisin, & Nourshargh, 2007). The cell population was verified using flow cytometry. Single cell suspensions were incubated with CD31-PE fluorophores, the respective isotype control as a negative control and unstained controls to define positivity. Isolated cells showed high expression of CD31 (*Flow cytometry data owned by Dr. Caporali and has not been shown*).

Endothelial cell (EC) isolation from the hindlimb of C57BL/6J mice was performed by Dr. Andrea Caporali as described previously (Caporali *et al.*, 2011). Briefly, adductor muscles of mice were harvested, enzymatically digested immunomagnetically sorted using the same commercially available kit as detailed above (Miltneyl).

Isolated CD31+ cells from thoracic aorta and intramuscular vessels of the hindlimb adductor muscle were then processed for RNA extraction and cDNA synthesis by Lorraine Rose as described in section 2.5.1 and 2.5.2. qRT-PCR (as described in section 2.5.3) was performed on CD31+ cells by Christina Intrator.

2.3.5 Mitochondrial Isolation

Cardiac mitochondria were isolated from two pooled hearts by differential centrifugation as previously described(Frezza, Cipolat, & Scorrano, 2007). All glassware and buffers were cooled to 4^0C to avoid mitochondrial damage. In brief, two hearts (with atria removed) from 14-16week old naïve wild type and two hearts from *Tst* $^{-/-}$ mouse littermates were extracted on the same morning from mice following cervical dislocation. Hearts were washed briefly in ice-cold isolation buffer (IB) (mM; Sucrose 67, Tris/ HCl 50, KCl 50, EDTA 10, BSA 10%, pH 7.4) and immersed in a small glass flask containing fresh ice-cold isolation buffer. Hearts were minced with scissors on ice, washed with isolation buffer 3 times and homogenised in 5ml of IB with a potter Elvehjem homogeniser (using only 10 full strokes) to maintain mitochondrial integrity. Tissue homogenates were transferred to 50ml Falcon tubes and spun at 1800 x g for 10min at 4^0C. Supernatants were removed and placed in

cooled ultracentrifuge glass tubes (Beckmann) before being spun at 7700 x g for 10min using an ultracentrifuge to pellet the mitochondria. Following ultracentrifugation, the supernatants were carefully discarded, the pellet washed in respiration buffer containing (KCl 130mM, KH_2PO_4 5mM, 4-Morpholinepropanesulfonic acid (MOPS) 20mM, $Na_4P_2O_7$ 1μM, $CaCl_2$ 5μM, BSA 0.1%, pH 7.2) and spun again at 7700 x g for 10min. Following the second centrifugation step, the supernatant was carefully discarded and the remaining buffer in the tube (approximately 100μl) used to re-suspend the pure mitochondrial fraction by gentle pipetting. Mitochondria were kept on the ice and used within 4hours for respiration studies.

2.3.6 Mitochondrial respiration studies

Isolated cardiac mitochondrial respiration studies were carried out in an Oroboros Oxygraph 2K (Oroboros Instruments) two-chambered high resolution respirometer using DataLab software (Oroboros). Respiration buffer (as detailed above) was placed in both chambers of the Oroboros Oxygraph and equilibrated to ambient oxygen concentration for one hour before the chambers were closed. Both chambers had previously been calibrated for differences in sensor sensitivity by performing a zero oxygen (addition of excess dithionite) measurement followed by and air calibration using respiration buffer (as detailed above). Equal volumes of isolated cardiac mitochondria from naïve wild type or *Tst*$^{-/-}$ mice were injected directly into either left or right chambers using a Hamilton syringe and magnetically stirred and maintained at 37^0C. In the purposes of time, mitochondrial protein content was measured later the same day using a Bradford assay as detailed in section 2.2.5. Mitochondria from each genotype were alternated between left and right chambers on a daily basis to control for any potential remaining sensor differences in O_2 partial pressure detection. Respiratory substrates (malate, 2.5mM, glutamate, 5mM, succinate, 5mM, adenosine diphosphate, 2mM) and inhibitors (oligomycin, 2.5μM, FCCP, 100nM) were administered via the injection port throughout the experiment. Basal respiratory rate was calculated as the rate of O_2 consumption observed during a linear phase and corrected for protein.

IRI can cause considerable damage to mitochondria, which can lead to the opening of the mitochondrial permeability transition pore and cause apoptosis and necrosis (Yellon & Hausenloy, 2007). *In vitro* cardiac mitochondrial ischaemia-reperfusion experiments were performed as detailed previously (Ljubkovic *et al.*, 2006). Briefly, isolated naive cardiac mitochondria were permitted to consume all O_2 within the chamber until anoxia was achieved, initiating the ischaemic period. Following 20 minutes of ischaemia, the chamber

was opened to ambient air, permitting reperfusion. Upon stabilisation of the O_2 signal to ambient O_2 concentrations, the chamber was closed again and O_2 consumption again measured. Post-ischaemic respiratory rate was expressed as a percentage of pre ischaemic respiratory rate and corrected for protein.

Vessel Myography

Vascular function experiments were performed using the Mulvany-Halpern myograph (Multi-myograph 610M, Danish Myotech, Denmark). C57BL/6N and *Tst*$^{-/-}$ mice were killed by cervical dislocation and the thoracic aorta dissected and quickly placed in ice-cold PSS buffer containing (mM; $NaCl_2$ 119, $NaHCO_3$ 25, D-Glucose 5.5, KCl 4.7, $MgSO_4$ ($2H_2O$) 1.17, KH_2PO_4 1.18, $CaCl_2$ ($2H_2O$) 2.5, EDTA 27μM), for preservation before pinning to 1% agarose coated petri dish containing ice cold PSS. The mesenteric bed and attached intestinal tissue were exteriorised, dissected together and placed in PSS for preservation as described above. The first order mesenteric artery and aorta was cleaned of surrounding fat tissue in preparation for mounting and cut into transverse rings approximately 2.5 - 3.0mm in length. Briefly, one tungsten wire was held between the jaws of the myograph and secured at one end to one of the two myograph jaws. The arterial ring was carefully placed onto the wire and the wire stretched and secured at the opposing end of the same myograph jaw. A second wire was carefully inserted through the lumen of the vessel to avoid damage to the endothelium and secured at both ends of the opposing myograph jaw. Myograph baths were filled with fresh PSS buffer bubbled with 95% O_2/ 5% CO_2 and maintained at 37^0C at all times. Each arterial ring was stretched to its appropriate optimal resting tension for 45 minutes (Table 2-2). The optimal resting tension values were determined by previous normalisation experiments in the Dr. Paddy Hadoke group.

Vessel	Resting Tension
Thoracic aorta	7.36mN
Mesenteric artery	3mN

Table 2-2 Optimal resting tension (mN) for aortic and mesenteric vessels

Following the stretched equilibration period, aortic rings were exposed to high potassium concentrations with KPSS buffer containing, (mM; $NaCl_2$ 4.7, $NaHCO_3$ 25, D-Glucose 5.5, KCl 119, $MgSO_4$ ($2H_2O$) 1.17, KH_2PO_4 1.18, $CaCl_2$ ($2H_2O$) 2.5, EDTA 27μM), and

noradrenaline to evaluate their contractile responsiveness. Aortic vessels were exposed to three periods of KPSS incubation and washed with PSS several times between treatments. Mesenteric arteries were exposed to varying KPSS and adrenergic receptor agonist noradrenaline (NA, $1*10^{-6}$ M) treatments as follows; KPSS*2, NA alone *1, KPSS alone *1, KPSS + NA *1 with several PSS washes between treatments. Following the normalisation protocol, vascular reactivity to pharmacological agents constrictors and dilators were administered to confirm the endothelium was intact and responsive. Vessels were pre-constricted with phenylephrine (Sigma, $1*10^{-7}$M) to partially constrict the vessel and then subsequently administered with $1*10^{-5}$M acetylcholine (Sigma), an endothelium dependent vasodilator (Figure 2-4). If aortic and mesenteric vessels did not relax by 70% of pre-constriction values, they were omitted from further experiments. Vessels were rested in PSS for 30 minutes following KPSS & NA administration to avoid desensitisation before experimental protocols were performed as detailed below.

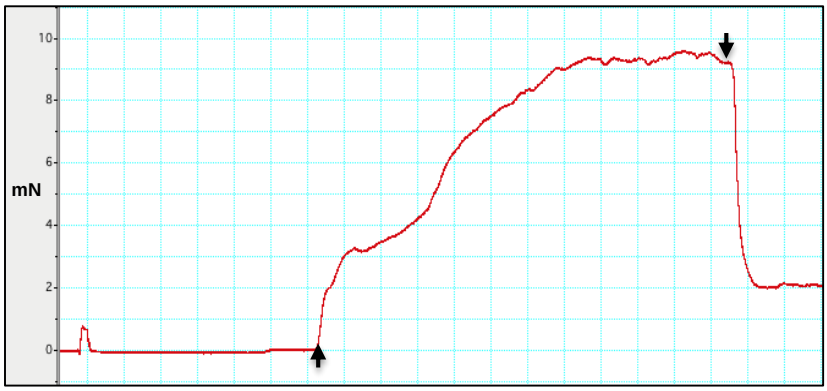

Figure 2-4 Diagram illustrating test for vascular endothelium

Vessel pre-constricted with $1*10^{-7}$M PE (left arrowhead) to a submaximal constriction before ACh ($1*10^{-5}$M) was added to bath (right arrowhead) to relax vessel. The vessel relaxed by 78% indicating the endothelium was intact and the vessel then used for experimentation.

Protocol

Phenylephrine (PE) and acetylcholine were added to PSS filled myography baths in increasing doses of half-log increments ($1x\ 10^{-9}$M – $3x\ 10^{-5}$M) to achieve cumulative drug dose response curves. Each dose was administered once the previous dose-dependent constriction (PE) or relaxation (ACh) had plateaued. Initially, dose response curves were obtained for PE, an α1-adrenergic receptor agonist, washed several times with PSS and vessels rested for 30 minutes. For ACh dose response curves, vessels were pre-constricted to 80% of PE-induced maximal vasoconstriction before ACh was administered. To determine if differences in channel activation were present in the *Tst* $^{-/-}$ vessels compared to controls, inhibitors against a variety of channels were incubated in the myograph bath for 20 minutes

prior to PE pre-constriction, before ACh dose curves were repeated (please see Table 2-3 for inhibitor details and bath concentrations). Channel inhibitors were present in myograph baths for the duration of dose response curves with ACh or SNP. Aortic samples were incubated with L-nitroarginine methyl ester (L-NAME, dissolved in PSS buffer, Alexis Biochemicals) and indomethacin (dissolved in PSS buffer, Sigma) to inhibit nitric oxide and cyclooxygenase respectively. Mesenteric samples were incubated with apamin (US Biologicals) and charybdotoxin (US Biologicals) to inhibit small and intermediate calcium activated K channels where H_2S has previously been shown to have effect (Mustafa *et al.*, 2011).

Drug	Target	Bath Concentration
L-NAME	Nitric oxide synthase	100μM
indomethacin	cyclooxygenase	10μM
apamin	small calcium activated potassium channel [SKCa]	1μM
charybdotoxin	intermediate calcium activated potassium channel [IKCa]	100nM

Table 2-3 Inhibitor details and concentrations used in myography protocols

Inhibitors were added to the organ bath 20 minutes before vessels were pre-constricted to 80% of their maximal constriction with phenylephrine.

Vascular tension (mN) data during all protocols was collected using AD Instruments transducers (Powerlab 8/30, MacLab 4/e) using LabChart 7 Pro software. Maximal vascular tensions were recorded corresponding to each dose of either PE or ACh. Functional responses to PE were normalised to the maximal response to KPSS or NA and ACh responses normalised to preconstruction tensions immediately before the first ACh dose.

2.4 Histology

2.4.1 Tissue collection

10-12week old wild type and *Tst* $^{-/-}$ mice were culled by cervical dislocation and the heart, liver, right kidney and thoracic aorta dissected. Atria were removed from heart tissue and all tissues either snap frozen on dry ice for protein and RNA extraction or fixed in 10% formalin for 24hours before being placed in 70% ethanol and wax embedded for histological analysis. For aortic western blotting experiments, the thoracic aorta was cleared of fat *in vivo*, cannulated with a 24G catheter (Terumo) and flushed with ice-cold PBS before being snap frozen in liquid nitrogen and stored at -80^{0}C.

2.4.2 Perfusion studies

At 4hours, 2days or 7days following CAL surgery, wild type and *Tst* $^{-/-}$ mice were perfused to remove the blood from the tissues. Perfusion was performed by Kieran McGregor, Katie Mylonas and Xiaofeng Zhao. Briefly, mice were weighed and anaesthetised with ketamine (50mg/kg)/ medatomidine (0.5mg/kg) administered intraperitoneally. Depth of anaesthesia was established by a lack of the pedal pain withdrawal reflex. An incision was made in the abdomen and the descending aorta was cannulated with a 24G catheter (Terumo). Blood was extracted from the descending aorta and placed in sodium citrate coated Eppendorff tubes. Blood samples were later spun at 6,000 x g for 6 minutes and the plasma isolated and frozen at -80^{0}C for further studies. Following blood withdrawal, ice-cold heparinised saline (10U/ mL in 0.9% saline) was perfused through the animal using a peristaltic pump at a physiological perfusion pressure of 100mmHg. The carotid artery was cut to allow full removal of the blood. For 7day post CAL gene expression assays, left ventricular infarct and border zones were snap frozen on dry ice for RNA extraction. For 4hour and 48hr post CAL hearts, the infarct zone was not clearly defined from surrounding border zone tissue and so left ventricular free wall tissue below the ligature was dissected and weighed. Ventricular tissue was cut in half; one half snap frozen on dry ice for protein extraction and the other half snap frozen on dry ice for RNA extraction for western blotting and real-time PCR experiments respectively. Alternatively, all left ventricular free **wall** tissue below the ligature was dissected and placed in ice-cold Hanks buffered saline solution without calcium and magnesium (HBSS[--]) for flow cytometry as discussed in section 1.5.8. Tissue extraction was always conducted by the same person to avoid inconsistencies when cutting tissues.

For histological experiments, the animal was perfused with 10% formalin (diluted in 0.9% saline) following heparinised saline perfusion. The whole heart, a portion of liver, the

right kidney and spleen were then removed and placed in 10% formalin for 24hours before being placed in 70% ethanol and wax embedded.

2.4.3 Immunohistochemistry for localisation of H_2S metabolic enzyme expression

Tissues were isolated as detailed in section 2.4.1. Tissues were specifically wax embedded to achieve a cross-axis view when cut. Paraffin wax blocks were cut using a microtome to achieve 5µm thickness, placed on glass slides and dried at room temperature overnight to allow firm adhesion to the slide. Slides were de-waxed with xylene (2*5mins), rehydrated through a series of graded ethanol concentrations (100%*2, 90%, 80%, 70% for 30seconds each) and washed in tap water.

Tissue fixation can cause protein cross-linking, which can mask protein antigens and prevent binding of primary antibodies. Cross-linked antigens were unmasked with a heat mediated antigen retrieval approach. Sections were placed in a sealed plastic container, submerged in 0.01M sodium citrate buffer (pH 6), and placed in a microwave on high power for 12 minutes until the buffer was boiling. The buffer was allowed to cool before slides were quenched in 3% H_20_2 for 5mins at RT to block endogenous peroxidases. Slides were washed in PBS and incubated with 10% goat blocking serum for 1hr at RT to block non-specific binding of secondary goat anti-rabbit antibodies. Following PBS washes (3*3min), avidin & biotin (Vector) were applied as per kit instructions to reduce non-specific binding of biotinylated antibodies. Following avidin & biotin application, sections were washed with PBS (3*3min), and incubated with rabbit raised-polyclonal antibodies overnight at 4^0C. Optimisation of primary antibody concentration (in dilutions ranging from 1:100 - 1:3000) was performed for each antibody in each tissue to achieve a strong signal with little to no background staining. Antibodies against CBS, CSE, MPST, TST and CD31 were raised in rabbit and sourced from Abcam. After several PBS washes (3*3min), biotinylated goat anti-rabbit secondary antibodies (1:500, Vector) were incubated for 1hr at RT before being washed off with PBS. Streptavadin horseradish peroxidase (Vector ABC reagent kit) was subsequently incubated (30mins at RT) which binds to the biotinylated secondary antibody and amplifies antigen signal by binding to multiple antigen sites. After several PBS washes, sections were incubated with the chromagen, 3-3'-diaminobenzidine (DAB, Vector) for the appropriate time. DAB reacts with peroxidase activity resulting in the development of a brown colour at antigen target sites. Sections were counterstained with Harris' Haematoxylin for 4 minutes to stain nuclei, rinsed in Scotts tap water and dehydrated through a series of graded ethanol concentrations (70%, 80%, 90%, 100%*2 for 30seconds each) and xylene

(5mins*2) before being mounted with DPX and coverslipped. Positive control tissues (where protein is notably most abundant) and negative control sections (omitting primary antibody incubation step) were used for all staining protocols. Sections were acquired using an Olypmus light microscope with Image Capture Pro 7 software.

2.4.4 Immunofluorescence staining for TST expression

Immunofluorescent co-localisation staining of CSE and TST staining with α-smooth muscle actin (α-SMA) was performed on heart tissue sections from 12wk old male C57BL/6 mice. CSE localisation within smooth muscle cells was used as a positive control for H_2S enzyme smooth muscle staining as described previously (Yang *et al.*, 2008). Paraffin embedded heart samples, 5µm thick were de-waxed, heat treated for antigen retrieval and blocked with goat serum, avidin & biotin as described above. Fluorescently conjugated α-SMA-Cy3 (Sigma) was co-incubated with primary antibodies for TST (Abcam) and CSE (Abcam) in the dark overnight at 4^0C. All further steps and washes were performed in the dark. Sections were washed in PBS and incubated with goat anti-rabbit secondary antibodies (Vector) for 1hr at RT. Following several PBS washes, fluorescently labelled strepavadin Alexa 488 (Life Technologies) was incubated for 1hr at RT in the dark and then washed with PBS. DAPI (Life Technologies) was incubated for 4 minutes at RT to stain for nuclei before mounting with Floromount G and coverslipped. Sections were imaged using a Zeiss Axiovert 200 fluorescent microscope with AxioVision Rel 4.8 software (Zeiss).

2.4.5 Haematoxylin and Eosin (H & E) staining

Haemotoxylin & Eosin staining was used to investigate morphological differences between wild type and *Tst*$^{-/-}$ mice in heart, liver and kidney tissues. Haematoxylin stains nuclei purple and Eosin stains cytoplasm pink. Tissue sections were deparrafinised with xylene, rehydrated with a series of graded ethanol concentrations and washed in tap water as described above. Slides were then immersed in Harris' Haemotoxylin solution (Sigma) for 4 minutes, washed in tap water and then placed in Scotts tap water (H_20 with ammonia) for 30seconds and washed again in tap water. Scotts tap water is a mild blueing reagent that causes Haematoxylin stained nuclei to turn blue and also enhances tissue adhesion to the slide which can otherwise be partially lost during graded ethanol and xylene dehydration steps. Slides were then immersed in Eosin for 10seconds until sufficient cytoplasmic staining was obtained and then washed in tap water. Slides were dehydrated by phased ethanol and xylene steps and mounted with DPX and coverslipped as described above.

2.4.6 Masson's Trichrome staining

Massons Trichrome staining was performed by Deborah Mauchline (Histology service, QMRI) on hearts from 7day post-CAL surgery mice for quantification of infarct size. Massons Trichrome (TCS Biosciences) stains collagen fibres blue, nuclei black and the cytoplasm red. Wild type and *Tst*$^{-/-}$ mice were perfusion fixed and the hearts extracted (as described above) and wax embedded. Slides were deparaffinised and rehydrated with xylene and ethanol as previously described above. Slides were placed in Weigert's haemotoxylin for 10min at RT, rinsed with dH_20 and incubated with phosphomolybdic-phosphotungstic acid solution for 15min until collagen lost its red appearance. Slides were subsequently incubated in aniline blue solution for 10min at RT, washed in dH_20 and further incubated in 1% acetic acid for 5 minutes. Slides were dehydrated by phased ethanol and xylene steps and mounted with DPX and coverslipped as described in chapter 2.4.3.

2.4.7 Picrosirius Red staining

Picrosirius Red (PSR) staining was performed on hearts from 7day post-CAL surgery mice for quantification of fibrosis. With PSR staining, collagen appears red and the background appears green in colour. Sections were stained by Deborah Mauchline (Histology service, QMRI). Slides were deparaffinised and rehydrated with xylene and ethanol as previously described and placed in PSR solution (0.1% Direct red, 0.1% Fast green and diluted 1:9 in Picric acid solution, Sigma) for 2hours at RT and then washed in tap water. Slides were dehydrated by phased ethanol and xylene steps and mounted with DPX and coverslipped as described previously.

2.4.8 Quantification

Sections were tiled at 4x magnification to generate whole heart images on Sterologer 3 and quantified using CapturePro5. Collagen (Picosirrius Red), scar area (Massons Trichome) and macrophage staining (Mac2) were calculated as percentage staining of left ventricle (LV). Scar thickness was calculated as average thickness from three points along the scar. First and last points were marked at the infarct border areas where 50% of viable tissue and 50% scar tissue were found. The third point was placed between the first two and average thickness along the scar calculated using ImagePro software. Infarct length was calculated as infarct length/ left ventricle length x 100.

2.5 Biochemical and Molecular Techniques

2.5.1 RNA extraction

Mice were culled by cervical dislocation, the tissues excised and then snap frozen on dry ice for RNA extraction. Hearts were dissected, the atria removed and the ventricles snap frozen, as was the right kidney and a portion of the liver. For CAL hearts, left ventricular myocardial tissue below the ligature incorporating the infarct and border zones were dissected and snap frozen. RNA was extracted from frozen tissues using a Trizol RNA extraction method. Samples were homogenised in RNase-free Eppendorff tubes with 1ml of ice-cold Trizol (Invitrogen) using autoclaved and RNA-Zap treated steel homogenised beads and homogenised for 1minute at a frequency of 30rpm/ second using the Retsch Vibration Mill. Samples were incubated at RT for 5 minutes before 0.2ml of chloroform (Fisher Scientific) was added and vigorously mixed for 15seconds and allowed to incubate for 10min at room temperature. Following the incubation period, samples were centrifuged for 15min at 12,000 x g at 4^0C to achieve a phase separation. Samples were separated into three distinct layers; a lower red-phenol phase, an interphase containing protein and a colourless upper phase containing RNA. The upper phase was transferred to an RNase-free eppendorff and the RNA precipitated with 0.5ml of ice-cold isopropyl alcohol (Fisher Scientific). Samples were centrifuged at 12,000 x g at 4^0C for 10 minutes and the supernatant discarded. The RNA pellet was washed with 1ml of ice-cold 70% ethanol (diluted in nuclease-free water, Qiagen) and centrifuged again at 12,000 x g at 4^0C for 5 minutes. Following washing step, the ethanol supernatant was discarded and the RNA pellet air-dried for 5min on wet ice before the RNA was eluted in 30µl of nuclease free water. RNA concentration was measured using a NanoDrop spectrophotometer (NanoDrop ND-1000, Thermo Fisher Scientific) at a wavelength of 230-280nm. RNA purity was identified by the A_{260}/ A_{280} ratio where values of 1.8 – 2.1 were deemed highly pure and were used for further analysis. Samples with A_{260}/ A_{280} ratio values outwith the appropriate range were not used for further analysis. Neat RNA samples were aliquoted to avoid repeated freeze-thaw damage and stored at -80^0C.

2.5.2 cDNA synthesis

Synthesis of cDNA was carried out in a two-step process. Firstly, 1µg of RNA was mixed with 1µl of 10mM dNTP mix (Applied Biosystems), 1µl random hexamers (Applied Biosystems) and 3µl of nuclease-free water and loaded into a Reverse Transcription system (Peltier Thermal Cycler 200, UK) at the following conditions; 65^0C *5mins, 0^0C *1min and held at 1^0C. Samples were then removed from the thermal cycler and supplemented with 4µl of 10x RT buffer (Applied Biosystems), 8.8µl of 25µM magnesium chloride (Applied Biosystems), 0.8µl RNase inhibitors (Applied Biosystems), 1µl multiscribe reverse transcriptase (Applied Biosystems), and 15.4µl of nuclease free water before returning to the Reverse Transcription system (Peltier Thermal Cycler 200, UK) at the following conditions; 25^0C *2mins, 42^0C *50mins, 70^0C *15mins and held at 4^0C. Samples were then diluted 1:2 with nuclease-free water and stored at -20^0C until needed. A control RNA sample was run in parallel with all samples and supplemented with all reagents except for reverse transcriptase and used as a negative control for all RT-PCR reactions.

2.5.3 Quantitative real-time PCR

The Applied Biosystems 7900HT fast real-time PCR system and applied biosystems taqman gene expression probes were used to measure the relative mRNA expression between tissues or the fold change differences in the same tissue of different genotypes using the $2^{\Delta\Delta Ct}$ method. The reaction mixture contained 10µl fast advanced mastermix (Applied Biosystems), 7µl RNase-free water, 1µl Taqman gene expression probes (Applied Biosystems, see table x for full details of probes used). The reaction mixture was added to 96well plates in duplicate and supplemented with 2µl of cDNA. Nuclease free water and reverse transcriptase-free RNA (as described above) served as two separate negative controls to determine if reagent contamination or genomic DNA amplification occurred during the PCR reaction respectively. Negative controls were plated in duplicate for all probes on each PCR plate. The 96well plate was centrifuged at 1000rpm *20seconds and placed in the ABI 7900HT PCR machine. The PCR reaction was performed at the following conditions; 95^0C *1:20min followed by 40cycles alternating between 95^0C *0:01min and 60^0C *0:20min). The data was used if the amplification curves were exponential before 35 cycles followed by a flat plateau. Taqman probes were obtained from Applied Biosystems. Probe sequences are not freely available from Applied Biosystems but primer numbers are detailed below (Table 2-4).

Quantification of relative expression was analysed using the ΔCt method to assess the presence of each gene in various tissues and using positive control tissue as reference (I.e. Liver used as a positive control tissue for *Tst*). Quantification of fold change was analysed using the $2^{\Delta\Delta Ct}$ method to compare upregulation/ downregulation of mRNA levels in the same tissue of different genotypes (WT vs. $Tst^{-/-}$). qRT-PCR was prepared and run as above (cDNA made using comparable concentrations of RNA) for both ΔCt and $2^{\Delta\Delta Ct}$ quantification approaches. TATA-binding protein (*Tbp*) was used as a housekeeping gene for all experiments involving enzymes of cytosolic origin (*Cbs, Cth, Mpst, Nos1, Nos2, Nos3, Ccl2, Ccr2, Icam1, Vcam*). Cytochrome oxidase IV (*Cox4i1*), a component of the mitochondrial respiratory chain was used as the housekeeping gene for experiments involving mitochondrial bound enzymes (*Tst, Sqrdl, Ethe1, Suox*) to normalise for differences in mitochondrial density between tissues. Neither *Tbp* nor *Cox4i1* expression was significantly changed by CAL treatment (Figure 2-5). *Gapdh* was used as an internal control gene when assessing *Tst* expression in endothelial cells only as *Gapdh* is the commonly used housekeeping gene for this cell type.

Gene	AB primer number
Cbs	Mm00460654_m1
Cox4i1	Mm01250094_m1
Cth	Mm00461247_m1
Ethe1	Mm00480916_m1
Gapdh	Mm99999915_g1
Mpst	Mm00460389_m1
Nos1	Mm00435175_m1
Nos2	Mm00440502_m1
Nos3	Mm00435217_m1
Sqr-dl	Mm00502443_m1
Suox	Mm00620388_g1
Tbp	Mm00446971_m1
Tst	Mm01195231_m1
Actr1b	Mm00525061_m1
Ccl2	Mm00441242_m1
Ccr2	Mm01216173_m1
Icam1	Mm00516023_m1
Vcam1	Mm01320970_m1

Table 2-4 Applied Biosystems probes for qRT-PCR

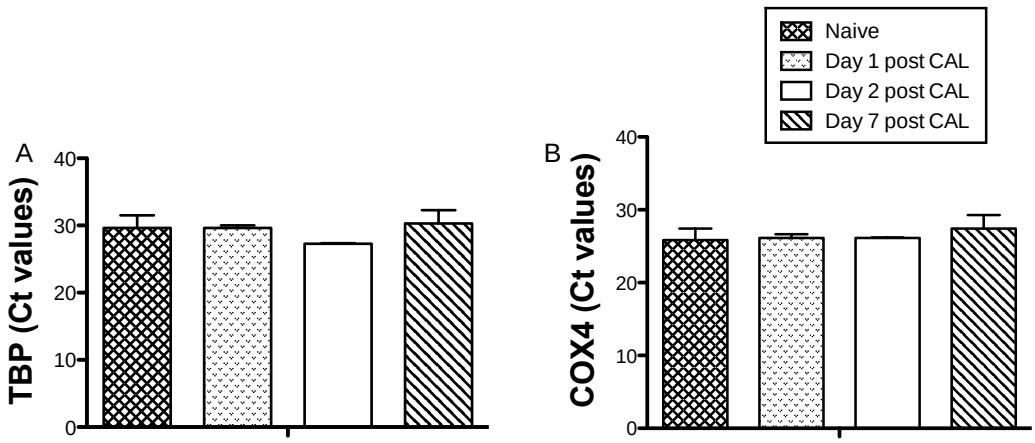

Figure 2-5 Internal control gene expression is unaltered in hearts following myocardial infarction

A) TBP and B) COX4 internal control gene expression expressed as cycle threshold (Ct) values in naïve hearts and at 1, 2 and 7 days following myocardial ischaemia. Values ± SEM, analysed by repeated measures ANOVA.

2.5.4 Protein extraction

Western blotting was performed on heart, liver, kidney and aortic tissues from naïve animals or on hearts from CAL operated mice from both *Tst-/-* and control groups. Frozen liver, heart and kidney tissues (20-100mg) were placed in a sterile Eppendorff tube containing ice-cold 1x RIPA buffer (Millipore), protease inhibitor cocktail (Sigma, 1:100) and phosphatase inhibitors cocktails 2 & 3 (Sigma, 1:100) to preserve protein quality. From CAL hearts, myocardium was isolated from the infarct and border zones below the ligature. Sterile steel homogenisation beads were added to the Eppendorff tube and the samples homogenised for 1minute at a frequency of 30rpm/ second using the Retsch Vibration Mill. Samples were centrifuged at 13,000rpm at 4^0C to pellet tissue debris and clear homogenate transferred to clean eppendorffs. Myocardial and aortic homogenates used for western blots investigating eNOS and Vasp protein expression were prepared by Alessandra Borgognone at the University of Birmingham. Frozen hearts and thoracic aortas were crushed under liquid nitrogen conditions and 10% (wt/vol) solution of tissues homogenate was prepared in homogenisation buffer containing ice-cold 100 mM Tris·HCL (pH 7.4), protease complete C tablet (Roche) per 50 ml, 2 mM sodium orthovanadate, and 5 mM sodium fluoride.

2.5.5 Bradford protein assay

Albumin protein standards (0, 25, 125, 250, 500, 750, 1000, 1500, 2000µg/ mL, Thermo Scientific) diluted in homogenisation buffer were plated in duplicate in a 96well flat-

bottomed plate alongside diluted sample homogenates. Samples were supplemented with kit reagents to initiate colour change and incubated at 37^0C for 30 minutes as per kit instructions. Samples were read at 562nm on a Spectrophotometer and sample protein levels quantified using the standard curve method using Excel. Aliquots of neat protein samples were diluted in homogenisation buffer to obtain equal protein concentrations (2-10µg protein/ µl) and frozen at -20^0C until required.

2.5.6 Western Blotting

Equal concentrations of heart, kidney & liver protein samples were run on 10-12% sodium dodecyl sulphate (SDS) gels SDS. 5% separating gel (30% acrylamide, 0.5M Tris buffer, 10% SDS, 10% Ammonium persulfide, dH_20 and TEMED) were set on top of 12% resolving gel (containing 30% acrylamide, 1.5M Tris buffer, 10% SDS, 10% Ammonium persulfide, dH_20 and TEMED). Protein samples (10-30µg protein) incubated with 6X sample buffer (0.35M Tris-Hcl, 0.35M SDS, 30% v/v glycerol, 0.6M DTT, 0.175mM bromophenol blue) and protein markers (Colorplus Prestained Protein Marker Broad Range, 7-175kDa, New England Biolabs) were boiled at 95^0C for 5min and centrifuged at 13,000rpm for 1min before loading into the gel. Electrophoresis was performed at 80V for 15min, then 120V for 1hr in running buffer containing (mM; Glycine 39, Tris 50 and SDS 2).
Following electrophoresis, the gel was placed in transfer buffer (mM; Tris 48, Glycine 40 SDS 1.2, 1:5 methanol: dH_20) and stacked with transfer buffer soaked extra-thick blot paper (Bio-Rad) and ECL nitrocellulose membranes (Amersham) on a Trans-Blot Semi Dry Transfer Cell (Bio-Rad). Protein transfer was ran for 90min using an appropriate milli-amplitude (mA) calculated from the following equation:

$$\boldsymbol{mA = Gel\ surface\ area\ (cm^2) \times 0.8}$$

Membranes were then blocked with 5% dried milk dissolved in Tris-Buffered Saline Tween (TBST; 1000mL 1X TBS, 1ml Tween 20) for 1hr at RT to eliminate non-specific binding of the antibodies. Following blocking, membranes were incubated with internal control antibodies Beta-actin (Abcam) or cytochrome oxidase IV (COX IV, Abcam) for 1hr at room temperature (RT), washed in TBST (3*15mins) and further incubated for 1hr at RT in the dark with Alexa-780 fluorescent secondary antibodies (Li-Cor) at 1:10,000 dilutions. The mitochondrial respiratory enzyme, cytochrome oxidase IV (COX IV) was used as an internal control for TST western blots and all other cytosolic bound enzymes normalised to tubulin.

After further washes (3*15mins), membranes were developed on the fluorescent detection Licor Odyssey developer where signal intensity was quantified using the Odyssey software package. Membranes were again blocked with 5% milk for 1hour at RT, briefly washed in TBST and then incubated with the primary antibodies for proteins of interest overnight at 4^0C with agitation. Antibody optimization was performed in dilutions ranging from 1:500 - 1:5000 in 5% BSA to determine working dilutions that resulted in good signal but little non-specific binding. Antibodies against CBS, CSE, MPST, TST, HO-1 and Trx1 were raised in rabbit and sourced from Abcam. Following washing (3*15mins), membranes were incubated for 1hr at RT in the dark with Alexa-780 fluorescent secondary antibodies (Li-Cor) at 1:10,000 dilutions. The membrane was again developed on the Licor Odyssey developer and internal control and protein of interest identified based on protein size using the protein ladder. Densitometric analysis was performed using the Odyssey software package, which quantified the relative intensity of the protein of interest and normalized it its own internal control to account for differences in sample loading and the efficiency of the protein transfer. Western blots were performed in duplicate and average normalised protein expression calculated. The relative intensity of each sample were then normalised to the mean of the control group (wild type naïve mice or wild type post-CAL mice).

For eNOS and Vasp phosphorylation studies performed by Alessandra Borgognone in the University of Birmingham, total eNOS (BD transduction laboratories), $eNOS^{Ser1177}$ (Cell signalling), total Vasp (Cell signalling), $Vasp^{239}$ (Cell signalling) and GAPDH (Abcam) blots were performed on 10% SDS gels and transferred onto PVDF membranes (Hybond P, Amersham). Following primary antibody incubation, membranes were washed with TBST and incubated with horseradish peroxidase (HRP)- conjugated anti-species secondary antibodies (GE healthcare) for 1 hr at room temperature and then exposed to enhanced chemiluminescence (ECL) detection reagent (Amersham) and exposed to ECL Hyperfilm (Amersham). The hyperfilm was then scanned and densitometric analysis performed using Adobe Photoshop. $eNOS^{Ser1177}$ was normalised to total eNOS and $Vasp^{Ser239}$ was normalised to total Vasp. Total eNOS and total Vasp blots were normalised to GAPDH.

2.5.7 TST enzyme activity assay

Tissue TST enzyme activity as measured by the formation of thiocyanate from potassium cyanide and thiosulfate as described previously (Hildebrandt & Grieshaber, 2008a) with modifications, in collaboration with Roderick Carter. Liver tissue was used for TST enzyme activity assays as TST is most abundant in liver tissue. Equal amounts of liver protein (100μg) were incubated at 30^0C with sodium thiosulfate (500mM, Sigma), potassium

phosphate (500mM, Sigma) and distilled water. Thiocyanate formation is catalysed by addition of potassium cyanide (50mM, Sigma) and incubated at room temperature for 10 minutes. The reaction is halted with 38% paraformaldehyde (Sigma) before 0.25M iron nitrate (Sigma) and 25% nitric acid (Sigma) are added to initiate colour change. Thiocyanate levels were measured spectrophotometrically at 460nm. Thiocyanate levels were corrected for background signal by subtracting the absorbance read in blank samples. Heat-treated wild type protein (95^0C for 5 minutes) was used a negative control in all experiments. Low enzyme activity observed in *Tst*$^{-/-}$ mice was deemed as artefact as wild type heat-treated tissue (95^0C *5mins) had similar spectrophotometric signal. TST enzyme activity assays were performed on liver tissue from *Tst*$^{-/-}$ and C57BL/6N mice in each experimental study as a means of genotyping.

2.5.8 Flow Cytometry

2.5.8.1 Circulating leukocytes

Circulating monocytes and neutrophils were measured in whole blood (30µl blood: 30µl 3.2% citrate) withdrawn from the tail vein in conscious mice at 2days post MI. Whole blood was placed in 5ml round bottomed FACS tubes, incubated with fluorescent antibodies against CD11b-AF700, Ly6C-PerCP5.5 and Ly6G-PacificBlue (BioLegend) for 30mins in the dark and washed with PBS[--] (without calcium and magnesium). Red blood cells were lysed with 1ml of Lysis buffer (1:10 in dH_20, BD FACS), washed with PBS[--] and centrifuged at 300 x g for 5 minutes and resuspended in 1ml PBS[--]. Auto florescent counting beads (50,000beads) were added to flow tubes immediately prior to sample readings on the LSR flow cytometer and used as reference values to quantify the total numbers of neutrophils, Ly6C^{high} and Ly6C^{low} monocytes per mL of blood. Sample measurement was stopped when the number of counting beads reached 5000 events. Neutrophils were identified as CD11b^{high}/ Ly6G^{high}/ Ly6C^{intermediate}. Monocytes subsets were identified as CD11b^{high}/ Ly6G^{low}/ **Ly6C^{high}** or CD11b^{high}/ Ly6G^{low}/ **Ly6C^{low}**. Cells were gated upon as described in Figure 2-6.

2.5.8.2 Infiltrated leukocytes

All left ventricular free wall cardiac tissue below the ligature was harvested from mice 2days after MI as described above. Tissues were chopped with scissors and placed into warmed (37^0C) MACS tubes containing a cocktail of Collagenase D (1.25mg/ml, Roche), DNase 1 (60U/ml, Roche) in HBSS and homogenised on a MACS dissociator (Macs Biotinyl Biotech) to digest the myocardium. Tissue samples were incubated in a water bath at 37^0C

for 30 minutes before being homogenised a second time on a MACS disrupter to increase the yield. Cells were filtered through a 70µm nylon mesh (Fisher brand), and centrifuged at 300 x g for 5 minutes at 4^0C and live counted using a Nucleocounter (Chemometec Nucleocassette).

Cells were washed with PBS[--], blocked with 10% mouse serum and incubated with fluorescent antibodies against CD45-PeCy7, CD11b-AF700, Ly6C-PerCP5.5 and Ly6G-PB (BioLegend), for 30mins in the dark and washed with PBS[--]. Cells were incubated with DAPI (1µg/ ml, Invitrogen) immediately prior to sample testing to identify dead cells ($DAPI^+$) when disrupted cell membranes were permeable to DAPI. Cells were incubated with counting beads and 30,000 bead events counted on the LSR, which approximately accounted for the entire sample. Live neutrophils were identified as DAPI ^{low}/ $CD45^{high}$/ $CD11b^{high}$/ $Ly6G^{high}$/ $Ly6C^{intermediate}$. Monocytes subsets were identified as either $DAPI^{low}$/ $CD45^{high}$/ $CD11b^{high}$/ $Ly6G^{low}$/ **$Ly6C^{high}$** or $DAPI^{low}$/ $CD45^{high}$/ $CD11b^{high}$/ $Ly6G^{low}$/ **$Ly6C^{low}$**. Neutrophil or monocyte subset numbers were calculated as total live cells multiplied by percentage of live neutrophils or live $Ly6C^{high}$ or $Ly6C^{low}$ monocytes within identified gates. Cells were gated upon as described in Figure 2-7. Unstained and isotype controls for CD45, CD11b, Ly6G and Ly6C were ran in parallel to all samples as negative controls to ensure the LSR cytometer compensations were within the correct range.

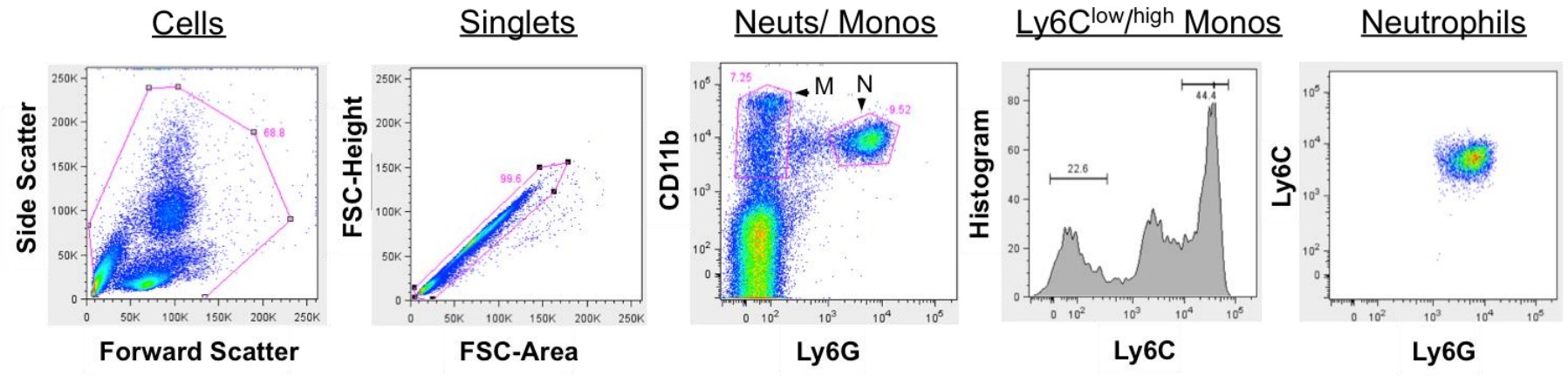

Figure 2-6 Flow cytometry gating strategy of blood from mice at 2days post CAL

Gating strategy for flow cytometry in blood from infarcted wild type C57BL/6N mouse heart at 2days post CAL with anti-CD11b, Ly6G and Ly6C (reading left to right). Cells were gated for granularity and size (by Side scatter-SSC and Forward Scatter-FSC) and singlet cells gated using FSC-H/ FSC-A (height/ area) to exclude cell clumps. Cells expressing CD11b were gated against Ly6G and used to identify monocytes (M) and neutrophil (N) cell populations. CD11b^{high} and Ly6G ^{high} cells were gated on to select for neutrophils. CD11b^{high} and Ly6G^{low} cells were gated on to select for monocytes (M). The monocyte population was separated into CD11b^{high}/ Ly6G^{low}/ Ly6C^{high} and CD11b^{high}/ Ly6G^{low}/ Ly6C^{low} populations. Neutrophils were further identified as CD11b^{high}/ Ly6G^{high}/ Ly6C^{intermediate}. *Abbreviations; FSC; forward scatter, Leuk; leukocyte, M; monocytes, N; neutrophils, SSC; side scatter, FSC; forward scatter.*

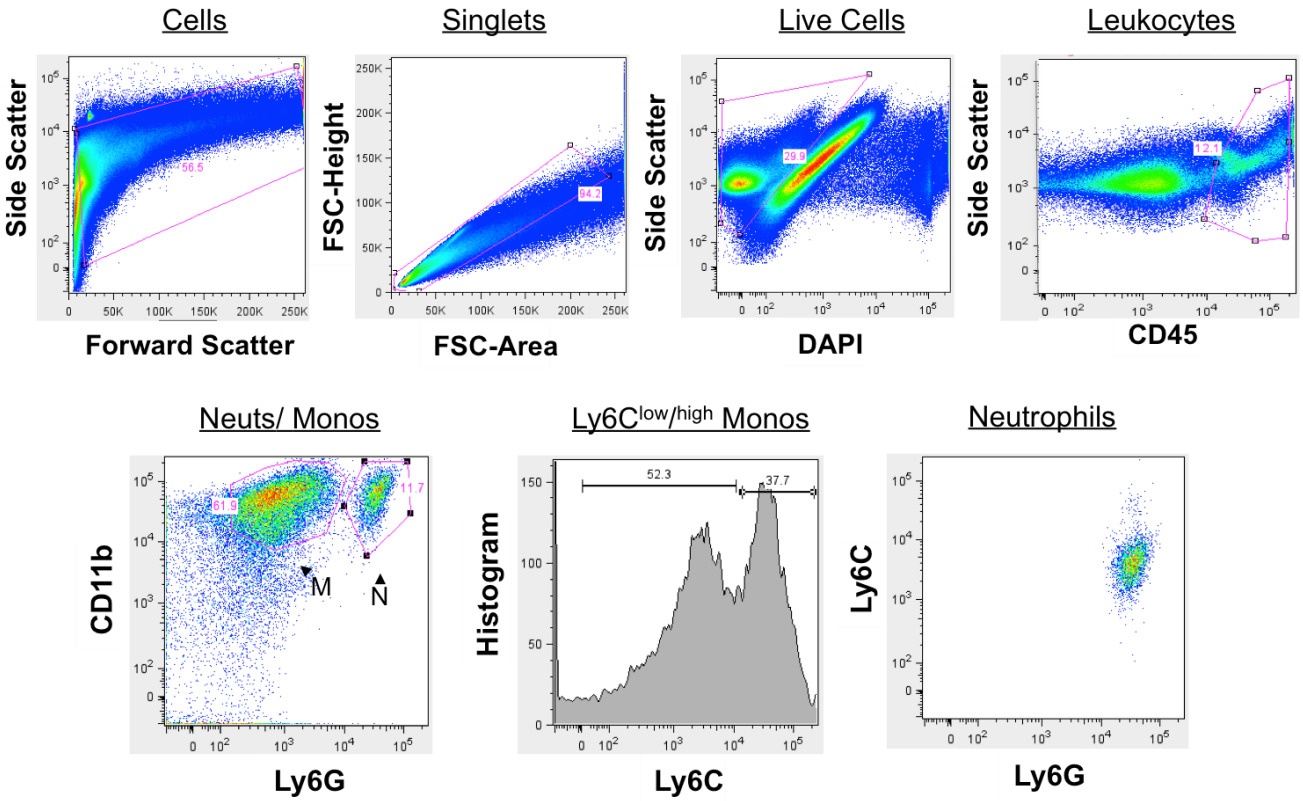

Figure 2-7 Flow cytometry gating strategy in digested hearts of mice at 2days post CAL

Gating strategy for flow cytometry from individual digested heart preparations from infarcted wild type C57BL/6N mouse heart at 2days post CAL stained with anti-CD45, CD11b, Ly6G, Ly6C and DAPI (reading top row left-right, then bottom row left-right). Cells were gated for granularity and size (by Side scatter-SSC and Forward Scatter-FSC) and singlet cells gated using FSC-H/ FSC-A (height/ area) to exclude cell clumps. Live cells were selected with a DAPI negative gate (Live cells were DAPI^{low}). Cells expressing high levels of the leukocyte marker CD45 were gated upon (Side Scatter-SSC/CD45+). Cells expressing CD11b were gated against Ly6G and used to identify monocytes (M) and neutrophil (N) cell populations. CD11b^{high} and Ly6G^{high} cells were gated on to select for neutrophils. The monocyte population was separated into CD11b^{high}/ Ly6G^{low}/ Ly6C^{high} and CD11b^{high}/ Ly6G^{low}/ Ly6C^{low} populations. Neutrophils were further identified as CD11b^{high}/ Ly6G^{high}/ Ly6C^{intermediate}. *Abbreviations; FSC; forward scatter, Leuk; leukocyte, M; monocytes, N; neutrophils, SSC; side scatter.*

2.5.9 H_2S Measurement - Bromophenol blue assay

Initial experiments to measure tissue H_2S production rates were performed with the bromophenol blue method as described previously (Geng *et al.*, 2004a). Fresh left ventricular myocardium and liver tissue from naïve C57BL6 mice were isolated and homogenized in ice-cold 50mM potassium phosphate buffer (pH 6.8) and then added to the reaction mixture of 100mM potassium phosphate (pH 7.4), 10mM L-cysteine (Sigma), 2mM pyridoxal 5'-phosphate (Sigma) and 10% (w/v) tissue homogenate. Cryovial test tubes (2ml; Simport Plastics, Belocil, Que) were used as the centre wells containing a 2cm X 1.5cm piece of Whatmann filter paper soaked in 0.5ml 1% zinc acetate as a trapping solution for H_2S. The centre wells of the reagent containing cyrovials were flushed with a slow stream of nitrogen gas, sealed with a layer of Parafilm and then capped. By transferring the flasks from ice to a 37^0C shaking water bath, the reaction was initiated. After incubation in the water bath for 90mins, 0.5ml of 50% trichloroacetic acid (Sigma) was added to stop the reaction. Flasks were flushed with nitrogen gas, sealed once more and placed in a water bath at 37^0C for another 60mins to ensure complete trapping of evolved H_2S by the zinc acetate solution as zinc sulfide. The centre tubes contents were transferred to test tubes, each of which contained 3.5ml of water after which 0.5ml of 20mM N, N-dimethyl-p-phenylenediamine sulphate in 7.2M HCl and 0.5ml of 30mM $FeCl_3$ (Sigma) in 1.2M HCl were added directly to the zinc acetate soaked Whatmann paper to initiate a colour change. The flasks were allowed stand for 20mins at room temperature and the absorbance of the resulting solution was measured at 670nm with a spectrophotometer (Molecular Devices, Sunnyvale, California, USA). A calibration curve of absorbance versus sulfide concentration was determined by using standards of the H_2S donor, Na_2S (as outlined in Figure 2-8). Bromophenol blue assays were deemed too insensitive to measure H_2S as concentrations below 1mM Na_2S were not linear (Figure 2-8). Tissue H_2S measurements with a specific H_2S electrode (discussed in further detail in chapter 2.5.10) were later adopted as a more sensitive method (lower detection limit within nM range) that could detect the rate of H_2S production and breakdown in real time.

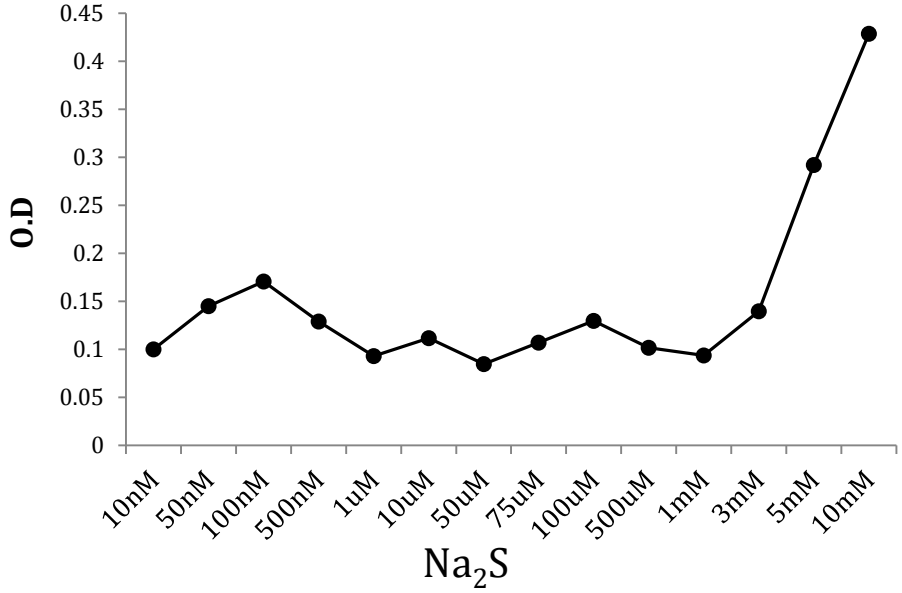

Figure 2-8 Bromophenol Blue method of H_2S detection

Optical density (O.D) values of Na_2S standards (nM – mM) using Bromophenol blue method.

2.5.10 H_2S electrode

The Hydrogen sulfide electrode was constructed during a lab visit to our collaborators, Professor Kenneth Olson and Eric DeLeon in the University of Notre Dame, Indiana, USA. The H_2S electrode is capable of measuring H_2S in the nM range compared to mM range as observed with the bromophenol blue assay. The electrode is based on the Doeller H_2S electrode design (Doeller *et al.*, 2005), with modifications.

A 0.6mm, 99.95% pure platinum wire (Alfa Aesar), which acted as the anode, was covered with a 2cm borosilicate capillary tube at its tip and heat-sealed to the platinum with a blow torch. The tip of the glass tube was then ground until the platinum is exposed on all sides and polished using ultrafine sandpaper under approximately 5ml of water to reduce vibration and avoid shattering the borosilicate glass. The platinum and glass were annealed overnight to strengthen the glass. Silastic tubing was heated in hot water and milked over the proximal end of the anode to provide electrical insulation from the cathode. Copper wiring was soldered onto the anode's platinum, which was used to conduct the amperometric signal away from the tip of the anode (discussed in more detail below). A 32G platinum wire (Alfa Aesar), which acted as the cathode, was spun around the anode 10-15times. The copper from the anode and platinum cathode were soldered into a 2-prong lemo connector (Lemo UK; FGG 00.02.CLAD35). An outer glass tube 2mm in diameter was cut to match the length of the platinum wire and a groove cut 2mm from its tip (please see electrode schematic and picture of completed electrode in Figure 2-9). The tip of the glass was covered with a gas permeable silicone membrane, secured with an O-ring that fitted into the glass groove and filled with 50mM ferricyanide solution (World Precision Instruments). The anode and cathode assembly was then immersed in the ferricyanide containing outer glass tube and in conjunction with a threaded sleeve, screwed into a customised acrylic chamber with a stopper to limit H_2S oxidation. The electrode was connected to a TBR4100 free radical analyser (World Precision Instruments) via the electrodes Lemo connector and equilibrated in 0.1M PBS overnight at 150mV polarising voltage. The TBR4100 was connected to an AD Instruments Powerlab 8/30 and signal was recorded in real time using LabChart 7 software (AD Instruments).

Daily calibrations of the H_2S sensor were carried out using standards of the H_2S donor compound, Na_2S (Sigma) to calculate tissue H_2S concentration in terms of current change (1μM H_2S/ nA). Na_2S was added to a glass vial and sealed with a rubber stopper (Fisher USA) before nitrogenated dH_20 was added with a syringe through the stopper to achieve a stock solution with a final concentration of 100mM Na_2S. A second syringe was sealed with a rubber stopper, filled with nitrogenated dH_20 and using a syringe, a set volume of stock

Na_2S was added to achieve a final concentration of 2mM. The acrylic chamber was filled with 1mL of dH_20 before Na_2S standards (0.5µM, 1µM, 5µM, 10µM) were administered with a 0.25mL bevelled Hamilton syringe through the injection port within the chamber stopper. As H_2S is added to the chamber, it permeates the sensor's membrane and dissociates to HS^-, which reduces ferricyanide to ferrocyanide (Figure 2-10). This chemical reduction donates electrons to the anode, creating a current potential that is proportional to H_2S concentration (Figure 2-11). H_2S standards were repeated 3 times before and after all tissue experiments. Baseline current is subtracted from the current produced by H_2S standards and the current (nA) produced by 1µM Na_2S is calculated to interpret tissue H_2S experiments.

Heart and liver tissue was extracted from wild type and *Tst*$^{-/-}$ mice, quickly washed in ice-cold Krebs solution and immersed in Krebs solution containing protease inhibitors (1:100). Atria were removed from hearts and a portion of liver was dissected. All homogenisation apparatus and tubes were pre-chilled on ice to preserve mitochondrial integrity. Tissues were homogenised in a potter Elvehjem homogeniser, centrifuged at 2,000rpm at 4^0C for 30seconds to pellet tissue particulate and kept on ice until used. All tissue was used within 6hours of collection. Tissue was placed into the closed H_2S chamber with Krebs solution at a ratio of 1:10 and stirred with a micro magnetic rod driven by magnetic stirrer underneath. For H_2S breakdown assays, 20µM Na_2S was administered to tissues and H_2S levels continuously monitored. The rate of H_2S breakdown was calculated when a linear breakdown phase was observed. Tissue H_2S breakdown was corrected for protein using a Bradford assay as described in chapter 2.5.5. Heat-treated (95^0C *5mins) wild type tissue and buffer alone were placed in the chamber and treated with 20µM Na_2S to illustrate little breakdown in the absence of fresh tissue. For H_2S production assays, tissue (1:10 with Krebs solution) was supplemented with H_2S synthetic enzyme substrates, L-cysteine (5mM) and pyridoxal-5-phosphate (1mM). The rate of H_2S production was calculated when a linear production phase was observed and corrected for protein. However, spontaneous H_2S generation with 5mM L-cysteine (but not pyridoxal 5' phosphate) was observed in buffer alone led to lower L-cysteine being tested (0.2-1mM). Spontaneous decomposition of L-cysteine into H_2S in aqueous solutions has been reported previously using gas chromatography techniques (Furne, Saeed, & Levitt, 2008). 1mM L-cysteine H_2S was deemed satisfactory and tissue-free L-cysteine samples were to be used to correct for spontaneous decomposition in tissue-containing samples. The H_2S polarographic electrode broke before the study was conducted and despite considerable efforts, could not be fixed prior to my departure from the lab.

A

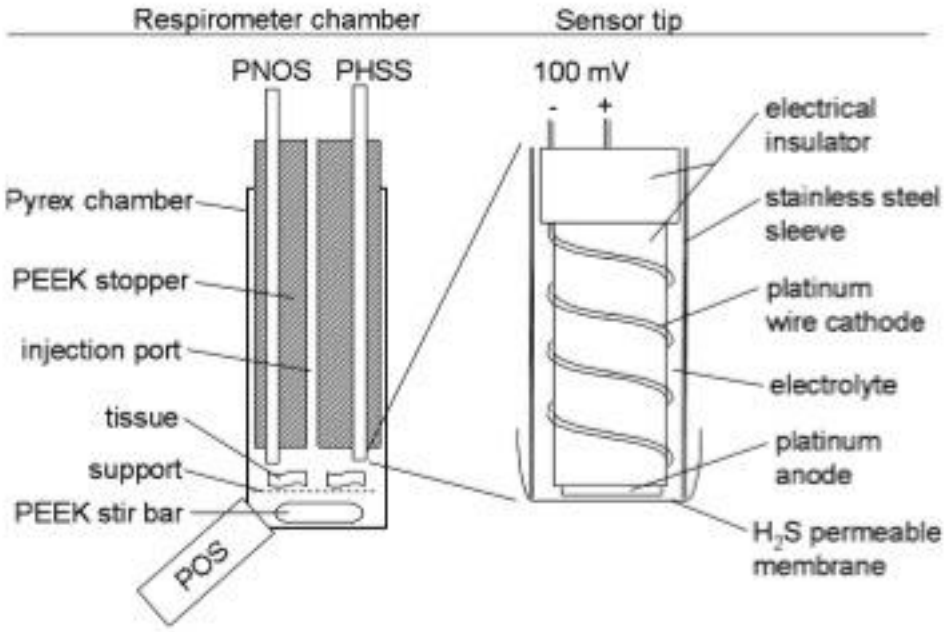

B

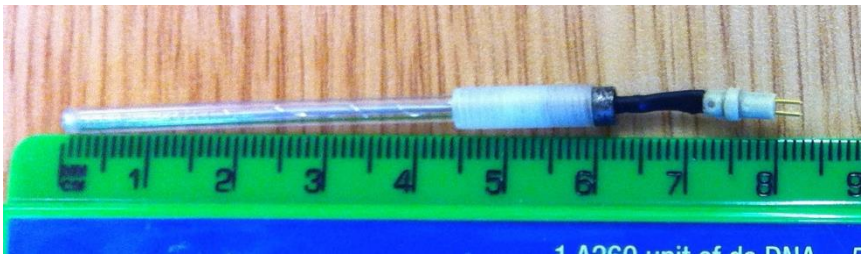

Figure 2-9 Schematic illustration of H_2S electrode construction

A) Diagram of prototype H_2S sensor obtained from (Doeller *et al.*, 2005). B) Picture of a completed H_2S sensor used H_2S measurement studies.

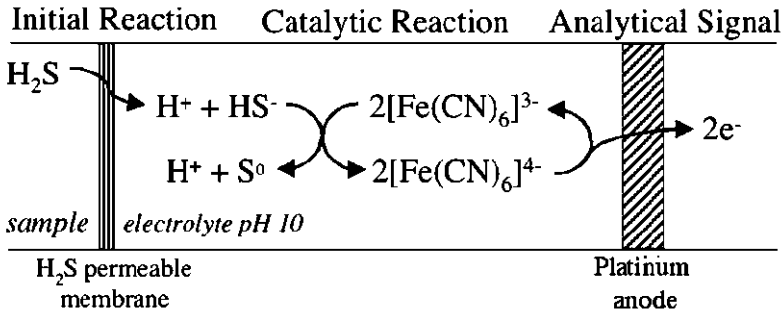

Figure 2-10 H_2S sensor redox chemistry

H_2S diffuses across the sensors membrane and reduces ferricyanide to ferrocyanide, which donates electrons to the anode creating a current proportional to H_2S concentration. Diagram obtained from (Doeller et al., 2005).

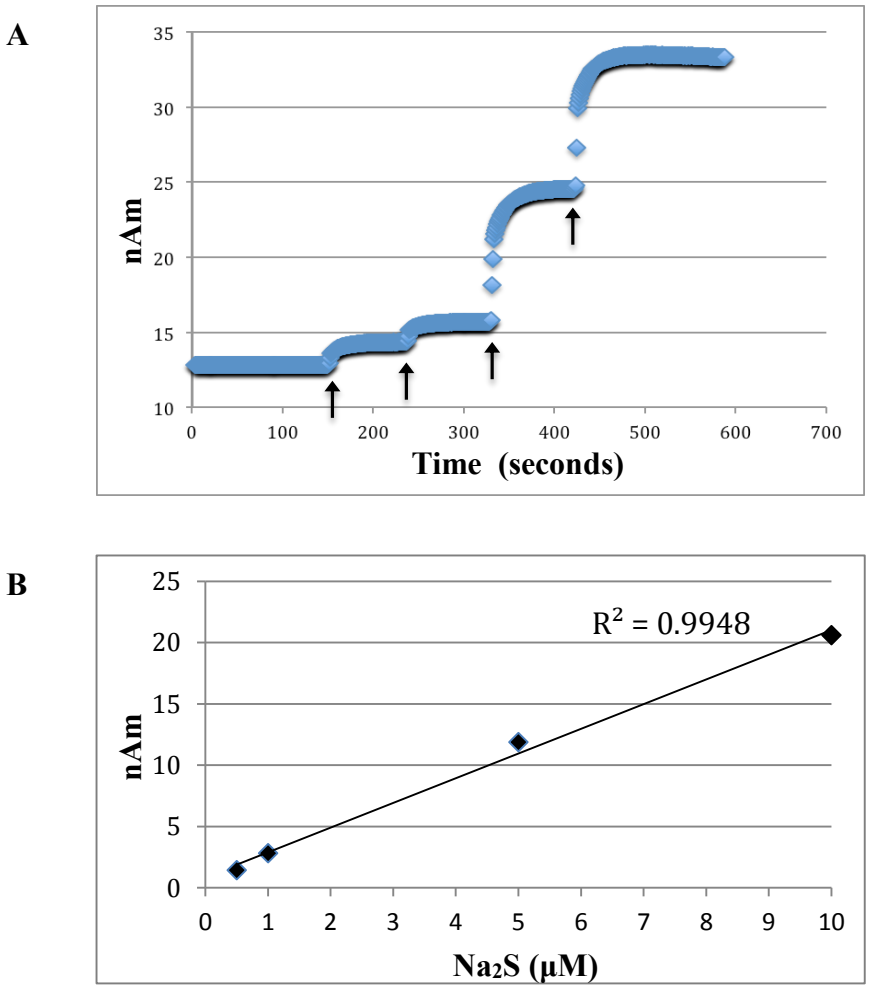

Figure 2-11 H_2S electrode responds to low concentrations of sulfide in real time

A) Representative calibration trace of the H_2S sensor using standards of a H_2S donor (Na_2S) administered to fresh normoxic dH20. Arrows from left to right illustrate H_2S donor administration of 0.5µM, 1µM, 5µM and 10µM. B) H_2S electrode displays a linear response to H_2S donor concentrations illustrating its sensitivity.

2.5.11 Monobromobimane assay – H_2S and thiosulfate measurements

Monobromobimane assays measuring H_2S and thiosulfate were performed by Dr. Martin Barrios-Llerena in the Morton group. Determination of H_2S and thiosulfate concentration in whole blood samples were performed by derivatization with monobromobimane (MBB) followed by HPLC separation and detection with a fluorescence detector as described previously (Tiranti *et al.*, 2009), with modifications.

Briefly, 50µl blood samples were collected into an Eppendorff tube containing 10µl of 46 mM MBB and incubated for 30 minutes in the dark. The MBB-sulfide was extracted with 1ml of 160mM EPPS/16mM diethylenetriaminepentaacetic acid (DTPA) pH 8, dried under nitrogen, reconstituted 4-fold with buffer A (10 mM tetrabutylammonium phosphate aqueous, 10% methanol, 45 mM acetic acid adjusted to pH 3.4) and injected into an Ultimate 3000 UHPLC+ focused system for identification and quantification. Separation was achieved by a gradient of buffer A to 100% Buffer B (10 mM tetrabutylammonium phosphate in methanol, 10% water, 45 mM acetic acid) for 45 minutes at 1 ml/min flow rate.

Separation was performed using an Ultimate 3000 UHPLC+ focused system, couple to a 4.0 × 125 mm LiChroCART 125-4, (LiChrospher 60 RP-select B, 5 µm, Merck KGaA), analytical column fitted with a guard column LiChroCART 10-2, Superspher 60 RP-select B cartridge and using a fluorescence detector (excitation 380 nm, emission 480 nm). Na_2S and sodium thiosulfate (Sigma) standards were performed in parallel with blood samples for determination of concentration.

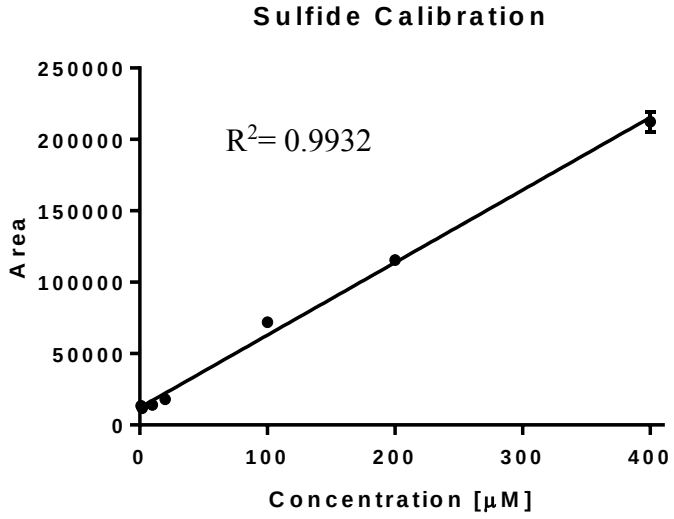

Figure 2-12 H_2S standard curve using monobromobimane HPLC method of detection

Linear response relationship between the fluorescence area of HPLC chromatograms as function of sulfide concentration, injecting 20 µL of standard sulfide solutions. Fluorescence trace was recorded at l_ex = 380 nm, l_em = 480 nm.

2.6 Statistical Analysis

Statistical analysis was performed using Graphpad Prism software. All values presented are as mean ± SEM. Analysis of survival was performed using a Chi squared test. Analysis of non-parametric data for cumulative water and urinary electrolyte balance were performed using two-tailed Mann-Whitney U test. Other comparisons are by unpaired two-tailed Student t-test, 1-way ANOVA and 2way ANOVA followed by post-hoc analysis using Tukeys Multiple Comparison test or Bonferoni post-hoc tests respectively. For full details, please see individual chapters. P values less than 0.05 were considered significant.

3 TST is expressed in the murine cardiovascular system and regulates H_2S synthesis and removal

3.1 Introduction

Hydrogen sulfide (H_2S) is an endogenously produced gaseous signalling molecule with a diverse set of therapeutic capabilities across its physiological range. Pharmacological H_2S donors limit myocardial infarction-(MI) induced injury (Szabo, 2007), reduce blood pressure via increased vasodilatation (Abe *et al.*, 1995) and suppress inflammation (Zhang *et al.*, 2014). H_2S donor compounds interact with endogenous nitric oxide (NO) to mediate these protective actions (Papapetropoulos *et al.*, 2009). H_2S is generated by the enzymes cystathionine beta synthase (CBS), cystathionine gamma lyase (CSE) and 3-mercaptopyruvate sulfurtransferase (3MST), as described in detail in section 1.1.1. CSE is considered the primary H_2S synthetic enzyme within the cardiovascular system and is highly expressed in the heart and vasculature. Cardiac specific CSE overexpressing (αMHC-CGL-Tg) mice produce more H_2S and are protected from myocardial ischaemia reperfusion injury (IRI) (Calvert *et al.*, 2010; Elrod *et al.*, 2007). αMHC-CGL-Tg mice have increased basal expression of the H_2S-sensitive antioxidant transcription factor, nuclear receptor factor-E2-related factor (Nrf2) and its downstream targets, hemeoxygenase 1 (HO-1) and thioredoxin (TRX1) in the heart, which help mediate their cardioprotective profile (Calvert *et al.*, 2010).

H_2S bioavailability is likely to be determined not only by local synthesis, but also by local removal. As high concentrations of H_2S can fatally inhibit mitochondrial respiration via cytochrome c (Modis *et al.*, 2013b; Szabó, 2007), H_2S bioavailability is tightly regulated to avoid such harmful effects by efficient breakdown within the mitochondria as described in detail in section 1.1.2. According to the Hildebrandt and Grieshaber H_2S breakdown model (Hildebrandt *et al.*, 2008b), thiosulfate sulfurtransferase (TST) is believed to utilise sulfite produced by a sulfur dioxygenase (ETHE1) in the mitochondria to form the stable metabolite thiosulfate, which is safely excreted in the urine. *Ethe1* deficient mice have retarded growth and die from sulfide toxicity by 40 days of age (Tiranti *et al.*,2009), supporting a vital role for the sulfide detoxification pathway. TST is most abundantly expressed in the liver, kidneys and colon (Nagahara *et al.*,1998). Sulfate reducing bacteria in the colon produce large amounts of H_2S and are widely believed to be involved in the aetiology of ulcerative colitis (Rowan *et al.*, 2009; Taniguchi *et al.*, 2009). Mice with ulcerative colitis have reduced TST enzyme activity in the colon (Taniguchi *et al.*, 2009), supporting a role for TST in H_2S removal.

Although TST has previously been shown to be present in whole heart homogenates (Nagahara *et al.*, 1998), nothing is known of its cellular localisation within the heart and vasculature or its role in regulating H_2S bioavailability. The work presented in this chapter aimed to address these issues by examining the expression and localisation of TST in the healthy murine heart and vasculature in comparison to the well-characterised H_2S synthetic enzymes. Additionally, using a novel *Tst* deficient (*Tst*$^{-/-}$) mouse, the current study aimed to investigate; (i) the extent to which TST plays a role in myocardial H_2S breakdown, (ii) whether the *Tst*$^{-/-}$ mouse suffers a similar pathology as the *Ethe1*$^{-/-}$ mouse due to H_2S over-exposure, or if it represented a milder model of altered H_2S breakdown (iii) if expression levels of the H_2S synthetic and catabolic enzymes were altered in response to altered H_2S breakdown in *Tst*$^{-/-}$ mice and (iv) if expression levels of the NO-synthesising enzymes are altered.

3.2 Methods

3.2.1 Mice

Male 10-12 week old C57BL/6J mice, bred in-house, were used for all characterisation experiments to identify the basal expression and localisation of the H_2S metabolising enzymes in the heart, liver and aorta. Male *Tst* knockout (*Tst*$^{-/-}$) and wild type C57BL6/N littermates aged 10-12 weeks were used for basal characterisation studies, unless otherwise stated.

Mice were culled by cervical dislocation and the heart, liver, right kidney and aorta removed and snap frozen on dry ice for either RNA or protein extraction. Alternatively, tissues were dissected and immersed into isolation buffer for mitochondrial isolation (see section 2.3.5) or immediately fixed in 10% formalin and processed for immunohistochemical and tissue morphological analysis as outlined in sections 2.4.3 and 2.4.5.

3.2.2 Real time PCR

Quantitative real time PCR was performed on heart, liver and kidney tissues of mice using Taqman probes as described in section 2.5.3. For full details of probes, please refer to Table 2-4. Equal concentrations of RNA was reverse transcribed for cDNA synthesis and used for PCR reactions when comparing gene expression between tissues or cell types. For heart versus liver, 1µg RNA was reverse transcribed to make cDNA. For CD31+ cells in aorta, intramuscular vessels of the hindlimb and liver, 50ng RNA was reverse transcribed for cDNA synthesis. Relative expression was calculated using the ΔCt method to identify gene expression in tissues of C57BL/6J mice. Fold Change was calculated using ΔΔCt method when comparing gene expression in the same tissue of different genotypes (WT vs. *Tst*$^{-/-}$). All PCR reactions were run in the same fashion. Christina Intrator conducted qRT-PCR of isolated endothelial cells. For full details, see section 2.5.3.

3.2.3 Western blotting

Western blotting was performed on heart, liver, kidney and aortic tissues of naïve mice using rabbit polyclonal antibodies as described in section 2.5.6.

3.2.4 Immunohistochemistry

Immunohistochemical staining for the localisation of the H_2S metabolising enzymes in heart, liver and aorta sections were performed using rabbit polyclonal antibodies. CD31 was used

as a positive control for vascular endothelial staining within aorta samples. For details of dilutions used and the full procedure, see section 2.4.3.

3.2.5 Immunofluorescent co-localisation staining

Immunofluorescent co-localisation staining of TST/ CSE and α-smooth muscle actin within myocardial vascular smooth muscle cells was performed on heart tissue sections from naive C57BL/6J mice as described in section 2.4.4.

3.2.6 Survival rate & Body Weight

Mice were checked regularly following birth until 20weeks of age to assess if TST loss impacted upon survival. A cohort of *Tst*$^{-/-}$ and wild type mice were weighed between 6-12weeks following birth to examine if TST loss impacted growth rates.

3.2.7 Echocardiography

Cardiac size, function and performance were evaluated by Doppler ultrasound in naïve mice at 6 and 10weeks of age as described in Section 2.2.2, performed by Adrian Thomson. Cardiac dimensional, functional and performance measurements were analysed in a single blinded fashion.

3.2.8 TST enzyme activity assay

TST enzyme activity assays were performed on liver homogenates of naïve *Tst*$^{-/-}$ and wild type mice as described in section 2.5.7. Wild type heat-treated protein (95^0C x 5minutes) was used as a negative control for all experiments.

3.2.9 Tissue H_2S breakdown assay

H_2S breakdown assays were performed on fresh heart and liver homogenates from *Tst*$^{-/-}$ and C57BL/6N wild type mice in a closed normoxic chamber using a H_2S amperometric electrode as described in section 2.5.10. All tissue homogenates were kept on ice and used within 6hours of collection.

3.2.10 H_2S and thiosulfate measurements

H_2S and thiosulfate levels were measured in the blood of *Tst*$^{-/-}$ and C57BL/6N wild type mice using the monobromobimane-HPLC method as described in section 2.5.11.

Monobromobimane assays were performed by Dr. Martin Barrios-Llerena in the Morton group.

3.2.11 Histology

Tissue morphological analysis was assessed using haematoxylin and eosin (H&E) staining performed on heart sections of adult *Tst*$^{-/-}$ and C57BL/6N wild type mice, see section 2.4.5. H&E sections were assessed by a rodent pathologist (James Baily) who was blinded to genotype to examine if any gross structural abnormalities existed.

3.2.12 Mitochondrial respiration

Mitochondria were isolated from two pooled hearts of *Tst*$^{-/-}$ or wild type mice aged 14-16 weeks as described in section 2.3.5. Mitochondria were placed into an Oroboros oxygraph in the presence of excess substrate (mM; Malate 2.5, Glutamate 5, Succinate 5, ADP 2) to stimulate state 3 respiration as detailed in section 2.3.6. Basal O_2 respiratory rate during state 3 respiration was calculated during the linear phase of O_2 consumption and corrected for protein by BSA assays as detailed in section 2.3.6 and 2.5.5.

3.2.13 Cardiomyocyte Isolation

Cardiomyocytes were isolated from whole mouse hearts of C57BL/6J mice using collagenase digestion mixture perfused through the heart using the Langendorff apparatus as detailed in section 2.3.3 and then lysed for protein analysis using Western blotting.

3.2.14 Endothelial cell Isolation

CD31+ endothelial cells were isolated from thoracic aorta and intramuscular vessels of the hindlimb of C57BL/6J mice by Lorraine Rose and Dr. Andrea Caporali. RNA was extracted from endothelial cells, and kindly donated as cDNA by Lorraine Rose and Dr. Andrea Caporali (50ng RNA was reverse transcribed to make cDNA). For full details on endothelial isolations, see section 2.3.4.

3.2.15 Statistical Analysis

All values presented are as mean ± SEM. Unless otherwise stated, comparisons are by unpaired two-tailed Student t-test. P values less than 0.05 were considered significant.

3.3 Results

3.3.1 The H_2S synthetic enzymes are expressed in the murine heart & liver

Quantitative real-time PCR confirmed the presence of the H_2S synthesising enzymes *Cbs*, *Cth* and *Mpst* in the hearts and livers of adult C57BL/6J mice. *Cth* gene expression was comparable in heart and liver tissues (Figure 3-1). *Cbs* gene expression was low in the heart in comparison to liver (Figure 3-1). *Mpst* gene expression was higher in the liver in comparison to heart (Figure 3-1).

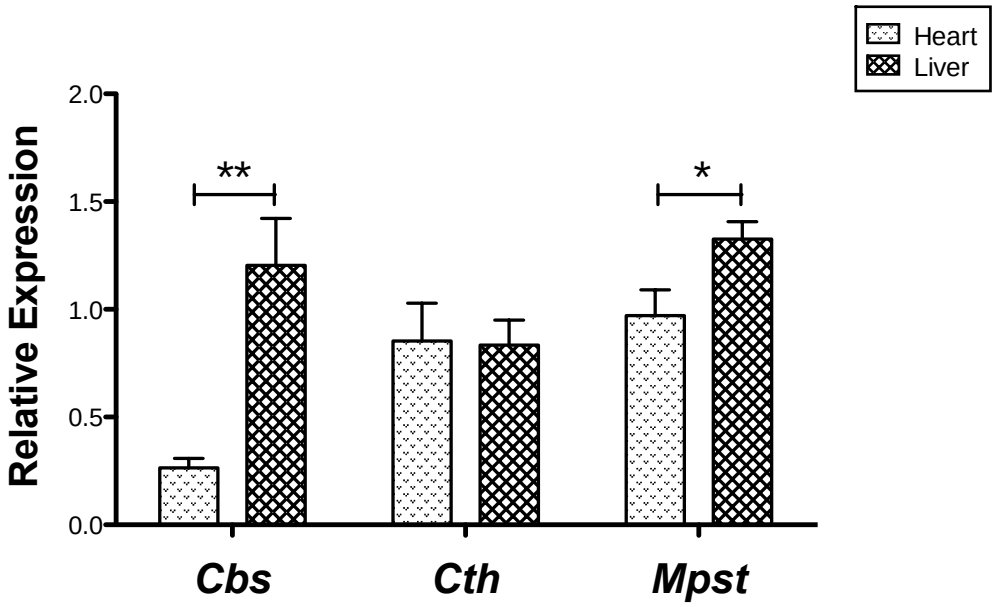

Figure 3-1 The H_2S synthetic enzymes are expressed in the murine heart and liver

Quantitative real time PCR analysis measuring mRNA levels of the H_2S synthetic enzymes *Cbs, Cth (Cse)* and *Mpst* in C57BL/6J hearts and livers. All data are normalised to the housekeeping gene β-actin (n=4/ tissue). Values are expressed as mean±SEM. *p < 0.05, **p < 0.01. *Abbreviations; Cbs; cystathionine-β-synthase, Cth; cystathionine-γ-lyase, Mpst; 3-mercaptopyruvate sulfurtransferase, A.U; arbitrary units.*

3.3.2 TST is expressed in the murine heart and vasculature

Quantitative real-time PCR and western blots confirmed the presence of *Tst* mRNA and TST protein in whole hearts and livers of C57BL/6J mice (Figure 3-2). TST protein is significantly more abundant in the liver compared to heart tissue (Figure 3-2). Western blots performed on mitochondria and cardiomyocytes isolated from whole hearts confirmed that TST is localised within the mitochondria of the heart and in isolated cardiomyocytes (Figure 3-2).

3.3.3 TST and CSE are expressed in aorta and are co-expressed in the coronary vasculature

Immunofluorescent co-localisation staining localised CSE and TST with α-SMA within vascular smooth muscle cells within the myocardium (Figure 3-3). TST and CSE protein expression was observed in whole aorta homogenates (Figure 3-3).

3.3.4 TST and H_2S synthetic enzymes are differentially expressed in the vascular endothelium and smooth muscle of the aorta

Immunohistochemical staining showed that CSE (Figure 3-4) was expressed in vascular smooth muscle of the aorta, but not in the endothelium (Figure 3-4). CBS and 3MST were both expressed in the endothelium with little staining observed within the smooth muscle (Figure 3-4). Quantitative real-time PCR confirmed the presence of *Tst* mRNA in CD31+ endothelial cells isolated from aorta and intramuscular vessels of the hindlimb of C57BL/6J mice (Figure 3-5).

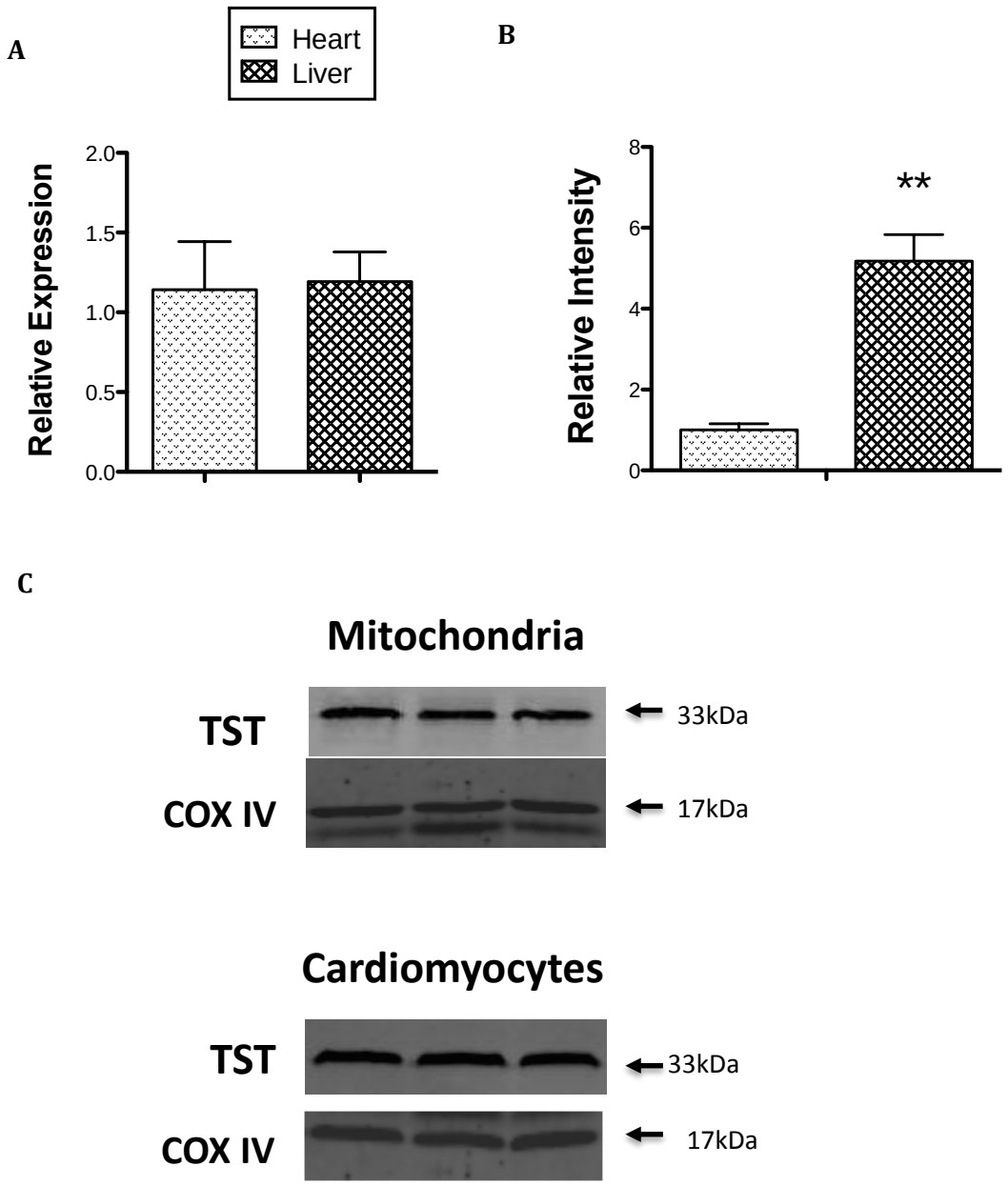

Figure 3-2 TST is expressed in mitochondrial fraction of murine heart and in cardiomyocytes but to a lesser extent than in liver

A) Quantitative real time PCR analysis measuring mRNA levels of the H_2S breakdown enzyme *Tst* in naïve C57BL/6J hearts and livers when normalised to the housekeeping gene, β-actin (n=4/ tissue). (B) Representative immunoblot and densitometric analysis of TST protein levels in C57BL/6J whole heart and liver tissue (n=4/ tissue). Data presented as relative intensity of protein expression when normalised to the mitochondrial internal control, COX IV. C) Representative immunoblot showing TST and COX IV expression in mitochondria and ventricular cardiomyocytes isolated from three whole hearts of naïve C57BL/6J mice. Values are expressed as mean±SEM. **$p < 0.01$.

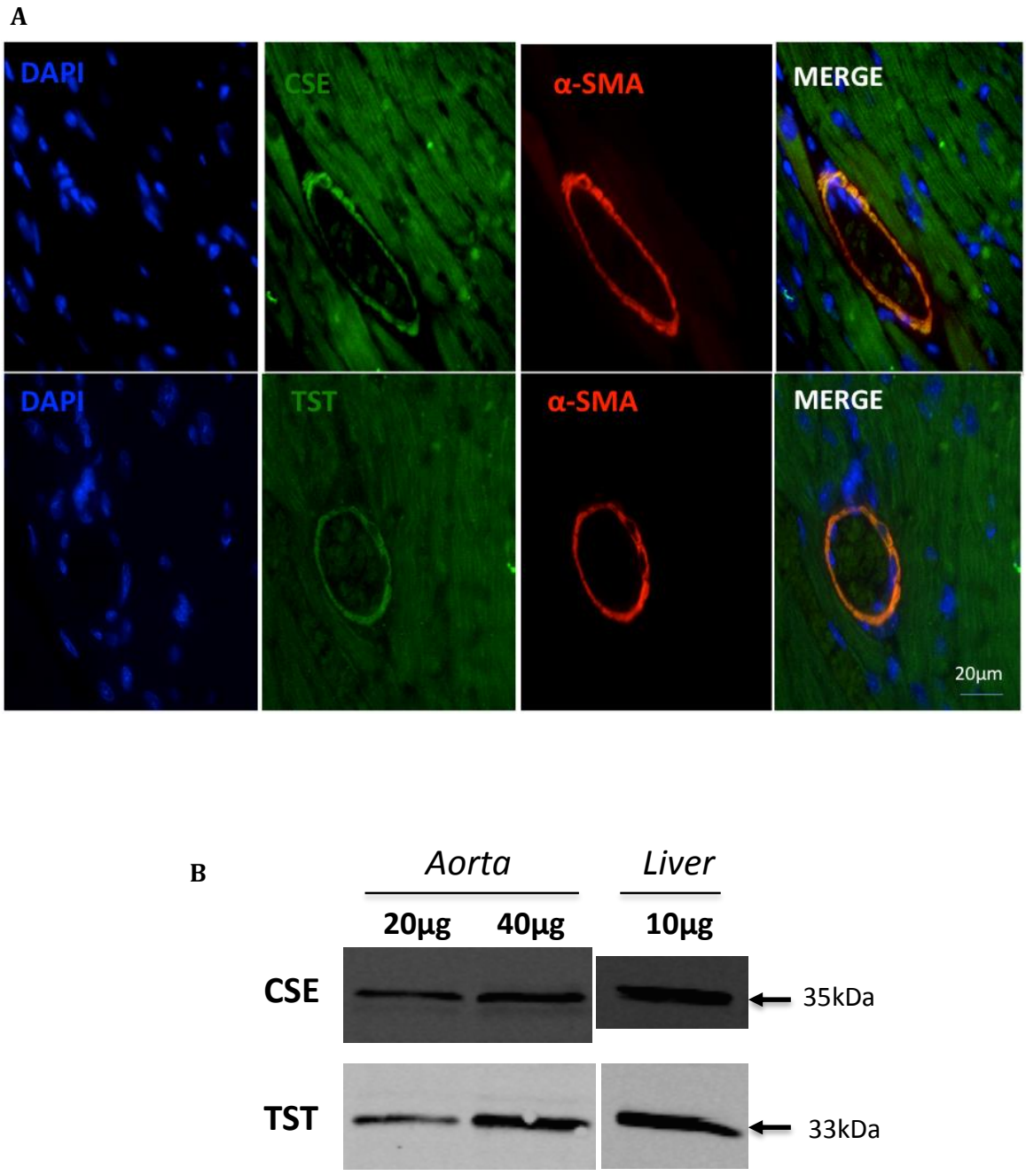

Figure 3-3 TST is localised with CSE in the coronary vasculature within smooth muscle and also in the aorta

A) Representative immunofluorescent co-localisation staining images of CSE & TST (Alexa488; green) with smooth muscle cell marker, alpha smooth muscle actin (α-SMA Cy3; red). Nuclei stained with DAPI for all sections (blue), scale bar is 20μm. B) Representative immunoblot showing increasing protein concentration (20μg, 40μg protein) signal response for CSE and TST expression in whole aorta and liver homogenates (positive control tissue) of naïve C57BL/6J mice.

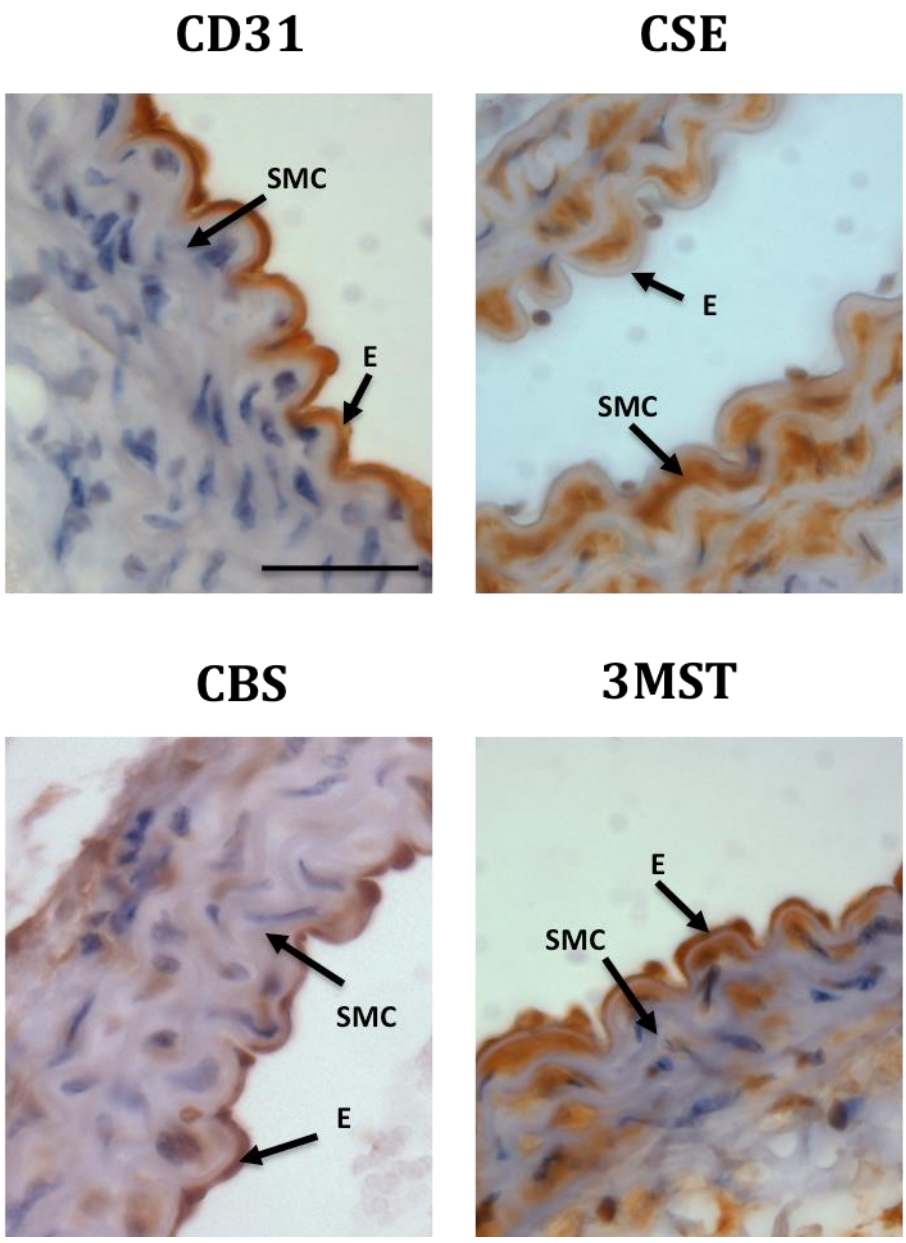

Figure 3-4 H_2S synthetic enzymes are expressed in endothelial and smooth muscle cells within the aorta

A) Immunohistochemical localisation staining of the H_2S synthetic enzymes, CSE, CBS and 3MST in the aorta of C57BL/6J mice. CD31 staining performed as positive endothelial cell control for comparative analysis. Sections photographed using an Olympus light microscope camera, 40x objective. Scale bar, 20μm. *Abbreviations; E; endothelium, SMC; smooth muscle cell.*

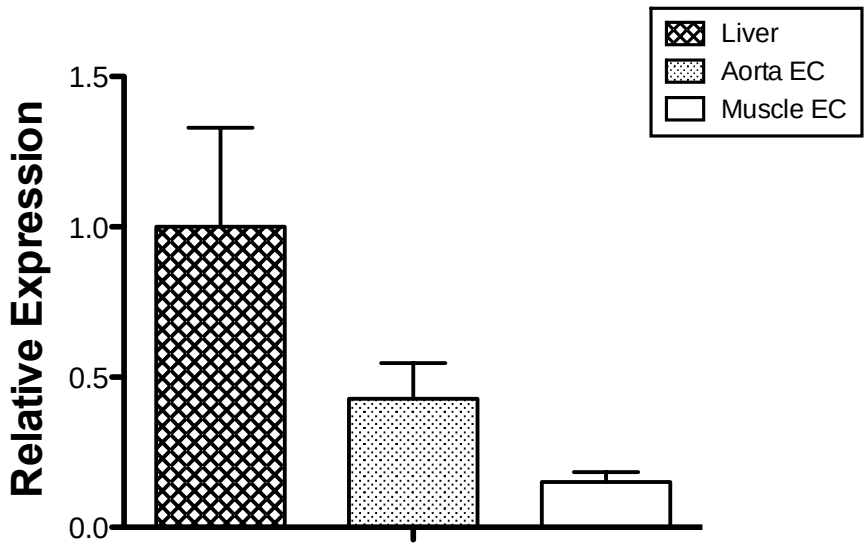

Figure 3-5 TST is expressed in the endothelium of aorta and small intramuscular vessels of mice

Quantitative real time PCR analysis measuring mRNA levels of *Tst* in isolated CD31+ endothelial cells (EC) from aorta and intramuscular vessels of the hindlimb. Liver used as positive control tissue. All data are normalised to the housekeeping gene GAPDH (n=5/ tissue). Values are expressed as mean±SEM.

3.3.5 TST deficient mice are grossly normal up to 12 weeks

3.3.5.1 TST is ablated in *Tst*$^{-/-}$ mice

Quantitative real-time PCR and western blotting confirm the loss of *Tst* mRNA and protein in heart, liver and kidney tissues of *Tst*$^{-/-}$ mice (Figure 3-6). TST enzyme activity assays confirm that TST enzymatic activity is lost in *Tst*$^{-/-}$ livers (Figure 3-6).

3.3.5.2 *Tst*$^{-/-}$ mice are grossly normal

Tst$^{-/-}$ mice survive to adulthood with no observed differences in body weight up to 12weeks of age (Figure 3-7). Kidney and liver organ weights in adult mice are comparable between groups when normalised to body weight (Figure 3-7).

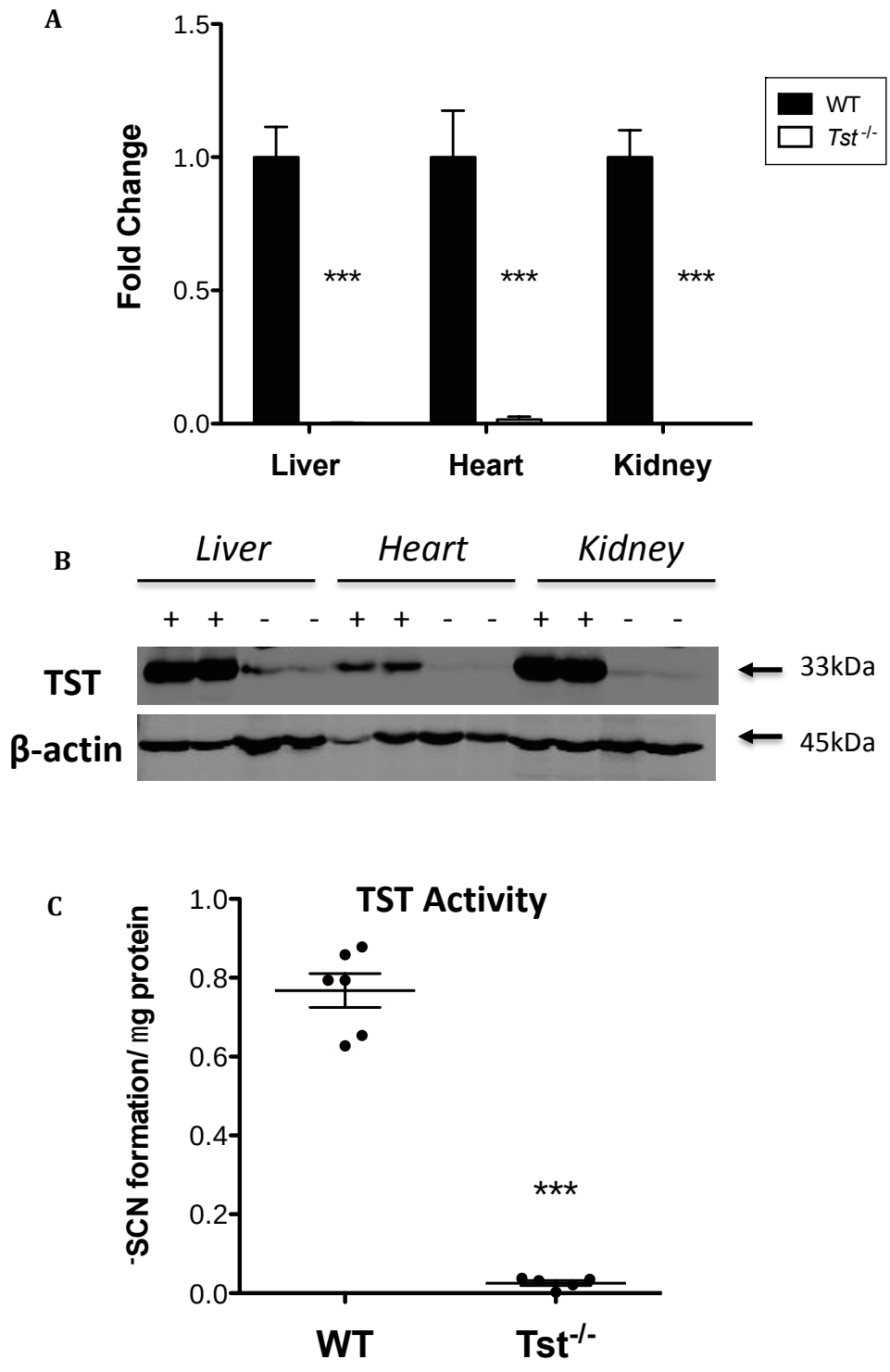

Figure 3-6 Confirmation of TST loss in *Tst*$^{-/-}$ mice

A) Quantitative real time PCR analysis measuring *Tst* mRNA levels in liver, heart and kidney tissues in *Tst*$^{-/-}$ and C57BL/6N wild type mice (n=4-5/ tissue/ group). Data normalised to the housekeeping gene *Cox4i1* and then normalised to level of wild type controls.
B) Representative western blot of TST protein expression in liver, heart and kidney tissues (10µg protein) in C57BL/6N wild type (+) and *Tst*$^{-/-}$ (-) mice. C) TST enzyme activity in fresh liver homogenates of *Tst*$^{-/-}$ and C57BL/6N control mice (WT; n=6, *Tst*$^{-/-}$; n=5). Values are expressed as mean±SEM. ***p < 0.001

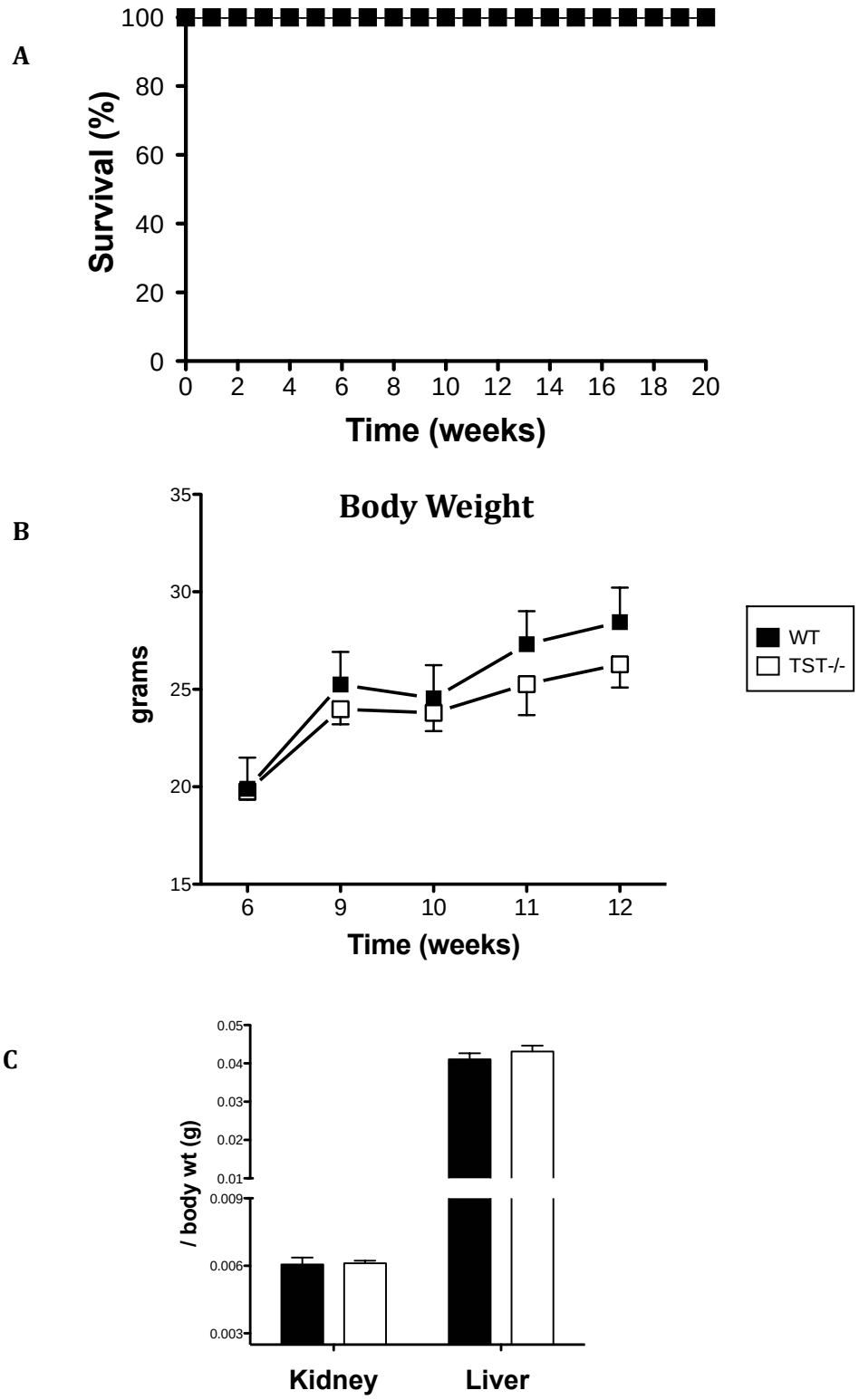

Figure 3-7 *Tst*$^{-/-}$ mice survive to adulthood and grow normally

A) Survival rates of *Tst*$^{-/-}$ mice. B) Body weight measurements in *Tst*$^{-/-}$ and wild type control mice at 6, 9, 10, 11 and 12weeks of age (n=6/ genotype). C) Organ weights of kidney and liver tissues normalised to body weight measured in 12week old *Tst*$^{-/-}$ and C57BL/6N wild type mice (WT; n=10, *Tst*$^{-/-}$; n=9). Values are expressed as mean±SEM.

3.3.6 H_2S balance is compromised in *Tst*$^{-/-}$ mice

3.3.6.1 Expression of mitochondrial H_2S breakdown enzymes are not altered in *Tst*$^{-/-}$ mice

In the heart and liver, quantitative real-time PCR showed that loss of *Tst* had no impact on the mRNA levels of the mitochondrial H_2S breakdown enzymes, *Sqrdl*, *Ethe1* or *Suox*. In the kidneys, PCR revealed a trend for reduced *Sqrdl*, *Ethe1* and *Suox* mRNA levels mice (Figure 3-8, *Sqrdl* P=0.13, *Ethe1* P=0.1, *Suox* P=0.09).

3.3.6.2 The rate of H_2S breakdown is reduced in the heart and liver of *Tst*$^{-/-}$ mice

Polarographic H_2S electrode experiments revealed that the rate of H_2S breakdown was significantly decreased in heart and liver homogenates from *Tst*$^{-/-}$ mice (Figure 3-9). In the heart and liver homogenates of *Tst*$^{-/-}$ mice, H_2S breakdown was reduced by 20% and 50% respectively when compared to controls.

3.3.6.3 *Tst*$^{-/-}$ mice have higher circulating H_2S and thiosulfate levels and increased urinary concentration of thiosulfate

Monobromobimane assays revealed that H_2S levels were approximately 7-fold higher in the blood of *Tst*$^{-/-}$ mice compared to controls (μM; WT; 30.3 ± 1.3, *Tst*$^{-/-}$; 227.1 ± 9.2) (Figure 3-10). Thiosulfate levels were approximately 30-fold higher in the blood of *Tst*$^{-/-}$ mice compared to controls (μM; WT; 2.15 ± 0.2, *Tst*$^{-/-}$; 66.3 ± 10.3) (Figure 3-10). Urinary thiosulfate levels are approximately 500-fold higher in the urine of *Tst*$^{-/-}$ mice compared to wild type controls (μM; WT; 4.99 ± 2.63, *Tst*$^{-/-}$; 2374.49 ± 318.94) (Figure 3-10).

3.3.6.2 H_2S-sensitive Nrf2 downstream targets TRX1 and HO-1 are not altered in *Tst*$^{-/-}$ hearts

Despite increased circulating levels of H_2S, expression of the H_2S-sensitive Nrf2 downstream target proteins TRX1 and HO-1 are comparable in heart tissue from of *Tst*$^{-/-}$ and C57BL/6N wild type littermates (Figure 3-11).

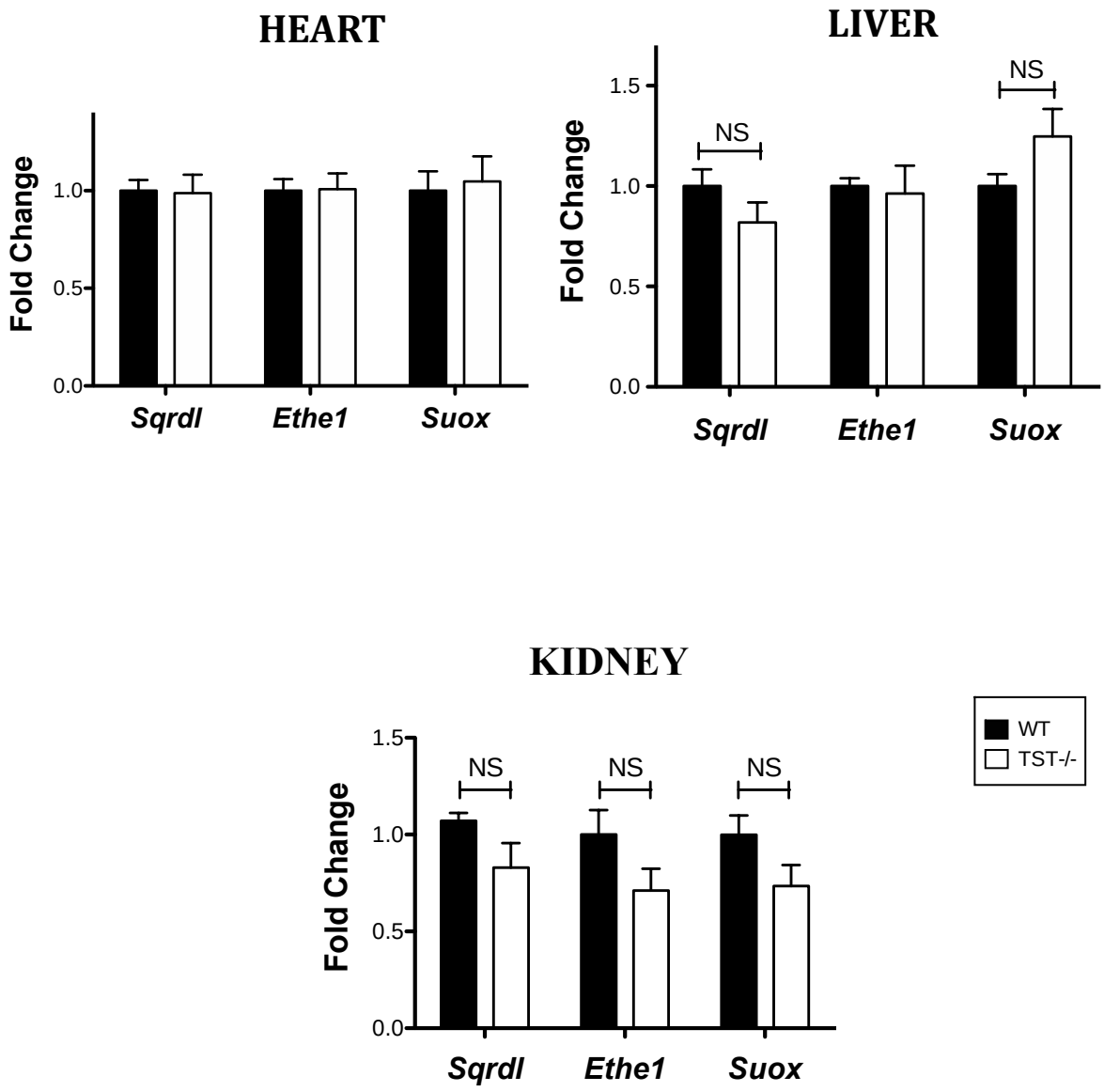

Figure 3-8 Expression of the mitochondrial H_2S breakdown enzymes is not modified in *Tst*$^{-/-}$ mice

Quantitative real time PCR analysis measuring mRNA levels of the mitochondrial H_2S breakdown enzymes, *Sqrdl, Ethe1* and *Suox* in heart (n=5/ genotype), liver (n=5/ genotype) and kidney (WT; n=7, *Tst*$^{-/-}$; n=8) tissues from *Tst*$^{-/-}$ and C57BL/6N wild type mice. Data normalised to the housekeeping gene *Cox4i1* and then normalised to level of wild type controls. Values are expressed as mean±SEM. *Abbreviations; Sqrdl; sulfide quinone oxidoreductase, Ethe1; sulfur dioxygenase, Suox; sulfide oxidase*

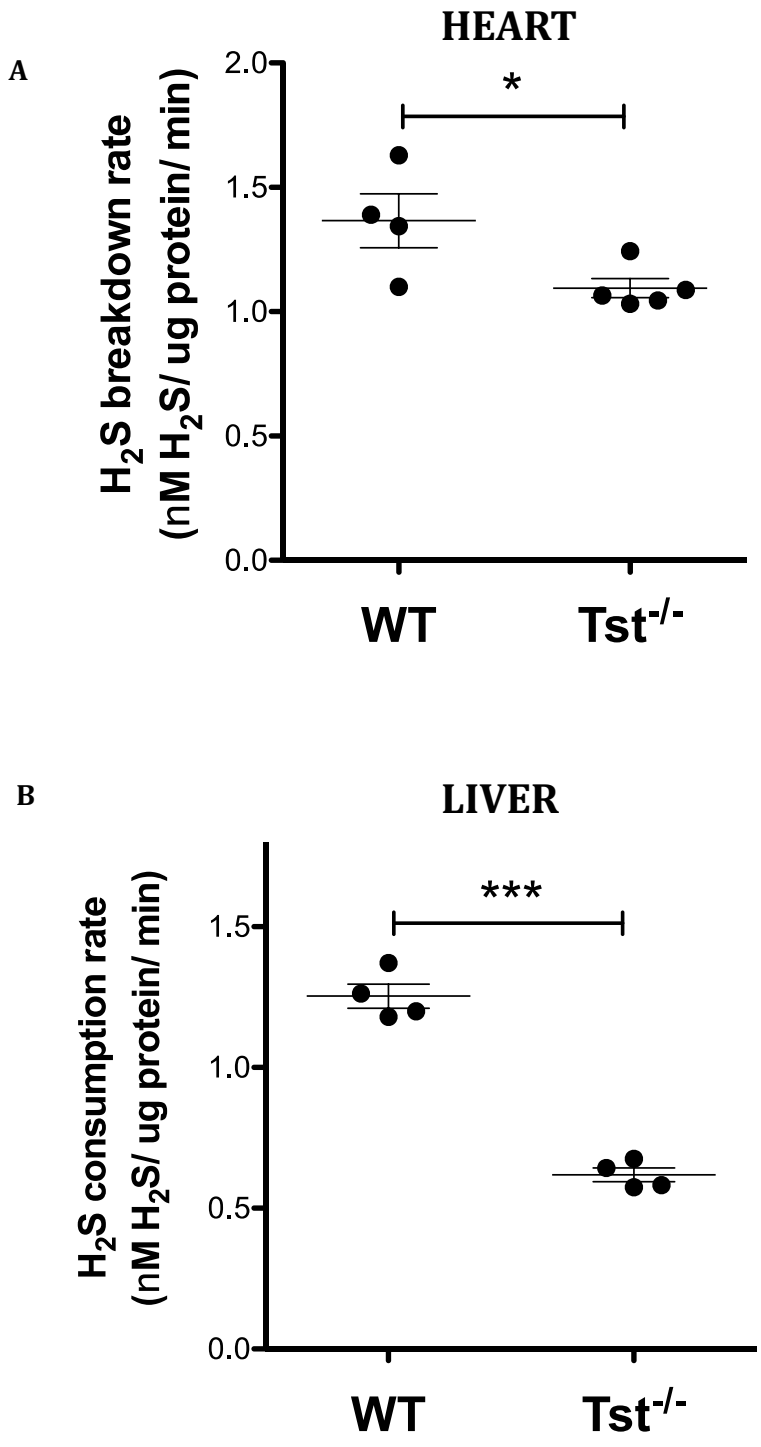

Figure 3-9 Rate of H_2S breakdown is reduced in heart and liver tissue of naïve *Tst*$^{-/-}$ mice

Rate of H_2S breakdown in normoxic fresh heart (A) and liver (B) homogenates of *Tst*$^{-/-}$ and C57BL/6N wild type mice. H_2S signal was continuously measured following administration of 20µM Na_2S in a closed chamber (WT; n=4, *Tst*$^{-/-}$; n=4-5) and corrected for protein. Values are expressed as mean±SEM. *$p < 0.05$, ***$p < 0.001$.

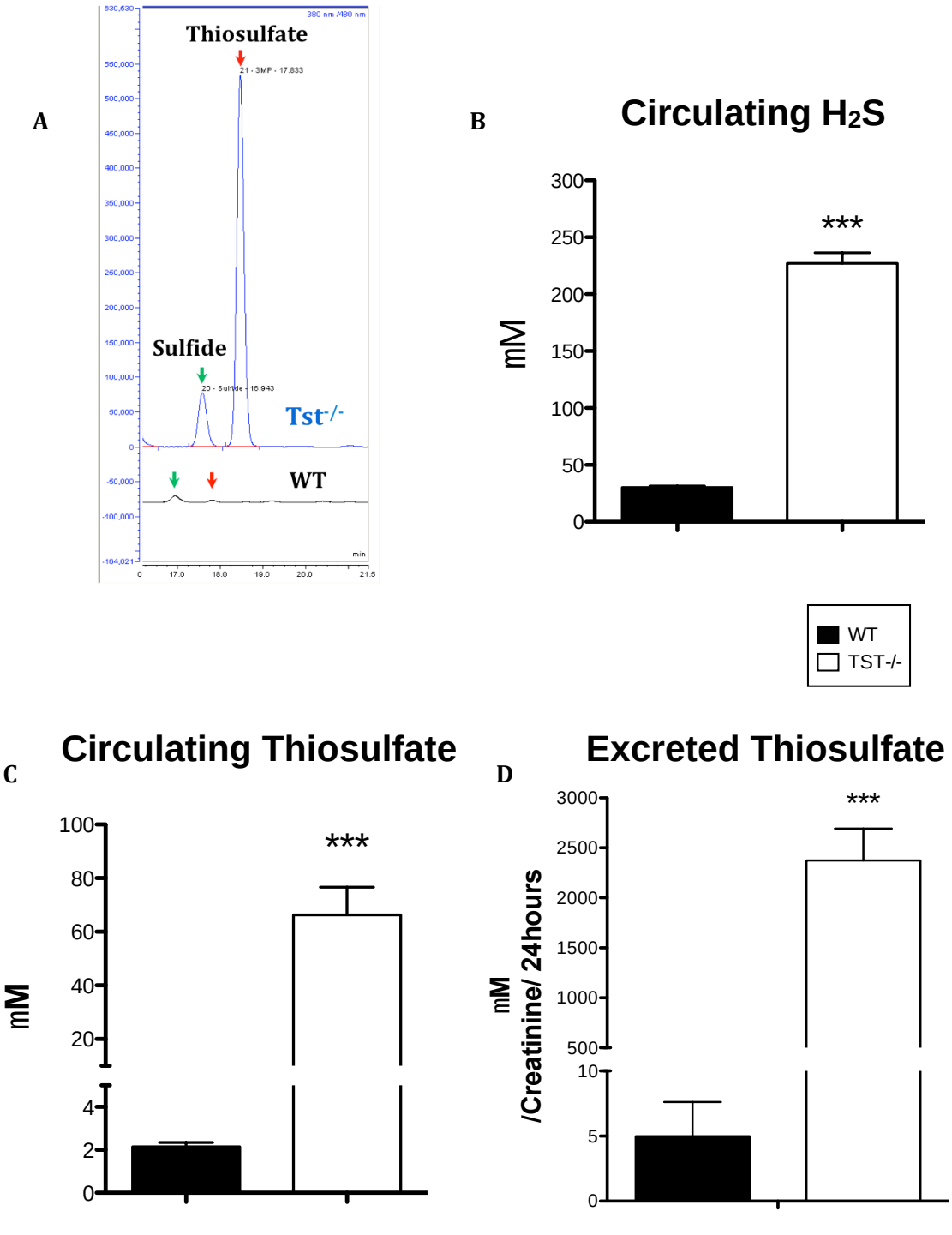

Figure 3-10 Circulating H_2S and thiosulfate levels are markedly higher in whole blood from *Tst*$^{-/-}$mice

A) Representative monobromobimane peak for H_2S and thiosulfate, measured by HPLC. B) H_2S (n=4/ group) and (C) thiosulfate levels in blood (n=4/ group) of *Tst*$^{-/-}$ and C57BL/6N wild type mice. D) 24hour excreted urinary thiosulfate levels normalised to creatinine in *Tst*$^{-/-}$ and C57BL/6N wild type mice (WT; n=4, *Tst*$^{-/-}$; n=5). Samples obtained from mice 4days following acclimatisation to metabolic cages. Values are expressed as mean±SEM. ***p < 0.001

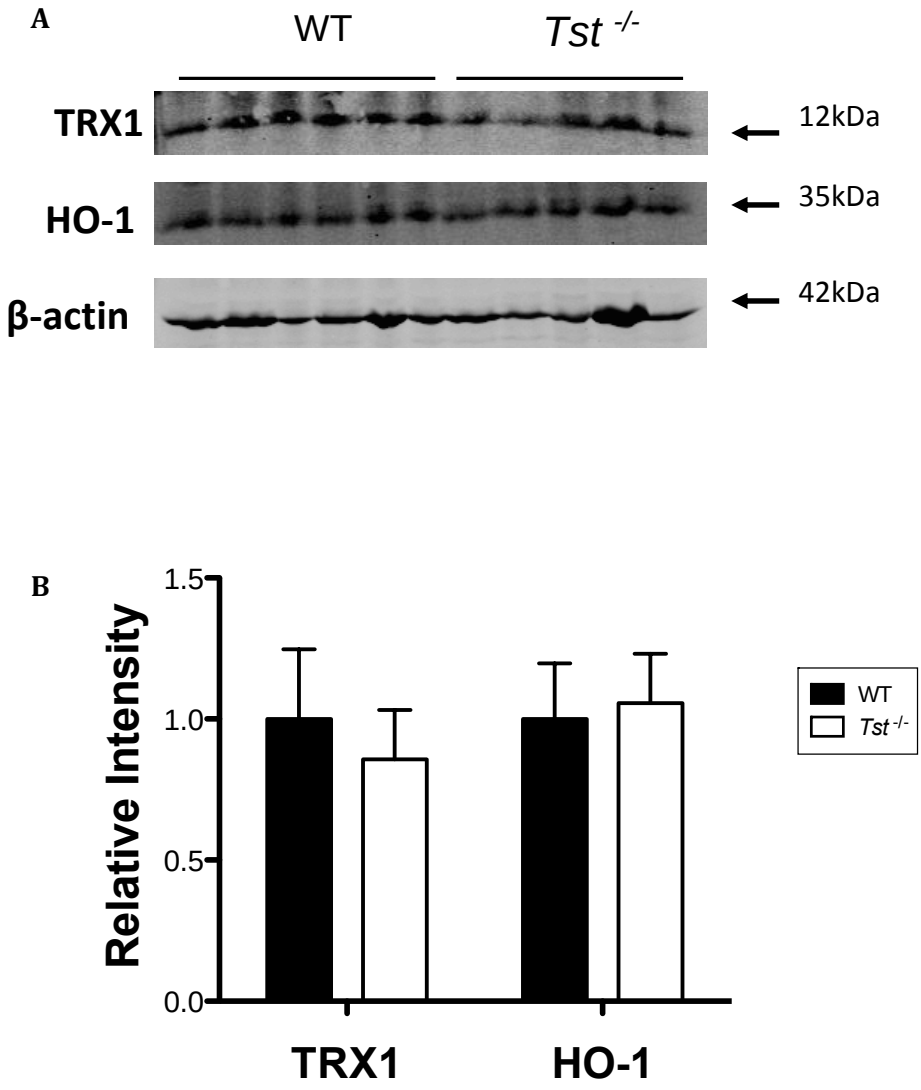

Figure 3-11 The H_2S-sensitive Nrf2 downstream target proteins are not altered in *Tst*$^{-/-}$ hearts under basal conditions

(A) Representative immunoblot and (B) densitometric analysis of TRX1 and HO-1 protein expression in hearts of naïve *Tst*$^{-/-}$ and C57BL/6N wild type mice. Data presented as relative intensity of protein expression when normalised to the internal control, β-actin and then normalised to level of C57BL/6N wild type controls (WT; n=4, *Tst*$^{-/-}$; n=5). Values are expressed as mean±SEM. *Abbreviations; TRX1; thioredoxin, HO-1; hemeoxygenase 1.*

3.3.7 H_2S synthetic enzyme expression is reduced in the hearts of *Tst*$^{-/-}$ mice

Tst$^{-/-}$ mice have significantly lower mRNA (Figure 3-12) and protein (Figure 3-12, P=0.011) levels of the H_2S synthetic enzyme CSE in their hearts. However, while *Mpst* (Figure 3-12) mRNA levels are lower in hearts from *Tst*$^{-/-}$ mice, western blots reveal that 3MST protein levels are comparable between groups (Figure 3-12, P=0.2). Cardiac CBS expression was unaffected by loss of *Tst* (Figure 3-12).

3.3.8 3MST is up-regulated in the liver mitochondria of *Tst*$^{-/-}$ mice

Quantitative real-time PCR revealed that hepatic mRNA levels of the H_2S synthetic enzymes *Cse* and *Cbs* were comparable to controls (Figure 3-13). Hepatic *Mpst* mRNA levels were significantly reduced in *Tst*$^{-/-}$ mice but western blotting revealed 3MST protein to be higher in mitochondria isolated from liver tissue (Figure 3-13).

3.3.9 CSE is upregulated in the kidneys of *Tst*$^{-/-}$ mice

Cbs mRNA levels tended to be lower in kidney tissue of *Tst*$^{-/-}$ mice (Figure 3-14, P=0.069) but western blots revealed that CBS protein tended to be higher in kidneys of *Tst*$^{-/-}$ mice compared to controls (Figure 3-14, P=0.09). Renal *Cse* mRNA levels were comparable between groups but CSE protein levels were higher in the kidneys of *Tst*$^{-/-}$ mice (Figure 3-14). *Mpst* mRNA (Figure 3-14) was reduced in *Tst*$^{-/-}$ kidneys but protein levels were comparable between groups (Figure 3-14).

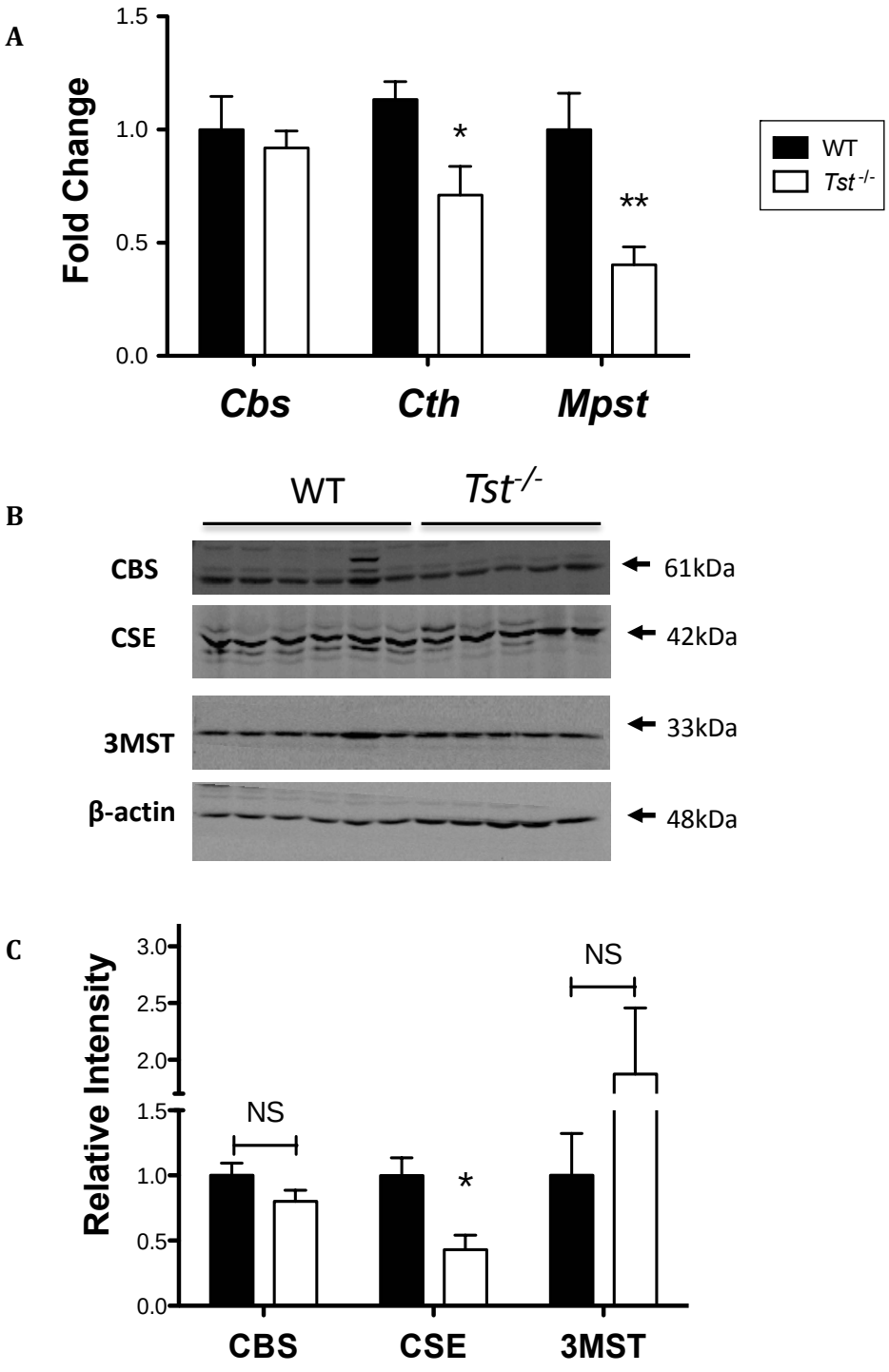

Figure 3-12 *Cth*/ CSE expression is reduced in the hearts of *Tst*$^{-/-}$ mice

A) Quantitative real time PCR analysis measuring mRNA levels of the H_2S synthetic enzymes *Cbs, Cth* and *Mpst* in heart tissue of *Tst*$^{-/-}$ and C57BL/6N wild type mice (WT; n=6, *Tst*$^{-/-}$; n=8/ gene/ group). Data normalised to the housekeeping gene *Tbp* and then normalised to level of wild type controls. Representative immunoblots (B) and densitometric analysis (C) of H_2S synthetic enzyme protein levels in heart tissue of *Tst*$^{-/-}$ and C57BL/6N wild type mice (WT; n=6, *Tst*$^{-/-}$; n=5). Data presented as relative intensity of protein expression when normalised to the internal control, β-actin and then normalised to level of C57BL/6N wild type controls. Values are expressed as mean±SEM. *$p < 0.05$, **$p < 0.01$.

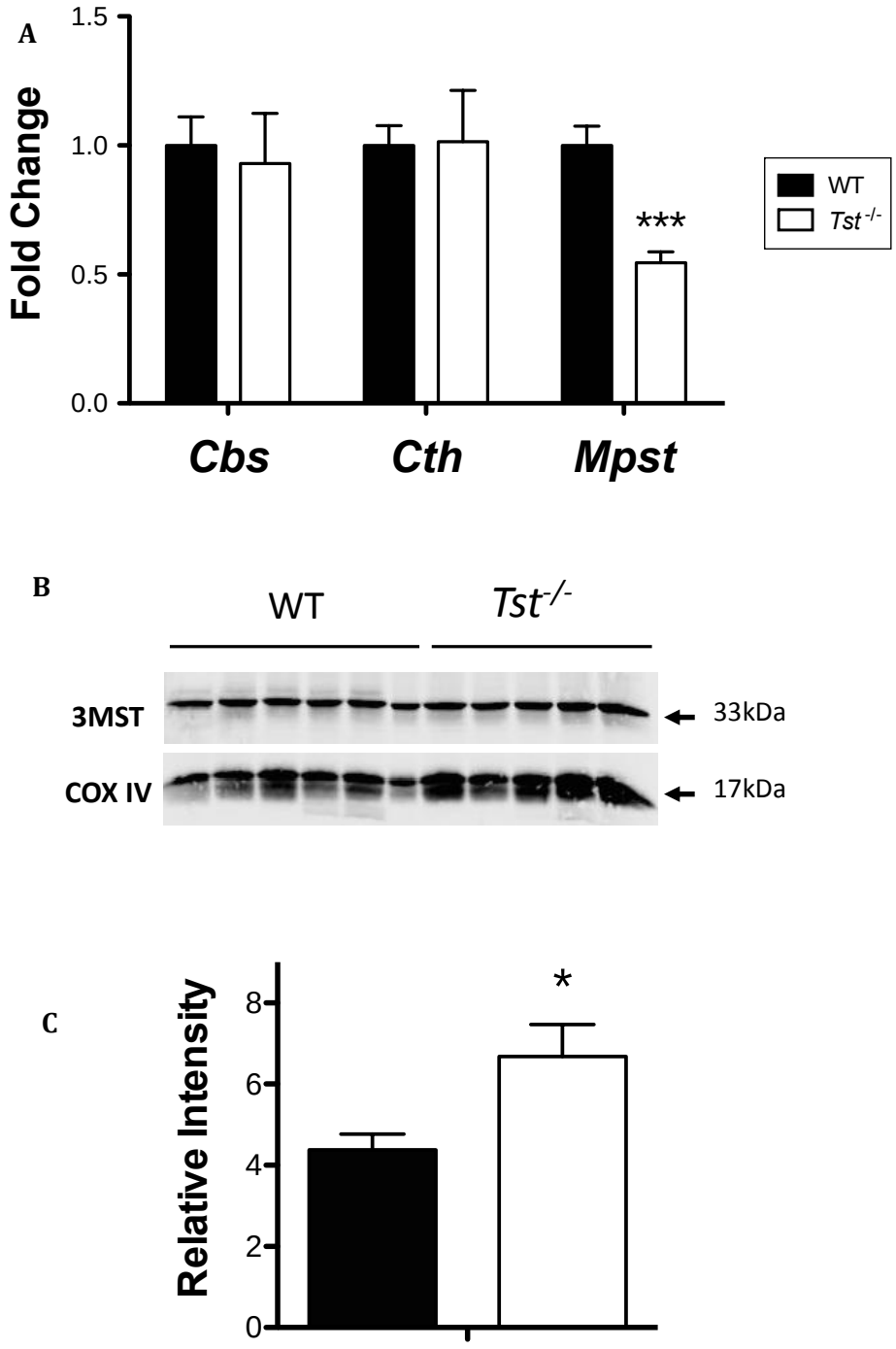

Figure 3-13 3MST protein expression is upregulated in hepatic mitochondria of *Tst*$^{-/-}$ mice

A) Quantitative real time PCR analysis measuring mRNA levels of the H_2S synthetic enzymes *Cbs, Cth* and *Mpst* in liver tissue of *Tst*$^{-/-}$ and C57BL/6N wild type mice (n=6-8/ gene/ group). Data normalised to the housekeeping gene *Tbp* and then normalised to level of wild type controls. Representative immunoblot (B) and densitometric analysis (C) of 3MST protein levels in isolated liver mitochondria of *Tst*$^{-/-}$ and C57BL/6N wild type mice (WT; n=6, *Tst*$^{-/-}$; n=5). Data presented as relative intensity of protein expression when normalised to the mitochondrial internal control, COX IV and then normalised to level of C57BL/6N wild type controls. Values are expressed as mean±SEM. *$p < 0.05$, ***$p < 0.001$

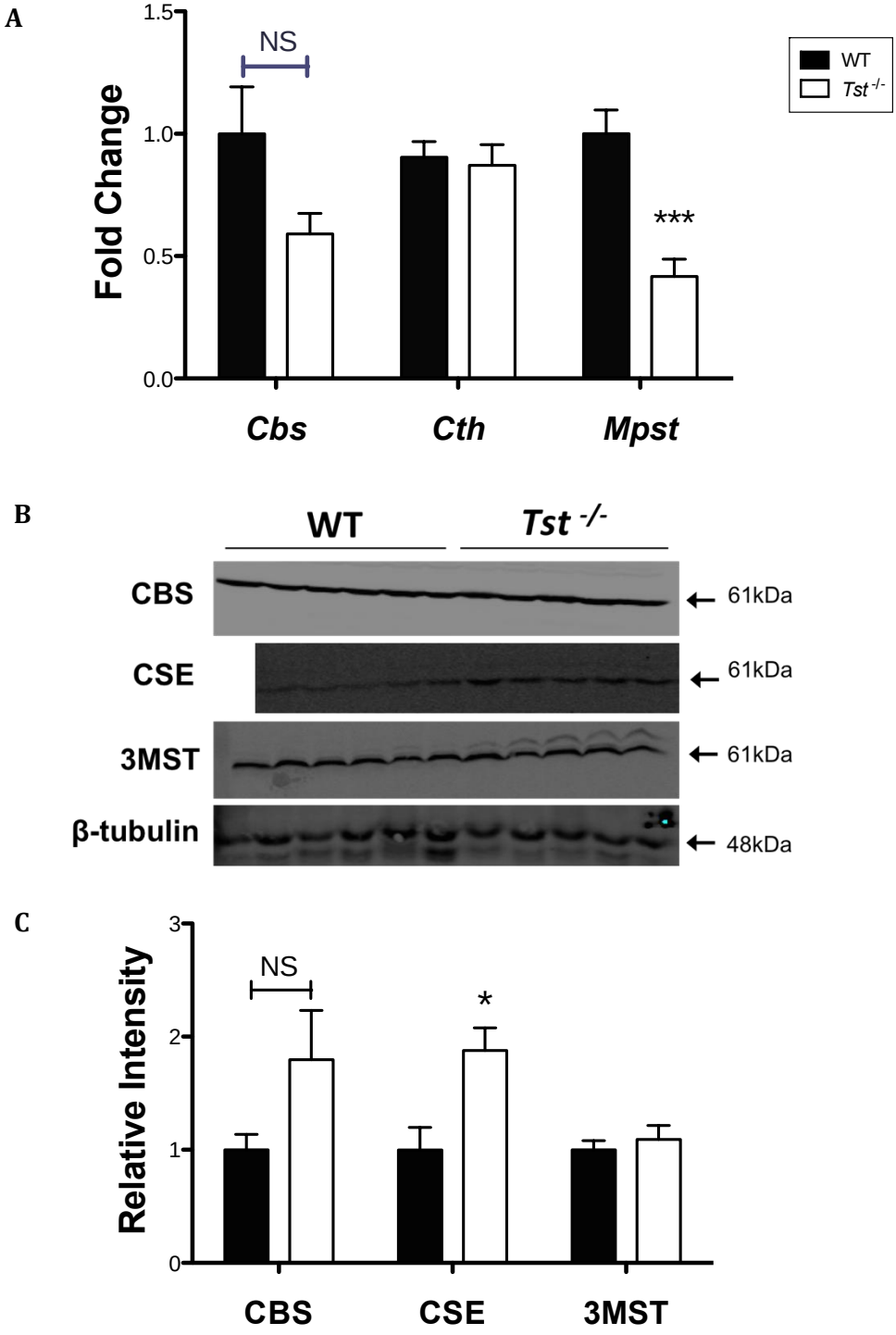

Figure 3-14 CSE expression is increased in *Tst*$^{-/-}$ kidneys

A) Quantitative real time PCR analysis measuring mRNA levels of the H_2S synthetic enzymes *Cbs, Cth* and *Mpst* in kidney tissue of *Tst*$^{-/-}$ and C57BL/6N wild type mice (n=8/ gene/ group). Data normalised to the housekeeping gene *Tbp* and then normalised to level of wild type controls. Representative immunoblots (B) and densitometric analysis (C) of H_2S synthetic enzyme CBS, CSE and 3MST protein levels in kidney tissue of *Tst*$^{-/-}$ and C57BL/6N wild type mice (CBS/ 3MST; WT; n=6, *Tst*$^{-/-}$; n=5, CSE; n=5/ group) when normalised to β-actin and then normalised to level of C57BL/6N wild type controls. Values are expressed as mean±SEM. *$p < 0.05$, ***$p < 0.001$

3.3.10 *Tst*$^{-/-}$ mice have altered eNOS expression in the heart

Quantitative real-time PCR revealed that mRNA levels for *Nos1*, *Nos2* and *Nos3* were comparable in the hearts of *Tst*$^{-/-}$mice and wild type littermates (Figure 3-17). Western blots performed on naïve hearts revealed that phosphorylation of the eNOS activation site, P-eNOS^{Ser1177} was comparable between groups but total eNOS was lower in *Tst*$^{-/-}$ hearts (Figure 3-16). A trend for reduced P-Vasp^{239} protein was present in *Tst*$^{-/-}$ hearts but failed to reach statistical significance (Figure 3-16, P=0.12).

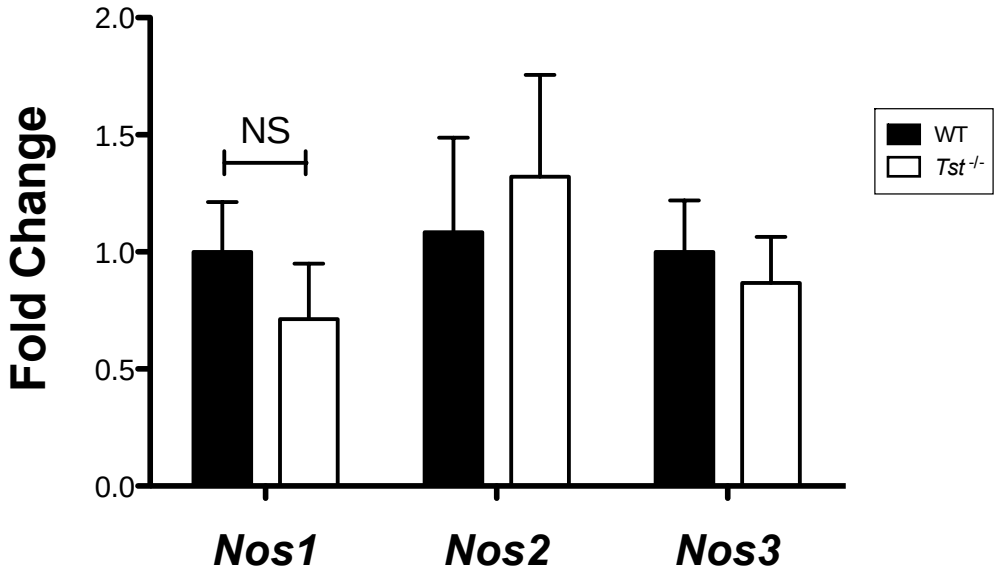

Figure 3-15 mRNA levels of NOS isoforms are not altered in *Tst*$^{-/-}$ hearts

Quantitative real time PCR analysis measuring mRNA levels of the nitric oxide isoforms, *Nos1/ nNOS* (WT; n=4, *Tst*$^{-/-}$; n=6), *Nos2/ iNOS* (n=5/ group) and *Nos3/ eNOS* (WT; n=7, *Tst*$^{-/-}$; n=8) in the heart of *Tst*$^{-/-}$ and C57BL/6N wild type mice. Data normalised to the housekeeping gene *Tbp* and then normalised to level of wild type controls. Values are expressed as mean±SEM.

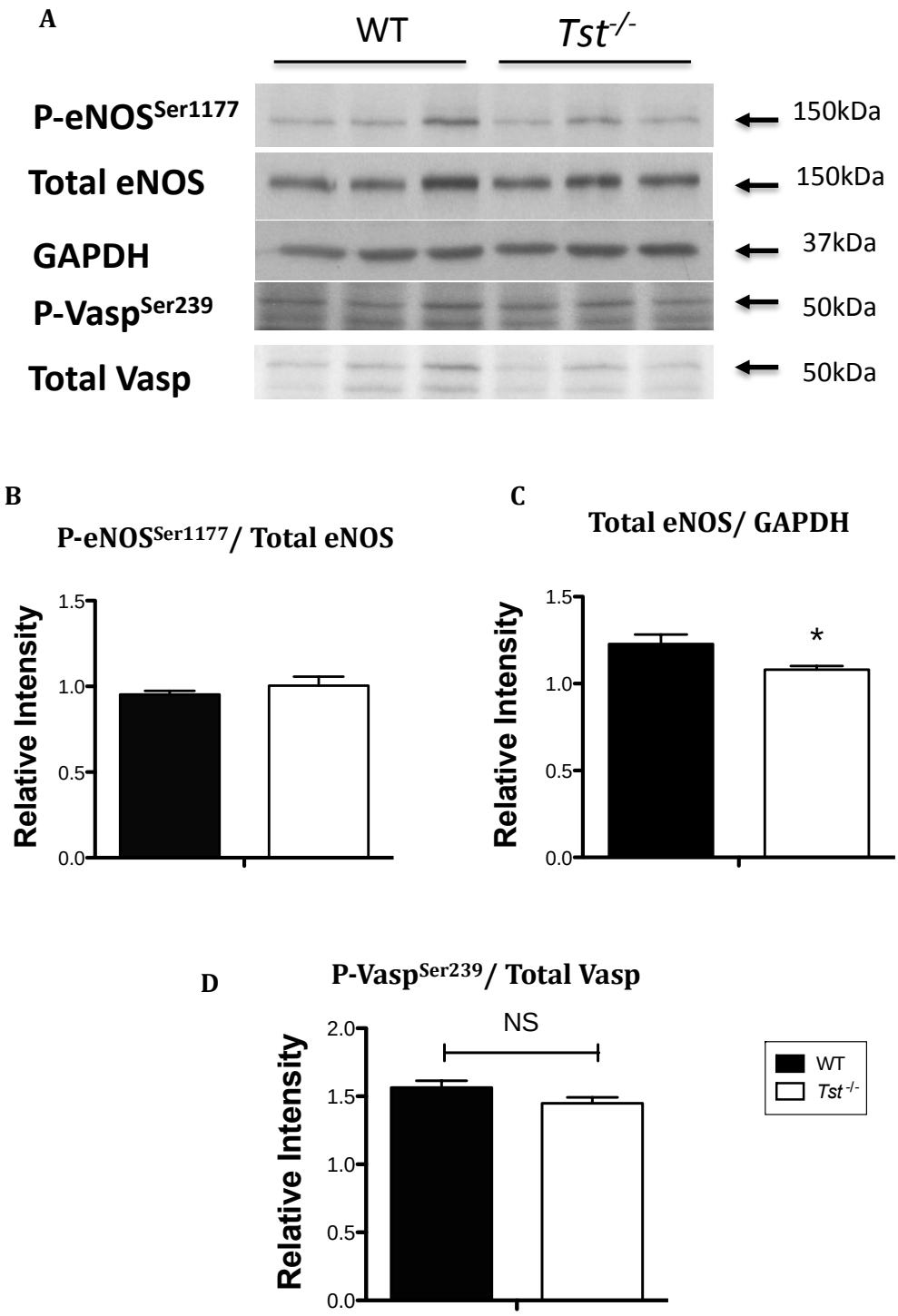

Figure 3-16 Cardiac eNOS protein levels are lower in *Tst*$^{-/-}$ mice

Representative immunoblot and densitometric analysis showing (A) phosphorylation of eNOS at the Serine1177 residue (P-eNOS^{Ser1177}), (B) total eNOS and (C) phosphorylation of Vasp at Serine239 residue (P-Vasp^{Ser239}) in heart tissue of *Tst*$^{-/-}$ and C57BL/6N wild type mice (WT; n=5, *Tst*$^{-/-}$; n=6). Data presented as relative intensity of protein expression when normalised to total eNOS (A), GAPDH (B) and total Vasp (C) and then normalised to level of C57BL/6N wild type controls. Values are expressed as mean±SEM. *p < 0.05

	Heart		***Liver***		***Kidney***	
Gene/ Protein	***mRNA***	***Protein***	***mRNA***	***Protein***	***mRNA***	***Protein***
Cbs/ CBS	N.D	N.D	N.D	-	N.D	N.D
Cth/ CSE	Reduced	Reduced	N.D	-	N.D	Increased
Mpst/ 3MST	Reduced	N.D	Reduced	Increased	Reduced	N.D
Nos1	N.D	-	-	-	-	-
Nos2	N.D	-	-	-	-	-
Nos3/ eNOS	N.D	Reduced	-	-	-	-
P-eNOS^{Ser1177}	-	N.D	-	-	-	-
P-Vasp^{239}	-	Reduced	-	-	-	-
TRX1	-	N.D	-	-	-	-
HO-1	-	N.D	-	-	-	-
Sqrdl	N.D	-	N.D	-	N.D	-
Ethe1	N.D	-	N.D	-	N.D	-
Suox	N.D	-	N.D	-	N.D	-

Table 3-1 Summary table of changes to mRNA and protein in heart, liver and kidney tissues in *Tst*$^{-/-}$ mice compared to wild type mice.

Summary data detailing changes in mRNA and protein expression in naïve *Tst*$^{-/-}$ tissues compared to wild type controls. Changes labelled as 'reduced' or 'Increased' are significantly different to controls as shown in Figures 3-8 to Figures 3-16. *Abbreviations; N.D; not different compared to wild type controls.*

3.3.11 *Tst*$^{-/-}$ mice have normal cardiac structure, function and mitochondrial respiration rates

Haematoxylin & Eosin stained heart sections revealed no gross morphological alterations in the hearts of *Tst*$^{-/-}$ mice (Figure 3-17). Heart weight to body weight ratios are comparable between C57BL/6N and in *Tst*$^{-/-}$ mice (Figure 3-17).

Ultrasound scanning showed that left ventricular size at end-systole and end-diastole were comparable between groups to controls at 6 and 10weeks of age (Table 3-2). Cardiac function, evaluated by ejection fraction and endocardial area change, was normal at 6 and 10weeks of age (Table 3-2). Fractional shortening was reduced in *Tst*$^{-/-}$ hearts at 6weeks of age but was comparable to controls at 10weeks of age (Table 3-2). Doppler scanning revealed that isovolumetric contraction, relaxation and ejection times were comparable between groups at both timepoints (Table 3-3). The load-independent measure of cardiac function, myocardial performance index, was similar in *Tst*$^{-/-}$ and WT mice at 6 and 10weeks of age (Table 3-3).

Basal mitochondrial respiration studies revealed that the O_2 consumption rate during state-3 respiration (Malate, succinate and ADP administration) was comparable in the mitochondria isolated from whole hearts of *Tst*$^{-/-}$ and control mice (Figure 3-18).

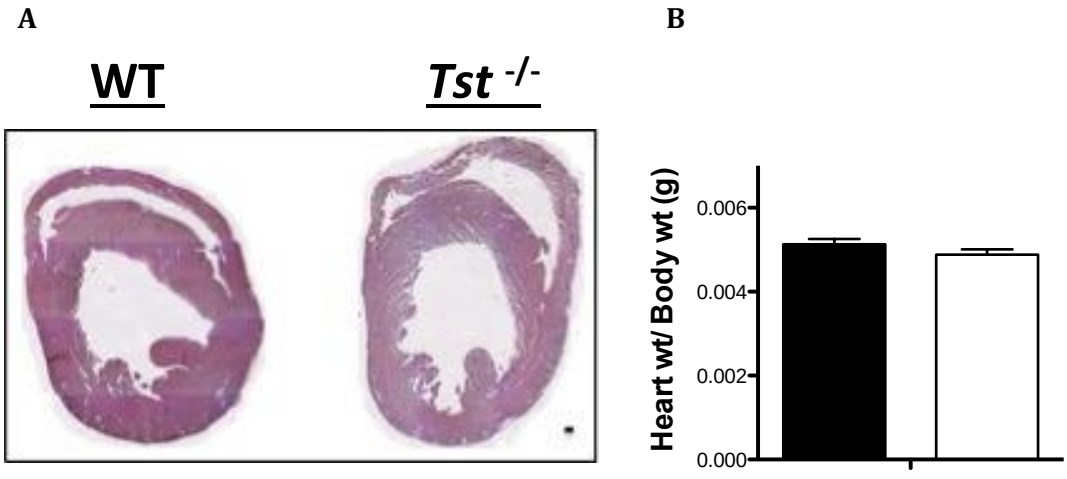

Figure 3-17 *Tst*$^{-/-}$ mice have normal heart morphology and heart weight

(A) Representative haematoxylin and eosin stained heart sections of *Tst*$^{-/-}$ and C57BL/6N wild type mice (WT; n=4, *Tst*$^{-/-}$; n =5). Scale bar is 20μm. B) Heart weight normalised to body weight measured in 12week old *Tst*$^{-/-}$ and C57BL/6N littermates (WT; n=10, *Tst*$^{-/-}$; n=9). Values are expressed as mean±SEM.

Group	Age (weeks)	LVESA (mm^2)	LVEDA (mm^2)	EF (%)	FS (%)	EAC (mm^2)
WT	6	12.3 ± 0.6	20.7 ± 0.9	58.5 ± 2.2	43.1 ± 2.4	8.6 ± 0.3
Tst $^{-/-}$	6	11.6 ± 0.5	20.2 ± 0.7	62.3 ± 1	34.5 ± 1.6*	8.8 ± 0.4
WT	10	13.9 ± 0.9	23 ± 0.3	58.9 ± 3.3	32.6 ± 1.5	9.3 ± 0.6
Tst $^{-/-}$	10	13.4 ± 0.7	23.1 ± 0.6	64.2 ± 2.1	35.4 ± 0.9	9.4 ± 0.3

Table 3-2 *Tst*$^{-/-}$ mice have normal heart size and function at 6 & 10weeks of age

2-dimensional long axis B-mode and short axis M-mode ultrasound scanning performed on anaesthetised naïve 6week and 10week old *Tst*$^{-/-}$ and C57BL/6N wild type mice (n=6/ group/ timepoint). Values are mean±SEM, analysed by 2-way ANOVA with Bonferroni post-hoc test, *p<0.05 WT vs. *Tst*$^{-/-}$ mice at 6weeks of age. *Abbreviations; LVESD (mm^2); left ventricular end systolic area, LVEDA (mm^2); left ventricular end diastolic area, EF (%); ejection fraction, FS (%); fractional shortening, EAC (mm^2); endocardial area change.*

Group	Age (weeks)	IVCT (ms)	IVRT (ms)	ET (ms)	MPI
WT	6	11.5 ± 0.8	13.5 ± 0.9	39.5 ± 1.5	0.63 ± 0.03
Tst $^{-/-}$	6	13.4 ± 1.3	13.7 ± 0.4	41.3 ± 0.9	0.66 ± 0.03
WT	10	10.7 ± 0.7	13.8 ± 0.8	38.5 ± 0.9	0.64 + 0.04
Tst $^{-/-}$	10	12.5 ± 1.7	12.6 ± 0.3	38.4 ± 1.3	0.64 + 0.04

Table 3-3 *Tst*$^{-/-}$ mice have normal cardiac performance at 6 & 10weeks of age

Doppler scanning performed on anaesthetised naïve 6 and 10wk old *Tst*$^{-/-}$ and C57BL/6N wild type mice, (n=6/ group/ timepoint). Values are mean±SEM, analysed by 2-way ANOVA. *Abbreviations; IVCT (ms, milliseconds); isovolumetric contraction time, IVRT (ms, milliseconds); isovolumetric relaxation time, ET (ms, milliseconds); ejection time, MPI (arbitrary units); myocardial performance index*

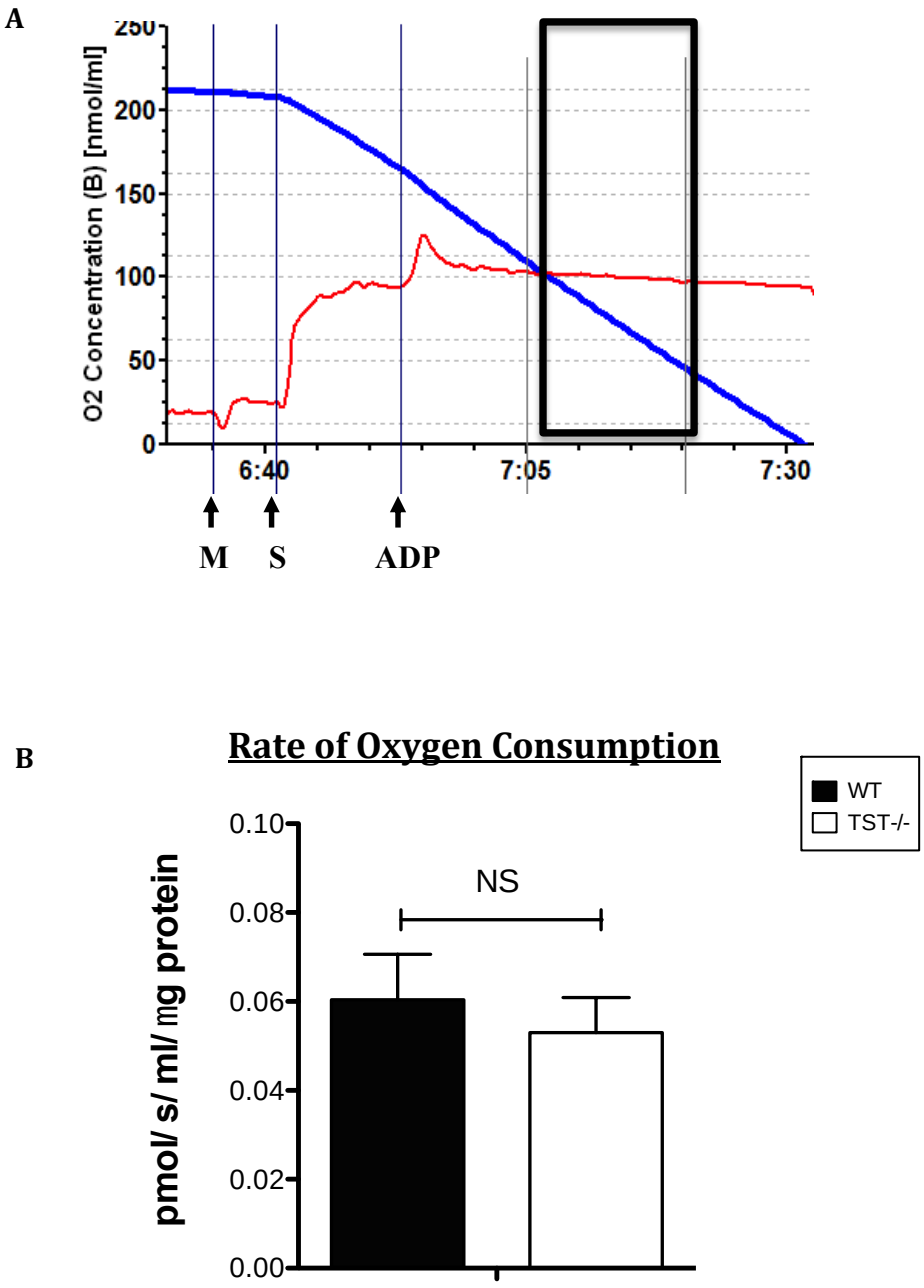

Figure 3-18 *Tst*$^{-/-}$ mice have normal cardiac mitochondrial respiratory rate

A) Representative mitochondrial respiration trace of C57BL6 control mouse showing timepoints of substrate administration to achieve state 3 respiration; malate (M), succinate (S) and ADP. Blue line represents mitochondrial O_2 consumption and red line denotes change of respiration with substrate administration. Black boxes represent the linear phase of O_2 consumption (blue line) used for measurements. B) Absolute respiratory rate during State 3_{ADP} respiration in isolated cardiac mitochondria when normalised to protein (WT; n=5, *Tst*$^{-/-}$; n=6, two hearts pooled per n number). Values are expressed as mean±SEM. *Abbreviations, ADP; adenosine diphosphate.*

3.4 Discussion

The aim of the current study was to investigate the expression and localisation of TST within the murine heart and vasculature and to establish the role that TST plays in regulating H_2S bioavailability in *Tst* deficient mice.

TST and the H_2S synthetic enzymes are expressed in the murine heart, liver and aorta

The expression and localisation of the H_2S synthetic enzymes in the murine heart and vasculature were assessed as a means to compare against *Tst* expression. Consistent with previous reports, the current study showed that the H_2S synthetic enzymes, *Cth* (CSE*), Cbs* and *Mpst* were present in the murine heart. *Cbs* mRNA levels were low in the heart compared to liver supporting previous reports that CBS plays a lesser role in cardiac H_2S production (Sen *et al.*,, 2008). Conversely, cardiac *Cth* and *Mpst* mRNA levels were both high in whole heart homogenates compared to liver tissue supporting previous findings (Geng *et al.*, 2004b; Nagahara *et al.*, 1998).

Several studies have shown that CSE is expressed in both the vascular endothelium and smooth muscle (Fu *et al.*, 2012a; Yang *et al.*, 2008; Zhao *et al.*, 2001) but the immunohistochemical staining presented here clearly suggests that CSE was present in aortic smooth muscle alone. CSE deficient mice produce less H_2S and suffer from vascular dysfunction caused by impaired hyperpolarisation within the endothelium and impaired activation of the ATP-sensitive potassium activated-ATP channels in smooth muscle of small mesenteric arteries (Mustafa *et al.*, 2011; Yang *et al.*, 2008). Therefore, it seems likely our antibody simply failed to detect endothelial CSE and additional studies with alternate antibodies may be required. CBS expression in the cardiovascular system remains controversial with several groups suggesting it is weakly expressed (Sen *et al.*, 2008; Zhao *et al.*, 2001). CBS is involved in homocysteine breakdown, which is essential in the process of producing the H_2S-synthetic enzyme substrate, L-cysteine. Silencing of CBS in human umbilical vein endothelial cells (HUVECs) with CBS shRNA reduces cellular proliferative potential and predisposes cells to premature senescence, which is exacerbated by administration of homocysteine (Albertini, 2012). CBS deficient mice develop hyperhomocysteinemia causing endothelial dysfunction, hypertension and vascular remodelling (Ovechkin *et al.*, 2006). The present study demonstrates the presence of immunoreactive CBS in aortic endothelial cells and together with literature, indicates that CBS plays a broader role in vascular health than is currently acknowledged. 3MST immunoreactivity in the endothelium of the aorta is consistent with previous reports

(Shibuya et al., 2009), indicating it plays a role in vascular function but as no specific 3MST inhibitors are currently available, this remains to be elucidated.

While TST was previously shown to be present in whole heart homogenate (Nagahara *et al.*, 1998), TST's cellular localisation within the cardiovascular system was unclear. The current study showed that TST was present in whole heart, isolated cardiomyocytes, myocardial vascular smooth muscle cells and the aorta in a similar pattern to CSE. Furthermore, western blots and qRT-PCR showed that TST is expressed in whole aortic homogenates and in endothelial cells from aorta and intramuscular vessels of the hindlimb. These data confirm that TST is also expressed in vasculature outwith the heart and blood vessels, raising the possibility that TST plays a role in vascular function (discussed in Chapter 4). TST's presence in the same tissues and cell types as the H_2S-synthesising enzymes was not surprising given the toxic effects of H_2S at high concentrations. As H_2S can freely diffuse across cell membranes, mitochondrial bound TST is well situated to prevent endogenous or exogenous sources of H_2S from inhibiting cytochrome c in the mitochondrial respiratory chain, which can be fatal. Immunohistochemical TST staining in aortic tissues was attempted but failed to show cellular specificity and due to time constraints, could not be properly optimised. Future studies should aim to optimise aortic TST immunohistochemical staining and perform immunofluorescent co-localisation staining with α-SMA and TST to elucidate if TST is present in aortic smooth muscle cells.

TST knockout mice survive, but how?

Upstream of TST, the sulfur dioxygenase ETHE1 participates in the H_2S breakdown pathway to form sulfite from SQR persulfide groups (Kabil *et al.*, 2014). *Ethe1* knockout (*Ethe1*$^{-/-}$) mice have retarded growth by post-natal day15 and impaired movement. These mice die at 5-6 weeks after birth due to sulfide toxicity (Tiranti *et al.*, 2009). Elevated liver, brain and muscle tissue H_2S levels in *Ethe1*$^{-/-}$ mice lead to tissue cytochrome c inhibition and reduced mitochondrial complex IV activity (Tiranti *et al.*, 2009). Surprisingly, *Ethe1*$^{-/-}$ mice have normal SQR and TST activities in all tissues despite cytochrome c inhibition, suggesting that ETHE1 plays a distinct yet vital role in the H_2S breakdown pathway.

TST has a putative role in the breakdown of H_2S but as no selective pharmacological inhibitors or knockout mice have been reported to date, its importance in this process was unclear. To investigate this, we used a novel TST deficient mouse. *Tst*$^{-/-}$ mice showed complete loss of TST mRNA, protein and enzyme activity confirming that the knockout strategy was effective. *Tst*$^{-/-}$ mice all survived to adulthood (20 weeks) with no differences in body weight, organ weight or organ morphology indicating that TST is not essential for

development and that other pathways are likely modified to retain H_2S within a non-toxic concentration range. However, *Tst*$^{-/-}$ mice have reduced H_2S breakdown rates in the heart and liver confirming that TST is involved in H_2S breakdown in these tissues. Impaired H_2S breakdown is more pronounced in *Tst*$^{-/-}$ livers, explained by markedly higher TST expression in liver compared to the heart. H_2S levels in the blood are also increased in *Tst*$^{-/-}$mice, yet these mice are viable and do not display the phenotypic characteristics seen in the *Ethe1*$^{-/-}$ mice. *In vitro* assays showed that the rate of H_2S breakdown was impaired in heart and liver tissues but exogenous H_2S was eventually catabolised. This may be because there is some redundancy in the system and other catabolic enzymes are able to take over H_2S removal to some extent. TST has a high affinity for ETHE1-derived sulfite in the H_2S breakdown pathway (Hildebrandt *et al.*, 2008a) but SUOX can also utilise sulfite to produce sulfate in an oxygen dependent manner (Kabil *et al.*, 2014). Expression of *Sqrdl, Ethe1* and *Suox* mRNA levels were comparable in heart and liver tissues of *Tst*$^{-/-}$ and control mice. Although not statistically different, likely because of insufficient sample numbers, *Suox* mRNA levels tended to be higher in *Tst*$^{-/-}$ livers. As the liver preferentially converts sulfide to sulfate (Bartholomew *et al.*, 1980), SUOX may play a vital role in mediating sulfite breakdown in *Tst*$^{-/-}$ mice. Western blotting assays were performed on heart, liver and kidney tissues to assess SQR, ETHE1 and SUOX protein levels with several antibodies but were unsuccessful. This area merits further investigation, including further optimisation of SUOX protein detection, and measurement of sulfite and sulfate levels to examine SUOX functional changes and the efficiency of its sulfite conversion.

Circulating H_2S levels in blood were found to be approximately 7-fold higher in *Tst*$^{-/-}$ mice indicating that total body sulfide levels is elevated. Bacterial flora in the colon produce vast amounts of H_2S, which is catabolised by efficient mitochondrial breakdown (Taniguchi *et al.*, 2009). The liver is perfused with venous blood from the digestive tract via the portal vein and given its capacity to catabolise H_2S, may act as a secondary barrier to limit colonic bacterial-derived H_2S from entering the circulation (Szabó *et al.*, 2014). TST is ubiquitously expressed in hepatocytes surrounding the portal vein and central vein of C57BL/6J mice (Appendix 1). Germ-free mice have markedly lower plasma H_2S levels compared to controls (Shen *et al.*, 2013) and so colonic bacterial-produced H_2S is believed to contribute to plasma H_2S levels (Szabó *et al.*, 2014). Due to expression of the H_2S synthetic enzymes in all tissues, colonic bacterial-produced H_2S is not believed to act as a source of H_2S to other tissues, confirmed by comparative tissue H_2S levels the liver, heart and kidneys of germ free mice (Shen *et al.*, 2013). H_2S is considered to play a role in the pathogenesis of colonic

ulcerative colitis (UC). Mice with pharmacologically induced-UC have maintained CSE expression but reduced TST mRNA, protein and enzyme activity in the colon indicating that impaired H_2S breakdown plays a vital role in UC (Taniguchi *et al.*, 2009). Therefore, it is expected that loss of TST in the colon of *Tst*$^{-/-}$ mice results in inefficient H_2S breakdown and subsequently, higher H_2S levels in the blood in contact with the gut. Hepatic perfusion from the digestive tract into the liver of *Tst*$^{-/-}$ mice via the portal vein may result in higher H_2S levels in the blood due to impaired hepatic H_2S breakdown. To definitively understand the source of plasma H_2S it will be important to measure tissue H_2S levels in *Tst*$^{-/-}$ mice, especially in the gut and liver.

Measurement of tissue H_2S in Tst$^{-/-}$ mice

H_2S measurements were attempted in *Tst*$^{-/-}$ mouse and control mouse tissues using a variety of methods with varying success including, (i) the methylene blue assay, (ii) polarographic electrode and (iii) monobromobimane analysis using HPLC. The widely used methylene blue assay relies upon incubating tissue samples with excess H_2S synthetic enzyme substrate L-cysteine (10mM), trapping produced sulfide with zinc acetate and following incubations with coloured reagents dissolved in strong acids (1.2-7.2M HCl), methylene blue is formed and measured spectrophotometrically to infer H_2S levels. There are several issues with this method, which have been previously reported including; (i) spectrophotometric interference of coloured substances, (ii) strong acidification treatments liberate stored sulfide giving false H_2S values and (iii) lack of sensitivity to measure H_2S concentrations in or below the μM range. In my hands, spectrophotometric optical density values obtained from the methylene blue method did not distinguish heat-treated (95^0C*5mins) negative control samples to regular samples confirming interference from coloured reagents. Following administration of Na_2S (a H_2S donor) standards, the assay failed to consistently detect sub-millimolar Na_2S concentrations and as a result, this approach of H_2S detection was abandoned.

The H_2S polarographic electrode is a more sensitive method where H_2S can be measured in the nM range in real time. H_2S production assays were employed using the same concentrations of the H_2S synthetic enzyme substrates as the methylene blue assay in hypoxic conditions to avoid H_2S breakdown by the oxygen dependent enzymes, ETHE1 and SUOX. Preliminary measurements revealed rapid H_2S production in the presence of 10mM L-cysteine. Upon further investigation, it was observed that L-cysteine administration in Krebs buffer or deionised water alone released large amounts of H_2S in normoxic and anoxic conditions in a concentration-dependent manner. Spontaneous decomposition of L-cysteine into H_2S in aqueous solutions has been reported previously using gas chromatography

techniques (Furne *et al.*, 2008). Based on Furne *et. al.* 2008 experiments, a second set of tissue H_2S experiments were planned using a 10-fold lower L-cysteine concentration and tissue-free L-cysteine samples to correct for spontaneous decomposition in tissue-containing samples. Unfortunately, the H_2S polarographic electrode broke before the study was conducted and despite considerable efforts, could not be fixed. Based on the requirement for L-cysteine substrate in both the methylene blue and the polarographic H_2S assays, I would argue that these assays are an indirect measure of combined H_2S synthetic enzyme activities and not actual H_2S levels. The monobromobimane (MBB) HPLC assay, which is widely accepted as a sensitive stable technique to measure H_2S, operates when MBB reacts with H_2S to produce sulfide-dibimane and the reactants are then detected at established peaks using HPLC. Whilst this technique has been effective to measure whole blood H_2S concentrations in *Tst*$^{-/-}$ mice, this approach has not yet been optimised for determining tissue H_2S levels.

Although it was not possible to assess absolute tissue H_2S in the present study, it was possible to assess the expression of cellular targets of H_2S as a surrogate marker. Cellular expression of nuclear receptor factor-E2-related factor (Nrf2) and its downstream targets thioredoxin (TRX1) and hemeoxygenase 1 (HO-1) are increased by H_2S (Calvert *et al.*, 2009). Cardiac specific CSE overexpressing mice also have increased expression of Nrf2, TRX1 and HO-1 protein in heart, which is attributed to their increased H_2S availability (Calvert *et al.*, 2009). In the current study myocardial TRX1 and HO-1 protein levels were comparable between groups suggesting that cardiac H_2S bioavailability is maintained.

High H_2S concentrations (>10μM) can decrease mitochondrial respiration via cytochrome c inhibition (Szabo *et al.*, 2014). Administration of the H_2S donor, Na_2S to isolated cardiac mitochondria dose-dependently reduces mitochondrial oxygen consumption (Elrod *et al.*, 2007). *Ethe1*$^{-/-}$ mice have elevated plasma and tissue H_2S levels and markedly impaired complex IV activity in isolated cardiac mitochondria (Tiranti *et al.*, 2009). Given the hearts vast energy requirements, any disruption or inhibition of mitochondrial function would be detrimental. Mitochondria isolated from *Tst*$^{-/-}$ hearts show comparable oxygen consumption rates to controls, supporting the conclusion H_2S does not accumulate to toxic levels in *Tst*$^{-/-}$ hearts under basal conditions. Furthermore, Doppler ultrasound scanning confirms that cardiac size, function and performance were comparable between *Tst*$^{-/-}$ and WT control mice at 6 and 10weeks of age. This is consistent with data showing normal cardiac morphology and heart weight to body weight ratios between groups. The lack of an underlying cardiac

phenotype facilitates the study of pathology in *Tst*$^{-/-}$ mice in myocardial infarction intervention studies, as outlined in the chapter 5.

However, these data prompt the question of how *Tst*$^{-/-}$ mice maintain cardiac H_2S levels when myocardial H_2S breakdown is impaired and circulating H_2S levels are increased. Evaluation of the myocardial H_2S synthetic enzymes in *Tst*$^{-/-}$ mice revealed reduction of *Cse*/CSE gene and protein levels, suggesting that a homeostatic negative feedback mechanism is triggered in the heart to limit H_2S synthesis when breakdown is reduced. Reduced CSE-mediated H_2S production could explain why cardiac TRX1 and HO-1 protein levels are comparable in *Tst*$^{-/-}$ and control mice. Activation of the negative feedback mechanism is likely triggered in *Tst*$^{-/-}$ hearts to enable the cardiac mitochondria and, subsequently, the whole heart to function normally. Reduced local CSE-mediated H_2S generation likely influences eNOS expression in hearts of *Tst*$^{-/-}$ mice, an effect reported in other studies (King *et al.*, 2014).

Although mRNA levels of the NOS enzymes are unaltered by loss of TST, total eNOS protein was lower in *Tst*$^{-/-}$ hearts. NO activated protein kinase G mediates phosphorylation of the vasodilator-stimulated phosphoprotein (VASP) at the serine239 residue (P-Vasp^{Ser239}) (Defawe *et al.*, 2010) and can be used as an indirect measure of NO availability. Vasp^{Ser239} tended to be lower in *Tst*$^{-/-}$ hearts, which is consistent with reduced cardiac total eNOS data indicating NO availability may also be lower in *Tst*$^{-/-}$ hearts. Indeed, CSE deficient mice have reduced eNOS activity and NO availability, and increase susceptibility to IRI (King *et al.*, 2014). Whilst cardiac CSE downregulation appears to be a protective strategy under basal conditions, it may be detrimental in pathophysiological states. CSE and eNOS have been previously shown to be important mediators of the hearts response to MI (Elrod *et al.*, 2006; 2007; King *et al.*, 2014; Sumeray, 2000) and reduced basal expression of both enzymes in the heart may be detrimental for *Tst*$^{-/-}$ mice following MI. The response of *Tst*$^{-/-}$ mice to CAL will be discussed in Chapter 5.

Dynamic regulation of tissue H_2S synthetic enzymes have been shown in a variety of injury models including kidney nephropathy (Yamamoto *et al.*, 2012), acute liver failure (Shirozu *et al.*, 2014) and pressure overload-induced heart failure (Kondo *et al.*, 2013), but the mechanism regulating their expression remains unclear. In the current study, the H_2S synthetic enzymes respond differently in heart, liver and kidney tissues of *Tst*$^{-/-}$ mice indicating that H_2S synthetic enzymes are likely to be regulated by integrated local and systemic H_2S responsive pathways. In kidneys from *Tst*$^{-/-}$ mice, CSE protein levels were higher and there was also a trend for increased CBS protein suggesting that renal H_2S levels may be further increased rather than limited by reduced synthesis. Although H_2S breakdown

rates were not measured in *Tst*$^{-/-}$ kidneys, increased H_2S production could detrimentally affect kidney function. This will be discussed further in Chapter 4.

3MST is characterised as a H_2S synthesising enzyme where it converts 3-mercaptopyruvate or thiosulfate into H_2S in concert with the endogenous reducing agent, thioredoxin (Mikami *et al.*, 2011). In the current study, *Mpst* mRNA expression is approximately halved in heart, liver and kidney tissues of *Tst*$^{-/-}$ mice. As *Mpst* is in close proximity to *Tst* on chromosome 15 (within 1 kb), it is possible the TST knockout strategy with 5′ and 3′ homology arms inadvertently extended too far and affected the *Mpst* sequence. Sequencing of the entire *Mpst* gene in *Tst*$^{-/-}$ mice should be performed in the future to examine this. Despite reduced mRNA levels, 3MST protein levels were comparable between heart and kidney tissues and were elevated in liver mitochondria of *Tst*$^{-/-}$ mice. As the sample preparation for mitochondrial isolation does not separate cytosolic fractions cleanly, it is unclear if increased mitochondrial 3MST expression is due to its upregulation or due to enhanced compensatory translocation from the cytosol. Although 3MST is characterised as a H_2S generating enzyme, it is possible it plays multiple roles depending on prevailing substrate and H_2S levels. TST and 3MST are evolutionarily related and share considerable similarities of their sequence and 3-dimensional structure (Cipollone *et al.*, 2007). Indeed, 3MST has previously been implicated in cyanide detoxification and is capable of converting cyanide to thiocyanate, albeit at a much increased Km (Cipollone *et al.*, 2007; Spallarossa *et al.*, 2004). Nagahara and colleagues 2013, who developed the first 3MST knockout mouse for anxiety-based studies, accidentally created a 3MST-TST double knockout during initial knockout development. Interestingly, the double knockouts were embryonic lethal (Nagahara *et al.*, 2013) supporting the vital functions of 3MST and TST and raising the intriguing possibility that 3MST may have the capacity to compensate for H_2S detoxification with TST deficiency. Through collaboration, we acquired a novel 3MST inhibitor. Our aim was to perform the H_2S breakdown assay in tissues pre-treated with the 3MST inhibitor but the H_2S electrode broke before these studies were performed and should be tested in future with new H_2S electrodes.

Whilst *Tst*$^{-/-}$ hearts show negative feedback on CSE levels to limit H_2S production, *Tst*$^{-/-}$ kidney and liver tissues do not. It may be that H_2S bioavailability is regulated through additional mechanisms in these tissues. H_2S availability is regulated by mitochondrial breakdown and efficient sulfide storage in the cell in either acid-labile sulfide stores or as bound sulfane sulfur and can be released under certain conditions (Shen *et al.*, 2012). Acid-labile sulfur stores consist of protein iron-sulfur clusters, which are ubiquitously expressed in

a variety of mitochondrial proteins and release H_2S in acidic conditions (Ishigami *et al.*, 2009). Alternatively, bound sulfane sulfur stores exist when sulfur covalently binds to another sulfur atom and can release H_2S under reducing conditions (Kabil *et al.*, 2014). Exogenous Na_2S is absorbed in rat brain homogenates as bound sulfane sulfur within 30minutes (Ishigami *et al.*, 2009). Administration of the reducing agent, dithiothreitol (DTT) released 45% more H_2S from Na_2S pre-treated brain homogenates than non-treated control samples supporting this mechanism (Ishigami *et al.*, 2009). Based on their redox sensitivity, such stores are believed to act as an emergency source of H_2S under pathophysiological conditions but the action of release and the precise conditions in which they liberate H_2S are poorly understood (Kolluru *et al.*, 2013). Whilst it has long been considered an innocuous metabolite of TST, thiosulfate is now categorised as a bound sulfane sulfur compound that can rapidly release H_2S under appropriate conditions (Mikami *et al.*, 2011). In mouse liver tissues, co-administration of thiosulfate with the pharmacological or endogenous reducing agents, dithiothreitol (DTT) or dihydrolipoic acid (DHLA), respectively, releases H_2S rapidly (Kolluru *et al.*, 2013; Mikami *et al.*, 2011; Olson *et al.*, 2013). Furthermore, DHLA can dose-dependently relax pre-constricted mouse and rat aortas with IC50s of 30μM (mouse) and 70μM (rat) reported, indicating that liberated H_2S stores can participate in biological functions (Olson *et al.*, 2013). However, there is no evidence to support the notion that bound sulfane sulfur is used in lieu of free H_2S for biological functions or H_2S signalling events (Kabil *et al.*, 2014). The current study shows that thiosulfate levels are markedly increased in in the blood and urine of *Tst*$^{-/-}$ mice. This surprising result contradicts previously held beliefs that TST produces thiosulfate in the H_2S breakdown pathway (Hildebrandt *et al.*, 2008b). Studies performed on lugworm reported that the affinity of TST for thiosulfate was lower than that of sulfite but showed that TST can utilise thiosulfate as substrate nonetheless (Hildebrandt *et al.*, 2008b). Although TST is involved in H_2S breakdown as discussed previously, the accepted view that TST converts ETHE1-derived sulfite into thiosulfate within the H_2S breakdown pathway clearly needs revision. Studies in bacteria suggest that thiosulfate is formed more efficiently by the SQR than by TST and may in fact be the source of its production (Jackson *et al.*, 2012). Certainly this data would help explain why *Ethe1*$^{-/-}$ and *Tst*$^{-/-}$ mice also have such high thiosulfate levels. That such significant thiosulfate levels are present in urine suggests the body cannot efficiently catabolise sulfide to sulfate for excretion and may be a compensatory mechanism to rid the body of H_2S. As selective inhibitors for SQR are not currently available, in-depth investigation to understand the role of the SQR in thiosulfate formation in *Tst*$^{-/-}$ mice cannot be currently tested. Future studies

should test SQR enzyme activity to determine if it is raised in *Tst*$^{-/-}$ mice in response to higher circulating H_2S levels.

In conclusion, the current study shows that TST is expressed in the murine cardiovascular system as well as the kidney and liver where it contributes to regulation of H_2S availability. The next chapter will investigate how changes in H_2S availability impacts upon blood pressure and vascular function and kidney sodium fluid handling.

4 *Tst* knockout mice have altered endothelial function and kidney electrolyte-fluid homeostasis

4.1 Introduction

Blood pressure is regulated by small resistance arteries and arterioles that determine the peripheral resistance and in the kidney through electrolyte-fluid handling leading to changes in extracellular volume. Experiments in Chapter 3 have shown that TST is expressed within the kidney and the vascular smooth muscle of the myocardial vasculature as well as in dorsal aorta and in endothelial cells of the aorta and small intramuscular vessels of the hindlimb. In kidneys from *Tst*$^{-/-}$ mice expression of CSE protein was higher indicating that kidney H_2S generation is likely to be elevated. H_2S levels are markedly higher in the blood of *Tst*$^{-/-}$ mice. Together these observations suggest that TST may have a role in controlling blood pressure through regulating the availability of H_2S. Experiments in this chapter were therefore aimed at investigation of blood pressure regulating mechanisms in *Tst*$^{-/-}$ mice.

Fluid homeostasis within the body is tightly regulated so that plasma osmolality and intravascular volume remain constant. Under physiological conditions, whole body water balance is regulated so that urinary excretion matches fluid intake and therefore, maintains plasma osmolality, blood volume and blood pressure. The renal nephron actively reabsorbs sodium and other electrolytes from the filtrate via several different sodium coupled exchangers and water reabsorption is dependent upon this process (Mullins *et al.*, 2006; Wang *et al.*, 2009), which is outlined in detail in section 1.1.5.3. The nephrons proximal convoluted tubule (PCT) reabsorbs ≈65% of the filtrates sodium and water content (Castrop *et al.*, 2014). The H_2S synthetic enzymes, CSE, CBS and 3MST are highly expressed in the kidney and have been localised to the PCT (Nagahara *et al.*, 1998; Yamamoto *et al.*, 2012). Administration of the H_2S donor NaHS to the renal artery of rats increases urinary flow rate and excretion of sodium, highlighting a potential role of endogenous H_2S in electrolyte-fluid homeostasis and blood pressure regulation (Xia *et al.*, 2009). TST is also highly expressed in the murine kidney and has been localised to the PCT (Sylvester *et al.*, 1990). TST expression and enzyme activity levels are comparable between kidney and liver tissues (Nagahara *et al.*, 1998) and as such, the kidney has classically been characterised as a cyanide detoxifying tissue given its exposure to cyanide in the blood (Cipollone *et al.*, 2007). Previous findings in this thesis show that TST mediates H_2S breakdown in heart and liver tissues and therefore, it is possible that TST indirectly regulates kidney tubular function via local H_2S availability

in the PCT. *Tst*$^{-/-}$ mice have increased CSE expression in the kidney and increased H_2S in blood indicating that the kidney is exposed to higher concentrations of H_2S. The experiments in this chapter are designed to investigate if loss of TST impacts upon kidney sodium-fluid handling and blood pressure regulation.

Pharmacological H_2S administration dose dependently reduces blood pressure (Yang *et al.*, 2008; Zhao *et al.*, 2001). The ability of H_2S to act as an endothelium derived hyperpolarising factor (EDHF), causing vasorelaxation, is thought to contribute to this blood pressure lowering effect (Hosoki *et al.*, 1997; Mustafa *et al.*, 2011; Yang *et al.*, 2008; Zhao *et al.*, 2001). The cardiovascular specific H_2S-synthetic enzyme, CSE is highly expressed in the endothelium and smooth muscle of the aorta (Fu, *et al.*, 2012a; Shibuya *et al.*, 2009; Yang *et al.*, 2008). As described in chapter 3, TST is expressed in whole aorta and endothelial cells from aorta and small arteries of the hindlimb of wild type mice indicating that TST may play a role in regulating vascular function by controlling H_2S availability. H_2S plays a major role in relaxing small resistance arteries, which are largely eNOS and COX independent. Within small mesenteric arteries, H_2S activates small and intermediate calcium activated potassium channels (SK_{Ca} and IK_{Ca}) in the endothelium and via diffusion into vascular smooth muscle, H_2S also activates ATP-sensitive potassium channels (K_{ATP}). During cholinergic stimulation, calcium is released within endothelial cells and activates calmodulin, which then binds to and stimulates CSE to produce H_2S (Mustafa *et al.*, 2011; G Yang *et al.*, 2008). Endothelial produced H_2S activates SK_{Ca} and IK_{Ca} channels, permitting intracellular K^+ efflux resulting in hyperpolarisation of endothelial cells and the whole vessel, causing relaxation (Mustafa *et al.*, 2011). Inhibition of the H_2S-sensitive SK_{Ca} and IK_{Ca} channels with apamin and charybdotoxin in isolated endothelial cells from mice attenuates acetylcholine-induced hyperpolarisation (Mustafa *et al.*, 2011). Hyperpolarisation of the whole vessel and vasorelaxation is attenuated when the endothelium is removed confirming that endothelial produced H_2S is vital in mediating mesenteric vasorelaxation (Mustafa *et al.*, 2011; Yang *et al.*, 2008). In contrast to small arteries, H_2S plays a minor role in the relaxation of the aorta (Hosoki *et al.*, 1997), which is largely eNOS and cyclooxygenase (COX) dependent. However, low doses of the nitric oxide (NO) donor sodium nitroprusside (10nM) enhance sensitivity to NaHS in isolated aortic rings (Hosoki *et al.*, 1997), highlighting the importance of H_2S-NO interactions in the vasculature. As *Tst*$^{-/-}$ mice have increased circulating levels of H_2S, it was hypothesised that vasodilatation would be increased and blood pressure reduced in *Tst*$^{-/-}$ mice. The potential for H_2S-NO crosstalk was investigated by detection of eNOS protein and its phosphorylation status, indicative of modified eNOS activity and NO

availability (King *et al.*, 2014). The present study aimed to investigate the influence of TST on the function of large conductance vessels (thoracic aorta), as well as smaller arteries (mesenteric) using myography. Furthermore, the vessel function experiments in this chapter were designed to investigate if (i) activation of the H_2S-sensitive SK_{Ca} and IK_{Ca} channels is enhanced in small mesenteric arteries from *Tst*$^{-/-}$ mice and (ii) if augmented H_2S-NO crosstalk alters the sensitivity to the NO inhibitor LNAME and the NO donor SNP in the aorta.

4.2 Methods

4.2.1 Blood pressure

Blood pressure was measured in anaesthetised wild type and *Tst*$^{-/-}$ mice via the right carotid artery using an intravascular Millar catheter as described in section 2.2.1. Blood pressure was allowed to equilibrate for 30 minutes before basal blood pressure was measured.

4.2.2 Metabolic cage water balance measurements

Male wild type and *Tst*$^{-/-}$ mice were acclimatised to single housed metabolic cages for 6 days prior to data acquisition and fed a standard ground RM1 diet (0.25% salt content) and given free access to water. Daily measurements of body weight, water & food intake, urine & faecal output were recorded at the same time of day following the acclimatisation period as described in section 2.2.5. To minimise natural daily fluctuations, mean values of water intake, urine excretion and urinary sodium, potassium and chloride measurements were calculated over an 8-day period following acclimatisation. Water or electrolyte balances (excretion – intake) were calculated as cumulative balances. Metabolic cage sample collections were performed in collaboration with Matthew Gibbins.

4.2.3 Urinary Electrolyte measurement

Urinary sodium and potassium levels and plasma potassium levels were measured using the Roche 9180 Electrolyte analyser as described in section 2.2.6. Urinary electrolyte values were multiplied by total urinary weight in a 24hr period to calculate total electrolyte excretion. Values were calculated as mean excretions over an 8-day period following metabolic cage acclimatisation. Urinary calcium and phosphate measurements were performed by Forbes Howie in the Clinical Analysis Core Services at the University of Edinburgh using commercially available colorimetric assays as described in section 2.2.6. Values were calculated as mean calcium and phosphate excretions on two consecutive days following metabolic cage acclimatisation. Values were multiplied by total urinary weight in a 24hr period to calculate total electrolyte excretion. As urine samples were collected at the same day each day, values were not corrected for creatinine.

4.2.4 Histology

Tissue morphological analysis was assessed using haematoxylin and eosin (H&E) staining performed on kidney sections of adult *Tst*$^{-/-}$ and wild type mice as described in section 2.4.5.

Kidney H&E sections were assessed by a rodent pathologist (James Baily) who was blinded to genotype to examine if any gross structural abnormalities existed.

4.2.5 Western blotting

Western blotting was performed using rabbit polyclonal antibodies as described in section 2.5.6. Immunoblots analysing total eNOS and P-eNOS^{Ser1177} protein levels in aortic tissues were carried out by Alessandra Borgognone in the University of Birmingham.

4.2.6 Wire myography

Vascular function was evaluated on isolated vessels using the Mulvany-Halpern myograph as described in section 2.3.7 Aorta and first order mesenteric arteries from *Tst*$^{-/-}$ and C57BL/6N wild type mice were isolated, placed onto stainless steel wires and passively stretched to their optimal resting tension in PSS filled myography baths as described in section 2.3.7. Vessel viability was assessed using high potassium solutions (KPSS) and noradrenaline (Aorta; KPSS alone; mesenteric arteries; KPSS and NA). Endothelium integrity was confirmed when pre-constricted vessels (70-80% of KPSS-mediated maximal constriction) relaxed by $\geq$70% of pre-constriction following the administration of acetylcholine (ACh, $1*10^{-5}$M). Vessels that relaxed by <70% following acetylcholine administration were not used for experimentation.

Vessels were treated with increasing half-log increments ($1x\ 10^{-9}$M – $3x\ 10^{-5}$M) of the α1-adrenergic receptor agonist phenylephrine (PE) to achieve cumulative drug dose response curves. Endothelium intact aortas and mesenteric arteries were preconstricted with PE to 80% of E_{max} (EC80) before cumulative additions of the endothelium dependent cholinergic receptor agonist, acetylcholine (ACh) or the endothelial independent nitric oxide donor sodium nitroprusside (SNP). To investigate the extent nitric oxide and cyclooxygenase play in aortic vasorelaxation, aortic rings were pre-incubated with and without inhibitors for nitric oxide (L-NAME, 100μM) and cyclooxygenase (Indomethacin, 10μM) prior to PE, ACh or SNP administration. To investigate the extent that small and intermediate calcium activated potassium channels (SK_{Ca} and IK_{Ca} respectively) play in vasorelaxation in small resistance arteries, mesenteric rings were incubated with and without Apamin (1μM) and Charybdotoxin (100nM) prior to ACh or SNP administration. Doses for all inhibitors were determined from the literature and previous experiments in the laboratory. Dose response curves were generated using non-linear regression curve fit approaches in Prism Graphpad 5.0.

4.2.7 Statistics

All values are expressed as mean ± SEM. Comparisons of blood pressure and 24hour mean differences in water intake and excretion and electrolyte excretory data were assessed by unpaired student t-tests. Non-parametric cumulative water and urinary electrolyte balance data were compared using two-tailed Mann Whitney U tests. Comparisons of vessel myography are by 2-way ANOVA with Bonferroni post-hoc tests comparing between genotype and pharmacological agonist doses. EC_{50} and E_{max} values were calculated using non-linear regression analysis on Prism Graphpad 5.0. Unpaired students t-tests were performed when comparing EC_{50} and E_{max} values between treated and non-treated groups or within groups of treated versus non-treated mice of the same genotype. P values less than 0.05 were considered significant.

4.3 Results

4.3.1 *Tst*$^{-/-}$ mice have normal blood pressure

Intracarotid blood pressure measurements revealed that in comparison to WT mice, adult *Tst*$^{-/-}$ mice have comparable systolic blood pressure (mmHg; WT; 96.2 ± 4.2, *Tst*$^{-/-}$; 98.5 ± 5.8), diastolic blood pressure (mmHg; WT; 74.2 ± 4.5, *Tst*$^{-/-}$; 67.6 ± 4.5) and mean arterial blood pressure (mmHg; WT; 81.5 ± 3.2, *Tst*$^{-/-}$; 77.8 ± 4.3).

4.3.2 *Tst*$^{-/-}$ mice are polydipsic and polyuric

Metabolic cage studies showed that *Tst*$^{-/-}$ mice drank significantly more water and produced significantly more urine than age matched WT controls. Urine osmolality was lower in *Tst*$^{-/-}$ mice compared to WT controls. The polydipsia and associated polyuria observed in *Tst*$^{-/-}$ mice consequently led to maintained cumulative water balance (water intake-urine output) that was not significantly different to wild type control mice (P=0.28). Body weight was similar between groups at all time-points (Appendix 2).

4.3.3 *Tst*$^{-/-}$ mice excrete significantly more sodium, potassium and chloride in their urine compared to control mice

Tst$^{-/-}$ mice excreted significantly more sodium, potassium and chloride in their urine compared to control mice (Figure 4-3). *Tst*$^{-/-}$ mice ate significantly more food and therefore, ingested significantly higher doses of sodium, potassium and chloride from their diet compared to wild type control mice (Appendix 2). *Tst*$^{-/-}$ mice remain in positive electrolyte balance and have comparable cumulative sodium, potassium and chloride balances relative to WT controls (Figure 4-3).

Urinary phosphate and calcium levels were measured to examine function within the proximal tubule and the thick ascending limb of Henle respectively. Urinary phosphate tended to be higher in *Tst*$^{-/-}$ mice (Table 4-1, P = 0.07). Urinary calcium excretion was comparable between groups (Table 4-1, P = 0.33). Haematoxylin & Eosin stained sections revealed no gross morphological alterations in the kidneys of *Tst*$^{-/-}$ mice (Table 4-1).

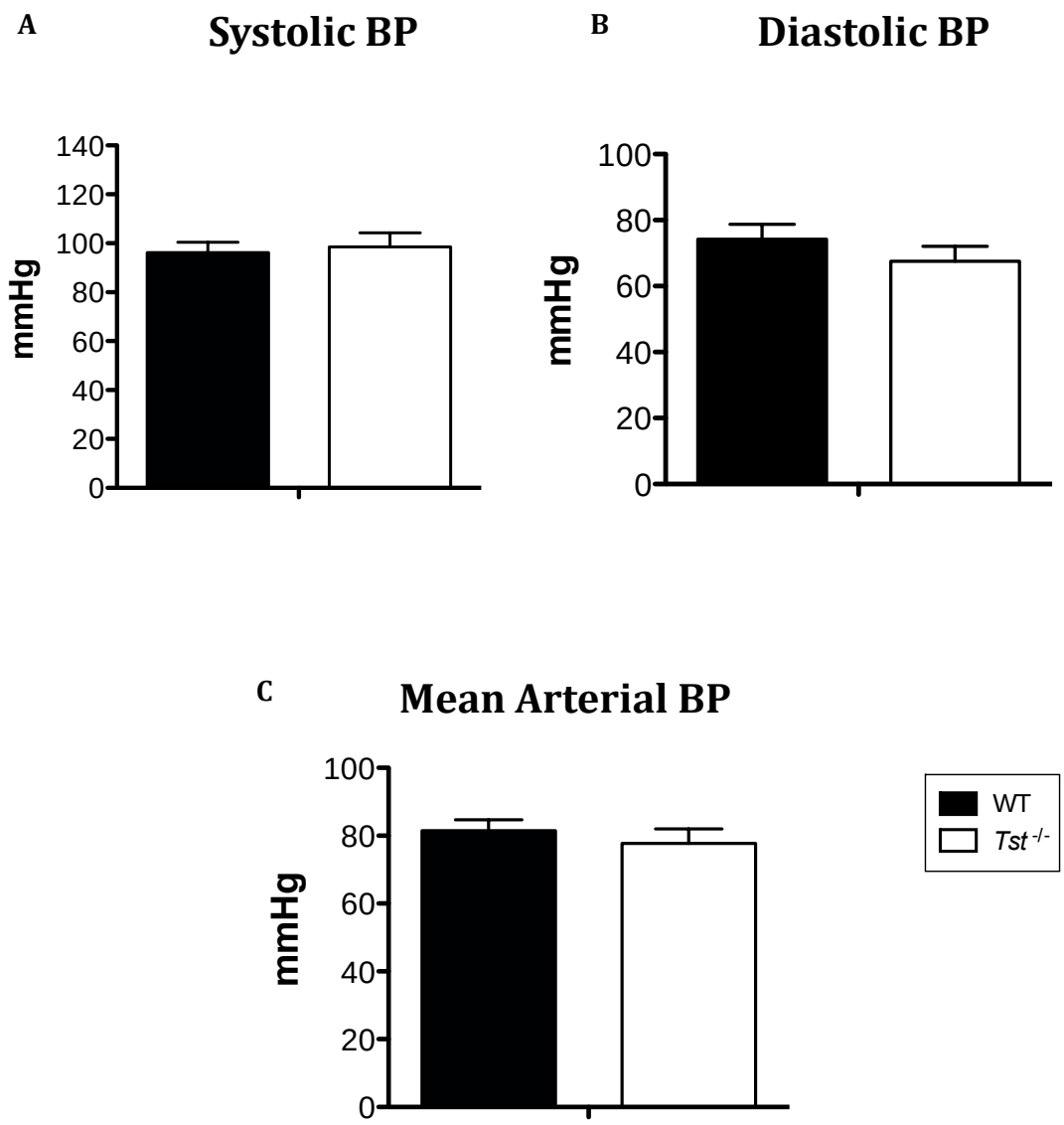

Figure 4-1 *Tst*$^{-/-}$ mice are normotensive

A) Systolic blood pressure, (B) diastolic blood pressure and (C) mean arterial blood pressure of anaesthetised adult *Tst*$^{-/-}$ and C57BL/6N wild type mice, measured by carotid cannulation (WT; n=8, *Tst*$^{-/-}$; n=11). Values are expressed as mean±SEM.

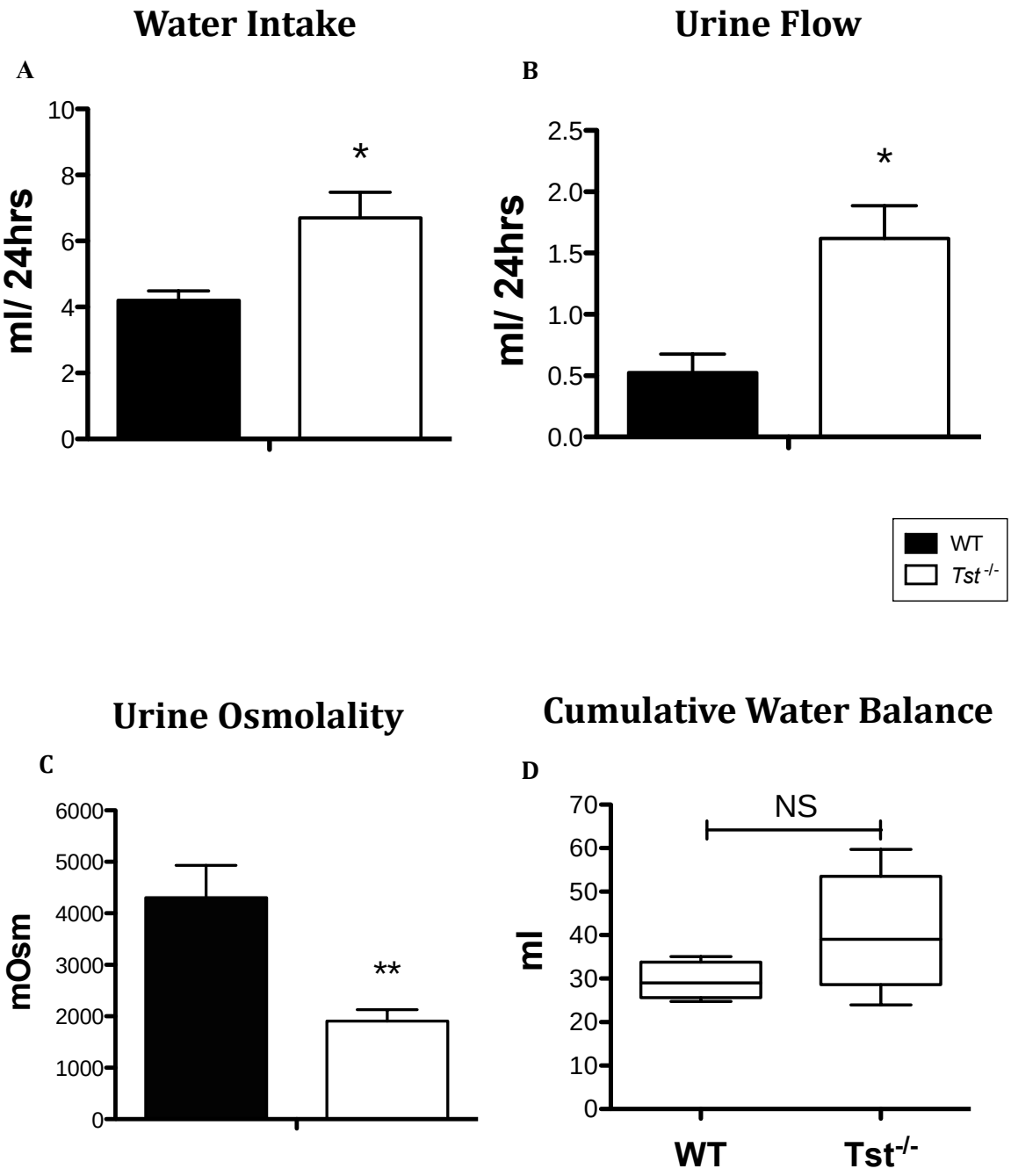

Figure 4-2 *Tst*$^{-/-}$ mice have higher water turnover than controls

Mean 24 hour water intake (A), urine output (B), urine osmolality (C) and D) cumulative water balance (water intake – urine excretion) calculated over the 8 day post-acclimatisation period in *Tst*$^{-/-}$ and C57BL/6N wild type mice (WT; n=4, *Tst*$^{-/-}$; n=5). Data are mean ± SEM. Statistical analysis was performed using student t-test (A-C) and Mann-Whitney U test (D). *p < 0.05, **p<0.01

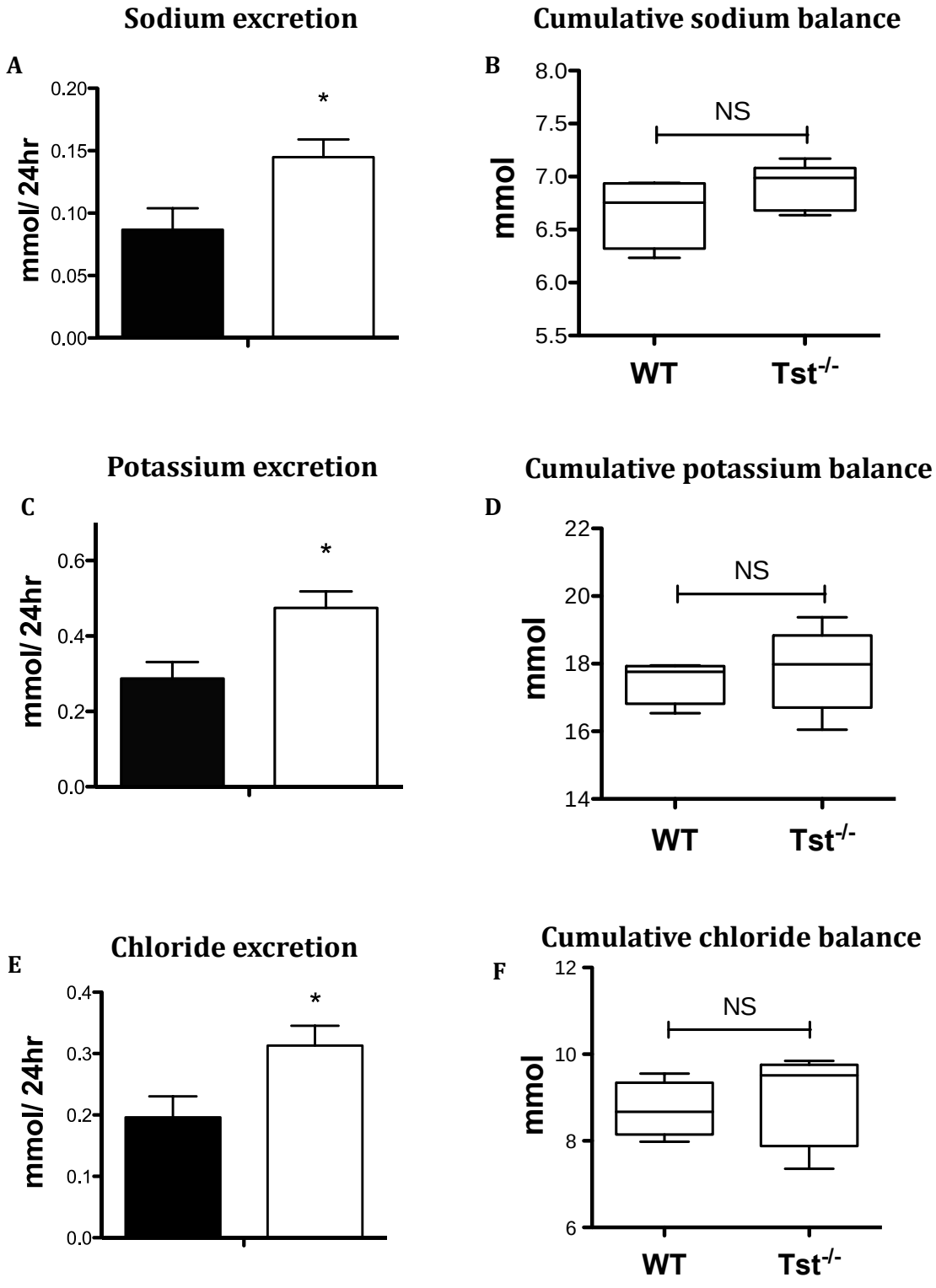

Figure 4-3 *Tst*$^{-/-}$ mice excrete more sodium, potassium and chloride compared to controls but remain in positive electrolyte balance

(A-C) Mean 24hour urinary sodium, potassium and chloride excretion in *Tst*$^{-/-}$ and C57BL/6N wild type mice. (D-F) Cumulative sodium, potassium and chloride balance (dietary intake - urinary excretion) over 8day post-acclimatisation period (WT; n=4,*Tst*$^{-/-}$; n=5). Values were corrected for total urinary volume in a 24hr period. Data are mean ± SEM. Statistical analysis was performed using student t-test (A-C) and Mann-Whitney U test (D-F). *$p < 0.05$

	WT	*Tst* $^{-/-}$
n	4	5
Phosphate	1.42 ± 0.28	2.48 ± 0.37
Calcium	3.57 ± 1.86	6.45 ± 2.12

Table 4-1 Urinary phosphate and calcium excretion are comparable between groups

Mean 24hour urinary phosphate and chloride excretion from *Tst*$^{-/-}$ and C57BL/6N wild type mice over a 2day post-acclimatisation period. Values were corrected for total urinary volume in a 24hr period. Data are mean ± SEM.

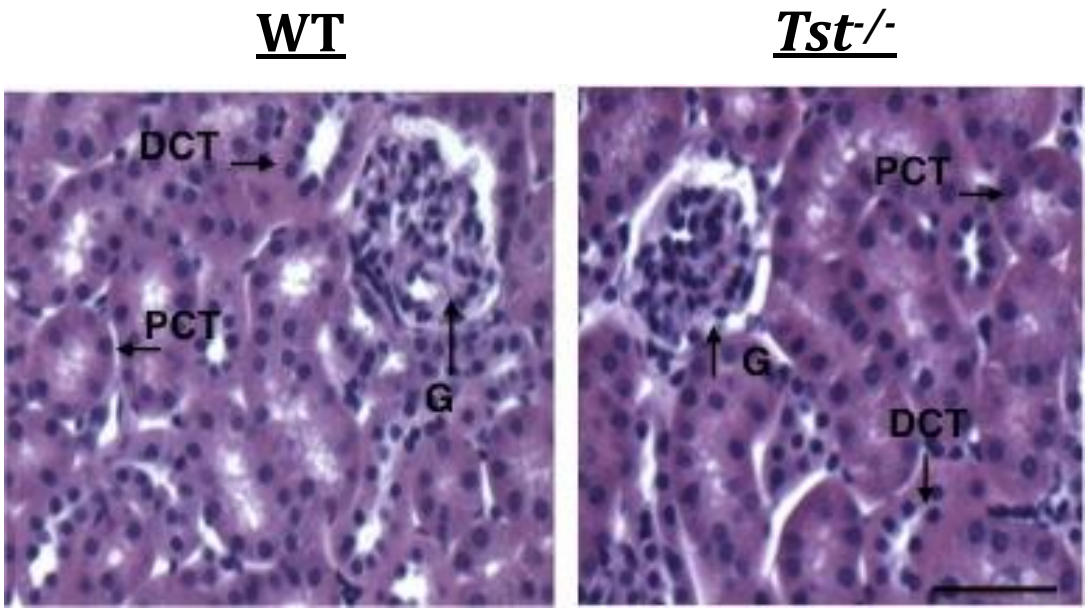

Figure 4-4 *Tst-/-* mice have normal kidney morphology

Representative haematoxylin and eosin stained kidney tissue of *Tst*$^{-/-}$ and C57BL/6N wild type mice (WT, n=4, *Tst*$^{-/-}$, n =5). Abbreviations*, G (glomerulus), PCT (proximal convoluted tubule, DCT (distal convoluted tubule).* Scale bar is 20µm.

4.3.4 *Tst*$^{-/-}$ mice have altered eNOS expression in aorta

Western blots performed on aorta showed that protein levels of P-eNOS^{Ser1177} were higher in *Tst*$^{-/-}$ mice but total eNOS protein levels were comparable between groups (Figure 4-5).

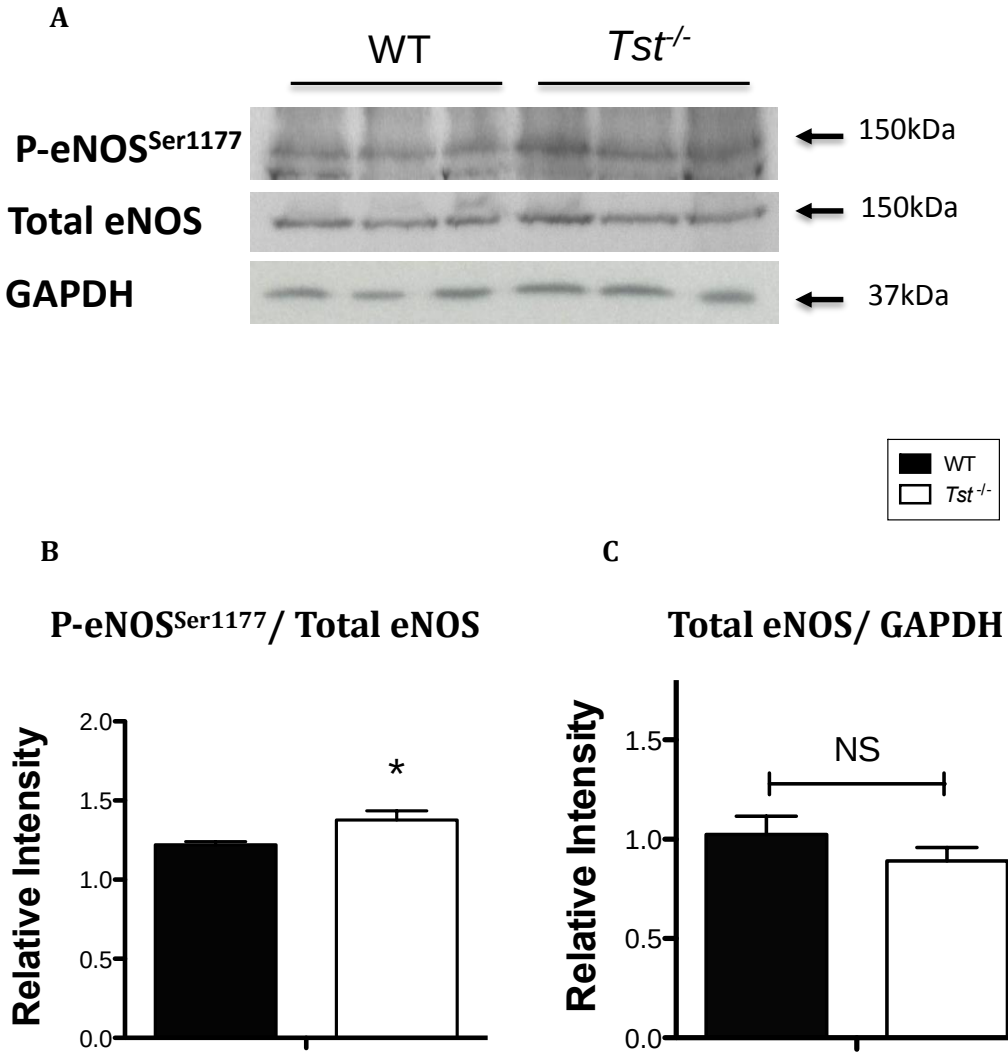

Figure 4-5 eNOS signalling is elevated in aorta of *Tst*$^{-/-}$ mice

A) Representative immunoblot and densitometric analysis showing (B) phosphorylation of eNOS at the Serine1177 residue (P-eNOS^{Ser1177}) and (C) total eNOS in naïve aortic tissue (WT; n=5, *Tst*$^{-/-}$; n=6). Data presented as relative intensity of protein expression when normalised to total eNOS (A) or GAPDH (B) and then normalised to level of C57BL/6N controls. Values are expressed as mean±SEM. *p < 0.05

4.3.5 Isolated vessels from WT and *Tst*$^{-/-}$ mice have similar responses to the α1-adrenergic agonist, PE

Cumulative addition of phenylephrine (PE) to isolated endothelium intact aorta and mesenteric arteries from WT and *Tst*$^{-/-}$ mice caused dose-dependent contraction (Figure 4-6). The response of aorta and mesenteric arteries to PE was similar between groups at all concentrations (Figure 4-6, Table 4-2).

4.3.6 *Tst*$^{-/-}$ vessels have mild endothelial dysfunction in small mesenteric arteries

Vessel pre-constriction with PE to 80% of maximal constriction (EC80) was equivalent in aorta and mesenteric arteries from WT and *Tst*$^{-/-}$ mice for all interventions.

Cumulative addition of ACh (Figure 4-7) or SNP (Figure 4-8) to isolated aortas and mesenteric arteries cause dose-dependent relaxation. The response to the endothelial dependent cholinergic receptor agonist ACh was comparable in aorta from WT and *Tst*$^{-/-}$ mice (Figure 4-7). There were no differences between groups for ACh EC_{50} or E_{max} (maximal relaxation) (Table 4-2). The responses to the endothelium independent, vascular smooth muscle cell relaxant agent, SNP were also comparable between groups (Figure 4-8, Table 4-2).

Mesenteric vessels from *Tst*$^{-/-}$ mice were less responsive to ACh than WT controls (Figure 4-7) and there was a significant (P=0.015) increase in EC_{50} relative to WT (Table 4-2). The maximal relaxation induced by ACh was not different in mesenteric arteries of *Tst*$^{-/-}$ mice compared to WT controls (Table 4-2). The responses to SNP within mesenteric arteries were comparable between groups (Figure 4-8). EC_{50} and E_{max} of SNP in mesenteric arteries were similar in WT and *Tst*$^{-/-}$ mice (Table 4-2).

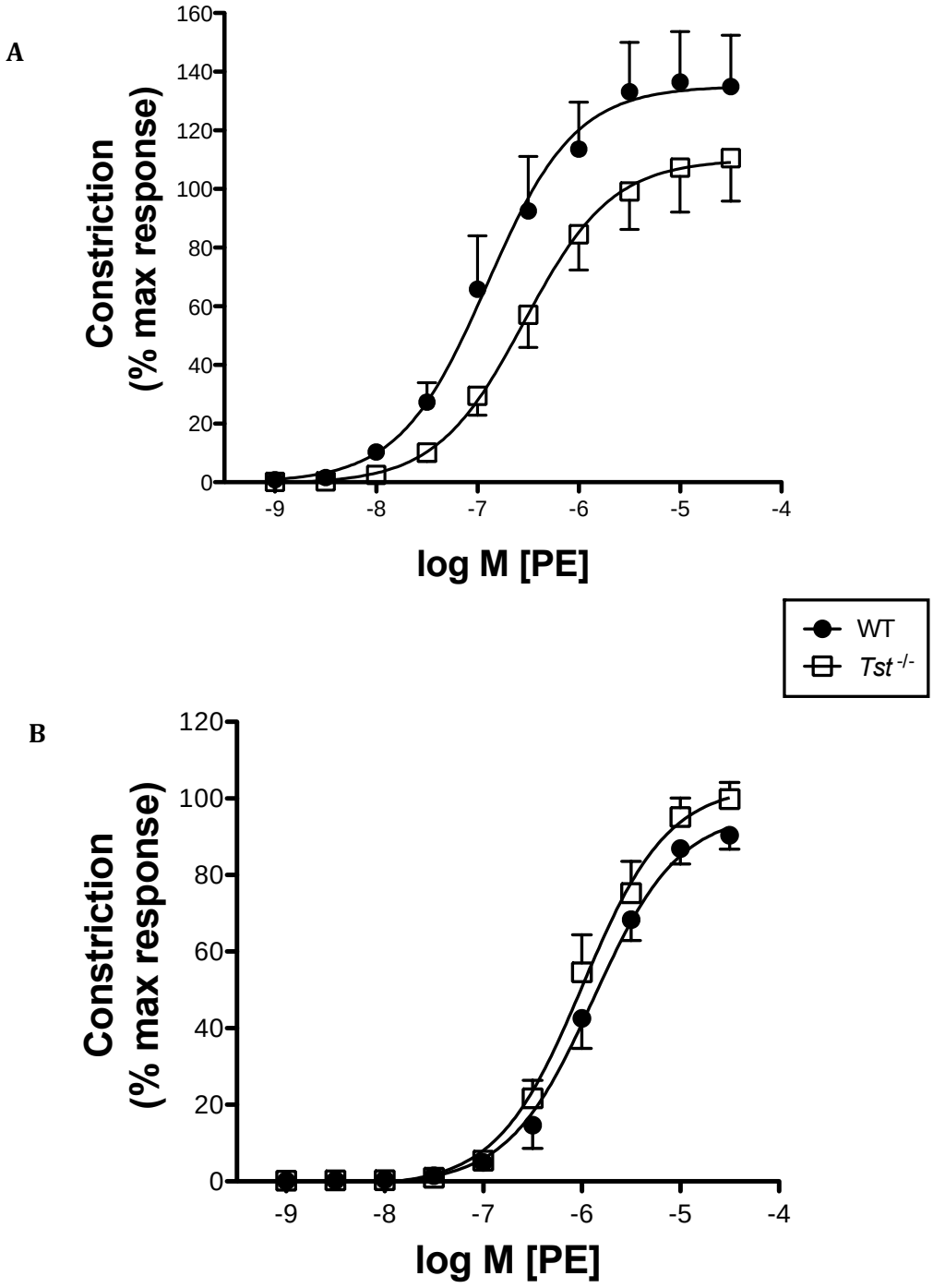

Figure 4-6 Contractile response to PE is normal in the vasculature of *Tst*$^{-/-}$ mice

Cumulative concentration response to PE ($1*10^{-9}$ – $3*10^{-5}$ M) in endothelial intact (A) aortic rings (n=6/ group) and (B) mesenteric artery rings (n=8/ group) isolated from C57BL/6N wild type and *Tst*$^{-/-}$ male mice. Vessel response to PE was expressed as percentage of maximal response to KPSS. Values are mean±SEM, analysed by 2-way ANOVA with Bonferroni post-hoc test. *Abbreviations; PE; phenylephrine*

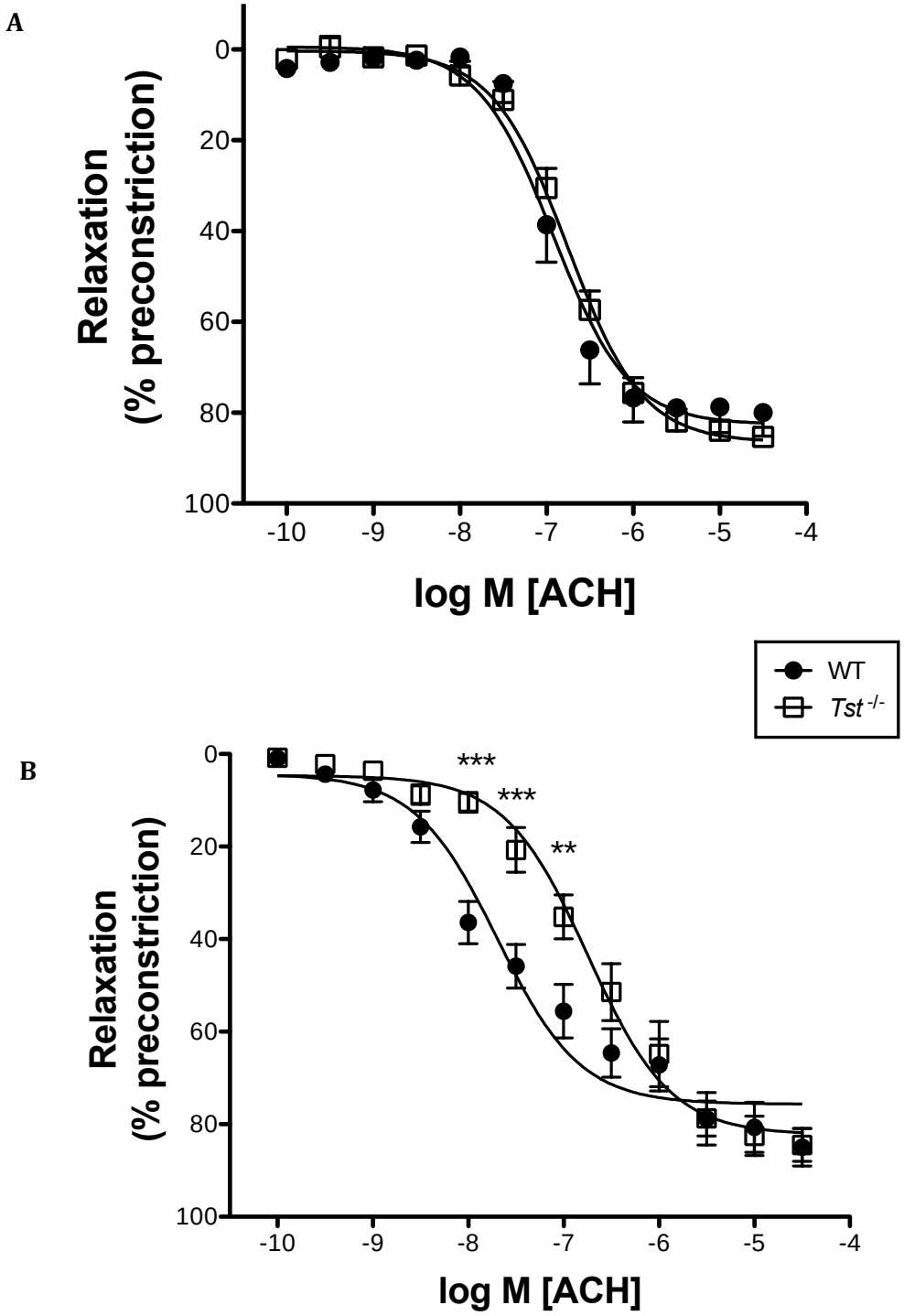

Figure 4-7 *Tst*$^{-/-}$ mice have mild endothelial dysfunction in small mesenteric arteries but not in aorta

Cumulative concentration response to Ach ($1*10^{-10}$ – $3*10^{-5}$ M) in endothelium intact (A) aortic rings (WT; n=5, *Tst*$^{-/-}$; n=7) and (B) mesenteric rings (WT; n=7, *Tst*$^{-/-}$; n=6) isolated from C57BL/6N wild type and *Tst*$^{-/-}$ male mice. Vessel response to ACh was expressed as percentage of vessel pre-constriction. Values are mean±SEM, analysed by 2-way ANOVA with Bonferroni post-hoc test. **p < 0.01, ***p < 0.001. *Abbreviations; ACh; acetylcholine.*

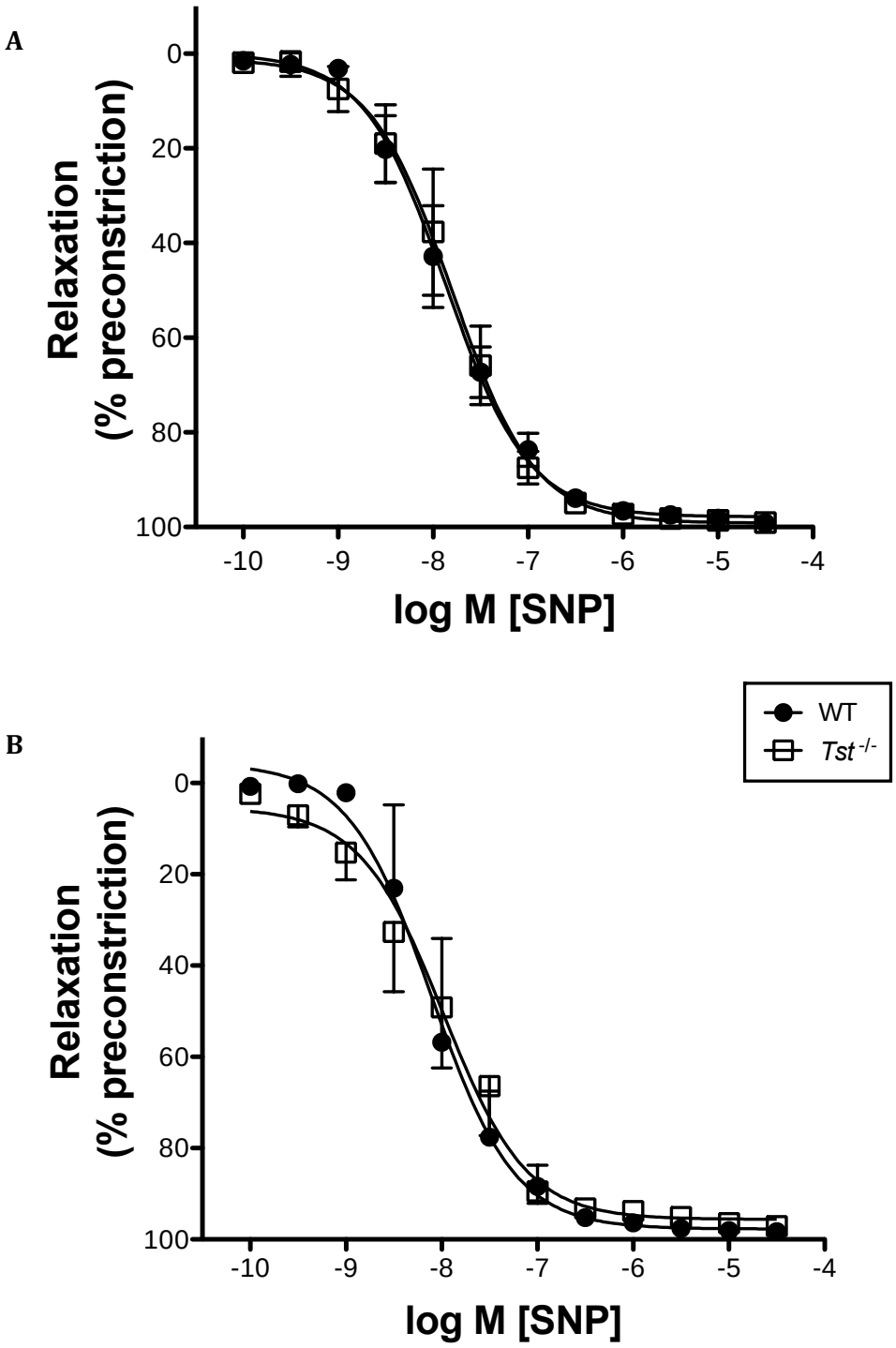

Figure 4-8 Relaxation response to nitric oxide donor, SNP is normal in the vasculature of *Tst*$^{-/-}$ *mice*

Cumulative concentration response to SNP ($1*10^{-10}$ – $3*10^{-5}$ M) in endothelium intact (A) aortic rings (WT; n=5, *Tst*$^{-/-}$; n=6) and (B) mesenteric rings (WT; n=3, *Tst*$^{-/-}$; n=6) isolated from C57BL/6N wild type and *Tst*$^{-/-}$ male mice. Vessel response to ACh was expressed as percentage of vessel pre-constriction. Values are mean±SEM, analysed by 2-way ANOVA with Bonferroni post-hoc test. *Abbreviations; SNP; sodium nitroprusside*

		Aorta		Mesentery	
		WT	*Tst* $^{-/-}$	WT	*Tst* $^{-/-}$
PE	n	6	6	8	8
	-logEC_{50} (M)	6.84 ± 0.20	6.51 ± 0.11	5.87 ± 0.12	5.96 ± 0.14
	E_{max} (% KPSS)	134.92 ± 17.5	110.53 ± 14.7	90.36 ± 3.62	99.58 ± 5.08
ACh	n	5	7	7	6
	-logEC_{50} (M)	6.91 ± 0.08	6.77 ± 0.08	7.5 ± 0.21	6.68 ± 0.21*
	E_{max} (% Relaxation)	80.05 ± 5.11	85.37 ± 2.05	85.01 ± 4.07	84.52 ± 3.53
SNP	n	5	6	3	6
	-logEC_{50} (M)	7.91 ± 0.15	7.83 ± 0.19	8.12 ± 0.26	8.10 ± 0.26
	E_{max} (% Relaxation)	99.21 ± 1.40	99.82 ± 1.12	98.34 ± 0.51	97.14 ± 0.72

Table 4-2 Contractile and relaxant responses of WT and *Tst*$^{-/-}$ mice

The EC_{50} (50% maximal constriction/ relaxation) and E_{max} (maximal constriction/ relaxation) were calculated for the contractile response to PE or relaxant response to ACh and SNP in endothelium intact aorta and mesenteric arteries isolated from C57BL/6N wild type and *Tst*$^{-/-}$ mice. Data are mean ± SEM. *p < 0.05; WT vs. *Tst*$^{-/-}$ in mesenteric arteries analysed by unpaired student t-test.

4.3.7 TST loss influences the basal release of NO and constrictor prostaglandins in the aorta

In the presence of the nitric oxide and cyclooxygenase inhibitors, LNAME and indomethacin, the maximal response to PE was only significantly increased in aortas from *Tst*$^{-/-}$ mice (Table 4-3). However, the IC50 for PE was not significantly changed by L-NAME and indomethacin in aortas isolated from WT and *Tst*$^{-/-}$ mice (Figure 4-9, Table 4-3).

4.3.8 NO and prostaglandins mediate endothelium dependent and independent vasodilatation in the aorta

Incubation with L-NAME and indomethacin reduced endothelium dependent relaxation to Ach (Figure 4-10). Maximal relaxation was reduced in both groups to a similar extent (Figure 4-10, Table 4-3). IC_{50} was not different between groups when pre-treated with L-NAME and Indomethacin (Table 4-3). In the presence of L-NAME and indomethacin, aortas from both WT and *Tst*$^{-/-}$ mice were both significantly more sensitive to the nitric oxide donor, SNP (Figure 4-10, Table 4-3). Maximal relaxation was not different within either group when comparing treated versus non-treated aortas (Table 4-3).

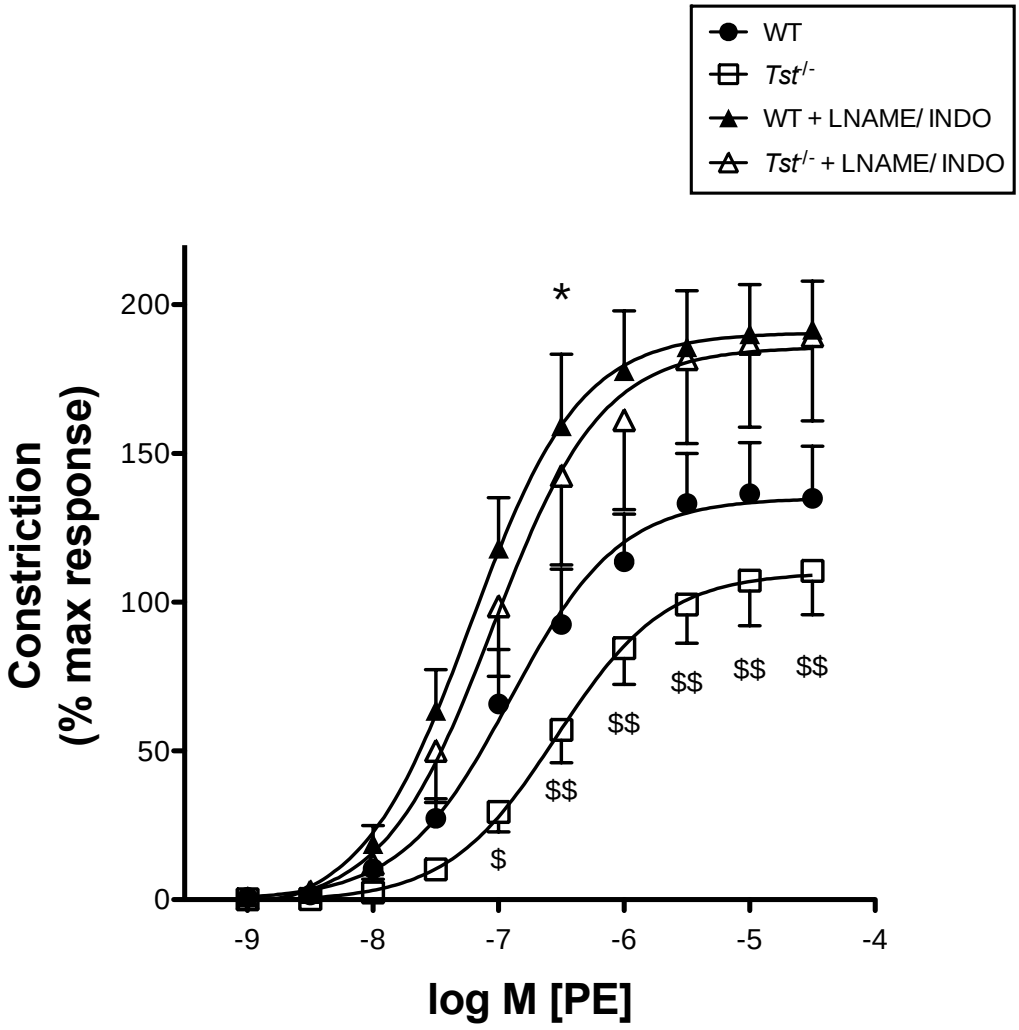

Figure 4-9 Nitric oxide and cyclooxygenase mediate the contractile response to PE in the aorta of WT and *Tst*$^{-/-}$ mice

Cumulative concentration response to PE ($1*10^{-9}$ – $3*10^{-5}$ M) in aortic rings pre-treated with LNAME (NO inhibitor) and indomethacin (cyclooxygenase inhibitor). Endothelium intact vessels were isolated from C57BL/6N wild type and *Tst*$^{-/-}$ mice (Non-treated; n=6/ group, Treated; WT; n=5, *Tst*$^{-/-}$; n=6). Vessel response to PE was expressed as percentage of maximal response to KPSS. Values are mean±SEM, analysed by 2-way ANOVA with Bonferroni post-hoc test. *$p < 0.05$ WT vs. WT [+] LNAME/ INDO. $; $p < 0.05$, $$; $p < 0.01$, *Tst*$^{-/-}$ vs. *Tst*$^{-/-}$ [+] LNAME/ INDO. *Abbreviations; PE; phenylephrine, LNAME; N(G)-nitro-L-arginine methyl ester, INDO; indomethacin.*

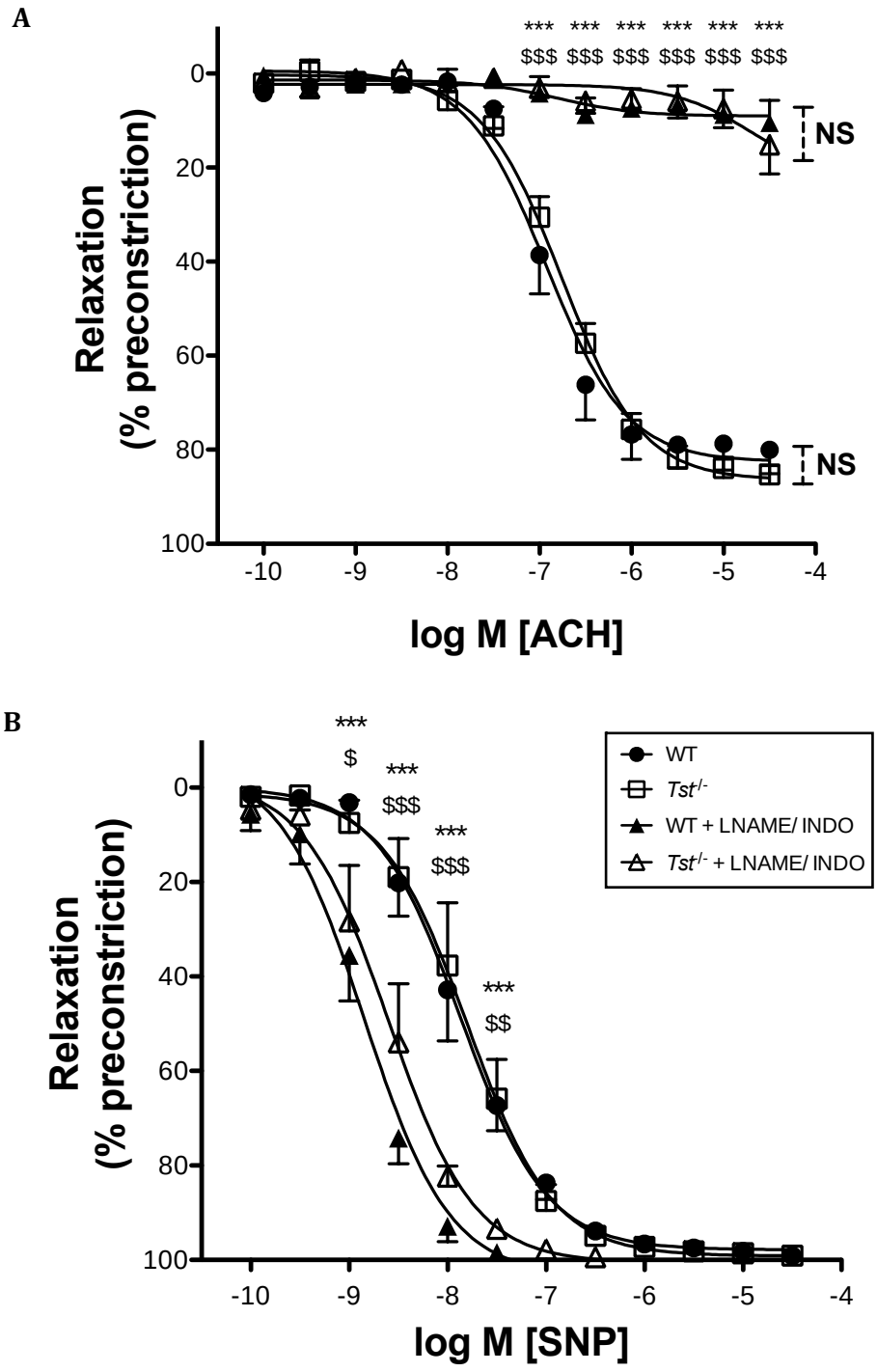

Figure 4-10 Nitric oxide and cyclooxygenase independent vasorelaxation in aortas of WT and *Tst*$^{-/-}$ mice

Cumulative concentration response to (A) ACh (Non-treated; WT; n=5, *Tst*$^{-/-}$; n=7, Treated; WT; n=4/ group) and (B) SNP (Non-treated; WT; n=5, *Tst*$^{-/-}$; n=6, Treated; n=5/ group) in aortic rings pre-treated with LNAME and indomethacin. Endothelium intact vessels were isolated from C57BL/6N wild type and *Tst*$^{-/-}$ mice. Vessel response to ACh and SNP were expressed as percentage of vessel pre-constriction. Values are mean±SEM, analysed by 2-way ANOVA with Bonferroni post-hoc test. ***$p < 0.001$ WT vs. WT [+] LNAME/ INDO. $; $p < 0.05$, $$; $p < 0.01$, $$$; $p < 0.001$ *Tst*$^{-/-}$ vs. *Tst*$^{-/-}$ [+] LNAME/ INDO

		WT		*Tst* $^{-/-}$	
		[-] LN/ INDO	[+] LN/ INDO	[-] LN/ INDO	[+] LN/ INDO
PE	n	6	5	6	6
	-logIC_{50} (M)	6.84 ± 0.20	7.21 ± 0.13	6.51 ± 0.11	7.02 ± 0.16
	E_{max} (% KPSS)	134.92 ± 17.5	191.78 ± 16.15	110.53 ± 14.7	189.43 ± 28.48*
ACh	n	5	4	7	4
	-logIC_{50} (M)	6.91 ± 0.08	6.12 ± 0.69	6.77 ± 0.08	6.42 ± 0.39
	E_{max} (% Relaxation)	80.05 ± 5.11	10.52 ± 4.77***	85.37 ± 2.05	15.22 ± 6.16***
SNP	n	5	5	6	5
	-logIC_{50} (M)	7.91 ± 0.15	8.90 ± 0.13**	7.83 ± 0.19	8.68 ± 0.17**
	E_{max} (% Relaxation)	99.21 ± 1.40	99.69 ± 1.11	99.82 ± 1.12	102.83 ± 0.30

Table 4-3 Intra-group analyses of the contractile or relaxant response in the aortas of WT and *Tst*$^{-/-}$ mice pre-treated with or without L-NAME and indomethacin

The IC_{50} and E_{max} (maximal constriction/ relaxation) were calculated for the contractile response to PE or relaxant response to ACh and SNP in endothelium intact aorta isolated from wild type and *Tst*$^{-/-}$ mice pre-incubated with [+] or without [-] LNAME and indomethacin. Data are mean ± SEM analysed by 2way non-repeated measures ANOVA. *p<0.05, **p<0.01, ***p<0.001 when comparing within genotype of treated versus non-treated aortas. *Abbreviations; LN; LNAME, INDO; indomethacin.*

4.3.9 Small and intermediate calcium activated potassium channels do not regulate constriction in small mesenteric arteries from WT or *Tst*$^{-/-}$ mice

The constrictor response to PE was unchanged in mesenteric arteries when pre-incubated with inhibitors of the small (SK_{Ca}) and intermediate calcium activated potassium channels (IK_{Ca}), apamin and charybdotoxin (Figure 4-11, Table 4-4).

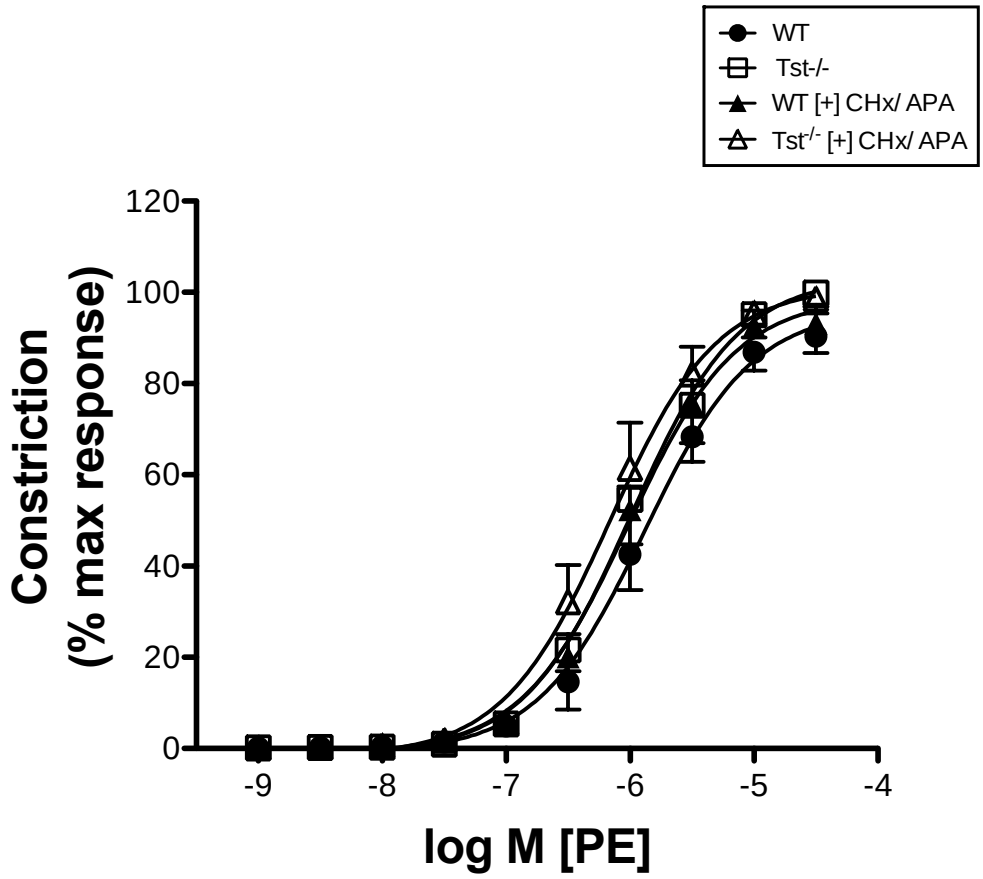

Figure 4-11 SK_{Ca} and IK_{Ca} channels do not mediate the contractile response to PE in the mesenteric arteries of WT and *Tst*$^{-/-}$ mice

Cumulative concentration response to PE in mesenteric rings pre-treated with apamin (SK_{Ca} inhibitor) and charybdotoxin (IK_{Ca} inhibitor). Endothelium intact vessels were isolated from C57BL/6N wild type and *Tst*$^{-/-}$ mice (Non-treated; n=8/ group, Treated; WT; n=7, *Tst*$^{-/-}$; n=5). Vessel response to PE was expressed as percentage of maximal response to KPSS. Values are mean±SEM, analysed by 2-way ANOVA. *Abbreviations; CHx, Charybdotoxin, APA; Apamin*.

4.3.10 Small and intermediate calcium activated potassium channels have an increased role in relaxation of small mesenteric arteries from *Tst*$^{-/-}$ mice

Incubation with apamin and charybdotoxin revealed a difference in the contribution of small and intermediate potassium channels to ACh induced relaxation in small mesenteric arteries (Figure 4-12). The ACh IC_{50} was significantly increased by apamin and charybdotoxin in mesenteric arteries of *Tst*$^{-/-}$ mice compared to WT (Figure 4-12, Table 4-4). While the maximum response to ACh was reduced by apamin and charybdotoxin in mesenteric vessels from *Tst*$^{-/-}$ mice (Figure 4-12, Table 4-4, P=0.019), this was unaffected in mesenteric vessels from control mice (Appendix 5).

In the presence of apamin and charybdotoxin there was evidence of a leftward shift of the SNP dose response curve in mesenteric vessels from *Tst*$^{-/-}$ mice compared to WT (Figure 4-13). However, whist SNP IC50 values tended to be lower in treated *Tst*$^{-/-}$ compared to treated WT vessels, these were not statistically different in the small sample groups (n=3/ group) tested (Table 4-4, P=0.26).

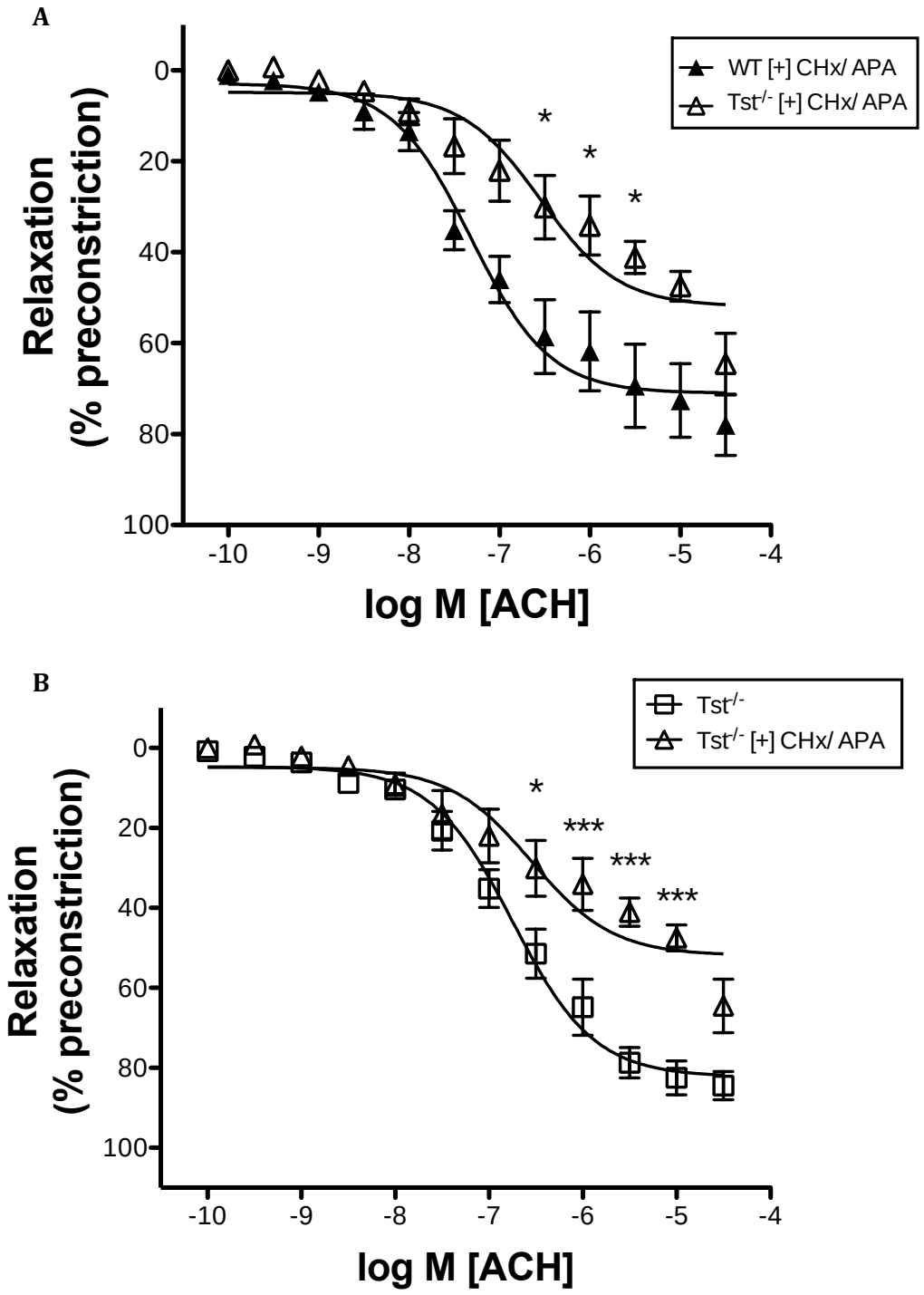

Figure 4-12 SK_{Ca} and IK_{Ca} channels mediate the relaxant response to ACh to a greater extent in *Tst*$^{-/-}$ mesenteric arteries

A) Cumulative concentration response to ACh in endothelial intact mesenteric rings of wild type and *Tst*$^{-/-}$ mice when pre-treated with apamin (SK_{Ca} inhibitor) and charybdotoxin (IK_{Ca} inhibitor) (WT; n=5, *Tst*$^{-/-}$; n=3). B) Comparative response to ACh in mesenteric vessels of *Tst*$^{-/-}$ mice when incubated with or without apamin and charybdotoxin (Non-treated; *Tst*$^{-/-}$; n=6, *Tst*$^{-/-}$ [+] CHx/ APA; *Tst*$^{-/-}$; n=3). Vessel response to ACh was expressed as percentage of vessel pre-constriction. Values are mean±SEM, analysed by 2-way ANOVA with Bonferroni post-hoc test. *$p < 0.05$, ***$p<0.001$.

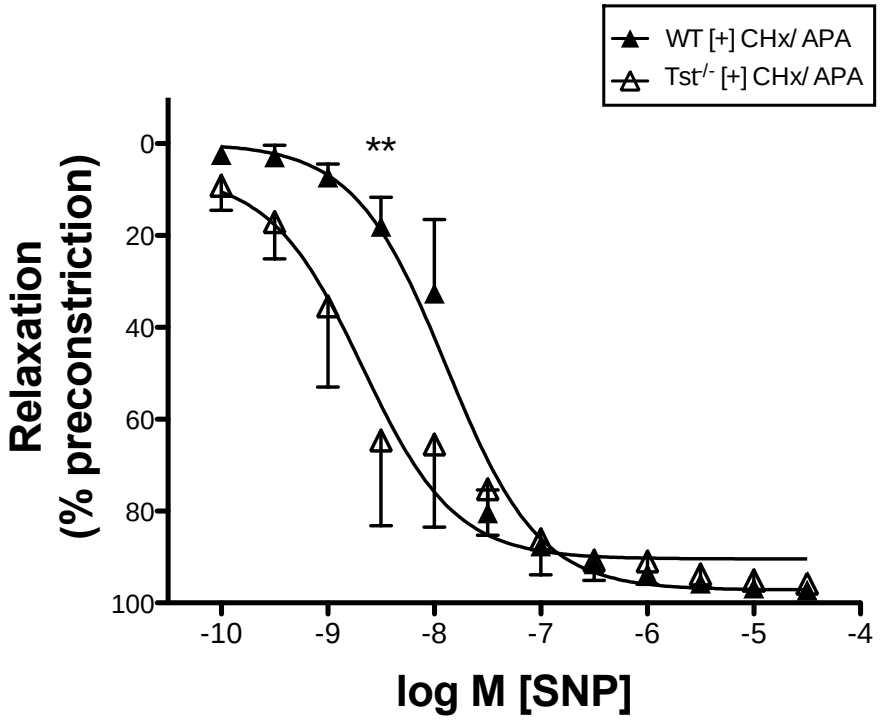

Figure 4-13 SK_{Ca} and IK_{Ca} mediate the relaxant response to SNP to a greater extent in *Tst*$^{-/-}$ mice

Cumulative concentration response to SNP in endothelial intact mesenteric rings of wild type and *Tst*$^{-/-}$ mice when pre-treated with apamin (SK_{Ca} inhibitor) and charybdotoxin (IK_{Ca} inhibitor) (n=3/ group). Vessel response to SNP was expressed as percentage of vessel pre-constriction. Values are mean±SEM, analysed by 2-way ANOVA with Bonferroni post-hoc test. **$p < 0.01$

		WT		*Tst* $^{-/-}$	
		[-] CHx/ APA	[+] CHx/ APA	[-] CHx/ APA	[+] CHx/ APA
PE	n	8	7	8	5
	-logIC_{50} (M)	5.87 ± 0.12	6.01 ± 0.08	5.96 ± 0.14	6.13 ± 0.15
	E_{max} (% KPSS)	90.36 ± 3.62	93.21 ± 3.65	99.58 ± 5.08	98.52 ± 1.99
ACh	n	7	5	6	3
	-logIC_{50} (M)	7.5 ± 0.21	7.3 ± 0.09	6.68 ± 0.21*	6.34 ± 0.44*
	E_{max} (% Relaxation)	85.01 ± 4.07	78.09 ± 6.64	84.52 ± 3.53	64.58 ± 6.67$^{\$}$
SNP	n	3	3	6	3
	-logIC_{50} (M)	8.12 ± 0.26	7.92 ± 0.12	8.10 ± 0.26	8.62 ± 0.53
	E_{max} (% Relaxation)	98.34 ± 0.51	97.24 ± 0.66	97.14 ± 0.72	95.87 ± 1.72

Table 4-4 Intra-group analyses of the contractile or relaxant response in the mesenteric arteries of *Tst*$^{-/-}$ mice pre-treated with and without Apamin and Charybdotoxin

The IC_{50} and E_{max} (maximal constriction/ relaxation) were calculated for the contractile response to PE or relaxant response to ACh in endothelium intact aorta isolated from WT and *Tst*$^{-/-}$ mice pre-incubated with [+] or without [-] apamin and charybdotoxin. Data are mean ± SEM analysed by 2way non-repeated measures ANOVA. *p<0.05 when comparing between genotypes of same treatment. $^{\$}$p<0.05 when comparing within genotype of treated versus non-treated vessels. *Abbreviations; CHx, Charybdotoxin, APA; Apamin*

4.4 Discussion

The vasorelaxant and blood pressure lowering effects of H_2S are well documented (Geng, Yang *et al.*, 2004b; Yang *et al.*, 2008; Zhao *et al.*, 2001). Circulating H_2S levels were found to be increased in *Tst*$^{-/-}$ mice (Chapter 3) and it was hypothesised that blood pressure would be reduced in these mice. Surprisingly this was not the case. However multiple alterations in the vascular and renal mechanisms regulating blood pressure have been identified in mice lacking TST, supporting a role for this pathway in the global control of blood pressure.

Blood pressure is regulated in part by peripheral resistance but the primary mechanism for long-term blood pressure regulation is through regulation of electrolyte-fluid homeostasis by the kidney. The kidneys tightly regulate sodium reabsorption via several sodium exchangers along the nephron, thus determining the volume of water to be reabsorbed to maintain plasma osmolality. Whilst several studies have shown that H_2S reduces blood pressure via vasorelaxation, few studies have investigated the role of electrolyte-fluid handling in the kidney.

TST plays a role in electrolyte-fluid handling in the kidney

The H_2S synthesising enzymes, CSE, CBS and 3MST have all been localised to the proximal convoluted tubule (PCT), the site for the majority of electrolyte and fluid reabsorption within the nephron (Nagahara *et al.*, 1998; Yamamoto *et al.*, 2012). Acute administration of NaHS or the H_2S synthetic enzyme substrate, L-cysteine to the left renal artery of rats dose dependently increased glomerular filtrate rate, urinary flow rate and urinary excretion of sodium and potassium but had no effect on urinary pH or mean arterial blood pressure (Xia *et al.*, 2009). Administration of the CBS or CSE inhibitors, AOAA or PPG to the left renal artery dose dependently decreases electrolyte and fluid loss (Xia *et al.*, 2009) showing that endogenous H_2S plays a role in tubular electrolyte-fluid handling. Although mean arterial blood pressure was not affected by tubular sodium and water losses, these studies were performed acutely and it is likely compensatory regulatory channels were acutely activated to maintain normotension. TST is highly expressed in the kidneys (Sylvester *et al.*, 1990) and has been localised to the renal PCT, but not the distal convoluted tubule (Sylvester *et al.*, 1990). In *Tst*$^{-/-}$ kidneys, protein levels of CSE and CBS are higher whilst mRNA levels of *Sqr-dl*, *Ethe1* and *Suox* tend to be lower than in WT mice (see section 3.3.6.1). The rate of H_2S breakdown is decreased by 50% in liver of *Tst*$^{-/-}$ mice. Although H_2S breakdown assays were not performed on kidney samples of *Tst*$^{-/-}$ mice, it is expected that the rate of H_2S breakdown is reduced given comparable TST protein expression and enzyme activity in

murine kidney and liver tissues (Nagahara *et al.*, 1998). Furthermore, *Tst*$^{-/-}$ mice have increased levels of circulating H_2S, and kidney CSE expression indicating local H_2S generation was also increased (see section 3.3.6.3 and 3.3.10). Together these data suggest that *Tst*$^{-/-}$ kidneys are exposed to higher levels of circulating and endogenous H_2S, which may not be efficiently catabolised. In the current study, metabolic cage experiments showed that *Tst*$^{-/-}$ mice are polydipsic, polyuric and excrete more sodium, potassium, chloride in their urine compared to wild type controls. The observed natriuretic and diuretic data are consistent with findings from Xia and colleagues (Xia *et al.*, 2009) and indicates that TST contributes to regulation of tubular electrolyte fluid handling, likely via regulation of H_2S availability in the PCT.

The Na^+/ K^+-ATPase pump is present in the basolateral membranes of PCT, TALH and the distal convolute tubules (DCT) and is critical in producing the electrochemical gradient necessary for the active movement of electrolytes from the filtrate into the cell (as outlined in section 1.1.5.3)(Amirlak *et al.*, 2000). Water reabsorption via AQP1 and 7 channels are dependent on this process. Inhibition of the Na^+/ K^+-ATPase with Ouabain or Bufalin, reduces Na^+/ K^+-ATPase activity and increases glomerular filtrate rate (GFR) and urinary sodium and potassium excretion in isolated perfused rat kidneys (Arnaud-Batista *et al.*, 2012; Cherniavsky-Lev *et al.*, 2014). *In vitro* studies performed on isolated renal basolateral membranes from rats showed that NaHS dose dependently reduced Na^+/ K^+-ATPase activity with 19% inhibition observed with 1μM NaHS treatment (Xia *et al.*, 2009). Inhibition of the Na^+/ K^+-ATPase activity with NaHS occurs via internalisation of the pump from the membrane to the cytosol (Ge *et al.*, 2014). Indeed, reduced Na^+/ K^+-ATPase activity in the PCT would explain why sodium, phosphate, potassium, calcium and water excretion is higher in *Tst*$^{-/-}$ mice. Localisation of TST at the PCT (Sylvester *et al.*, 1990) indicates that such inhibitory actions would be tightly regulated by H_2S breakdown. However in *Tst*$^{-/-}$mice, high circulating H_2S levels, locally elevated H_2S production by CSE and reduced H_2S breakdown in the kidney may inhibit Na^+/ K^+-ATPase activity in the PCT and impair reabsorption of electrolyte and water. Future studies should investigate Na^+/ K^+-ATPase activity in isolated basolateral membranes from *Tst*$^{-/-}$ kidneys. Additionally, microperfusion studies are required to confirm if sodium handling is impaired in the PCT of *Tst*$^{-/-}$ mice. As the Na^+/ K^+-ATPase pump is also present in the TALH and DCT, which are responsible for 20-25% of NaCl reabsorption from filtrate (Mullins *et al.*, 2006), it seems possible that increased H_2S in filtrate of *Tst*$^{-/-}$ mice may also reduce reabsorption at these regions of the nephron by diffusing through apical membranes. This may explain why electrolyte-fluid

malreabsorption in the PCT is not effectively compensated downstream. More in-depth examination of these regions using microperfusion techniques is warranted.

Sodium and water losses decrease extracellular fluid volume, which acutely activate several neurohormonal systems to increase vascular tone and enhance reabsorption of sodium and water in the kidney (McKinley *et al.*, 2004). The renin angiotensin aldosterone system (RAAS) is acutely activated and vasopressin released to reabsorb more sodium and water along the nephron (Mullins *et al.*, 2006). However, the brain eventually corrects for sodium and water deficits by changes in behaviour, namely by increased ingestion of sodium (i.e. salt appetite) and the stimulation of thirst (McKinley *et al.*, 2004). Osmoreceptors in the brain and neural inputs from cardiac baroreceptors detect small changes in plasma osmolality and hypovolemia respectively and are actively engaged with the central nervous system to maintain blood volume and osmolality through behaviour change (McKinley *et al.*, 2004). *Tst*$^{-/-}$ mice compensate for electrolyte and water losses by increasing food intake (Appendix 2) and water intake to remain in electrolyte and water balance indicating that their behaviour has been altered to offset losses in the kidney. Plasma renin concentrations were comparable between groups (Appendix 3) suggesting that sodium and water losses had occurred for extended periods of time. In a separate study performed by Clare McFadden in the Morton lab, *Tst*$^{-/-}$ mice also drank more water than wild type controls when singly housed in regular cages for an 8-day period, confirming the polydipsic phenotype (unpublished data, Appendix 4). As the RM1 diet not only contains sodium but all necessary electrolytes required, increased appetite in *Tst*$^{-/-}$ mice restored sodium, potassium and chloride balance. Due to time restraints, neither aldosterone nor vasopressin have been measured in *Tst*$^{-/-}$ mice and should be performed in future.

Tst$^{-/-}$ *mice have altered eNOS expression in aorta*

Small resistance arteries play a significant role in the development of hypertension (Intengan *et al.*, 2000). Impaired endothelium-dependent relaxation in small resistance arteries and arterioles reduces the lumen diameter leading to increased peripheral resistance and blood pressure (Intengan *et al.*, 2000). The aorta is a large conductance artery and therefore makes little contribution to peripheral resistance or blood pressure maintenance. However, the isolated aorta provides a good model for characterisation of endothelial function, in particular where this is focused on nitric oxide (NO), as this gasotransmitter is an important mediator of aortic relaxation. In the present study, the aorta was selected to permit interrogation of H_2S-NO crosstalk. While vasorelaxation of the aorta is largely NO and

cyclooxygenase (COX) dependent, H_2S has previously been shown to account for up to 25% of vasorelaxation in endothelium intact murine aorta (Hosoki *et al.*, 1997).

The current study showed that *Tst*$^{-/-}$ mice have increased P-eNOS^{Ser1177} protein expression but no difference in total eNOS expression in naïve aortas compared to controls, suggesting increased bioavailability of NO. These data are reminiscent of those recently reported in the myocardium of CSE knockout (*Cse*$^{-/-}$) mice that have reduced H_2S availability. The myocardium of *Cse*$^{-/-}$ mice was reported to have reduced myocardial P-eNOS^{Ser1177} but total eNOS protein comparable to wild type controls (King *et al.*, 2014). This was accompanied by reduced levels of cardiac and plasma NO metabolites. Furthermore, administration of H_2S donors to *Cse*$^{-/-}$ mice increased myocardial P-eNOS^{Ser1177} and NO availability compared to vehicle treated mice but also had no effect on total eNOS protein expression (King *et al.*, 2014). These data indicate that eNOS activity (P-eNOS^{Ser1177}) rather than eNOS abundance per se is targeted by H_2S to alter NO availability. However it remains unclear how H_2S increases eNOS activity and NO availability and is an active area of research within the field. NO bioavailability was not directly measured in the present study but together the data would suggest that it would be increased in vessels from *Tst*$^{-/-}$ mice, secondary to increased H_2S availability. H_2S availability could be influenced by increased circulating H_2S levels in *Tst*$^{-/-}$mice, but also by locally reduced H_2S breakdown in the endothelium. TST is expressed in whole aorta homogenates and in isolated CD31+ endothelial cells from aorta and small intramuscular vessels of the murine hind limb of C57BL/6J mice (Chapter 3). These data support a role for TST as an indirect regulator of eNOS activity via reduced H_2S breakdown and helps explain why P-eNOS^{Ser1177} is increased in aortas from *Tst*$^{-/-}$ mice.

In functional myography studies, loss of TST had no direct impact upon PE-induced vasoconstriction, which was also found by Matt Gibbins in the Morton group (unpublished data). However, importantly, inhibition of nitric oxide synthase by L-NAME and indomethacin revealed a potentially increased contribution of NO and/or COX metabolites to regulation of contraction in arteries from *Tst*$^{-/-}$ mice. These data may indicate that NO availability is higher in *Tst*$^{-/-}$aortas, consistent with increased P-eNOS^{Ser1177} findings. Due to time constraints, the current study did not measure the H_2S content or expression of H_2S synthetic enzymes in *Tst*$^{-/-}$ aortas and as such, it is unknown what contribution these may have made to the observed outcomes. Further studies should assess H_2S production and the expression profile of the H_2S synthetic enzymes in aorta to fully elucidate this.

The data presented here provide further evidence for significant tissue specific crosstalk between H_2S and eNOS, which is likely influenced by TST-mediated H_2S breakdown within the aortic endothelium. As previous reports have localised CSE in the endothelium of the aorta, it is likely that TST's primary role in this cell type is to prevent locally produced H_2S or circulating H_2S from inhibiting mitochondrial respiration. Future studies should measure the rate of H_2S breakdown in isolated aortic endothelial cells from *Tst*$^{-/-}$ mice.

Tst$^{-/-}$ *mice have mild endothelial dysfunction in small mesenteric arteries*

Resistance in small arterioles plays a major role in blood pressure maintenance (Intengan *et al.*, 2000). Relaxation of the mesenteric arteries involves H_2S and is largely NO and COX independent (Mustafa *et al.*, 2011). H_2S is released in these arteries in response to mobilisation of intracellular Ca^{2+} by ACh, causing calmodulin activation and stimulation of Ca^{2+} -calmodulin sensitive CSE (Yang *et al.*, 2008). ACh-induced H_2S generation causes hyperpolarisation of endothelial cells by activating of small and intermediate calcium activated potassium channels (SK_{Ca} and IK_{Ca}) channels and also activates ATP-sensitive potassium (K_{ATP}) channels in vascular smooth muscle causing vasorelaxation in mesenteric arteries of mice (as outlined in section 1.1.5.5, Figure 1.7) (Mustafa *et al.*, 2011; Paul *et al.*, 2012). Inhibition of SK_{Ca} and IK_{Ca} channels with apamin and charybdotoxin attenuates hyperpolarisation in isolated aortic endothelial cells of mice and partially reduces NaHS mediated vasorelaxation in isolated mesenteric arteries (Mustafa *et al.*, 2011). In endothelial cells isolated from aorta of *Cse*$^{-/-}$ mice, ACh-mediated hyperpolarisation is abolished and is associated with reduced H_2S-mediated activation of SK_{Ca} and IK_{Ca} channels in endothelium, contributing to their vascular dysfunction and hypertension (Mustafa *et al.*, 2011). Studies with apamin and charybdotoxin in the present study reveal an enhanced contribution of the SK_{Ca} and IK_{Ca} channels to relaxation in small arteries from *Tst*$^{-/-}$mice, potentially caused by increased local H_2S availability. TST is expressed in endothelial cells of small intramuscular vessels of the hindlimb suggesting that enhanced SK_{Ca} and IK_{Ca} channel activation in small mesenteric arteries of *Tst*$^{-/-}$mice is indirectly caused by reduced H_2S breakdown in the endothelium. However, maximal relaxation to ACh in these arteries was not enhanced and sensitivity was, if anything, reduced. Further compensatory mechanisms may therefore be engaged in these arteries and this merits further investigation.

As H_2S-induced SK_{Ca} and IK_{Ca} channel activation only constitutes 10-20% of total NaHS mediated vasorelaxation in rat mesenteric arteries (Mustafa *et al.*, 2011), the answer likely lies in how the other H_2S-sensitive channels function. Activation of K_{ATP} channels in

vascular smooth muscle cells mediates ≈70% of NaHS- induced vasorelaxation in mesenteric arteries (Mustafa *et al.*, 2011). Upon cholinergic stimulation, CSE-produced H_2S diffuses to smooth muscle and activates K_{ATP} channels, permitting potassium entry into the cell causing smooth muscle relaxation and vasodilatation (as detailed in section 1.1.10, Figure 1.7). Administration of the K_{ATP} channel blocker glibenclamide attenuates NaHS-mediated vasorelaxation (Mustafa *et al.*, 2011; Zhao *et al.*, 2001). Reduced H_2S levels in *Cse*$^{-/-}$ mice prevents K_{ATP} channel opening and is thought to underlie the majority of their vascular dysfunction and hypertension (Mustafa *et al.*, 2011). K_{ATP} channel inhibitor studies were attempted on wild type and *Tst*$^{-/-}$mesenteric arteries in the present study. However, pre-incubation with glibenclamide (dissolved in 0.1 and 0.01% DMSO in PSS) prevented stable PE pre-constrictions at EC80 and spontaneous relaxations meant that neither ACh nor SNP curves could not be performed. Unfortunately it was not possible to optimise this protocol within the time available for the resent study. However, as the maximal response to ACh is comparable between non-treated WT and *Tst*$^{-/-}$mesenteric arteries, it is expected that K_{ATP} channels are not affected in this model.

NO and COX mediate ≈10% of the maximal response to ACh in small mesenteric arteries. Whilst responses to SNP were comparable between non-treated WT and *Tst*$^{-/-}$ mesenteric vessels, sensitivity to SNP was enhanced in *Tst*$^{-/-}$vessels when pre-treated with apamin and charybdotoxin. These data may indicate an increase in the sensitivity of guanylate cyclase that could have resulted from a change in its activation by endogenous NO. These mechanisms and the role of H_2S-NO crosstalk require further investigation. H_2S has also been shown to activate Kv7 voltage activated potassium channels in arterial smooth muscle of rat aortic rings (Martelli *et al.*, 2013). Whilst outside the scope of the current study, it is possible that these channels are responsible for the observed mild endothelial dysfunctional phenotype in *Tst*$^{-/-}$mesenteric vessels and this should also be examined in the future. Additionally, its possible that the high circulating H_2S concentrations found in *Tst*$^{-/-}$ mice harms the endothelium and lack of TST in endothelium prevents efficient H_2S removal. Electron microscopy should be performed on isolated small mesenteric arteries and resistance arterioles to investigate if the structure of the endothelium is damaged.

Despite the severe endothelial dysfunction observed in mesenteric arteries of *Cse*$^{-/-}$ mice (<25% maximal response to methacholine), systolic blood pressure is only increased by 15-20mmHg compared to controls. These data indicate that modulation of other regulatory systems prevents a more severe hypertensive phenotype, possibly via kidney sodium-fluid handling.

The results presented here suggest that TST plays a relatively minor role in regulating vascular function, likely via modulation of H_2S availability and cross talk with NO. In the aorta the contribution of NO appears to be enhanced in mice lacking TST, potentially through reduced H_2S breakdown in the endothelium. In small mesenteric arteries, there is mild endothelial dysfunction and sensitivity to NO is enhanced through a mechanism that may involve activation of endothelial K^+ channels, but this remains to be defined. These effects may be due to reduced H_2S breakdown by TST in the endothelium, but could also be secondary to increased circulating H_2S or to changes in local H_2S production. Higher levels of H_2S may cause direct cytotoxicity and endothelial damage. Meanwhile, increased water and electrolyte excretion in *Tst*$^{-/-}$ mice suggest that TST is involved in tubular function, especially within the PCT and possibly the TALH. TST may therefore be a potential future diuretic drug target but in depth *ex vivo* and *in vivo* studies are required to accurately localise its site and mechanism of action.

5 Response of mice with global deletion of Tst to *in vivo* and *ex vivo* models of Myocardial Infarction

5.1 Introduction

Experiments in Chapter 3 have shown that TST is expressed in the smooth muscle of the cardiac vasculature and within cardiomyocytes. Global deletion of the *Tst* gene had no impact on basal cardiac function, structure or mitochondrial function under physiological conditions. In the $Tst^{-/-}$ mouse heart, H_2S breakdown rates were reduced by approximately 20% and circulating H_2S levels were approximately 7-fold higher in $Tst^{-/-}$ mice. In heart tissue, protein levels of the H_2S-activated nuclear factor-E2-related factor (Nrf2) downstream targets, thioredoxin (TRX1) and heme oxygenase-1 (HO-1) were comparable between groups. Importantly, protein levels for the cardiac specific H_2S-synthetic enzyme, cystathionine gamma lyase (CSE) were reduced in the $Tst^{-/-}$ heart, suggesting a homeostatic negative feedback mechanism to maintain myocardial H_2S bioavailability at non-toxic levels. Total endothelial nitric oxide (eNOS) protein levels were reduced in the hearts of $Tst^{-/-}$ mice identifying a cross talk between H_2S and nitric oxide (NO) signalling that has been observed by others (King *et al.*, 2014). Experiments in chapter 4 showed that $Tst^{-/-}$ mice were normotensive despite altered sodium-fluid handling in the kidney and mild endothelial dysfunction in the small mesenteric arteries. Currently, little is known about the expression pattern of the *Tst* gene or its role in H_2S bioavailability under pathophysiological conditions such as myocardial infarction (MI).

Initial infarct size due to ischaemic injury and the subsequent infarct healing response are both integral determinants of cardiac functional outcome and the degree of cardiac remodelling after MI. Reperfusion therapies reduce infarct size and mortality rates from acute MI, but reperfusion itself causes irreversible injury to cardiomyocytes (Yellon *et al.*, 2007) so that cardiac dysfunction and subsequent heart failure are still evident when patients are followed up at 5 years post-MI (Velagaleti *et al.*, 2008). The pathogenesis of permanent ligation and reperfusion injury are well characterised and covered in section 1.1.6.1.

Although H_2S donor therapy is effective in reducing infarct size following permanent coronary artery ligation (CAL) (Zhang *et al.*, 2014; Zhu *et al.*, 2006), the majority of research investigates the cardioprotective effects of H_2S using IRI models of MI. Due to the different aetiologies of injury and healing caused by CAL and IRI, many facets of the cardioprotective profile of H_2S in CAL models remain unclear. Single dose administration of

pharmacological H_2S donors at the time of reperfusion can reduce infarct size and improve ejection fraction in mice when assessed at 3 days after IRI (Elrod *et al.*, 2007). The cardioprotective profile of H_2S in IRI models operates via several mechanisms including; preserved mitochondrial function (Elrod *et al.*, 2007), stimulation of anti-oxidant and anti-apoptotic gene transcription (Calvert et al., 2009) and reduced leukocyte infiltration (Elrod *et al.*, 2007). Administration of the H_2S donor Na_2S to mice increases expression of the antioxidant transcription factor, nuclear receptor factor-E2-related factor (Nrf2) and its downstream targets, thioredoxin (Trx1) and heme-oxygenase 1 (HO-1) (Calvert *et al.*,, 2009) by 24hours. This response alleviates damage associated with reperfusion-induced oxidant stress generation. Although single-dose administration of H_2S can reduce injury acutely when given shortly before and/ or at the time of reperfusion (Elrod *et al.*, 2007; Johansen *et al.*, 2006), single doses fail to protect against cardiac dysfunction and ventricular remodelling by 4 weeks after IRI (Calvert *et al.*, 2010). However, H_2S donor treatment administered at reperfusion and then daily for 7 days after IRI increases Nrf2 expression by 7 days and improves cardiac outcome by 4 weeks after IRI (Calvert *et al.*, 2010) suggesting that early and sustained delivery of H_2S during the first week after injury is essential for long-term protection. Mice with cardiomyocyte-specific overexpression of the H_2S synthetic enzyme CSE (αMHC-CGL-Tg) produce more H_2S and have increased basal expression of the H_2S-sensitive Nrf2, Trx1 and HO-1 in the heart (Calvert *et al.*, 2009). At 72 hours post IRI, αMHC-CGL-Tg mice have reduced infarct size (Elrod *et al.*, 2007) and by 4 weeks after IRI have improved cardiac outcomes compared to wild type controls (Calvert *et al.*, 2010). However, by 7 days after CAL, 30% of αMHC-CGL-Tg mice die and by 4 weeks post-CAL, cardiac function is not improved compared to controls (Calvert *et al.*, 2010) indicating that the effects of H_2S in different MI models are more complex than previously thought. Therefore, investigation of when and to what extent the heart regulates CSE and other H_2S metabolic enzymes in the infarcted myocardium within 7 days after CAL is warranted.

Leukocyte infiltration is considered harmful in acute IRI but is vital in the process of healing in mouse models of permanent ligation. The stages of leukocyte infiltration are well defined and highlighted in section 1.1.6.4. Infarct healing after injury is orchestrated by infiltrating neutrophils, monocyte subsets ($Ly6C^{high}$ and $Ly6C^{low}$) and the macrophages derived from them which all respond to different chemokine signals released from the injured myocardium during the early and late healing phases (Nahrendorf *et al.*, 2010). Leukocytes remove dead cardiomyocytes and initiate the process that results in formation of a collagen rich scar to ensure maintenance of cardiac structural integrity (Nahrendorf *et al.*, 2010). Leukocyte

recruitment is vital for myocardial repair (Dewald *et al.*, 2005), excessive early neutrophil and Ly6C^{high} monocyte recruitment can destabilise the repair process and lead to cardiac rupture (Frangogiannis, 2012).

H_2S has anti-inflammatory actions. H_2S treatment reduces leukocyte infiltration and pro-inflammatory cytokine expression following IRI (Elrod *et al.*, 2007) but it is unclear if this effect is secondary to reduced myocardial damage. Intravital microscopy experiments showed that H_2S dose-dependently inhibited aspirin-induced leukocyte adherence in mesenteric venules of rats in a K_{ATP} channel-dependent manner (Sivarajah *et al.*, 2006). Furthermore, in models of inflammation such as carrageenan-induced paw oedema or air pouch inflammation, H_2S treatment reduced leukocyte infiltration and oedema, which was abrogated in rats pre-treated with the CSE or K_{ATP} channel inhibitors, β-cyano-l-alanine (BCA) and glibenclamide respectively (Sivarajah *et al.*, 2006). These data suggested that vascular CSE mediated H_2S production reduced leukocyte adhesion via K_{ATP} channel activation (Zanardo *et al.*, 2006). As leukocyte recruitment is an essential element of infarct healing following CAL, it seems unlikely the heart would endogenously produce H_2S during the infarct-healing phase, which would otherwise limit leukocyte infiltration and hamper necrotic tissue removal and stable scar formation.

The experiments in this chapter were designed to investigate the regulation of TST and the H_2S synthetic enzymes CSE and 3-mercaptopyruvate sulfurtransferase (3MST) following permanent coronary artery ligation. Using *in vivo* and *ex vivo* MI models, this chapter aimed to establish TSTs role in the response of the heart to ischaemia and how it regulates infarct healing following injury.

5.2 Methods

5.2.1 *In vivo* coronary artery ligation

Male C57BL/6N wild type or *Tst*$^{-/-}$ mice aged 18-20 weeks were used for *in vivo* myocardial infarction experiments. Mice underwent permanent coronary artery ligation (CAL) for induction of myocardial infarction, with un-operated mice serving as baseline controls as described in section 2.2.3. Surgery was conducted by Dr Katie Mylonas and by Xiaofeng Zhao. Mice were checked daily following CAL surgery and any deaths recorded. Post-mortem analysis was carried out on dead mice to establish the cause of death. Cardiac rupture was identified as cause of death when the chest cavity was filled with blood.

Study one

Heart tissue was collected from naïve adult male C57BL/6J mice or from C57BL/6J mice at 1 day, 2 days or 7 days after CAL surgery for analysis of gene expression by qRT-PCR and protein expression by western blotting. Infarct and infarct border zone tissue was dissected from the left ventricular free wall below the ligature for RNA extraction and for protein extraction as detailed in section 2.5.1 and 2.5.4 respectively. Taqman probes for H_2S metabolic enzymes were used to assess changes in gene expression at the timepoints indicated above. For full details of Taqman probes, please refer to Table 1-4, section 2.5.3.

For western blotting experiments, an equal amount of myocardial infarct and border zone protein was loaded into SDS gels for electrophoresis, transferred onto nitrocellulose membranes and incubated with antibodies for CSE and 3MST. For full details of the procedure, please refer to section 2.5.6.

Study two

Tst$^{-/-}$ mice and wild type littermates underwent CAL surgery. Cardiac size and function were evaluated in surviving mice by echocardiography 7 days after coronary artery ligation surgery as described in section 2.2.2. Adrian Thomson performed echocardiography scanning. Cardiac dimensional and functional measurements were analysed in a single blinded fashion. Following echocardiography, mice were anaesthetised and perfusion fixed with formalin as described in section 2.4.2. Perfusions were carried out by Dr Katie Mylonas and by Xiaofeng Zhao. The hearts were dissected, fixed for 24hours in 10% formalin and processed for histology. Infarct scar characteristics and collagen deposition were assessed in heart sections stained with Massons Trichrome and Picrosirius Red. Staining was performed by Deborah Mauchline (Histology Service). Quantification of scar area, scar thickness, infarct length or

collagen deposition was carried out on Stereologer Analyser 3 using CapturePro5 software. Further details are discussed in section 2.4.8.

Study three

Blood was withdrawn (30µl blood: 30µl 3.2% citrate) from the tail vein in conscious *Tst*$^{-/-}$ and wild type control mice at 2 days post MI to measure leukocyte mobilisation of monocytes and neutrophils, using flow cytometry. Blood samples were incubated with antibodies against CD11b, Ly6C and Ly6G at 1:50 dilution and the red blood cells lysed as described in section 2.5.8. Cells were incubated with counting beads (50,000 beads/ µl) immediately before samples were run in the LSR Fortessa. Samples were run until 5000 counting bead events were detected. The gating strategy to identify circulating leukocyte populations is detailed in Figure 2-6, section 2.5.8.1.

Immediately following blood withdrawal, wild type and *Tst*$^{-/-}$ mice were put under terminal anaesthesia, perfused with PBS and the hearts were removed to investigate leukocyte recruitment by flow cytometry. Dr. Katie Mylonas performed the perfusions. All left ventricular free wall tissue below ligature was dissected, placed in collagenase disassociation solution and cells dissociated as detailed in section 2.5.8.2. Cells were incubated with antibodies; CD45, CD11b, Ly6G, Ly6C at 1:50 dilution. Cells were incubated with DAPI (1:1000 dilution) and counting beads (50,000 beads/ µl) immediately before samples were run in the LSR Fortessa. Samples were run until 30,000 counting bead events were detected. The gating strategy to identify infiltrated leukocyte populations is detailed in Figure 2-7, section 2.5.8.2.

Study four

Heart tissue was collected from wild type and *Tst*$^{-/-}$ mice at 4hours and 2 days after CAL surgery for analysis of gene expression by qRT-PCR and protein expression by western blotting. Mice were perfused with PBS by Dr. Katie Mylonas and all the left ventricular free wall below the ligature was dissected and cut into 2 pieces – one half was used for RNA extraction and the other for protein extraction as described in section 2.5.1 and 2.5.4 respectively. Taqman probes for inflammatory chemoattractant and adhesion molecules were used to assess changes in gene expression at 2 days post-CAL. For full details of Taqman probes, please refer to Table 2-4, section 2.5.3.

For western blotting experiments, equal amounts of infarcted cardiac protein was loaded into SDS gels for electrophoresis, transferred onto nitrocellulose membranes and

incubated with antibodies for CSE, 3MST, TRX1 and HO-1. For full details of the procedure, please refer to section 2.5.6.

5.2.2 *Ex vivo* ischaemia and reperfusion in buffer perfused heart

Hearts were quickly isolated from male wild type or *Tst*$^{-/-}$ mice aged 12-13 weeks for *ex vivo* perfusion in Langendorff mode as detailed in section 2.3.1. Ischaemia was induced for 30 minutes followed by 2hours reperfusion. Upon completion of the *ex vivo* IRI protocol, the ligature was re-tied and Evans blue solution (1% w/v in 0.9% saline) was perfused into the heart to identify the area at risk and the heart washed in 0.9% saline to remove excess Evans Blue stain. All myocardium above the ligature was discarded and the hearts then frozen at -20^{0}C for subsequent analysis of infarct size by 2, 3, 5-triphenyltetrazolium chloride staining as detailed in section 2.3.2. These experiments were conducted in collaboration with Emma Batchen.

5.2.3 *In vitro* mitochondrial ischaemia reperfusion injury

Mitochondria were isolated from two pooled hearts of wild type or *Tst*$^{-/-}$ male mice aged 14-16 weeks as described in section 2.3.5. Mitochondria were placed into a closed chambered Oroboros oxygraph and exposed to excess substrate and ADP to stimulate maximal respiration as detailed in section 2.3.6. Basal O_2 respiratory rate was calculated during the linear phase of O_2 consumption. Ischaemia was considered initiated when mitochondria consumed all O_2 within the chamber. Following a 20 minute ischaemic period, the chamber was opened to ambient O_2 to simulate reperfusion injury. Upon stable O_2 equilibrium within the chamber, the chamber was re-sealed and ischaemic respiratory recovery rate calculated as post ischaemic respiratory rate as percentage of pre-ischaemic respiratory rate.

5.2.4 Statistical Analysis

All values presented are as mean±SEM. Analysis of survival was performed using a Chi squared test. Unless otherwise stated, comparisons are by unpaired two-tailed Student t-test. 1-way ANOVA followed by post-hoc analysis using Tukeys Multiple Comparison test was performed on PCR results for the H_2S metabolic genes at various timepoints during the infarct-healing phase following CAL. P values less than 0.05 were considered significant.

5.3 Results

5.3.1 H_2S metabolic enzyme mRNA level is dynamically regulated in the early infarct healing phase

Quantitative real-time PCR analysis revealed that *Cth* mRNA was downregulated in infarct border zone of C57BL/6J hearts by day 1 (Figure 5-1) and day 2 post-CAL (Figure 5-1) compared to naïve controls but recovered to baseline levels by day 7 (Figure 5-1). *Mpst* mRNA expression was also downregulated in C57BL/6J hearts by day 1 and day 2 post-CAL (Figure 5-1) but remained significantly lower by day 7 (Figure 5-1). Western blots performed on separate myocardial infarct tissue samples confirm that cardiac CSE and 3MST protein are significantly lower by day 2 post-CAL (Figure 5-2). In comparison, *Sqrdl*, *Ethe1*, *Tst* and *Suox* mRNA are markedly upregulated in C57BL/6J hearts (TST upregulated ≈12-fold) by day 2 post-CAL (Figure 5-1) and returned to baseline levels by day 7. No differences were observed in cardiac expression of housekeeping genes at any timepoint post-CAL (see figure 2-5, section 2.5.3).

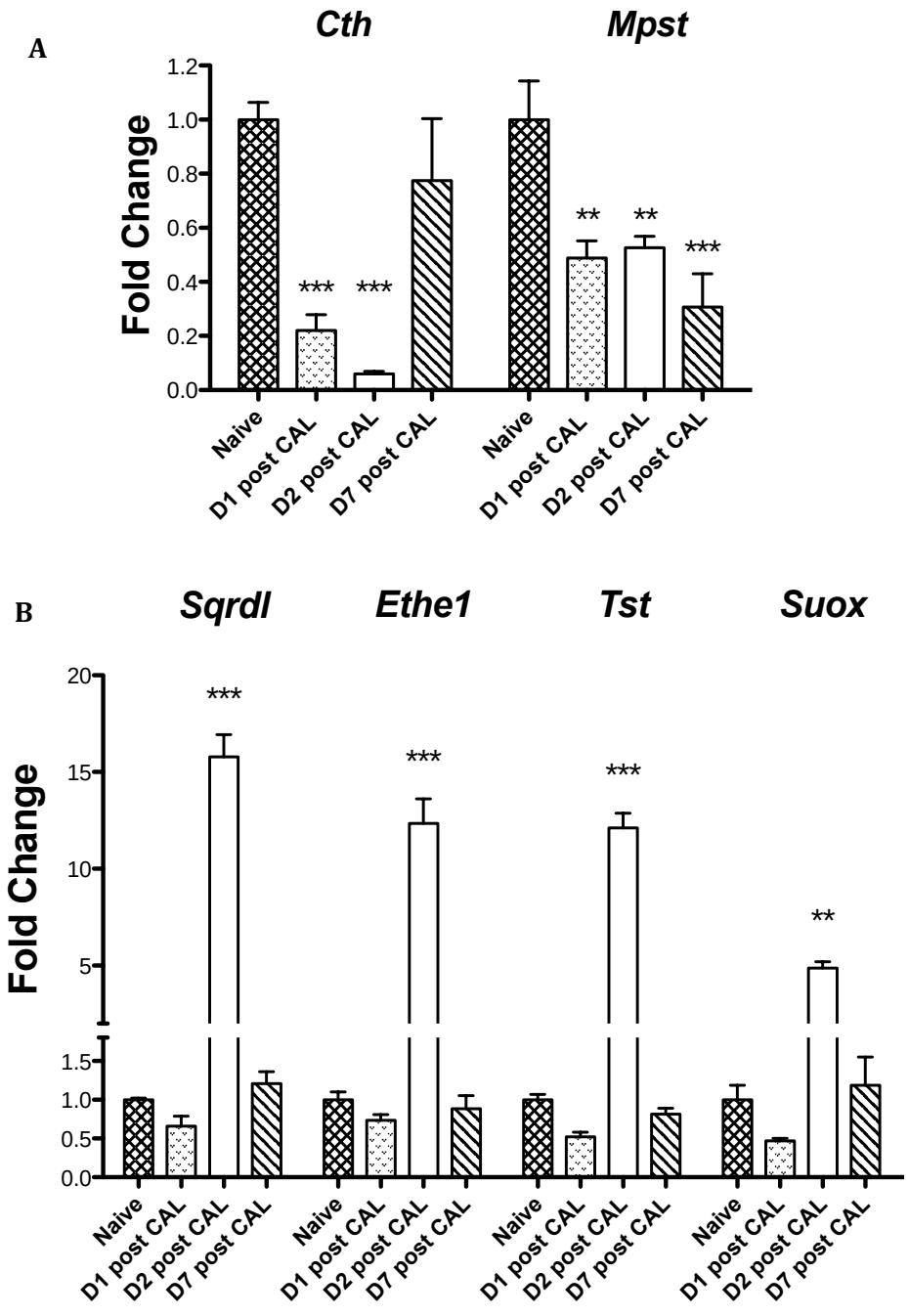

Figure 5-1 Cardiac mRNA expression of H_2S metabolic enzymes is regulated during early infarct healing phase to limit H_2S bioavailability

A) Quantitative real time PCR analysis measuring mRNA levels of H_2S synthetic enzymes, *Cth* and *Mpst* (A) and H_2S breakdown enzymes, *Sqrdl, Ethe1, Tst* and *Suox* (B) in naïve C57BL/6J hearts and in myocardial infarct and infarct border zone tissue of C57BL/6J mice at 1, 2 and 7 days after coronary artery ligation (CAL) surgery (n=4/ timepoint). All data are normalised to the housekeeping genes; *Tbp* (A) or *Cox4i1* (B) and then normalised to expression level of naïve controls. Values are expressed as mean±SEM. *p < 0.05, **p < 0.01, ***P < 0.001 vs. naïve by 1way ANOVA with Tukeys post hoc test. *Abbreviations; D1, D2, D7 post-CAL; day 1, day 2 or day 7 post coronary artery ligation, Cth; cystathionine gamma lyase, Mpst; 3-mercaptopyruvate sulfurtransferase, Sqrdl; sulfide quinone oxidoreductase, Ethe1; sulfur dioxygenase, Tst; thiosulfate sulfurtransferase, Suox; sulfide oxidase.*

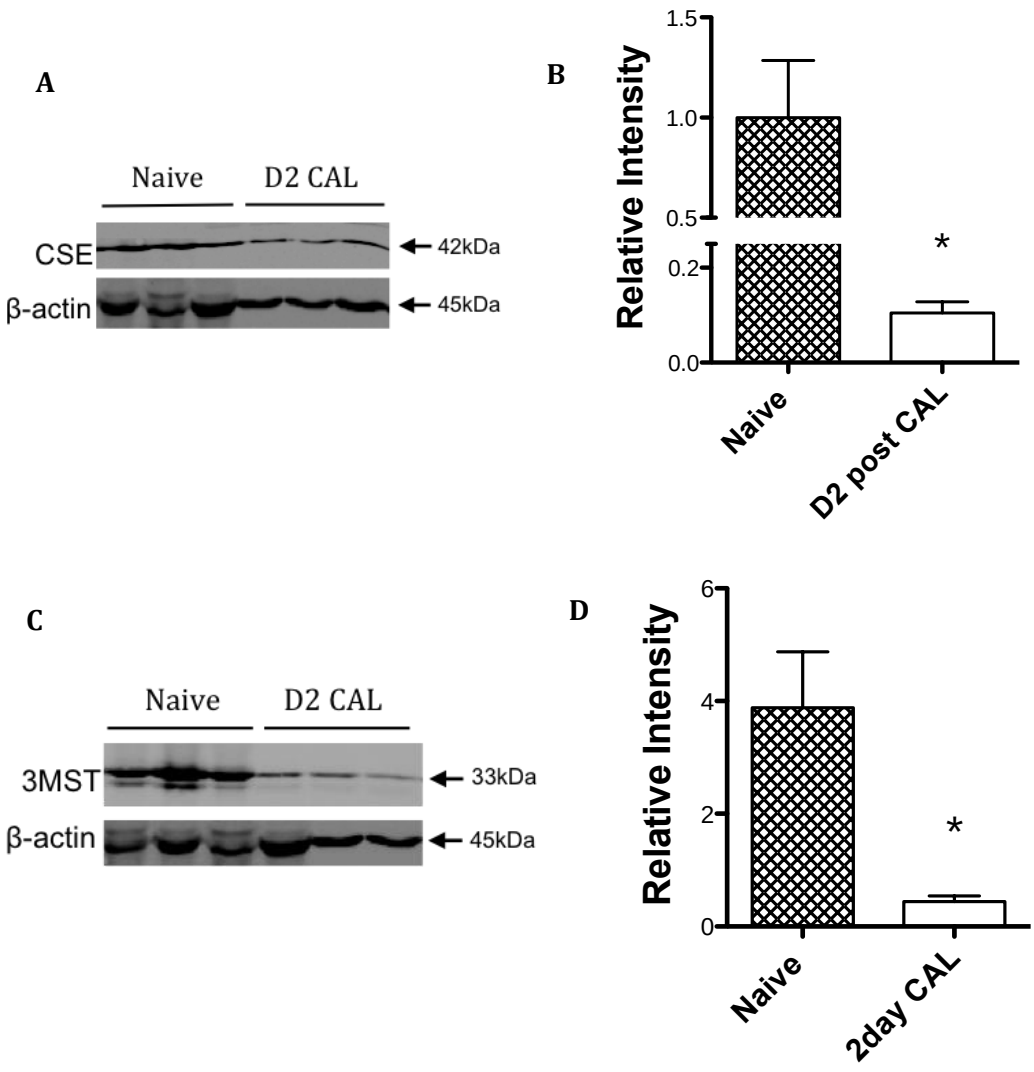

Figure 5-2 Protein levels of H_2S synthetic enzymes are reduced by 2days post-CAL

Representative immunoblots and densitometric analysis of CSE (A-B) and 3MST (C-D) protein levels in naïve and day 2 post-CAL myocardial infarct and infarct border zone tissue of C57BL/6N mouse hearts (Naive; n=5, 2day CAL; n=4). Data presented as relative intensity of protein expression when normalised to the internal control, β-actin and then normalised to level of C57BL/6N wild type controls. Values are expressed as mean±SEM, *p < 0.05

5.3.2 *Tst*$^{-/-}$ mice have increased mortality and worsened cardiac outcomes at 7 days post-CAL

At 7 days post-CAL, mortality rates were significantly higher in *Tst*$^{-/-}$ compared to C57BL/6N mice (Figure 5-3). Survival rate was 87.5% in C57BL/6N wild type mice and 50% in *Tst*$^{-/-}$ mice, and in both groups, death was due to cardiac rupture, evidenced at post-mortem investigation by blood in the chest cavity. At 7 days after CAL, heart rate was comparable between groups (Figure 5-3). LVESA and LVEDA were higher in both groups at 7 days post-CAL compared to baseline measurements (Figure 5-3, $P < 0.01$). *Tst*$^{-/-}$ mice had increased LVESA and LVEDA compared to C57BL/6N wild type mice at 7 days post-CAL (Figure 5-3). CAL surgery decreased fractional area change (FAC) in both groups compared to baseline (Figure 5-3, $P < 0.01$) whilst fractional shortening (FS) was only decreased in the *Tst*$^{-/-}$ group compared to baseline measurements (Figure 5-3, $P < 0.001$). By 7 days after CAL, FAC and FS were reduced in *Tst*$^{-/-}$ compared to control mice (Figure 5-3).

5.3.2.1 Myocardial chemokine and adhesion molecule gene expression is normal in *Tst*$^{-/-}$ mice

Quantitative real-time PCR analysis revealed that mRNA levels for the monocyte chemoattractant protein MCP-1/ *Ccl2* and the MCP-1 receptor, *Ccr2* tended to be lower in infarcted hearts of *Tst*$^{-/-}$ mice at 2 days post-CAL but were not statistically different (Figure 5-4). Levels of mRNA for the adhesion molecules *Icam1* and *Vcam* were comparable between groups (Figure 5-4) in infarcted hearts of *Tst*$^{-/-}$ mice at 2 days post-CAL.

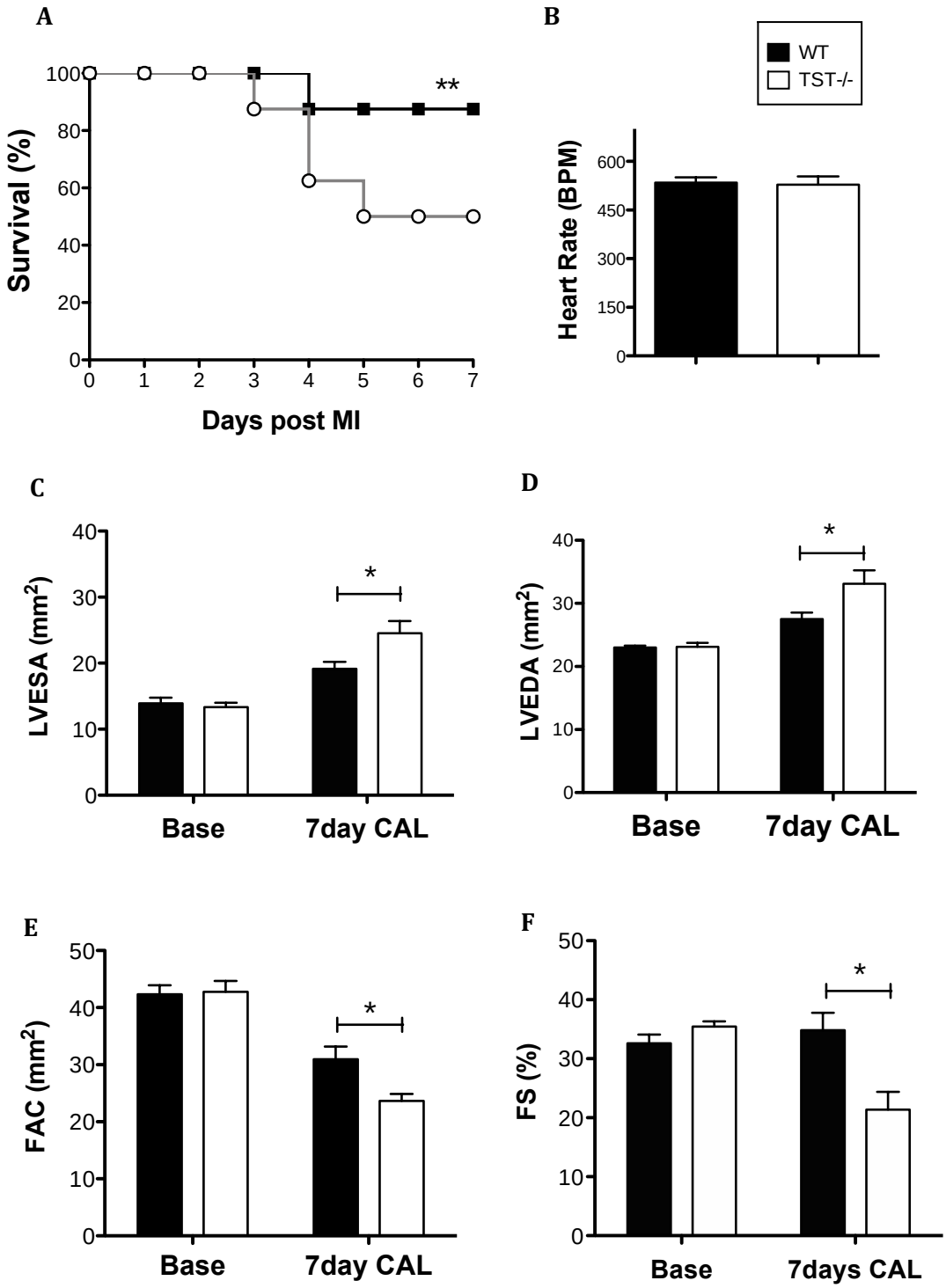

Figure 5-3 Loss of TST is detrimental to cardiac outcome by 7 days after CAL surgery

A) Survival rates following coronary artery ligation, analysed by Chi^2 test (n=8/ group). Two-dimensional B-mode and M-mode ultrasound images and paw electrode signals were analysed for (B) heart rate (bpm), (C) LVESA (mm^2), (D) LVEDA (mm^2), (E) FAC (mm^2) and (F) FS (%), (WT; n=6, *Tst*$^{-/-}$; n=4). Values are expressed as mean±SEM. *p<0.05 WT 7 days CAL vs. *Tst*$^{-/-}$ 7 days CAL by unpaired student t-test. *Abbreviations; BPM; beats per minute, LVESA; left ventricular-(LV) end systolic area, LVEDA; LV end diastolic area, FAC; fractional area change, FS; fractional shortening.*

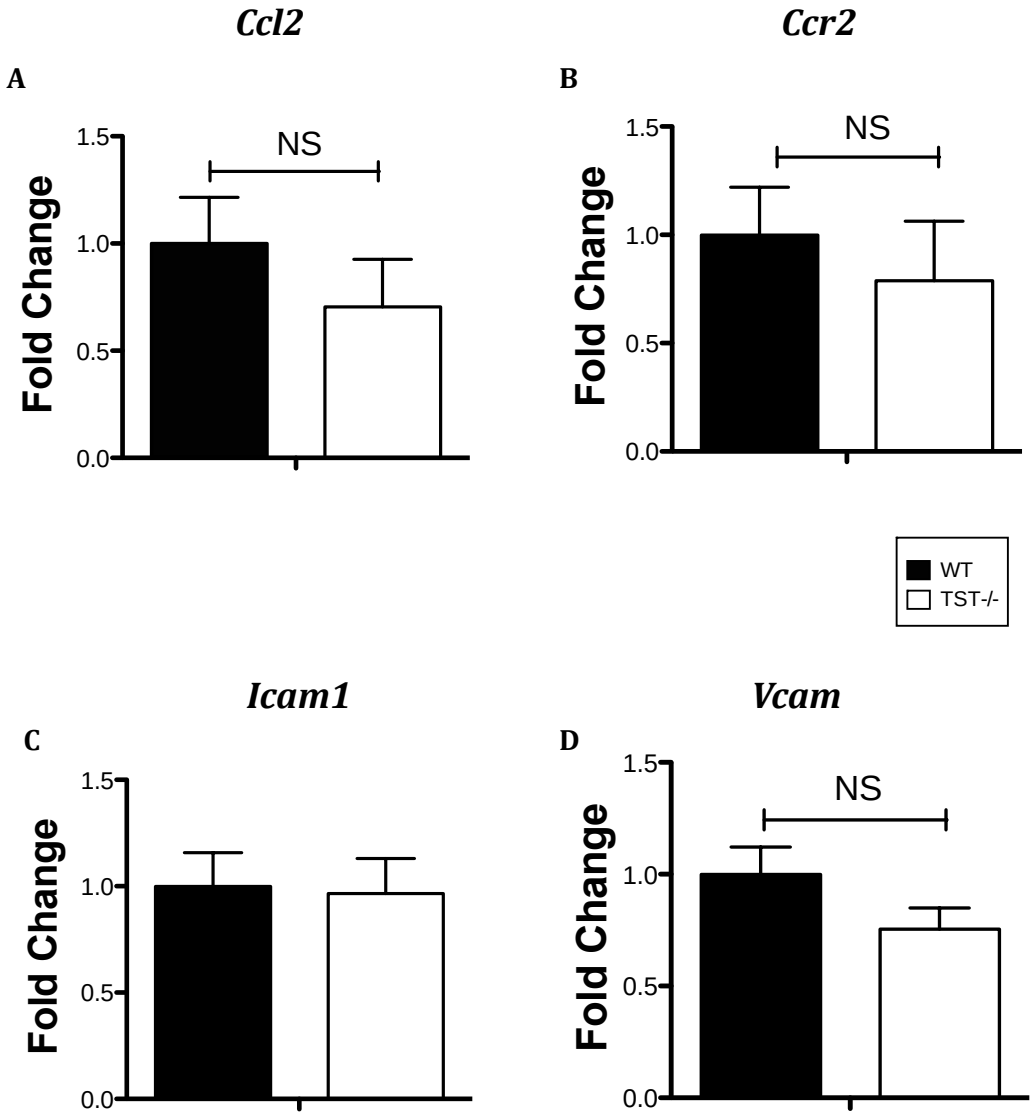

Figure 5-4 mRNA levels of chemokine and adhesion molecules is normal in infarcted hearts of *Tst*$^{-/-}$ mice at 2 days post-CAL

Quantitative real time PCR analysis measuring mRNA levels of the chemokine MCP-1/ *Ccl2* (A), the MCP-1 receptor *Ccr2* (B) and adhesion molecules, *Icam1* (C) and *Vcam* D) in myocardial infarct and infarct border zone tissue of *Tst*$^{-/-}$ and C57BL/6N control mice at 2 days after coronary artery ligation (CAL) surgery (WT; n=4, *Tst*$^{-/-}$; n=5). All data are normalised to the housekeeping gene *Tbp* and then normalised to expression level of wild type controls. Values are expressed as mean±SEM. *Abbreviations; MCP-1/ Ccl2; monocyte chemoattractant protein 1, Ccr2; chemokine receptor 2, Icam1; intracellular adhesion molecule, Vcam; vascular cell adhesion molecule.*

5.3.3 Increased rupture incidence is not due to excessive leukocyte recruitment into the damaged heart

At 2 days post-CAL, flow cytometry showed that leukocyte mobilisation in the blood is comparable between *Tst*$^{-/-}$ and C57BL/6N mice (Figure 5-5). Circulating numbers of neutrophils, Ly6C^{high} and Ly6C^{low} monocytes were similar in the blood at 2 days post-CAL (Figure 5-5). In CAL-operated *Tst*$^{-/-}$ and wild type littermates, numbers of recruited neutrophils, Ly6C^{high} and Ly6C^{low} monocytes to the heart were comparable between groups at 2 days post-CAL (Figure 5-5).

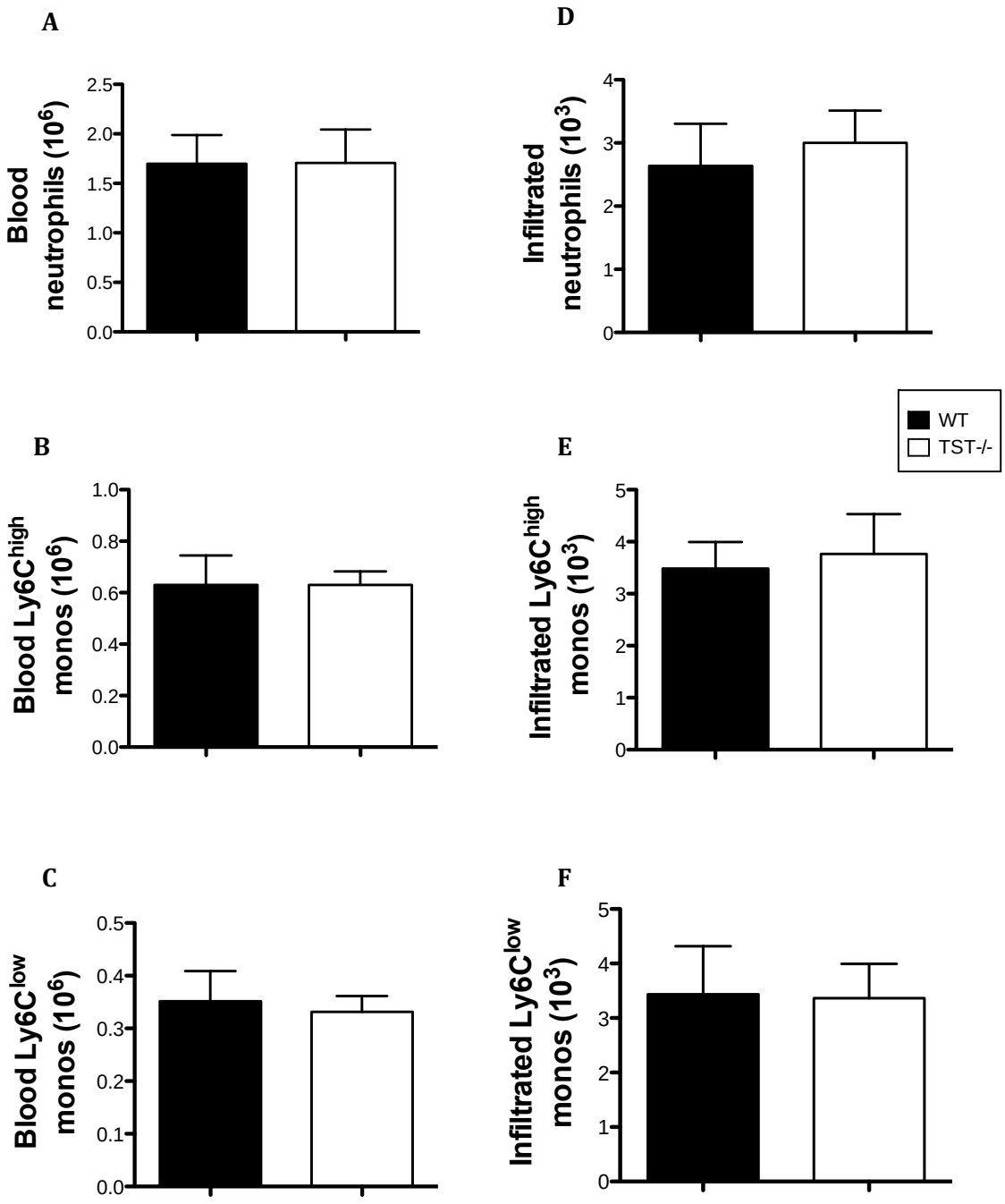

Figure 5-5 Loss of TST has no impact on leukocyte mobilisation or recruitment into the damaged heart at 2 days post-CAL

Flow cytometric analysis detailing the numbers of circulating blood A) neutrophils (CD11b^{high}/ Ly6G^{high}/ Ly6C^{intermediate}) B) Ly6C^{high} monocytes (CD11b^{high}/ Ly6G^{low}/ Ly6C^{high}) and C) Ly6C^{low} monocytes (CD11b^{high}/ Ly6G^{low}/ Ly6C^{low}) in whole blood of *Tst*$^{-/-}$ and C57BL/6N control mice at 2 days following CAL surgery, WT; n=11, *Tst*$^{-/-}$; n=9. Flow cytometric analysis of the number of D) infiltrated live neutrophils (DAPI^{low}/ CD45^{high}/ CD11b^{high}/ Ly6G^{high}/ Ly6C^{intermediate}), E) Ly6C^{high} monocytes (DAPI^{low}/ CD45^{high}/ CD11b^{high}/ Ly6G^{low}/ Ly6C^{high}) and F) Ly6C^{low} monocytes (DAPI^{low}/ CD45^{high}/ CD11b^{high}/ Ly6G^{low}/ Ly6C^{low}) in digested hearts of *Tst*$^{-/-}$ and C57BL/6N control mice at 2 days following CAL surgery, n=5/ group. Values are mean±SEM.

5.3.4 Macrophage recruitment is similar in surviving mice at 7 days post-CAL

At 7 days after surgery, macrophage infiltration, assessed by Mac 2 immunostaining was comparable between wild type and *Tst*$^{-/-}$ mice by day 7 (Figure 5-6). Mac 2 immunostaining was observed in the infarct and border zones but not the remote myocardium.

5.3.5 Surviving *Tst*$^{-/-}$ mice form stable scars and have similar scar areas to controls by 7 days post-CAL

Collagen deposition, assessed by Picrosirius Red staining was comparable between C57BL/6N wild type and *Tst*$^{-/-}$ mice (Figure 5-7). Scar area, evaluated by Massons Trichrome staining was similar between groups at 7 days after CAL (Figure 5-7). Infarct width and infarct length were comparable between groups (Figure 5-7).

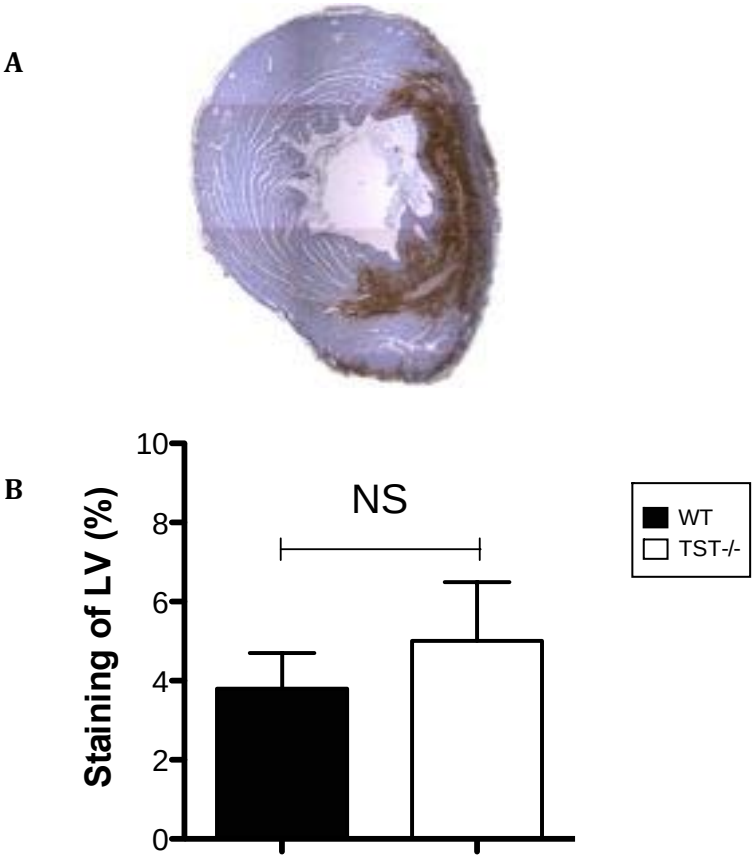

Figure 5-6 Macrophage staining in the myocardial infarct area is similar between groups at 7 days post-CAL

Representative tiled 7day post-CAL heart section immunostained with anti-Mac2 antibody (A). Quantification of Mac2 macrophage staining as percentage of LV (B) in wild type and *Tst*$^{-/-}$ hearts at 7 days after CAL (WT; n=5, *Tst*$^{-/-}$; n=3). Values are expressed as mean±SEM.

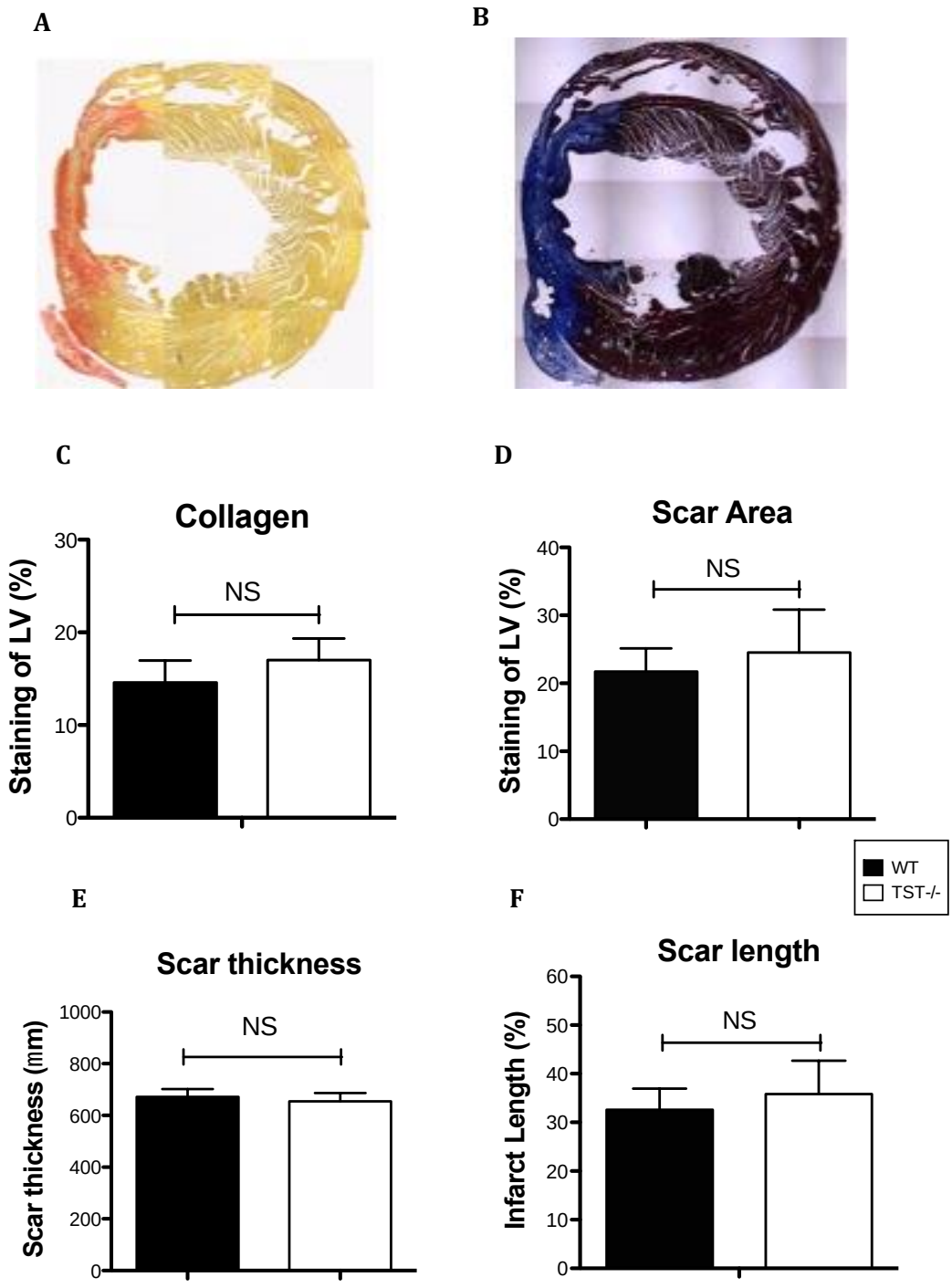

Figure 5-7 Histological analysis reveals similar collagen deposition and fibrosis between groups by 7 days after MI

Representative tiled images of sections stained with Picrosirius Red (A) for collagen deposition and Massons Trichrome (B) to stain infarct fibrosis. C) Collagen deposition and, D) scar formation as percentage of left ventricle were evaluated from Picrosirius Red and Massons Trichrome stained sections. E) Scar thickness was averaged from three points across the scar, evaluated from Massons Trichrome stained sections. F) Scar length expressed as percentage of the left ventricle in Massons Trichrome stained sections (WT; n=5, *Tst*$^{-/-}$; n=3). Values are expressed as mean±SEM

5.3.6 Loss of TST leads to dysregulation of H_2S synthetic enzyme expression at 48hours after CAL

Cardiac protein expression of the H_2S synthetic enzymes, CSE and 3MST were assessed by western blotting at 4hrs and 48hrs after CAL. At 4hrs post-CAL, cardiac CSE and 3MST protein levels were comparable between wild type and *Tst*$^{-/-}$ hearts (Figure 5-8). In comparison, by 48hrs post-CAL, CSE and 3MST protein levels were significantly upregulated by approximately 2-fold and 4-fold respectively in *Tst*$^{-/-}$ hearts (Figure 5-9).

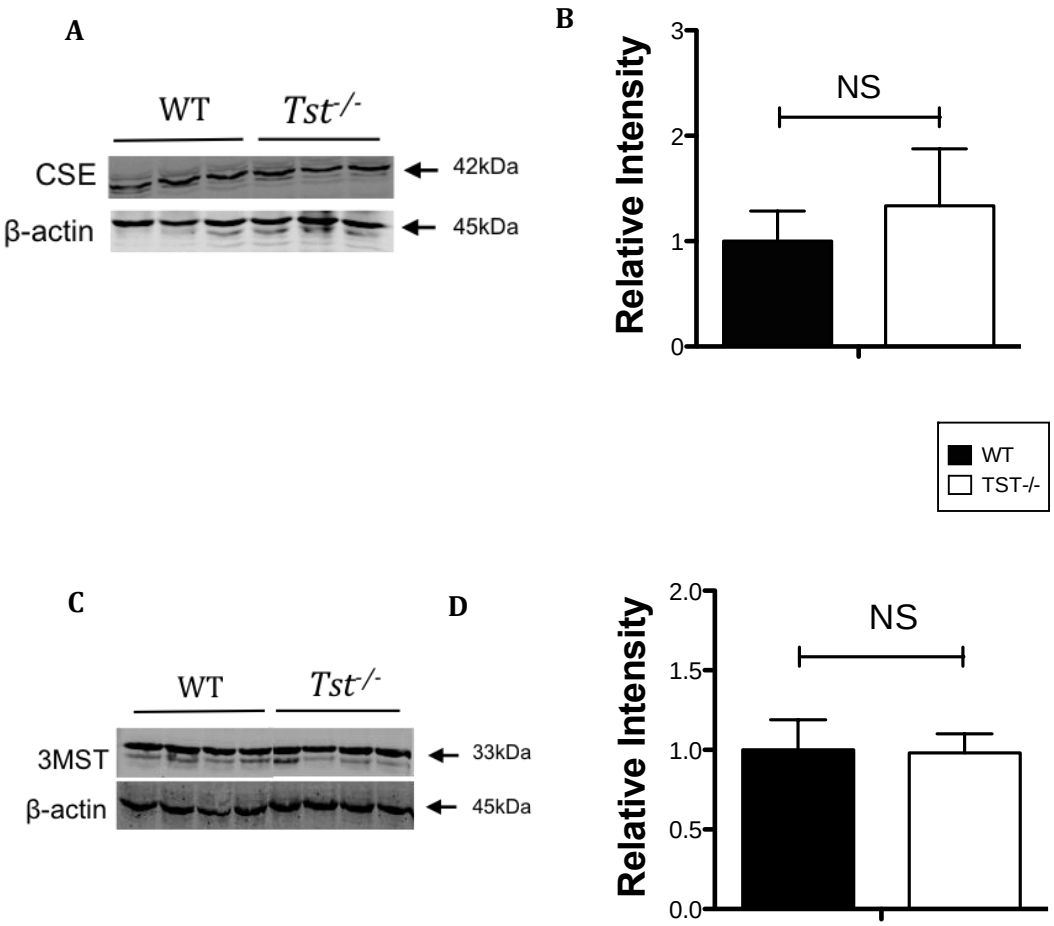

Figure 5-8 H_2S synthetic enzymes are comparable between groups at 4hours after CAL

Representative immunoblot and densitometric analysis of CSE (A-B) and 3MST (C-D) protein levels in myocardial infarct and infarct border zone tissue of *Tst*$^{-/-}$ and C57BL/6N wild type mice at 4hours post-CAL. Data presented as relative intensity of protein expression when normalised to the internal control, β-actin and then normalised to level of C57BL/6N wild type controls (WT; n=5, *Tst*$^{-/-}$; n=4). Values are expressed as mean±SEM.

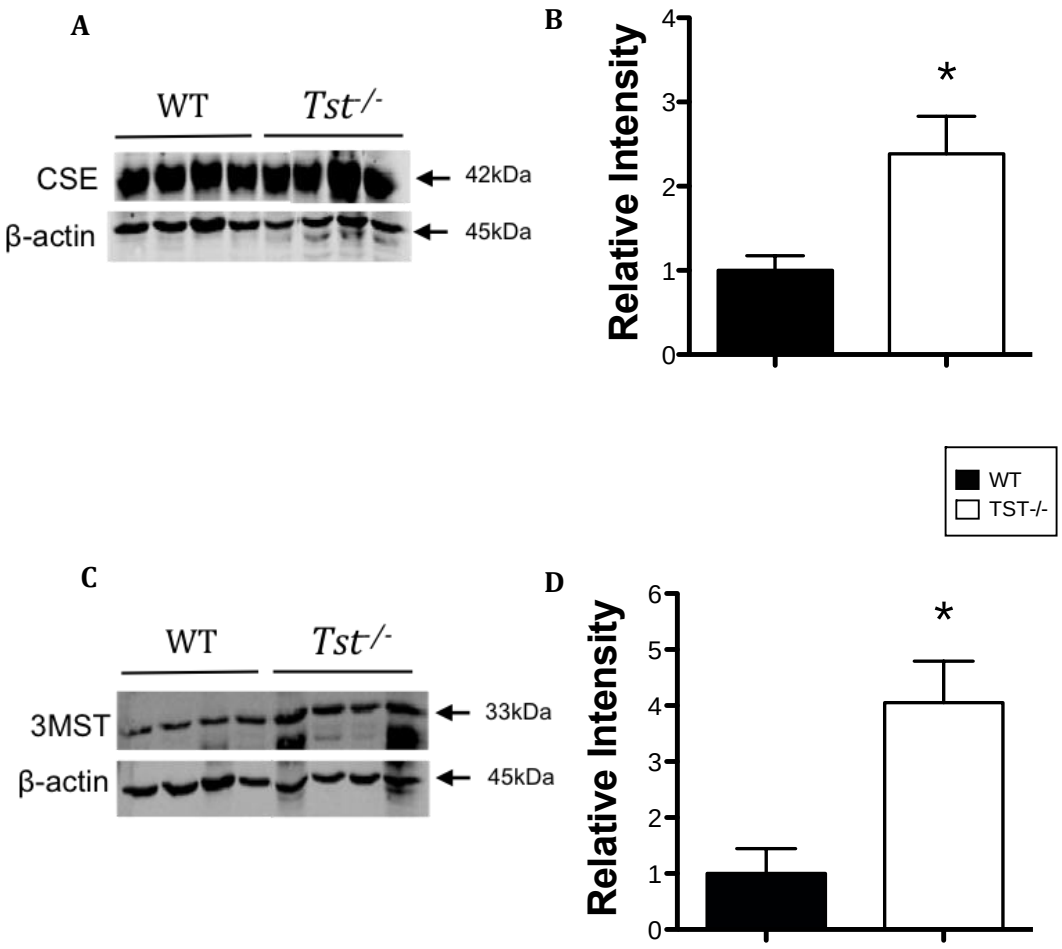

Figure 5-9 Loss of TST alters the protein expression of H_2S synthetic enzymes at 48hours post-CAL surgery

Representative immunoblot and densitometric analysis of cardiac CSE (A-B) and cardiac 3MST (C-D) protein levels in myocardial infarct and infarct border zone tissue of *Tst*$^{-/-}$ and C57BL/6N wild type at 48hours post-CAL. Data presented as relative intensity of protein expression when normalised to the internal control, β-actin and then normalised to level of C57BL/6N wild type controls (n=4/ group). Values are expressed as mean±SEM. *$p < 0.05$.

5.3.7 Nrf2 downstream anti-oxidant proteins are increased in *Tst*$^{-/-}$ mice at 48hrs after MI

Cardiac protein expression of the nuclear receptor factor 2 (Nrf2) regulated downstream anti-oxidant proteins, thioredoxin (Trx1) and heme-oxygenase-1 (HO-1), were assessed by western blotting at 4hrs and 48hrs after CAL. At 4hours after CAL, Trx1 protein appeared to be downregulated in *Tst*$^{-/-}$ hearts compared to controls, but did not reach statistical significance (Figure 5-10, P=0.08). By 48hrs post-CAL, Trx1 and HO-1 protein levels were significantly upregulated by approximately 10-fold and 40-fold respectively in *Tst*$^{-/-}$ hearts compared to wild type CAL controls (Figure 5-10).

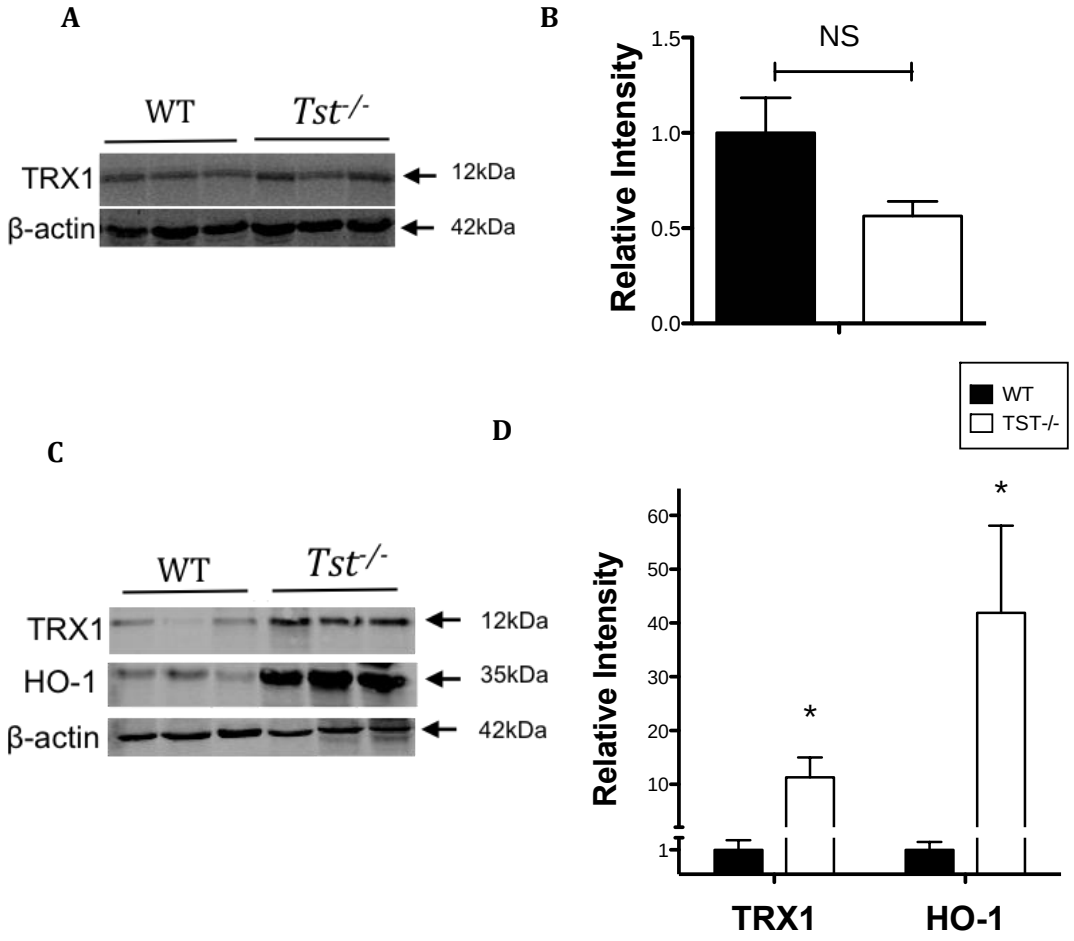

Figure 5-10 Nrf2 downstream targets TRX1 and HO-1 are higher by 48hours post-CAL

(A-B) Representative immunoblot and densitometric analysis of TRX1 protein levels in myocardial infarct and infarct border zone tissue of *Tst*$^{-/-}$ and C57BL/6N wild type at 4hours post-CAL. (C-D) Representative immunoblot and densitometric analysis of Trx1 and HO-1 protein levels in myocardial infarct and infarct border zone tissue of *Tst*$^{-/-}$ and C57BL/6N wild type at 48hours post-CAL. Data presented as relative intensity of protein expression when normalised to the internal control, β-actin and then normalised to level of C57BL/6N wild type controls (WT; n=4, *Tst*$^{-/-}$; n=5). Values are expressed as mean±SEM. *p < 0.05.
Abbreviations; TRX1; thioredoxin, HO-1; hemeoxygenase 1.

5.3.8 *Tst*$^{-/-}$ cardiomyocytes are more susceptible to *ex vivo* ischaemia reperfusion injury

The area at risk (AAR) was comparable between groups (Figure 5-11, WT; 29.4 ± 6.0, *Tst*$^{-/-}$; 31.8 ± 6.9) indicating that ligature placement around the coronary artery was consistent between groups. Infarct size as percentage of AAR was significantly higher in the *Tst*$^{-/-}$ group compared to C57BL/6N wild type controls (WT; 64.6 ± 5.9 vs. *Tst*$^{-/-}$; 88.2 ± 2.3, Figure 5-11, P = 0.012).

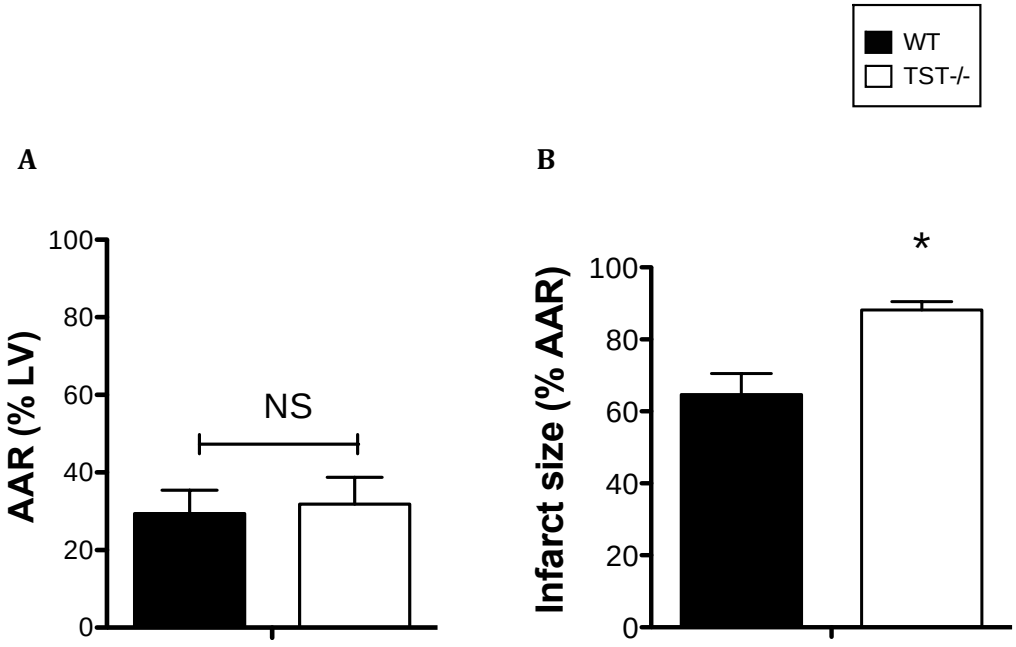

Figure 5-11 Infarct size is significantly increased following *ex vivo* model of ischaemia reperfusion injury

A) TTC stained area at risk (AAR) expressed as a percentage of the left ventricle. B) TTC stained infarct size as a percentage of area at risk. WT; n=5, *Tst*$^{-/-}$; n=4. Values are expressed as mean±SEM, *p<0.05

5.3.9 Myocardial mitochondrial respiration is diminished but comparable between groups following *in vitro* ischaemia reperfusion injury

In vitro ischaemia reperfusion injury (IRI) reduces cardiac mitochondrial oxygen consumption when compared to baseline readings (Figure 5-12). Mitochondrial respiratory recovery rate was similar between groups following *in vitro* IRI (Figure 5-12, WT; 70.9% ± 4.2% vs. *Tst*$^{-/-}$; 69.2% ± 4.2%).

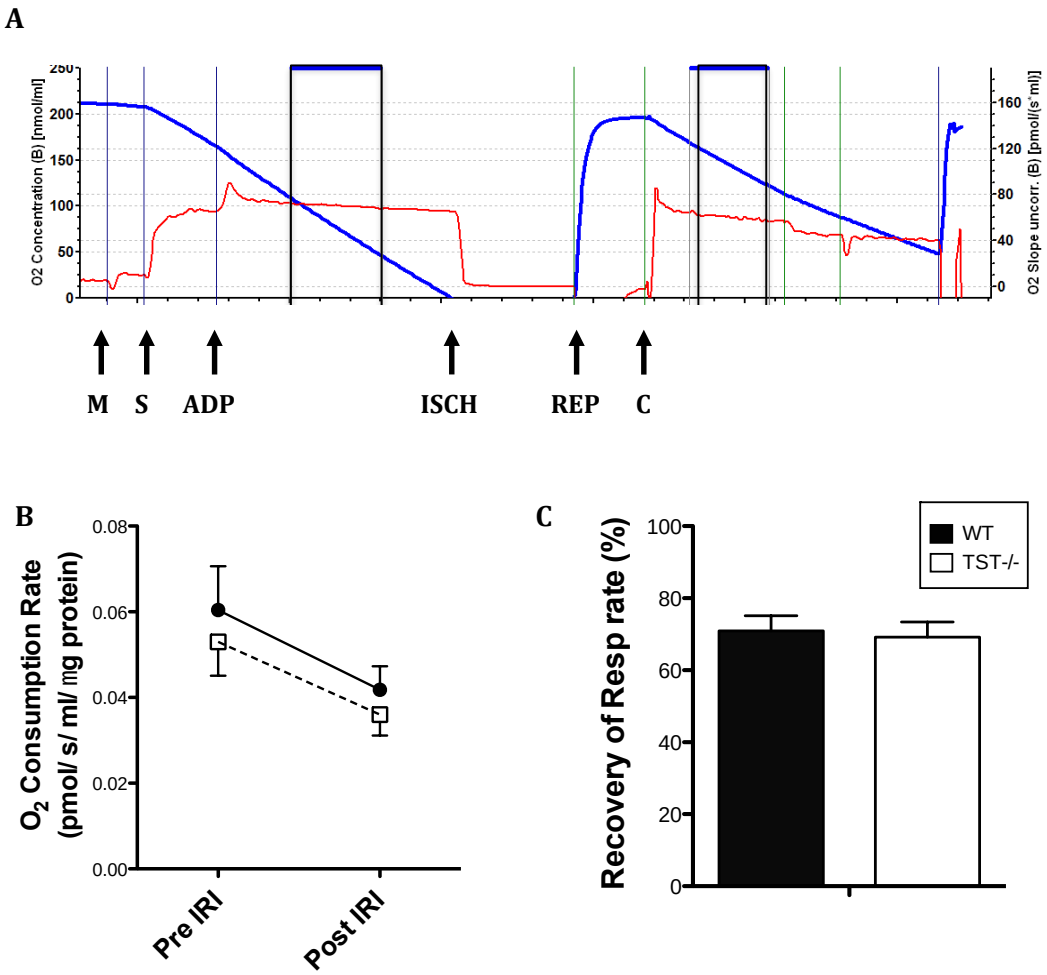

Figure 5-12 Isolated *Tst*$^{-/-}$ cardiac mitochondria show similar response to *in vitro* ischaemia reperfusion insult when compared to controls

A) Representative mitochondrial respiration trace showing timepoints of substrate administration to achieve state 3 respiration; malate (M), succinate (S) and ADP. Figure details the onset of ischaemia (ISCH), reperfusion (REP) and when the chamber was closed to atmosphere (C). Blue lines represents mitochondrial O_2 consumption and red line denotes change of respiration with substrate administration or O_2 depletion/ reintroduction (ischaemia/ reperfusion). Black boxes represent the linear phase of O_2 consumption (blue line) used for measurements. B) Oxygen consumption rate before and after ischaemia reperfusion injury (IRI) when normalised to protein. C) Oxygen consumption rate following IRI expressed as a percentage of pre-ischaemic respiration of same genotype and normalised to protein. WT; n=5, *Tst*$^{-/-}$; n=6, two hearts pooled per n number. Values are expressed as mean±SEM.

5.4 Discussion

The aims of the current study were (i) to evaluate how myocardial H_2S metabolic enzymes respond following coronary artery ligation (CAL) and (ii) to establish whether TST plays a role in regulating the response to ischaemia and/or infarct healing. This study showed that the heart actively regulates H_2S metabolic enzymes during the early and late infarct-healing phases and that loss of TST leads to dysregulation of this process. Loss of TST is detrimental to the heart, causing increased susceptibility to acute ischaemia and reperfusion injury, increased risk of cardiac rupture and enhanced detrimental structural and functional remodelling in survivors.

Dynamic Regulation of H_2S metabolic enzymes

Considerable cellular damage and cell death occurs in the minutes to hours following the onset of ischaemia. The early infarct-healing phase recruits neutrophils and pro-inflammatory monocyte/macrophages to the site of injury in the hours-days following MI to remove dead cardiomyocytes and cellular debris (Frangogiannis, 2012). Anti-inflammatory pro-repair monocyte/ macrophages dominate the cellular milieu from day 3-4 post MI onwards and initiate angiogenesis within infarcted tissue and form stable scar tissue. H_2S administration has been repeatedly shown to promote protection in models of acute myocardial ischaemia reperfusion injury (IRI) (Elrod *et al.*, 2007; Johansen *et al.*, 2006) and myocardial infarction (MI) induced by coronary artery ligation (CAL) (Zhu *et al.*, 2006). However, little is known of the extent to which endogenous H_2S synthetic and breakdown enzymes are regulated in the myocardium following injury.

In the current study, myocardial mRNA levels for the H_2S synthetic enzymes, *Cth* and *Mpst* were reduced during the early infarct healing phase at day 1 and 2 post-CAL, correspondingly protein levels were reduced at day 2 post-CAL compared to unoperated controls. Conversely, at 2 days post-CAL, myocardial mRNA levels for the H_2S breakdown enzymes *Tst, Sqrdl, Ethe1, Suox* levels were all markedly upregulated when compared to unoperated controls. Unfortunately insufficient tissue was collected to permit confirmation of protein levels in infarcted tissue. H_2S donors limit leukocyte recruitment to the heart following IRI or CAL (Elrod *et al.*, 2007; Zhang *et al.*, 2014). At 24hours post-CAL, cardiac H_2S levels were reported to fall as increased numbers of CD11b+/ Gr-1+ monocytes were mobilised into the blood from the spleen and recruited into the infarcted hearts of mice (Zhang *et al.*, 2014). In rats, *Cth* gene expression was lower by 2 days post-CAL (Zhu *et al.*,

2006) in agreement with the present findings. The data presented here and in the literature infers that during the early infarct-healing phase, the emphasis is on removal of H_2S, rather than production and this may help to ensure that inflammatory cells can infiltrate into the damaged tissue. TST is expressed in cardiomyocytes, myocardial vascular smooth muscle and in endothelial cells of aorta and intramuscular vessels (see sections 3.3.2 - 3.3.4) in a similar pattern to CSE, which may contribute to observed changes in expression. It is unclear if early pro-inflammatory leukocytes express TST, which may explain the timing of increased mRNA expression and should be investigated in future studies.

By 7 days post-CAL, during the second phase of infarct healing, mRNA levels of *Cth* and the H_2S breakdown enzymes are normalised relative to unoperated mice, although mRNA levels of the minor cardiovascular relevant H_2S generating enzyme *Mpst* remain reduced. This is a period of active angiogenesis in the healing myocardium (McSweeney *et al.*, 2010). H_2S donors have been reported to stimulate angiogenesis following MI via upregulation of vascular endothelial growth factor (VEGF) (Qipshidze *et al.*, 2012). In the current study, insufficient tissue was available to determine protein levels of the H_2S metabolic enzymes or cardiac H_2S levels at 7 days post-CAL so it was not possible to determine to what extent this was regulated during this phase of infarct healing. Together these data demonstrate the dynamic nature of H_2S metabolism in the infarcted heart during infarct healing phase and support a greater importance of TST and the other mitochondrial H_2S breakdown enzymes.

Myocardial rupture, infarct healing and structural/functional remodelling

Cardiac rupture is a fatal complication following MI, which typically occurs at the infarct border zone (Gao *et al.*, 2005). In C57BL/6 mice, cardiac rupture peaks at days 3-5 post-CAL due to ventricular wall thinning and reduced ventricular tensile strength (Gao *et al.*, 2005). According to the VALIANT trial, 8% of patient deaths within the first 30 days after MI were due to cardiac rupture (Shamshad *et al.*, 2010), with rupture incidence peaking between 5-10 days following MI. In the current study, the frequency of cardiac rupture is approximately 40% higher in $Tst^{-/-}$ mice compared to controls by 5 days post-CAL. Surviving $Tst^{-/-}$ mice have greater cardiac dysfunction and dilatation at 7 days post-CAL compared to controls. Cardiac function and remodelling following CAL are determined by the initial infarct size as well as by the quality of infarct healing. The evidence for changes in TST expression, together with detrimental outcomes in $Tst^{-/-}$ mice indicates that TST may play a vital role in these events. A variety of risk factors increase the likelihood of cardiac

rupture including, (i) infarct size, (ii) dysregulated leukocyte infiltration and (iii) haemodynamic status (Gao *et al.*, 2012).

(i) Infarct size

Initial infarct size is a key factor determining functional outcome and the extent of ventricular remodelling following injury. In C57BL/6J mice, cardiac rupture frequency markedly increases when infarct size exceeds 30% of the left ventricle (LV) corresponding to reduced ventricular tensile strength (Gao *et al.*, 2005). Early infarct size was not directly assessed in the present study in mice with permanent ligation. However, the observation that infarct size was increased in isolated perfused hearts from *Tst*$^{-/-}$ mice subjected to ischaemia and reperfusion, without any increase in the area at risk, suggests that the myocardium is more susceptible to injury in the absence of TST.

Robust production of H_2S from CSE is likely to be important in protection of the heart during the first minutes and hours after induction of ischaemia. Indeed, pharmacological inhibition of the H_2S synthesising enzyme CSE with PAG, administered to rats for 7 days prior to CAL, leads to increased infarct size and mortality compared to vehicle treated controls (Zhu *et al.*, 2006). Previous findings in this thesis (Chapter 3) show that expression of CSE is reduced in *Tst*$^{-/-}$ hearts under basal conditions (see section 3.3.8), perhaps as a result of a homeostatic negative feedback loop to limit H_2S production and avoid cytotoxicity. Thus reduced initial H_2S availability might account for increased injury in *Tst*$^{-/-}$ mice. In support of this hypothesis, protein levels of the H_2S-sensitive Nrf2 downstream target TRX1 show a downward trend at 4hours post-CAL in *Tst*$^{-/-}$ compared to WT hearts. Nitric oxide availability is another critical determinant of ischaemic injury (Scherrer-Crosbie *et al.*, 2001). Indeed protection of the heart by H_2S donors may be dependent upon NO. H_2S donor administration leads to phosphorylation of the eNOS activation site, phospho-eNOS^{S1177}. This is associated with increased myocardial NO availability and reduced IRI-induced damage in CSE-deficient mice (King *et al.*, 2014). Furthermore H_2S donor treatment has no effect on infarct size when administered to eNOS deficient mice or mice with mutated phospho-eNOS^{S1177}, confirming a role for eNOS in H_2S-mediated cardioprotection (King *et al.*, 2014). It is therefore important to note that hearts from *Tst*$^{-/-}$ mice also have reduced expression of eNOS protein (see section 3.3.11). CSE deficient mice have reduced cardiac H_2S and NO availability and increased infarct size compared to controls (King *et al.*, 2014), highlighting the importance of H_2S-NO crosstalk in mediating injury. eNOS derived NO is also an important determinant of myocardial infarct healing and remodelling (Scherrer-

Crosbie *et al.*, 2001). In comparison with the current study, mortality rates of eNOS deficient mice is approximately 40% higher than controls by 7 days post-CAL, whilst surviving eNOS deficient mice have reduced fractional shortening and greater left ventricular dilatation by 28 days post-CAL (Scherrer-Crosbie *et al.*, 2001). Therefore, it is likely that homeostatic feedback loops between H_2S breakdown and synthetic enzymes in the heart also influence myocardial H_2S-NO crosstalk and predisposes *Tst*$^{-/-}$ mice to increased injury, dysfunction, dilatation and rupture. eNOS protein expression and NO levels were not measured following CAL. It will be important to assess these and the expression of nNOS and iNOS, as both are alternative sources of NO in the injured myocardium. Due to mechanical failure of the H_2S electrode cardiac H_2S levels could not be directly measured in post-CAL hearts, this should also be addressed in future experiments.

Mitochondrial respiration

At low concentrations (0.1-1μM), H_2S can stimulate mitochondrial respiration by acting as an electron donor at complex 2 in the electron transport chain to produce ATP (Modis *et al.*, 2013b; Szabo *et al.*, 2014). However, higher concentrations of H_2S (3-30μM) can acutely inhibit mitochondrial bioenergetics (Modis *et al.*, 2013b) at cytochrome c in the respiratory chain.

Under basal conditions, *Tst*$^{-/-}$ mice have impaired H_2S breakdown in the heart and likely reduce cardiac CSE expression as a compensation to avoid H_2S-mediated cytochrome c inhibition. Previous findings show that respiratory rate is normal in mitochondria isolated from naive *Tst*$^{-/-}$ hearts (see section 3.3.12). In the current study, *in vitro* IRI studies performed on isolated cardiac mitochondria from naïve *Tst*$^{-/-}$ and control mice showed comparable respiratory recovery rates following injury. However, interpretation of these studies is limited by the removal of the cytosolic fraction, which contains the H_2S synthetic enzymes. Under *in vivo* hypoxic and *in vitro* calcium overload conditions (which occurs in myocardial IRI), CBS and CSE can translocate from the cytosol to the mitochondria in hepatocytes and mesenteric smooth muscle cells respectively, increasing H_2S production, mitochondrial respiration and ATP production (Fu *et al.*, 2012a; Teng *et al.*, 2013). However, it is currently unclear if H_2S enzyme translocation occurs in cardiac mitochondria following IRI or CAL-induced ischaemia. At 2 days post-CAL, protein expression of CSE, 3MST, TRX1 and HO-1 was increased in *Tst*$^{-/-}$ hearts, consistent with higher H_2S levels. If confirmed, increased myocardial H_2S levels the absence of TST at 2 days post-CAL could feasibly inhibit mitochondrial respiration and contribute to increased injury in *Tst*$^{-/-}$ mice. Future studies should investigate cardiac mitochondrial respiration at 2 days post-CAL.

(ii) *Early infarct healing and leukocyte recruitment*

Although H_2S reduces infarct size and mortality at 24-48hours post-CAL (Zhang *et al.*, 2014; Zhu *et al.*, 2006), no studies (to the authors knowledge) have yet investigated if regular administration of H_2S during the infarct-healing phase following CAL improves cardiac outcome. Cardiac specific CSE overexpressing mice (αMHC-CGL-Tg), produce more H_2S and have increased Nrf2 activation leading to greater protection from myocardial IRI (Calvert *et al.*, 2010; Elrod *et al.*, 2007). However, by 7 days after CAL, αMHC-CGL-Tg mice had a 30% mortality rate and by 4 weeks post-CAL, showed no improvement in cardiac function compared to controls (Calvert *et al.*, 2010). Although the authors failed to acknowledge the cause of death in the αMHC-CGL-Tg group, mortalities began from day 2 post-CAL, at a similar time to when we observe suppression of myocardial CSE expression in C57BL/6J mice. In the current study, protein levels of CSE and 3MST were significantly higher in *Tst*$^{-/-}$ hearts at day 2 post-CAL, 1 day prior to the onset of cardiac rupture in these mice. As mentioned previously, increased protein levels of CSE, 3MST, TRX1 and HO-1 in *Tst*$^{-/-}$ hearts at day 2 post-CAL are consistent with higher H_2S availability. Together these data infer that in models of CAL, raised cardiac CSE expression may be detrimental, leading to greater susceptibility to rupture and cardiac dysfunction in surviving mice, possibly due to elevated H_2S levels. Future studies should aim to administer CSE inhibitor compounds at day 2 post-CAL to *Tst*$^{-/-}$ mice to determine if CSE is involved in mitigating cardiac injury.

Ischaemia initiated by CAL elicits an intense inflammatory response mediated by activation of Toll-like receptors and the complement cascade (Ghigo 2014). Although essential for infarct repair, exaggerated or prolonged early neutrophil and Ly6C^{high} monocyte recruitment can impair the healing process leading to adverse remodelling and increased risk of rupture (Frangogiannis, 2012). Suppression of inflammatory cell recruitment is also detrimental to wound healing and leads to exaggerated cardiac remodelling (Frangogiannis, 2012). Several studies have demonstrated the anti-inflammatory effects of H_2S donors in models of inflammation and MI (Zanardo *et al.*, 2006). In cultured RAW264.7 macrophages, the H_2S donor, GYY4137 dose dependently inhibited lipopolysaccharide induced-NF-kB activation and expression of the pro-inflammatory cytokines, TNF-α and IL-1β (Whiteman, 2010). Administration of the H_2S donor, NaHS immediately before and 1hour following CAL suppresses myocardial leukocyte infiltration and expression of the inflammatory cytokines TNF-α and IL-1β at 24hours post-CAL (Zhang *et al.*, 2014). Although the Zhang 2014 study confirmed previous findings that H_2S limits inflammation following injury, it did not assess the effects of H_2S on infarct healing at later timepoints.

The current study used day 2 post-CAL as a key time-point to investigate whether alteration of leukocyte recruitment was responsible for detrimental wound healing in *Tst*$^{-/-}$mice because (i) *Tst* mRNA levels were markedly elevated in C57BL/6J mice at day 2 post-CAL (ii) CSE and 3MST protein expression is higher in *Tst*$^{-/-}$ hearts at day 2 post-CAL, and (iii) cardiac rupture incidence began at day 3 post-CAL permitting investigation prior to animal mortalities.

However, careful analysis using flow cytometry failed to detect any alteration in either the numbers of neutrophils and Ly6C^{high} monocytes detected in the blood after MI, or in those present in the infarcted left ventricle. Analysis of mRNA levels of myocardial MCP-1/ *Ccl2*, the MCP-1 receptor *Ccr2* and the adhesion molecule *Icam1* and *Vcam* also failed to reveal any modification in inflammatory signalling in hearts from *Tst*$^{-/-}$ mice. Alteration of the initial inflammatory response to infarction may not therefore account for increased cardiac rupture in these mice.

In the second infarct-healing phase that follows MI an orchestrated response is initiated by several different cell types to suppress pro-inflammatory signalling and promote repair (Frangogiannis, 2012). Defective resolution of post-infarction leukocyte response may lead to adverse cardiac remodelling and cardiac rupture (Frangogiannis, 2012; Ghigo *et al.*, 2014). From day 3-4 post-MI the monocyte/macrophage population becomes a more predominantly anti-inflammatory, pro-repair phenotype (Ly6C^{low}), under the influence of chemokines e.g. IL-4 and IL-13, generated in the healing myocardium by other cells, including fibroblasts and T cells. Promotion of these pro-repair monocytes/macrophages leads to increased angiogenesis, reduced infarct expansion and improved retention of cardiac function (McSweeney *et al.*, 2010). Growth factors including TGF-β that stimulate fibroblast to myofibroblast differentiation are necessary for collagen synthesis and deposition during scar formation (Gao *et al.*, 2012). Scar formation at the site of cardiomyocyte loss increases the tensile strength of the heart and is vital in preventing rupture (Gao *et al.*, 2012). Administration of H_2S-donors to human atrial fibroblasts *in vitro* markedly reduces TGF-β induced proliferation and differentiation into myofibroblasts, evident by reduced α-SMA mRNA levels and α-SMA immunoreactivity (Sheng *et al.*, 2013). In the current study, comparable numbers of Ly6C^{low} monocytes were detected in the blood and in digested hearts at 2 days post-CAL. However, it would be of interest to determine the extent to which the pro-repair process is initiated and sustained in *Tst*$^{-/-}$ heart. Studies carried out here do not support any reduction of macrophage content, or collagen deposition in mice surviving to 7 days after CAL. Future studies should measure myofibroblast and collagen content in

infarcted hearts of surviving mice at day 4-5 post-CAL to confirm that rupture is not caused by delayed removal of necrotic tissue and impaired collagen scar tensile strength when rupture incidence peaks. Additionally, pro-resolution inhibitory factors at day 4-5 post-CAL should be measured to identify if defective inflammatory resolution is the cause of the adverse cardiac remodelling and/or rupture.

(iii) Haemodynamic status

Heart rate and blood pressure are known risk factors influencing cardiac rupture following MI, which act as a force to facilitate wall tearing (Gao *et al.*, 2012). MI-induced cardiomyocyte loss and the replacement with stiff scar tissue alters ventricular contractility and stroke volume resulting in temporarily reduced blood pressure (Sutton *et al.*, 2000). To compensate, numerous neurohormonal factors are quickly activated such as the sympathetic adrenergic system, the renin angiotensin-aldosterone system (RAAS) and the release of endothelin, which increase heart rate, contractility of non-infarcted myocardium, vasoconstriction and fluid and sodium retention to temporarily maintain cardiac output and blood pressure (Sutton *et al.*, 2000). Telemetry observations indicate that cardiac rupture is preceded by marked increases in heart rate and blood pressure, typically when the mice are most physically active (Gao *et al.*, 2005; van den Borne *et al.*, 2008).

Although the current study did not measure heart rate prior to cardiac rupture at days 3-5 post MI, heart rate was comparable in anaesthetised *Tst*$^{-/-}$ and control mice at baseline and at 7 days after CAL. However, as heart rate is depressed with inhaled isoflurane to ensure clear echocardiographic image acquisition, the anaesthesia may mask the real values and so heart rate cannot be ruled out as a possible cause of cardiac rupture in these mice.

As outlined previously, TST is present in myocardial vascular smooth muscle and endothelial cells from large and small conductance arteries (see section 3.3.3 and 3.3.4). Under basal conditions, *Tst*$^{-/-}$ mice have mild endothelial dysfunction in small mesenteric arteries (see section 4.3.6), but remain normotensive, possibly via altered renal sodium handling (see section 4.3.3). However, it is unknown if *Tst*$^{-/-}$ mice maintain blood pressure regulation following MI. Blood pressure assessment was attempted in anaesthetised mice at day 2 post-CAL but insufficient numbers were carried out to permit statistical analysis and should be performed with larger sample groups in the future. However, given murine cardiac rupture typically occurs at night when mice are most active, telemetry studies should ideally

be performed to monitor heart rate and blood pressure in conscious mice during the initial 7 days after MI.

6 General Discussion

Numerous studies have characterised the ability of H_2S to dilate blood vessels, reduce blood pressure and protect the heart from MI-induced injury. It is recognised that local H_2S bioavailability is mediated by its enzymatic production and breakdown within the cell. However little is known of what impact H_2S breakdown has on net H_2S availability or indeed, how it regulates vascular function, blood pressure or the response to MI. The data described in this thesis tested the hypothesis that TST was present in the murine heart and vasculature and is actively involved in regulating local H_2S availability by efficient breakdown. Furthermore, it was hypothesised that TST loss would lead to increased H_2S availability and ultimately, would reduce blood pressure via increased vasodilatation and reduce injury following MI.

TST expression has been reported in several tissues throughout the body where it is thought to be involved in cyanide and H_2S breakdown (Nagahara *et al.*, 1998). Data in this thesis showed that TST is expressed in heart, liver, aorta and kidney tissues and in endothelial cells from aorta and small intramuscular vessels of the hindlimb (Chapter 3). Mice deficient for TST had significantly higher H_2S levels in the blood and a reduced rate of H_2S breakdown in the heart and liver. Together, these data supported our original hypothesis that TST is present in the heart where it regulates H_2S breakdown (Chapter 3). These data showcase the first viable mouse model of altered H_2S breakdown that do not present with associated H_2S-mediated cytotoxic complications observed in *Ethe1*$^{-/-}$ mice (Tiranti *et al.*, 2009).

TST utilises thiosulfate created at the SQR

Data in this thesis showed that *Tst*$^{-/-}$ mice had significantly higher levels of thiosulfate in plasma and urine, suggesting that contrary to previous conclusions (Hildebrandt *et al.*, 2008b), TST primarily utilises thiosulfate rather than producing it. A revision of the H_2S breakdown pathway has recently been proposed and this provides insight into why thiosulfate levels are higher in *Tst*$^{-/-}$ mice. Jackson and colleagues show that the SQR produces thiosulfate using the ETHE1-derived sulfite as SQR-borne persulfide acceptor (Jackson *et al.*, 2012). In vitro studies performed using purified recombinant human SQR expressed in E.coli showed that breakdown of H_2S by SQR using sulfite as the persulfide acceptor is a rapid and efficient reaction at physiological pH, resulting in thiosulfate formation (Jackson *et al.*, 2012). Moreover, Jackson and colleagues argue that thiosulfate formation by human SQR is approximately 10-fold faster than the rate of thiosulfate

formation by rat or bovine TST (Jackson et al., 2012). In this model SQR oxidises H_2S to persulfide, which is transferred to the acceptor sulfite, forming thiosulfate (Figure 6-1). TST then transfers sulfur from SQR-derived thiosulfate to gluthathione (GSH) forming gluthathione disulphide (GSSH) and simultaneously regenerates sulfite for the SQR reaction. GSSH provides substrate for ETHE1, producing sulfite that can be further converted to sulfate by SO and excreted or ETHE1-derived sulfite can be recycled to aid thiosulfate creation by the SQR. To date, evidence supporting this model had been lacking in mammalian models but higher thiosulfate levels observed in *Tst*$^{-/-}$ mice supports it. Loss of TST would appear to disrupt the efficiency of this pathway, increasing the accumulation of thiosulfate and reducing the rate of H_2S breakdown, as shown in heart and liver tissues. It is unclear what tissues are directly responsible for increased circulating thiosulfate and H_2S levels in *Tst*$^{-/-}$ mice but it seems likely that the colon and liver should play a major role. TST is highly expressed in the colon (Taniguchi *et al.*, 2009) to aid in the removal of bacterial-derived H_2S and therefore it is expected that loss of TST impairs H_2S breakdown and leads to increased concentrations of H_2S and thiosulfate in the blood. The hepatic portal vein receives venous blood from the digestive tract and accounts for approximately 75% of hepatic blood flow. TST is highly expressed in liver (Nagahara *et al.*, 1998) and as such, the liver is believed to act as a secondary barrier preventing colonic bacterial-derived H_2S from entering the systemic circulation via the central vein (Szabo *et al.*, 2014). The rate of H_2S breakdown is reduced by 50% in livers of *Tst*$^{-/-}$ mice indicating that the hepatic H_2S breakdown barrier is impaired and likely contributes to increased levels of H_2S and thiosulfate in the blood. However, although the rate of H_2S breakdown is reduced in heart and liver tissues from Tst-/- mice, H_2S is eventually catabolised, albeit at a slower rate indicating the system has compensated for TST loss. *Sqrdl* expression was not statistically different in heart, liver and kidney tissues of *Tst*$^{-/-}$ mice whilst higher thiosulfate levels in blood indicates that tissue SQR function is not impaired and indeed, may be enhanced to effectively catabolise high circulating H_2S when in contact with body tissues. Western blotting was attempted to measure SQR protein abundance but was unsuccessful on several occasions, warranting further investigation. Significantly higher concentrations of thiosulfate in urine of *Tst*$^{-/-}$ mice suggest that without TST, the body cannot adequately breakdown thiosulfate for sulfite and sulfate generation and subsequently, excretes it as waste. The Morton group is in the process of optimising assays to measure sulfite and sulfate levels as surrogate markers of ETHE1 and SO enzyme activity respectively, but these experiments were not completed at the time of writing. In-depth investigation of the H_2S breakdown

pathway in *Tst*$^{-/-}$ mice is warranted to understand how the pathway is adapted in the absence of TST.

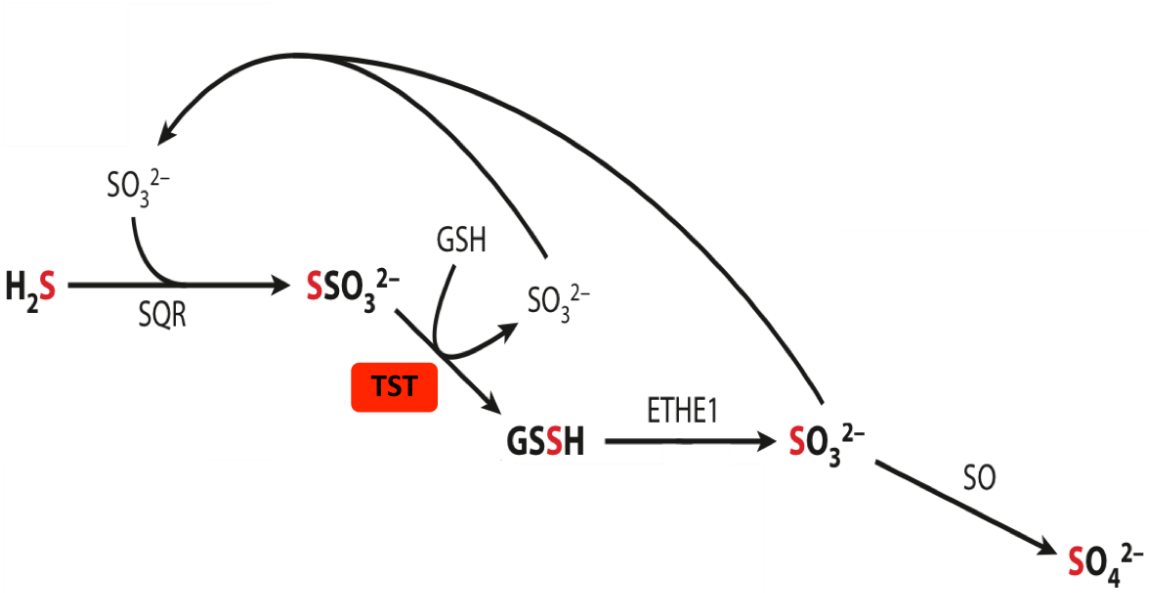

Figure 6-1 The Jackson mitochondrial H_2S oxidation pathway

H_2S is oxidised by the SQR forming thiosulfate, using sulfite as the SQR-persulfide acceptor. TST transfers sulfur from thiosulfate to glutathione, forming glutathione disulfide (GSSH) and further oxidised by ETHE1 to sulfite. ETHE1 derived sulfite can be recycled and used by the SQR or further oxidised to sulfate by sulfite oxidase and excreted. Diagram modified from (Kabil, Vitvitsky, & Banerjee, 2014).

Loss of TST activates a homeostatic negative feedback mechanism in the heart but not in kidney

TST is co-expressed in the same tissues as the H_2S synthetic enzymes, indicating that locally generated H_2S is tightly regulated by local breakdown within the mitochondria. Loss of TST alters the expression of CSE in heart and kidney tissues suggesting that TST may play an indirect role in its regulation. However, opposing effects were observed; CSE expression is reduced in the heart but increased in the kidney suggesting that alternate mechanisms are activated in these tissues.

Reduced CSE expression in hearts of *Tst*$^{-/-}$ mice supports the hypothesis that a homeostatic feedback mechanism exists in the murine heart. This is likely a protective mechanism to limit local H_2S generation and avoid H_2S-mediated cytotoxicity, supported by findings that cardiac structure and function is normal in *Tst*$^{-/-}$ mice compared to controls. Although, it remains unclear how CSE is downregulated in hearts of *Tst*$^{-/-}$ mice, it seems plausible that

the cell detects high levels of circulating H_2S and subsequently suppresses CSE production. Additionally, it's possible that intracellular signalling occurs between the cells sulfur storage pools and cytosolic bound CSE in heart, which regulates H_2S synthesis depending on whether sulfur pools are full or not. At 6 weeks following transaortic constriction (TAC) surgery, bound sulfane sulfur stores are reduced in the murine heart and correspond with increased myocardial CSE expression (Kondo 2013). Administration of the H_2S donor, SG1002 increases myocardial bound sulfane sulfur stores and normalises CSE expression to sham levels, supporting this hypothesis. Thiosulfate is recognised as bound sulfane sulfur present in the cells sulfur storage pools, which can be converted to H_2S under reducing conditions. The exogenous and endogenous reducing agents dithiothreitol (DTT), dihydrolipoic acid (DHLA) and thioredoxin (Trx1) rapidly generate H_2S from thiosulfate, which can exert biological effects such as vasodilatation in isolated aortas of mice or rats (Kolluru *et al.*, 2013; Mikami *et al.*, 2011; Olson *et al.*, 2013; Shen *et al.*, 2012). Therefore, high thiosulfate levels may be partly responsible for reduced CSE expression in *Tst*$^{-/-}$ hearts. Little is understood of how CSE or sulfur stores are regulated and are both active areas of research within the H_2S field. Future studies should measure cardiac CSE expression and enzyme activity following acute administration of the DTT, DHLA or Trx1 to determine if liberation of stored sulfane sulfur coincides with modified CSE expression or activity. It is possible that H_2S generation in the heart is more tightly regulated than other tissues studied to ensure that cardiac output is maintained to permit whole body perfusion.

It remains unclear why this negative feedback mechanism is not activated in the kidney of *Tst*$^{-/-}$ mice, especially given its exposure to high levels of H_2S in the blood/ filtrate. However, increased CSE expression in kidneys may not be caused by a dysfunctional feedback mechanism but perhaps a secondary effect to vascular dysfunction in small resistance arteries, which will be discussed in detail below. Unfortunately, due to issues with a batch of internal control antibodies, it is unknown if CSE protein levels are altered in the liver of *Tst*$^{-/-}$ mice and should be performed in future studies.

TST and blood pressure regulation

The ability of H_2S to relax blood vessels has long been considered the mechanism underlying its blood pressure lowering effects (Yang *et al.*, 2008; Zhao *et al.*, 2001). CSE is expressed in the vascular endothelium and smooth muscle and CSE deficient mice present with marked endothelial dysfunction in small mesenteric arteries and hypertension. Work in this thesis showed that TST is also expressed in endothelium of aorta and intramuscular vessels of the hindlimb (Chapter 3) suggesting that it may play a role in vascular function in small resistance vessels via regulation of H_2S availability. We hypothesised that loss of TST would increase H_2S availability and increase vasodilatation in small mesenteric arteries, lowering blood pressure. Myography experiments showed that *Tst*$^{-/-}$ mice have mild endothelial dysfunction of small mesenteric vessels (Chapter 4), contradicting this hypothesis. It remains unclear why *Tst*$^{-/-}$ mice have endothelial dysfunction but may be caused by endothelial damage induced by high H_2S levels in blood, warranting further investigation. Similar dysfunction in resistance vessels of *Tst*$^{-/-}$ mice would contribute to increased peripheral resistance and could increase blood pressure. Currently, it is unknown if *Tst*$^{-/-}$ mice have increased peripheral vascular resistance and this should be assessed alongside myography studies performed on smaller resistance arteries.

Increased sodium and water excretion in *Tst*$^{-/-}$ mice may be due to a pressure natriuresis (PN) response initiated by the kidney to maintain normotension. The PN response directly inhibits sodium reabsorption in the proximal convoluted tubule (PCT) by a cascade of paracrine and biophysical events, which increases excretion of sodium and water in urine, lowering extracellular fluid volume and normalising blood pressure (as detailed in background section 1.1.5.1) (Ivy *et al.*, 2014; McDonough *et al.*, 2003). Paracrine signalling is believed to be involved in the PN response by internalising sodium transporters such as the NHE3 and the Na^+/ K^+-ATPase pump from the membrane to the cytosol, resulting in reduced activity and sodium reabsorption (McDonough et al., 2003), but this mechanism is not well understood. The Na^+/ K^+-ATPase pump is present in the PCT, thick ascending limb of Henle (TALH) and the distal convoluted tubule (DCT) and is critical in producing the electrochemical gradient necessary for the movement of electrolytes and water from the filtrate into the cell via sodium cotransporters. Interestingly, NaHS has been reported to inhibit Na^+/ K^+-ATPase activity in renal basolateral membranes of rats due to internalisation, resulting in increased excretion of sodium, potassium and water (Ge *et al.*, 2014; Xia *et al.*, 2009). Considering that CSE, CBS and 3MST are localised in the PCT (Nagahara *et al.*, 1998; Yamamoto *et al.*, 2012), locally synthesised H_2S may act as a paracrine signalling molecule involved in the

acute PN response by inhibiting the Na^+/ K^+-ATPase pump and resultantly, impairing sodium reabsorption. TST is also expressed in the PCT (Sylvester *et al.*, 1990) and may indirectly regulate such a PN response by moderating H_2S bioavailability. Work presented in this thesis shows that CSE protein is increased whilst CBS protein tends to be higher in kidneys of *Tst*$^{-/-}$ mice suggesting that local H_2S generation is enhanced, and may be responsible for electrolyte malreabsorption. A strong trend for increased urinary phosphate excretion in *Tst*$^{-/-}$ mice suggests that the Na^+-Pi cotransporter is impaired and indicates that the PCT is the source of sodium and water losses in *Tst*$^{-/-}$ mice. The Na^+-Pi cotransporter is heavily reliant on the electrochemical gradient produced by the Na^+/ K^+-ATPase pump for sodium and phosphate reabsorption and serves as a surrogate marker of PCT function. This may be caused by a PN response initiated by CSE and CBS-mediated H_2S production. Inhibitor studies should be performed in the future to investigate if the CSE and CBS inhibitors, DL-propargylglycine (PAG) and aminooxyacetic acid (AOAA) can normalise electrolyte and water losses in *Tst*$^{-/-}$ mice. Unfortunately, small group numbers fail to provide statistical power for phosphate measurements and numbers should be increased in the future.

However, it cannot be ruled out that the natriuretic and diuretic phenotype in *Tst*$^{-/-}$ mice is simply due to the combined effects of high circulating H_2S levels, increased local H_2S production and reduced H_2S breakdown in the kidney causing direct inhibition of the Na^+/ K^+-ATPase in the PCT (Figure 6-2). As the Na^+/ K^+-ATPase is also present in the TALH and DCT, it is possible that increased H_2S in filtrate may also inhibit Na^+/ K^+-ATPase at these regions of the nephron by diffusing through apical membranes (Figure 6-2). This may explain why sodium losses were not compensated downstream of the PCT in *Tst*$^{-/-}$ mice, particularly in the TALH where 20-25% of total NaCl reabsorption from filtrate occurs by NKCC2 action. Although H_2S breakdown assays were not performed on kidney tissues, TST expression and enzyme activity in the kidney and liver are comparable (Nagahara *et al.*, 1998) and suggests that kidney H_2S breakdown is also markedly impaired and should be confirmed in future studies.

More in-depth investigation using specific experimental models of PN is warranted to elucidate if H_2S acts as a paracrine-signalling molecule in the PN response. The PN response can be experimentally replicated by surgically ligating the mesenteric and celiac arteries of mice causing incremental increases in MABP. Cannulation of the ureter allows collection of urine to measure urinary excretion of sodium and water during arterial pressure ramps (Ivy *et al.*, 2014). Healthy mice undergoing this procedure excrete more sodium and maintain

normal blood pressure (Ivy *et al.*, 2014). Using this experimental model, future studies should measure (i) the enzyme activities of TST and the H_2S synthetic enzymes (ii) H_2S levels (iii) Na^+/ K^+-ATPase activity and (iv) sodium and water excretion in control mice during pressure ramps to determine if H_2S is involved in PN-induced sodium malreabsorption in the kidney to maintain normotension. Ideally, this should be performed using TST inhibitors, as high circulating H_2S levels in *Tst*$^{-/-}$ mice cannot be controlled for. Unfortunately there are currently no commercially available selective TST inhibitors. Attempts were made by the Scott Webster drug discovery group, (QMRI, University of Edinburgh) to synthesise several in-house TST inhibitors but tests performed by the Morton lab have found that they lack selectivity and their use has since been discontinued.

PROXIMAL CONVOLUTED TUBULE

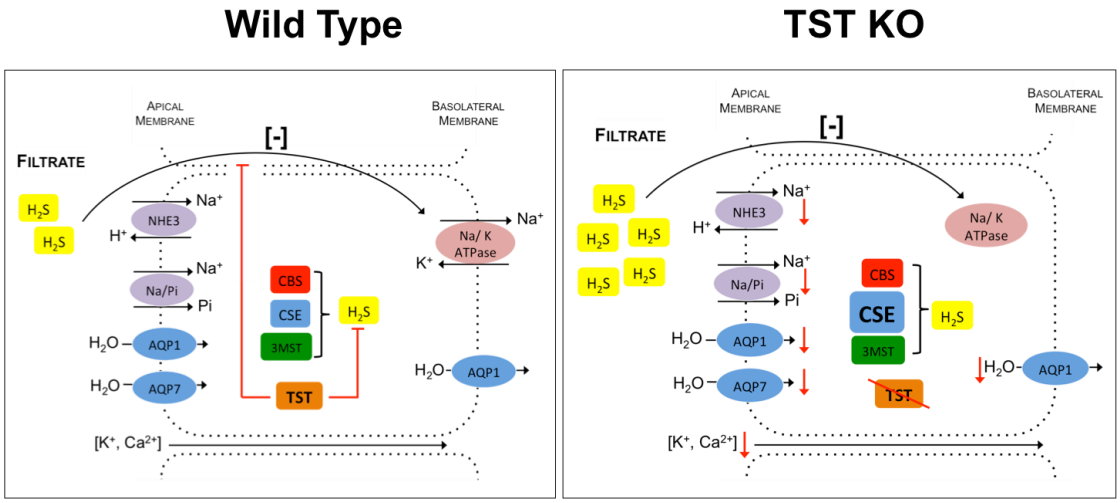

THICK ASCENDING LIMB OF HENLE

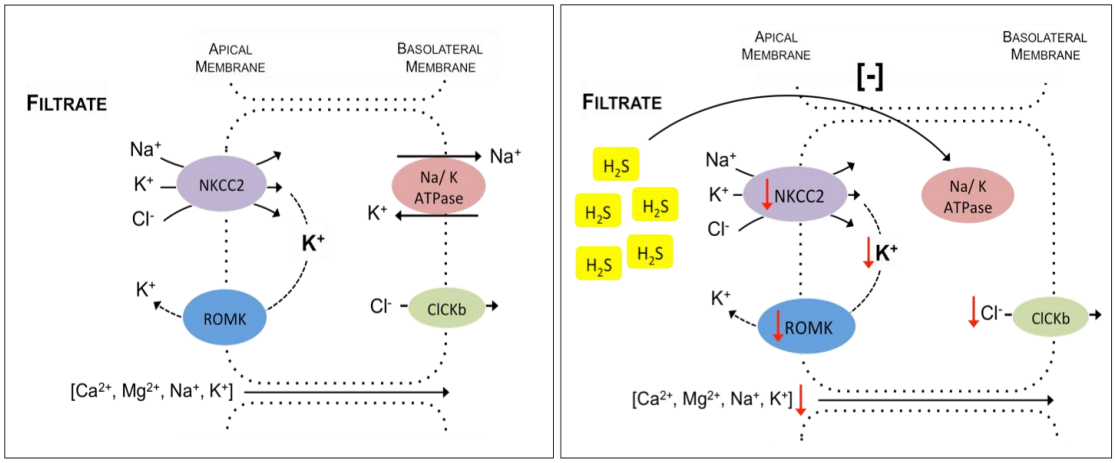

Figure 6-2 Model of increased electrolyte excretion in *Tst*$^{-/-}$ mice

TST prevents locally synthesised and circulating H_2S from internalising the Na^+/ K^+-ATPase in the proximal convoluted tubule (top left panel) and the thick ascending limb of Henle (bottom left panel). Loss of TST in the PCT of *Tst*$^{-/-}$ mice increases internalisation of the Na^+/ K^+-ATPase by CSE-mediated H_2S production (top right panel) and high circulating H_2S levels (top and bottom right panels) leading to reduced reabsorption of electrolytes and water.

TST is critical in regulating the heart's response to injury

The work in this thesis establishes that the mitochondrial bound TST is expressed in the cardiomyocytes and vasculature of the heart. We hypothesised that reduced H_2S breakdown in *Tst*$^{-/-}$ hearts would increase H_2S availability and protect the heart from MI. However, contrary to our hypothesis, *Tst*$^{-/-}$ mice are significantly more susceptible to injury. The precise mechanism causing this effect is unclear but it is likely that multiple factors occurring locally (as discussed in detail in chapter 5) and systemically are involved. Langendorff studies showed that cardiomyocytes are more susceptible to injury in the absence of TST, evident by increased infarct size following IRI. This is likely caused by reduced CSE expression that protects the heart from excessive H_2S generation under basal conditions but may predispose the heart to enhanced injury following MI. Reduced CSE-mediated H_2S generation is likely responsible for lowered eNOS expression under basal conditions and together, likely impair the hearts ability to acutely release H_2S and NO following injury, leading to increased damage. Reduced H_2S-NO crosstalk has been reported in CSE deficient mice, increasing their vulnerability to MI (King *et al.*, 2014). Future Langendorff studies should administer H_2S or NO donors during ischaemia to rescue *Tst*$^{-/-}$ hearts from IRI-induced injury.

Thiosulfate can be recycled to form H_2S by 3MST and the endogenous reducing agent, Trx1 (Mikami *et al.*, 2011) and has been hypothesised to act as an emergency sulfide source during ischaemia to stimulate ATP production via electron donation at complex 2 by the SQR (Olson, 2012). Increased myocardial expression of 3MST and Trx1 at 2days post CAL could generate toxic high concentrations of H_2S from high circulating thiosulfate levels, leading to inhibition of mitochondrial respiration in *Tst*$^{-/-}$ hearts, prompting cardiac dysfunction (Disatnik *et al.*, 2013; Neubauer, 2007). I hypothesise that TSTs utilisation of thiosulfate limits its conversion to H_2S by 3MST and Trx1 and this may explain why TST expression is markedly upregulated in control hearts at 2days post CAL. Under basal conditions, myocardial 3MST and Trx1 expression are comparable between groups suggesting that circulating thiosulfate would not be converted to H_2S when oxygen supply is sufficient to drive mitochondrial ATP production. This is supported by *in vitro* and *in vivo* findings showing comparable cardiac mitochondrial respiration and cardiac function between *Tst*$^{-/-}$ and WT mice. Future studies should measure thiosulfate and H_2S levels in the blood and heart tissue at 2days post CAL in *Tst*$^{-/-}$ mice to see if falling thiosulfate levels coincide with increased H_2S levels. Furthermore, isolated mitochondrial functional

experiments should be performed on *Tst*$^{-/-}$ and control hearts collected at 2day post CAL to determine if H_2S-mediated dysfunction is responsible for poorer post MI outcome.

Following MI-induced cardiomyocyte loss, activation of the renin angiotensin-aldosterone system (RAAS) and release of endothelin increase vasoconstriction and retention of sodium and water to temporarily maintain cardiac output and blood pressure (Sutton *et al.*, 2000). Loss of TST causes mild vascular dysfunction in small mesenteric arteries (Chapter 4) but blood pressure is not affected under basal conditions. However, it is possible that a combination of sympathetic stimulation, endothelin release and RAAS stimulation following MI may cause excessive vasoconstriction in small arteries and increase fluid and sodium retention in *Tst*$^{-/-}$ mice leading to cardiac rupture and cardiac dilatation in surviving mice. As outlined in chapter 5, blood pressure measurements were attempted on mice 1 day prior to the onset of rupture, but insufficient numbers were tested to permit statistical analysis. However, MI-induced cardiac rupture typically occurs at night when mice are most active and therefore, blood pressure measurements performed on unconscious mice during the day may not be the best approach. Therefore telemetry and metabolic cage studies should be performed in unison to monitor blood pressure and fluid retention in conscious mice during the initial 7 days after MI to elucidate if neurohormonal stimulated haemodynamic alterations contribute to increased cardiac rupture risk in *Tst*$^{-/-}$ mice.

Although the H_2S field has been preoccupied with CSE transgenic models and pharmacological H_2S donors to ensure protection from IRI, little consideration has been afforded to what impact such treatments may place upon the mitochondrial H_2S breakdown enzymes. Here, we show that TST is critical in mediating the hearts response to injury in IRI and permanent ligation models (Chapter 5). TST is increased during the early healing phase and loss of TST increases the rate of rupture. To date, 11 polymorphisms in the TST gene have been identified in healthy humans (Billaut-Laden *et al.*, 2012) and mice suffering from inflammatory bowel disease (IBD) have reduced TST expression and activity in the colon (Taniguchi *et al.*, 2009). It is unknown if TST activity is reduced in the colon of IBD patients or if TST activity is impaired in their hearts, which may predispose them to enhanced injury following unreperfused MI. Cardiac specific CSE overexpressing mice (αMHC-CGL-Tg^{+}) have increased H_2S availability in the heart but fail to preserve cardiac function by 4weeks following permanent ligation and this may be due to an impaired infarct healing response (Calvert *et al.*, 2010). From the data presented in this thesis (Chapter 5), control hearts actively downregulate the H_2S synthetic enzymes and upregulates the H_2S breakdown

enzymes during the early healing phase. Early stage clinical trials using the H_2S donor SG1002 on heart failure patients are underway and should these drugs be administered to patients who did not receive reperfusion therapy, it is possible that SG1002 may inadvertently cause harm, especially if given regularly during the early infarct-healing phase.

Concluding remarks and future directions

Global loss of TST modifies several organ systems simultaneously confirming the ubiquitous expression of TST and highlighting its role in the vasculature and in the heart's response to MI. However, *Tst*$^{-/-}$ mice have increased H_2S levels in blood, altering tissue H_2S synthetic enzyme expression and making tissue effects difficult to interpret. Although Langendorff studies show that TST plays a critical role in the heart's response to injury in isolation from other systems and circulating levels of H_2S and thiosulfate, a more specific transgenic mouse model is warranted to understand the mechanism causing the cardiac rupture and poorer post MI outcomes in *Tst*$^{-/-}$ mice. Future studies require tissue specific TST knockout models and inducible transgenic mice to fully elucidate the role of TST in these organ systems and its role following injury. This data shows that TST is beneficial for vascular health and is critical following MI. As such, future studies may attempt to stimulate TST during the early infarct-healing phase following unreperfused MI to reduce cardiac rupture and improve cardiac outcome. Furthermore, these data may accelerate the development of TST inhibitors for use as loop diuretics in the kidney or as treatments in haemorrhagic shock patients to reduce vasodilatation but obviously, further work as detailed above needs to be completed to understand the actions involved in these processes. Moreover, these data will further the understanding of the H_2S breakdown pathway in the mitochondria and provide the H_2S field with an alternative mouse model to investigate the complexity of H_2S biology following permanent ligation. It is becoming clearer that H_2S may not be a wonder molecule in all injury models and the data outlined here supports that excessive H_2S may in fact be detrimental to the early healing phase after unreperfused MI.

7 References

Abe, K., & Kimura, H. (1995). The Possible Role of Hydrogen Sulfide as an Endogenous Neuromodulator. *The Journal of Neuroscience*, *16*(3); 1066–1071.

Albertini, E. (2012). Cystathionine beta synthase modulates senescence of human endothelial cells. *Aging*, *4* (10); 664-673

Althaus, M., Urness, K. D., Clauss, W. G., Baines, D. L., & Fronius, M. (2012). The gasotransmitter hydrogen sulphide decreases Na+ transport across pulmonary epithelial cells. *British Journal of Pharmacology*, *166*(6), 1946–1963.

Amemiya, M., Loffing, J., Lotscher, M., Kaissling, B., Moe, O., & Alpern, R. (1995). Expression of NHE-3 in the apical membrane of rat renal proximal tubule and thick ascending limb, *Kidney International*, (48), 1206-1215.

Amirlak, I., & Dawson, K. (2000). Bartter syndrome: an overview. *Quarterly Journal Medicine*, *93*, 207–215.

Arnaud-Batista, F. J., Costa, G. T., Oliveira, I. M. B., Costa, P. P. C., Santos, C. F., Fonteles, M. C., Uchoa, D.E., Silveira, E.R., Cardia, B. A., Carvalho, K.M., Amaral, L.S., Pocas, E.S., Quintas, L.E., Noel, F., Nascimento, N.R., (2012). Natriuretic effect of bufalin in isolated rat kidneys involves activation of the Na+-K+-ATPase-Src kinase pathway. *AJP: Renal Physiology*, *302*(8), F959–F966.

Bartholomew T.C., Powell G.M., Dodgson K.S., and Curtis C.G, (1980). Oxidation of sodium sulphide by rat liver, lungs and kidney. *Biochemical Pharmacology* (29) 2431–2437.

Bhat, Y., Vinayaka, G., & Sreelakshmi, K. (2012). Antenatal Bartter Syndrome: A Review. *International Journal of Pediatrics*, *2012*(6), 1–5.

Bian, J. S. (2005). Role of Hydrogen Sulfide in the Cardioprotection Caused by Ischemic Preconditioning in the Rat Heart and Cardiac Myocytes. *Journal of Pharmacology and Experimental Therapeutics*, *316*(2), 670–678.

Billaut-Laden, I., Allorge, D., Crunelle-Thibaut, A., Rat, E., Cauffiez, C., Chevalier, D., Houdret, N., Lo-Guidice, J. M., Broly, F. (2012). Evidence for a functional genetic polymorphism of the human thiosulfate sulfurtransferase (Rhodanese), a cyanide and H2S detoxification enzyme. *Toxicology*, *225*(1), 1–11.

Bohlender, J., Menard, J., Edling, O., Ganten, D., & Friedrich, L. (1998). Mouse and rat plasma renin concentration and gene expression in (mRen2)27 transgenic rats, *Am J Physiol* (5Pt 2), 1450–1456.

Cai, M., Wang, M., Moore, P. K., Jin, H., Yao, T., & Zhu, Y. C. (2007). The novel proangiogenic effect of hydrogen sulfide is dependent on Akt phosphorylation.

Cardiovascular Research, *76*(1), 29–40.

Calvert, J. W., Elston, M., Nicholson, C. K., Gundewar, S., Jha, S., Elrod, J. W., Ramachandran, A., Lefer, D. J. (2010). Genetic and Pharmacologic Hydrogen Sulfide Therapy Attenuates Ischemia-Induced Heart Failure in Mice. *Circulation*, *122*(1), 11–19.

Calvert, J. W., Jha, S., Gundewar, S., Elrod, J. W., Ramachandran, A., Pattillo, C. B., Kevil, C. G., Lefer, D. J. (2009). Hydrogen Sulfide Mediates Cardioprotection Through Nrf2 Signaling. *Circulation Research*, *105*(4), 365–374.

Caporali, A., Meloni, M., Vollenkle, C., Bonci, D., Sala-Newby, G. B., Addis, R., Spinetti, G., Losa, S., Masson, R., Baker, A.H., Agami, R., le Sage, C., Condorelli, G., Madeddu, P., Martelli, F., Emanuaeli, C. (2011). Deregulation of microRNA-503 Contributes to Diabetes Mellitus-Induced Impairment of Endothelial Function and Reparative Angiogenesis After Limb Ischemia. *Circulation*, *123*(3), 282–291.

Carden, D., & Granger, D. (2000). Pathophysiology of ischaemia-reperfusion injury. *The Journal of Pathology*, *190*(3), 255-266.

Castrop, H., & Schiessl, I. M. (2014). Physiology and pathophysiology of the renal Na-K-2Cl cotransporter (NKCC2). *American Journal Physiology: Renal Physiology*, *307*(9), 991–1002.

Chen, L., Daum, G., Chitaley, K., Coats, S.A., Bowen-Pope, D.F., Eigenthaler, M., Thumati, N. R., Walter, U., Clowes, A.W. (2004). Vasodilator-stimulated phosphoprotein regulates proliferation and growth inhibition by nitric oxide in vascular smooth muscle cells, *Arterioscler Thromb Vasc Biol*, *24*(8), 1403-1408.

Cherniavsky-Lev, M., Golani, O., Karlish, S. J. D., & Garty, H. (2014). Ouabain-induced Internalization and Lysosomal Degradation of the Na+/K+-ATPase. *Journal of Biological Chemistry*, *289*(2), 1049–1059.

Cipollone, R., Ascenzi, P., & Visca, P. (2007). Common themes and variations in the rhodanese superfamily. *IUBMB Life*, *59*(2), 51–59.

Cortese-Krott, M., Fernandez, B., Santos, J. L. T., Mergia, E., Grman, M., Nagy, P., Kelm, M., Butler, A., Feelisch, M. (2014). Nitrosopersulfide (SSNO(-)) accounts for sustained NO bioactivity of S-nitrosothiols following reaction with sulfide. *Redox Biology*, *2*(C), 234–244.

Danson, E., Choate, J., & Paterson, D. (2005). Cardiac nitric oxide: Emerging role for nNOS in regulating physiological function. *Pharmacology & Therapeutics*, *106*(1), 57–74.

Defawe, O. D., Kim, S., Chen, L., Huang, D., Kenagy, R. D., Renné, T., Walter, U., Daum, G., Clowes, A.W. (2010). VASP phosphorylation at serine239 regulates the effects of NO on smooth muscle cell invasion and contraction of collagen. *Journal of*

Cellular Physiology, *222*(1), 230–237.

Dewald, O., Zymek, P., Winkelmann, K., Koerting, A., Ren, G., Abou-Khamis, T., Michael, L.H., Rollins, B. J., Entman, M. L., Frangogiannis, N. G. (2005). CCL2/Monocyte Chemoattractant Protein-1 Regulates Inflammatory Responses Critical to Healing Myocardial Infarcts. *Circulation Research*, *96*(8), 881–889.

Disatnik, M. H., Ferreira, J. C. B., Campos, J. C., Gomes, K. S., Dourado, P. M. M., Qi, X., & Mochly-Rosen, D. (2013). Acute Inhibition of Excessive Mitochondrial Fission After Myocardial Infarction Prevents Long-term Cardiac Dysfunction. *Journal of the American Heart Association*, *2*(5), 461–467.
Doeller, J. E., Isbell, T. S., Benavides, G., Koenitzer, J., Patel, H., Patel, R. P., Lancaster, J. R., Darley-Usmar, V. M., Kraus, D.W. (2005). Polarographic measurement of hydrogen sulfide production and consumption by mammalian tissues. *Analytical Biochemistry*, *341*(1), 40–51.

Elrod, J. W., James, J. M., Bryan, N., Langston, W., Szot, J., Gebregzlabher, H., Janssens, S., Feelisch, M., Lefer, D.J. (2006). Cardiomyocyte-Specific Overexpression of NO Synthase-3 Protects Against Myocardial Ischemia-Reperfusion Injury. *Arteriosclerosis, Thrombosis, and Vascular Biology*, *26*(7), 1517–1523.

Elrod, J., Calvert, J. W., Morrison, J., Doeller, J., Kraus, D. W., Tao, L., Jiao, X., Scalia R., Kiss, L., Szabo, C., Kimura, H., Chow, C. W., Lefer, D. J. (2007). Hydrogen sulfide attenuates myocardial ischemia-reperfusion injury by preservation of mitochondrial function. *Proceedings of National Academy of Science*, *104*, 15560–15565.

Elsey, D. J., Fowkes, R. C., & Baxter, G. F. (2010). Regulation of cardiovascular cell function by hydrogen sulfide (H_2S). *Cell Biochemistry and Function*, *28*(2), 95–106.

Frangogiannis, N. G., (2012). Regulation of the Inflammatory Response in Cardiac Repair. *Circulation Research*, *110*(1), 159–173.

Frangogiannis, N. G., & Entman, M. (2002). The inflammatory response in myocardial infarction. *Cardiovascular Research*, *53*, 31–47.

Frezza, C., Cipolat, S., & Scorrano, L. (2007). Organelle isolation: functional mitochondria from mouse liver, muscle and cultured filroblasts. *Nature Protocols*, *2*(2), 287–295.

Fu, M., Zhang, W., Wu, L., Yang, G, Li, H., & Wang, R. (2012a). Hydrogen sulfide (H_2S) metabolism in mitochondria and its regulatory role in energy production. *Pnas*, *109*(8), 2943–2948.

Fu, M., Zhang, W., Yang, G., & Wang, R. (2012b). Is cystathionine gamma-lyase protein expressed in the heart? *Biochemical and Biophysical Research Communications*, *428*(4), 469–474.

Furne, J., Saeed, A., & Levitt, M. D. (2008). Whole tissue hydrogen sulfide concentrations are orders of magnitude lower than presently accepted values. *American Journal Physiology: Regulatory, Integrative and Comparative Physiology*, *295*(5), 1479–1485.

Gao, X. M., White, D., Dart, A., & Du, X. J. (2012). Post-infarct cardiac rupture: Recent insights on pathogenesis and therapeutic interventions. *Pharmacology & Therapeutics*, *134*(2), 156–179.

Gao, X., Xu, Q., Kiriazis, H., Dart, A., & Du, X. J. (2005). Mouse model of post-infarct ventricular rupture: time course, strain- and gender-dependency, tensile strength, and histopathology. *Cardiovascular Research*, *65*(2), 469–477.

Garlid, K. D., & Halestrap, A. P. (2012). The mitochondrial K_{ATP} channel—Fact or fiction? *Journal of Molecular and Cellular Cardiology*, *52*(3), 578–583.

Ge, S.-N., Zhao, M.-M., Wu, D.-D., Chen, Y., Wang, Y., Zhu, J.-H., Cai W. J., Zhu, Y. Z., Zhu Y. C. (2014). Hydrogen Sulfide Targets EGFR Cys797/Cys798 Residues to Induce Na +/K +-ATPase Endocytosis and Inhibition in Renal Tubular Epithelial Cells and Increase Sodium Excretion in Chronic Salt-Loaded Rats. *Antioxidants & Redox Signaling*, *21*(15), 2061–2082.

Geng, B., Chang, L., Pan, C., Qi, Y., Zhao, J., Pang, Y., Du, J., Tang, C. (2004a). Endogenous hydrogen sulfide regulation of myocardial injury induced by isoproterenol. *Biochemical and Biophysical Research Communications*, *318*(3), 756–763.

Geng, B., Yang, J., Qi, Y., Zhao, J., Pang, Y., Du, J., & Tang, C. (2004b). H_2S generated by heart in rat and its effects on cardiac function. *Biochemical and Biophysical Research Communications*, *313*(2), 362–368.

Ghigo, A., Franco, I., Morello, F., & Hirsch, E. (2014). Myocyte signalling in leucocyte recruitment to the heart. *Cardiovascular Research*, *102*(2), 270–280.

Guyton, A. (1987). Renal Function Curve - a key to understanding the pathogenesis of hypertension. *Hypertension*, (10), 1–7.

Hausenloy, D. J., & Yellon, D. M. (2013). Myocardial ischemia-reperfusion injury: a neglected therapeutic target. *Journal of Clinical Investigation*, *123*(1), 92–100.

Hildebrandt, T. M., & Grieshaber, M. K. (2008a). Redox regulation of mitochondrial sulfide oxidation in the lugworm, Arenicola marina. *Journal of Experimental Biology*, *211*(16), 2617–2623.

Hildebrandt, T. M., & Grieshaber, M. K. (2008b). Three enzymatic activities catalyze the oxidation of sulfide to thiosulfate in mammalian and invertebrate mitochondria. *FEBS Journal*, *275*(13), 3352–3361.

Hosoki, R., Matsuki, N., & Kimura, H. (1997). The Possible Role of Hydrogen Sulfide as an Endogenous Smooth Muscle Relaxant in Synergy with Nitric Oxide. *Biochemical and Biophysical Research Communications*, *237*, 527–531.

Hu, Y., Chen, X., Pan, T.-T., Neo, K. L., Lee, S. W., Khin, E. S., Moore, P. K., Bian, J. S. (2007). Cardioprotection induced by hydrogen sulfide preconditioning involves activation of ERK and PI3K/Akt pathways. *Pflügers Archiv - European Journal of Physiology*, *455*(4), 607–616.

Intengan, H., & Schiffrin, E. (2000). Structure and Mechanical Properties of Resistance Arteries in Hypertension. *Hypertension*, *36*, 312–318.

Ishigami, M., Hiraki, K., Umemura, K., Ogasawara, Y., Ishii, K., & Kimura, H. (2009). A Source of Hydrogen Sulfide and a Mechanism of Its Release in the Brain. *Antioxidants & Redox Signaling*, *11*(2), 205–214.

Ivy, J. R., & Bailey, M. A. (2014). Pressure natriuresis and the renal control of arterial blood pressure. *The Journal of Physiology*, *592*(18), 3955–3967.

Jackson, M. R., Melideo, S. L., & Jorns, M. S. (2012). Human Sulfide:Quinone Oxidoreductase Catalyzes the First Step in Hydrogen Sulfide Metabolism and Produces a Sulfane Sulfur Metabolite. *Biochemistry*, *51*(34), 6804–6815.

Jeanes, H. L., Tabor, C., Black, D., Ederveen, A., & Gray, G. A. (2008). Oestrogen-mediated cardioprotection following ischaemia and reperfusion is mimicked by an oestrogen receptor (ER) agonist and unaffected by an ER antagonist. *Journal of Endocrinology*, *197*(3), 493–501.

Johansen, D., Ytrehus, K., & Baxter, G. F. (2006). Exogenous hydrogen sulfide (H2S) protects against regional myocardial ischemia–reperfusion injury. *Basic Research in Cardiology*, *101*(1), 53–60.

Kabil, O., & Banerjee, R. (2014). Enzymology of H_2S Biogenesis, Decay and Signaling. *Antioxidants & Redox Signaling*, *20*(5), 770–782.

Kabil, O., Vitvitsky, V., & Banerjee, R. (2014). Sulfur as a Signaling Nutrient Through Hydrogen Sulfide. *Annual Review of Nutrition*, *34*(1), 171–205.

Kimura, H. (2010). Hydrogen sulfide: its production, release and functions. *Amino Acids*, *41*(1), 113–121.

Kimura, H. (2014). Hydrogen Sulfide and Polysulfides as Biological Mediators. *Molecules*, *19*(10), 16146–16157.

King, A. L., Polhemus, D. J., Bhushan, S., Otsuka, H., Kondo, K., Nicholson, C. K., et al. (2014). Hydrogen sulfide cytoprotective signaling is endothelial nitric oxide synthase-nitric oxide dependent. *Proceedings of the National Academy of Sciences*,

111(8), 3182–3187.

King, A., & Lefer, D. (2011). Cytoprotective actions of hydrogen sulfide in Ischaemia-reperfusion injury. *Experimental Physiology*, 840–846.

Koivumaki, J. T., Takalo, J., Korhonen, T., Tavi, P., & Weckstrom, M. (2009). Modelling sarcoplasmic reticulum calcium ATPase and its regulation in cardiac myocytes. *Philosophical Transactions of the Royal Society: Mathematical, Physical and Engineering Sciences*, *367*(1896), 2181–2202.

Kolluru, G. K., Shen, X., Bir, S. C., & Kevil, C. G. (2013). Hydrogen Sulfide Chemical biological: Pathophysiological roles and detection. Nitric Oxide. *Nitric Oxide*, *35*(C), 5–20.

Kondo, K., Bhushan, S., King, A. L., Prabhu, S. D., Hamid, T., Koenig, S., Murohara, T., Predmore, B. L., Gojon, G., Sr., Gojon, G, Jr., Wang, R., Karusula, N., Nicholson, C. K., Calvert, J. W., Lefer, D. J., (2013). H_2S Protects Against Pressure Overload-Induced Heart Failure via Upregulation of Endothelial Nitric Oxide Synthase. *Circulation*, *127*(10), 1116–1127.

Li, L., Rose, P., & Moore, P. K. (2011). Hydrogen Sulfide and Cell Signaling. *Annual Review of Pharmacology and Toxicology*, *51*(1), 169–187.

Ljubkovic, M., Mio, Y., Marinovic, J., Stadnicka, A., Warltier, D. C., Bosnjak, Z. J., & Bienengraeber, M. (2006). Isoflurane preconditioning uncouples mitochondria and protects against hypoxia-reoxygenation. *American Journal of Physiology: Cell Physiology*, *292*(5), 1583–1590.

Maron, B. A., & Loscalzo, J. (2009). The Treatment of Hyperhomocysteinemia. *Annual Review of Medicine*, *60*(1), 39–54.

Martelli, A., Testai, L., Breschi, M. C., Lawson, K., McKay, N. G., Miceli, F., et al. (2013). Vasorelaxation by Hydrogen sulfide involves activation of K_v7 potassium channels. *Pharmacological Research*, *70*(1), 27–34.

McDonough, A., Leong, P. K., & Yang, L. (2003). Mechanisms of pressure natriuresis. *Annals of the New York Academy of Sciences*, (986), 669–677.

McKinley, M. J., & Johnson, A. (2004). The Physiological Regulation of Thirst and Fluid Intake. *News in Physiological Sciences*, *19*(1), 1–6.

McSweeney, S. J., Hadoke, P. W. F., Kozak, A. M., Small, G. R., Khaled, H., Walker, B. R., & Gray, G. A. (2010). Improved heart function follows enhanced inflammatory cell recruitment and angiogenesis in 11 HSD1-deficient mice post-MI. *Cardiovascular Research*, *88*(1), 159–167.

Mikami, Y., Shibuya, N., Kimura, Y., Nagahara, N., Ogasawara, Y., & Kimura, H. (2011). Thioredoxin and dihydrolipoic acid are required for 3-mercaptopyruvate

sulfurtransferase to produce hydrogen sulfide. *Biochemical Journal*, *439*(3), 479–485.

Mikami, Y., Shibuya, N., Ogasawara, Y., & Kimura, H. (2013). Biochemical and Biophysical Research Communications. *Biochemical and Biophysical Research Communications*, *431*(2), 131–135.

Modis, K., Asimakopoulou, A., Coletta, C., Papapetropoulos, A., & Szabo, C. (2013a). Oxidative stress supports the cellular bioenergetic effect of the 3-mercaptopyruvate sulfurtransferase/ hydrogen sulfide pathway. *Biochemical and Biophysical Research Communications*, *433*(4), 401–407.

Modis, K., Coletta, C., Erdelyi, K., Papapetropoulos, A., & Szabo, C. (2013b). Intramitochondrial hydrogen sulfide production by 3-mercaptopyruvate sulfurtransferase maintains mitochondrial electron flow and supports cellular bioenergetics. *The FASEB Journal*, *27*(2), 601–611.

Mullins, L. J., Bailey, M. A., & Mullins, J. J. (2006). Hypertension, Kidney, and Transgenics: A Fresh Perspective. *Physiological Reviews*, *88*(2), 709–746.

Mustafa, A. K., Sikka, G., Gazi, S. K., Steppan, J., Jung, S. M., Bhunia, A. K., Barodka, V. M., Gazi, F. K., Barrow, F. K., Wang, R., Amzel, L. M., Berkowitz, B. E., Snyder, S. H. (2011). Hydrogen Sulfide as Endothelium-Derived Hyperpolarizing Factor Sulfhydrates Potassium Channels. *Circulation Research*, *109*(11), 1259–1268.

Nagahara, N., I, T., Hitoshi, K., & Nishino, T. (1998). Tissue and subcellular distribution of mercaptopyruvate sulfurtransferase in the rat: confocal laser fluorescence and immunoelectron microscopic studies combined with biochemical analysis. *Histochemistry and Cell Biology*, *110*, 243–250.

Nagahara, N., Nagano, M., Ito, T., Shimamura, K., Akimoto, T., & Suzuki, H. (2013). Antioxidant enzyme, 3-mercaptopyruvate sulfurtransferase-knockout mice exhibit increased anxiety-like behaviors: a model for human mercaptolactate-cysteine disulfiduria. *Scientific Reports*, *3*, 1038-1043.

Nahrendorf, M., Pittet, M. J., & Swirski, F. K. (2010). Monocytes: Protagonists of Infarct Inflammation and Repair After Myocardial Infarction. *Circulation*, *121*(22), 2437–2445.

Neubauer, S. (2007). The Failing Heart — An Engine Out of Fuel. *New England Journal of Medicine*, *356*(11) 1140–1151.

Ogasawara, Y., Isoda, S., & Tanabe, S. (1994). Tissue and Subcellular Distribution of Bound and Acid-Labile Sulfur and the Enzymatic capacity for sulfide production in the rat. *Biol. Pharm. Bull.*, *17*, 1535–1542.

Olson, K. R. (2012). Mitochondrial adaptations to utilize hydrogen sulfide for energy and signaling. *Journal of Comparative Physiology B.*, *182*(7), 881-897

Olson, K. R., DeLeon, E. R., Gao, Y., Hurley, K., Sadauskas, V., Batz, C., & Stoy, G. (2013). Thiosulfate: a readily accessible source of hydrogen sulfide in oxygen sensing. *American Journal Physiology; Regulatory Integrative and Comparitive Physiology, 305*(6), 592–603.

Ovechkin, A. V., Tyagi, N., Sen, U., Lominadze, D., Steed, M. M., Moshal, K. S., & Tyagi, S. C. (2006). 3-Deazaadenosine mitigates arterial remodeling and hypertension in hyperhomocysteinemic mice. *American Journal of Physiology: Lung Cellular and Molecular Physiology*, *291*(5), 905–911.

Papapetropoulos, A., & Szabo, C. (2009). Hydrogen sulfide is an endogenous stimulator of angiogenesis. *Proceedings of National Academy of Science, 106*(51), 21972–21977.

Paul, B., & Snyder, S. H. (2012). H_2S signalling through protein sulfhydration and beyond. *Nature Reviews Molecular Cell Biology*, *13*(8), 449–507.

Polhemus, D. J., & Lefer, D. J. (2014). Emergence of Hydrogen Sulfide as an Endogenous Gaseous Signaling Molecule in Cardiovascular Disease. *Circulation Research, 114*(4), 730–737.

Polhemus, D. J., Calvert, J. W., Butler, J., & Lefer, D. J. (2014). The Cardioprotective Actions of Hydrogen Sulfide in Acute Myocardial Infarction and Heart Failure. *Scientifica, 2014*(9), 1–8.

Qipshidze, N., Metreveli, N., Mishra, P. K., Lominadze, D., & Tyagi, S. (2012). Hydrogen Sulfide Mitigates Cardiac Remodeling During Myocardial Infarction via Improvement of Angiogenesis. *International Journal of Biological Sciences*, *8*(4) 430–441.

Reichelt, M. E., Willems, L., Hack, B. A., Peart, J. N., & Headrick, J. P. (2008). Cardiac and coronary function in the Langendorff-perfused mouse heart model. *Experimental Physiology*, *94*(1), 54–70.

Rowan, F. E., Docherty, N. G., Coffey, J. C., & O'Connell, P. R. (2009). Sulphate-reducing bacteria and hydrogen sulphide in the aetiology of ulcerative colitis. *British Journal of Surgery*, *96*(2), 151–158.

Scherrer-Crosbie, M., Ullrich, R., Bloch, K., Nakajima, H., Nasseri, B., Aretz, T., Lindsey, M. L., Vancon, A. C., Huang, P.L., Lee, R. T., Zapol, W. M., Picard, M. H. (2001). Endothelial Nitric Oxide Synthase Limits Left Ventricular Remodeling After Myocardial Infarction in Mice. *Circulation*, *104*(11) 1286–1291.

Sen, U., Vacek, T. P., Hughes, W. M., Kumar, M., Moshal, K. S., Tyagi, N., Metreveli, N., Hayden, M. R., Tyagi, S. C. (2008). Cardioprotective Role of Sodium Thiosulfate on Chronic Heart Failure by Modulating Endogenous H_2S Generation. *Pharmacology*, *82*(3), 201–213.

Shamshad, F., Kenchaiah, S., Finn, P., Soler-Soler, J., McMurray, J., Velazquez, E., Maggioni, A. P., Califf, R. M., Solomon, S. D. (2010). Fatal myocardial rupture after acute myocardialinfarction complicated by heart failure, left ventriculardysfunction, or both: The VALsartan In Acute myocardial iNfarcTion Trial (VALIANT). *American Heart Journal*, *160*(1), 145–151.

Shen, X., Carlström, M., Borniquel, S., Jädert, C., Kevil, C. G., & Lundberg, J. O. (2013). Free Radical Biology and Medicine. *Free Radical Biology and Medicine*, *60*(C), 195–200.

Shen, X., Peter, E. A., Bir, S., Wang, R., & Kevil, C. G. (2012). Analytical measurement of discrete hydrogen sulfide pools in biological specimens. *Free Radical Biology and Medicine*, *52*(11-12), 2276–2283.

Sheng, J., Shim, W., Wei, H., Lim, S. Y., Liew, R., Lim, T. S., et al. (2013). Hydrogen sulphide suppresses human atrial fibroblast proliferation and transformation to myofibroblasts. *Journal of Cellular and Molecular Medicine*, *17*(10), 1345–1354.

Shibuya, N., Mikami, Y., Kimura, Y., Nagahara, N., & Kimura, H. (2009). Vascular Endothelium Expresses 3-Mercaptopyruvate Sulfurtransferase and Produces Hydrogen Sulfide. *Journal of Biochemistry*, *146*(5), 623–626.

Shirozu, K., Tokuda, K., Marutani, E., Lefer, D., Wang, R., & Ichinose, F. (2014). Cystathionine γ-Lyase Deficiency Protects Mice from Galactosamine/Lipopolysaccharide-Induced Acute Liver Failure. *Antioxidants & Redox Signaling*, *20*(2), 204–216.

Sivarajah, A., McDonald, M. C., & Thiemermann, C. (2006). The production of hydrogen sulfide limits myocardial ischemia and reperfusion injury and contributes to the cardioprotective effects of preconditioning with endotoxin, but not ischemia in the rat, *Shock*, *26*(2), 154–161.

Sodha, N. R., Clements, R. T., Feng, J., Liu, Y., Bianchi, C., Horvath, E. M., Szabo, C, Stahl, G. L., Sellke, F.W. (2009). Hydrogen sulfide therapy attenuates the inflammatory response in a porcine model of myocardial ischemia/reperfusion injury. *The Journal of Thoracic and Cardiovascular Surgery*, *138*(4), 977–984.

Spallarossa, A., Forlani, F., Carpen, A., Armirotti, A., Pagani, S., Bolognesi, M., & Bordo, D. (2004). The "Rhodanese" Fold and Catalytic Mechanism of 3-Mercaptopyruvate Sulfurtransferases: Crystal Structure of SseA from Escherichia coli. *Journal of Molecular Biology*, *335*(2), 583–593.

Sumeray, M. S., Rees, D. D., Yellon, D. M. (2000). Infarct Size and Nitric Oxide Synthase in Murine Myocardium. *J Mol Cell Cardiol*, *32*(1), 35–42.

Sun, Y. G., Cao, Y. X., Wang, W. W., Ma, S. F., Yao, T., & Zhu, Y. C. (2008).

Hydrogen sulphide is an inhibitor of L-type calcium channels and mechanical contraction in rat cardiomyocytes. *Cardiovascular Research*, *79*(4), 632–641.

Sutton, M. G. S. J., & Sharpe, N. (2000). Left Ventricular Remodeling After Myocardial Infarction: Pathophysiology and Therapy. *Circulation*, *101*(25), 2981–2988.

Sylvester, D., & Sander, C. (1990). Immunohistochemical localization of rhodanese. *Histochemical Journal*, *22*, 197–200.

Szabó, C. (2007). Hydrogen sulphide and its therapeutic potential. *Nature Reviews Drug Discovery*, *6*(11), 917–935.

Szabó, C., Ransy, C., Módis, K., Andriamihaja, M., Murghes, B., Coletta, C., Olah, G., Yanagi, K., Bouillaud, F. (2014). Regulation of mitochondrial bioenergetic function by hydrogen sulfide. Part I. Biochemical and physiological mechanisms. *British Journal of Pharmacology*, *171*(8), 2099–2122.

Taniguchi, E., Matsunami, M., Kimura, T., Yonezawa, D., Ishiki, T., Sekiguchi, F., Nishikawa, H., Maeda, Y., Ishikura, H., Kawabata, A. (2009). Rhodanese, but not cystathionine-γ-lyase, is associated with dextran sulfate sodium-evoked colitis in mice: A sign of impaired colonic sulfide detoxification? *Toxicology*, *264*(1-2), 96–103.

Teng, H., Wu, B., Zhao, K., Yang, G, Wu, L., & Wang, R. (2013). Oxygen sensitive mitochondrial accumulation of cystathionine β-synthase mediated by Lon protease. *Proceedings of National Academy of Science*, *110*(31), 12679–12684.

Tiranti, V., Viscomi, C., Hildebrandt, T., Di Meo, I., Mineri, R., Tiveron, C., Levitt, M. D., Prelle, A., Fagiolari, G., Rimoldi, M., Zeviani, M. (2009). Loss of ETHE1, a mitochondrial dioxygenase, causes fatal sulfide toxicity in ethylmalonic encephalopathy. *Nature Medicine*, *15*(2), 200–205.

van den Borne, S. W. M., Cleutjens, J. P. M., Hanemaaijer, R., Creemers, E. E., Smits, J. F. M., Daemen, M. J. A. P., & Blankesteijn, W. M. (2008). Increased matrix metalloproteinase-8 and -9 activity in patients with infarct rupture after myocardial infarction. *Cardiovascular Pathology*, *18*(1), 37-43.

van der Horst, I. C. C., Voors, A. A., & van Veldhuisen, D. J. (2007). Treatment of heart failure with ACE inhibitors and beta-blockers. *Clinical Research in Cardiology*, *96*(4), 193–195.

Velagaleti, R. S., Pencina, M. J., Murabito, J. M., Wang, T. J., Parikh, N. I., D'Agostino, R. B., Levy, D., Kannel, W. B., Vasan, R. S. (2008). Long-Term Trends in the Incidence of Heart Failure After Myocardial Infarction. *Circulation*, *118*(20), 2057–2062.

Wang, X., Armando, I., Upadhyay, K., Pascua, A., & Jose, P. A. (2009). The

regulation of proximal tubular salt transport in hypertension: an update. *Current Opinion in Nephrology and Hypertension*, *18*(5), 412–420.

Whiteman, M. (2010). The Effect of Hydrogen Sulfide Donors on Lipopolysaccharide-Induced Formation of Inflammatory Mediators in Macrophages, *Antioxidants & Redox signalling*, *12*(10) 1147-1154.

Whiteman, M., Le Trionnaire, S., Chopra, M., Fox, B., & Whatmore, J. (2011). Emerging role of hydrogen sulfide in health and disease: critical appraisal of biomarkers and pharmacological tools. *Clinical Science*, *121*(11), 459–488.

Woodfin, A., Voisin, M. B., & Nourshargh, S. (2007). PECAM-1: A Multi-Functional Molecule in Inflammation and Vascular Biology. *Arteriosclerosis, Thrombosis, and Vascular Biology*, *27*(12), 2514–2523.

Xia, M., Chen, L., Muh, R. W., Li, P. L., & Li, N. (2009). Production and Actions of Hydrogen Sulfide, a Novel Gaseous Bioactive Substance, in the Kidneys. *Journal of Pharmacology and Experimental Therapeutics*, *329*(3), 1056–1062.

Yamamoto, J., Sato, W., Kosugi, T., Yamamoto, T., Kimura, T., Taniguchi, S., et al. (2012). Distribution of hydrogen sulfide (H2S)-producing enzymes and the roles of the H2S donor sodium hydrosulfide in diabetic nephropathy. *Clinical and Experimental Nephrology*, *17*(1), 32–40.

Yang, G, Wu, L., Jiang, B., Yang, W., Qi, J., Cao, K., Meng, Q., Mustafa, A. K., Mu, W., Zhang, S., Snyder, S. H., Wang, R. (2008). H_2S as a Physiologic Vasorelaxant: Hypertension in Mice with Deletion of Cystathionine -Lyase. *Science*, *322*(5901), 587–590.

Yellon, D., & Hausenloy, D. (2007). Myocardial Reperfusion Injury. *The New England Journal of Medicine*, *357*, 1121–1135.

Yuan, S., Patel, R. P., & Kevil, C. G. (2015). Working with nitric oxide and hydrogen sulfide in biological systems. *American Journal of Physiology: Lung Cellular and Molecular Physiology*, *308*(5), 403–415.

Zanardo, R. C., Brancaleone, V., Distrutti, E., Fiorucci, S., Cirino, G., & Wallace, J. L. (2006). Hydrogen sulfide is an endogenous modulator of leukocyte-mediated inflammation. *The FASEB Journal*, *20*(12), 2118–2120.

Zhang, H., Moochhala, S. M., & Bhatia, M. (2008). Endogenous Hydrogen Sulfide Regulates Inflammatory Response by Activating the ERK Pathway in Polymicrobial Sepsis. *The Journal of Immunology*, *181*(6), 4320–4331.

Zhang, R., Sun, Y., Tsai, H., Tang, C., Jin, H., & Du, J. (2012). Hydrogen Sulfide Inhibits L-Type Calcium Currents Depending upon the Protein Sulfhydryl State in Rat Cardiomyocytes. *PLoS ONE*, *7*(5), 370-373.

Zhang, Y., Li, H., Zhao, G., Sun, A., Zong, N., Li, Z., Zhu, H., Zou, Y., Yang, X., Ge, J. (2014). Hydrogen Sulfide Attenuates the Recruitment of CD11b+Gr-1+ Myeloid Cells and Regulates Bax/Bcl-2 Signaling in Myocardial Ischemia Injury. *Scientific Reports*, *4*, 1-7.

Zhao, W., Zhang, J., Lu, Y., & Wang, R. (2001). The vasorelaxant effect of H_2S as a novel endogenous gaseous Katp channel opener. *The EMBO Journal*, *20*, 6008–6016.

Zhu, Y. Z., Wang, Z. J., Ho, P., Loke, Y. Y., Zhu, Y. C., Huang, S. H., Tan, C. S., Whiteman, M., Lu, J., Moore, P. K. (2006). Hydrogen sulfide and its possible roles in myocardial ischemia in experimental rats. *Journal of Applied Physiology*, *102*(1), 261–268.

8 Appendices

Appendix 1 Immunohistochemical localisation of TST and the H2S synthetic enzymes in livers of C57BL/6J mice

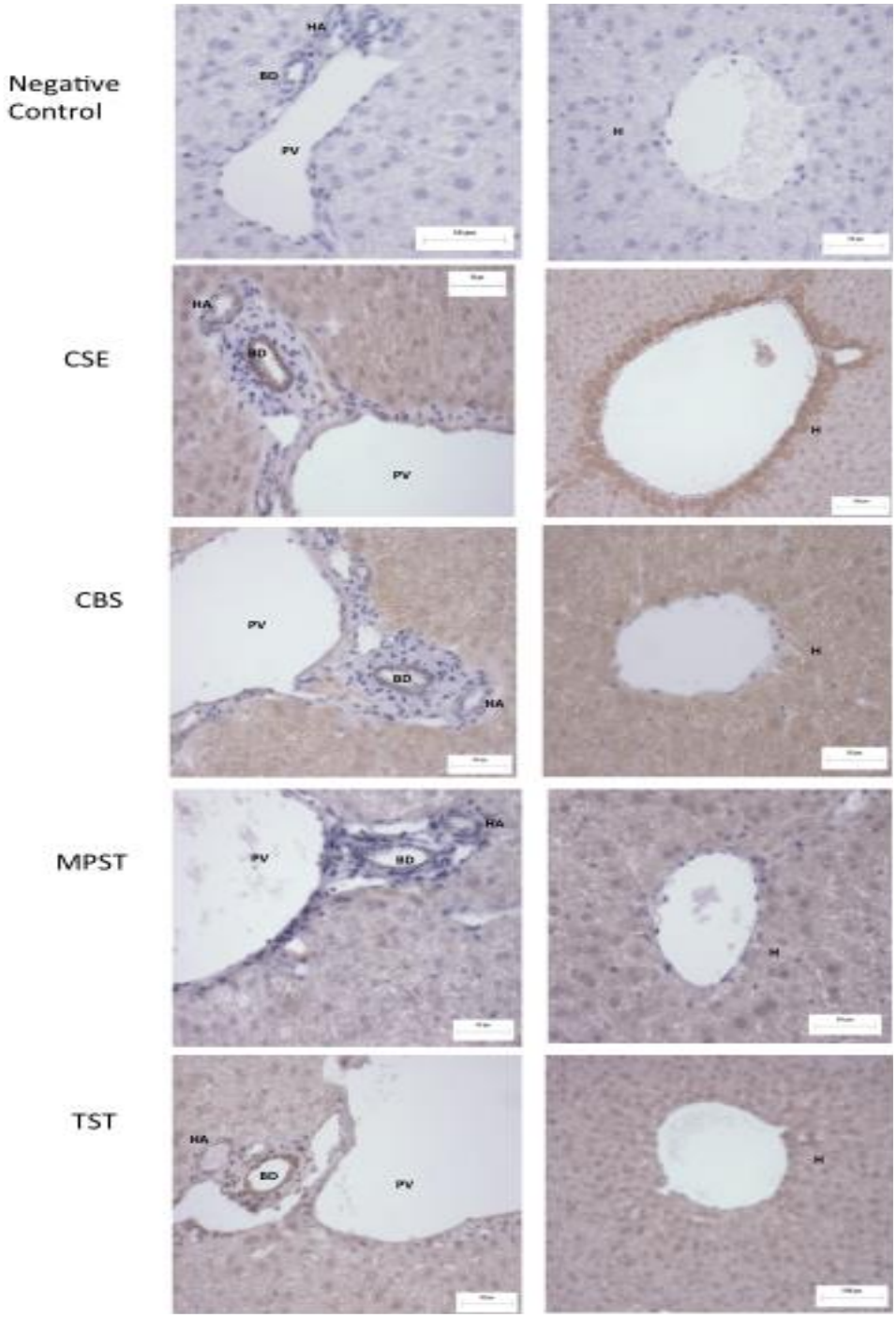

Sections photographed using an Olympus light microscope camera. Sections illustrate negative control stained sections (top row) and positive DAB staining (brown) in hepatic portal tracts (left column), and hepatic central veins (right columns). Abreviations; PV (portal vein), HA (hepatic artery), BD (bile duct), H (hepatocytes). Scale bar, 50μm.

Appendix 2 *Tst*$^{-/-}$ ingest more sodium, potassium and chloride from diet

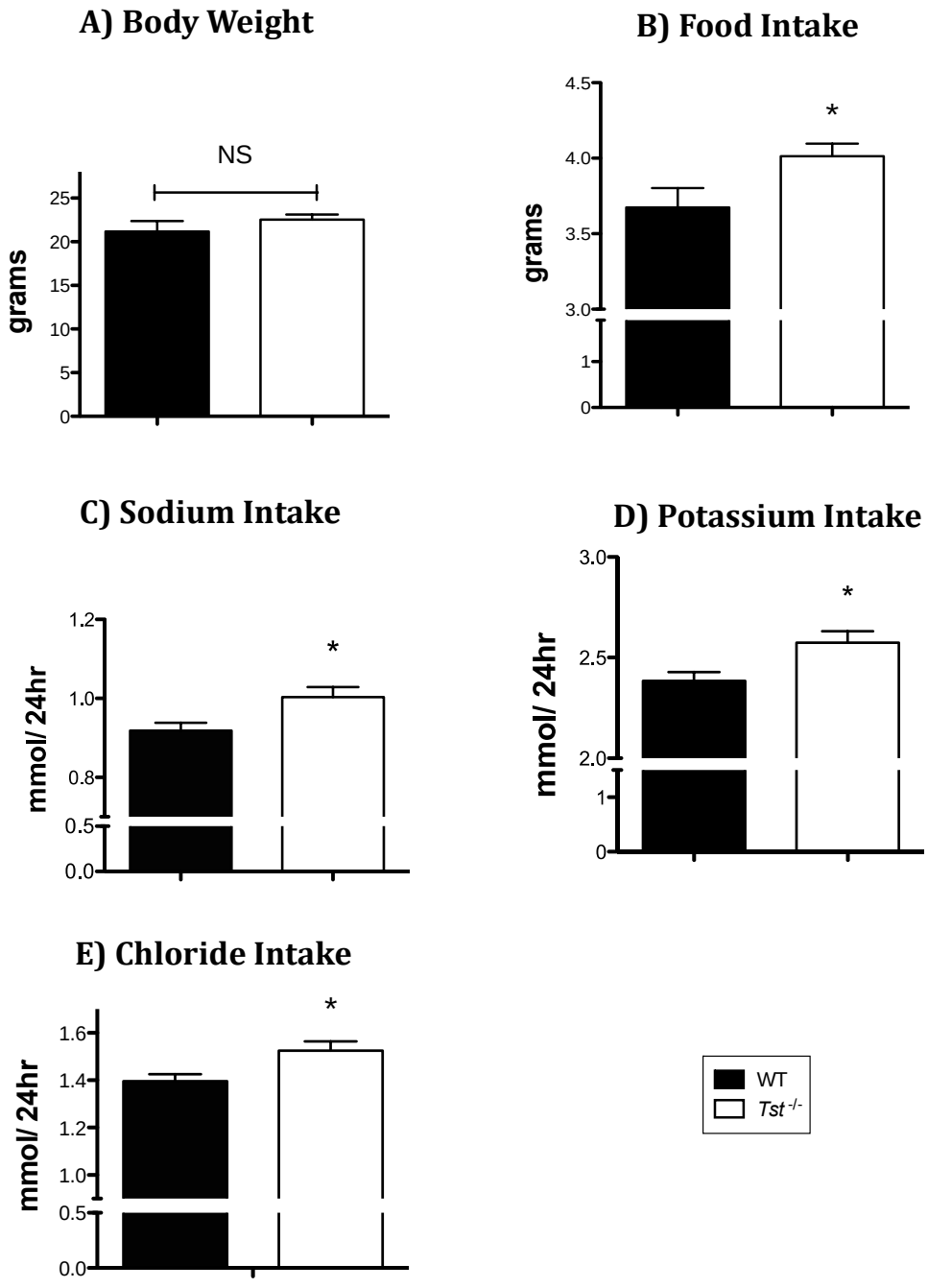

Mean body weight (A) and mean food take (B) over 8day post-acclimatisation period (WT; n=4,*Tst*$^{-/-}$; n=5). (C-E) Mean 24hour sodium, potassium and chloride intake over 8day post-acclimatisation period (WT; n=4,*Tst*$^{-/-}$; n=5). Electrolyte intake [food intake (g) x (g) of Na^+, K^+ or Ca^{2+} in RM1 diet]. Data are mean ± SEM. Statistical analysis was performed using unpaired student t-test *p < 0.05

Appendix 3 Plasma renin concentrations are not altered in *Tst*$^{-/-}$ mice

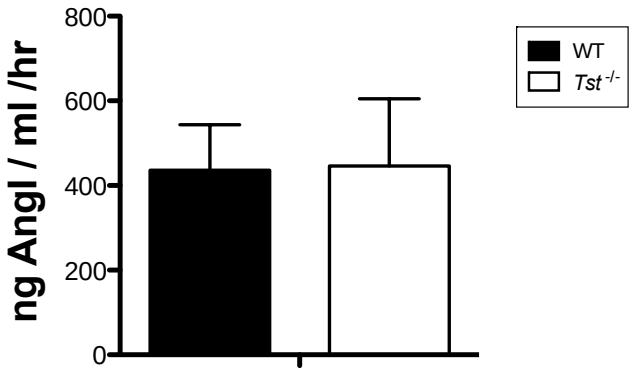

Radioimmunoassay detecting plasma renin concentration in plasma from 12week old WT and *Tst*$^{-/-}$ mice (n=4/ group). Data are mean ± SEM. [Assay performed by Dr. Chris Kenyon as previously described (Bohlender, menard, Edling, Ganten, & Friedrich, 1998)]

Appendix 4 Independent observations of polydipsic phenotype in *Tst*$^{-/-}$ mice

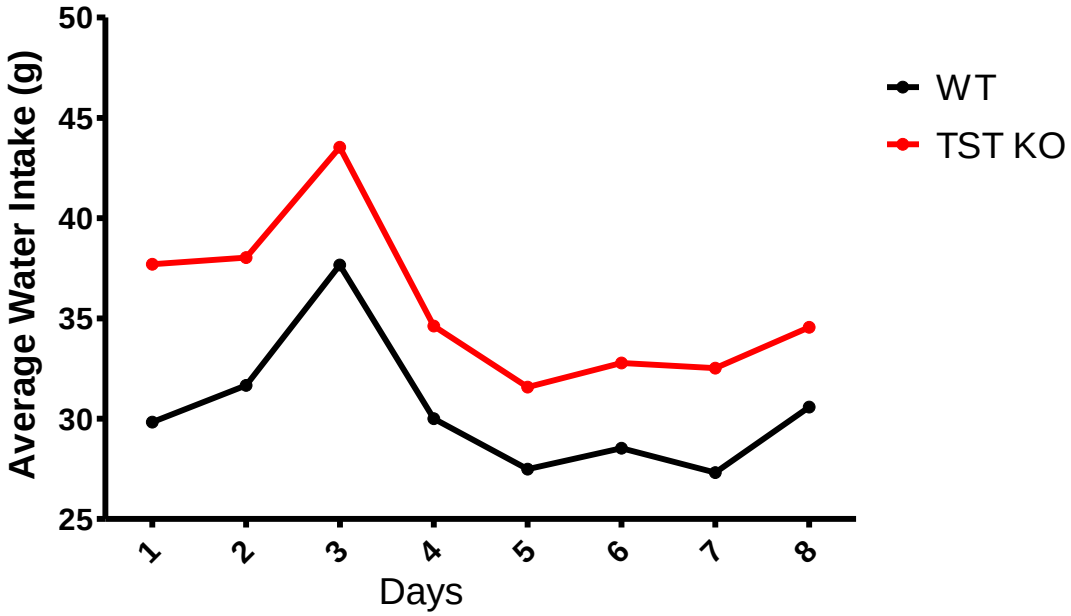

Average daily water intake *Tst*$^{-/-}$ and C57BL/6N wild type littermates in single housed regular cages over 8days period (n=3/group). Unpublished data from Clare Mc Fadden, University of Edinburgh.

Appendix 5 Contribution of SK_{Ca} and IK_{Ca} channels to the relaxant response to ACh in isolated mesenteric arteries from C57BL/6N wild type

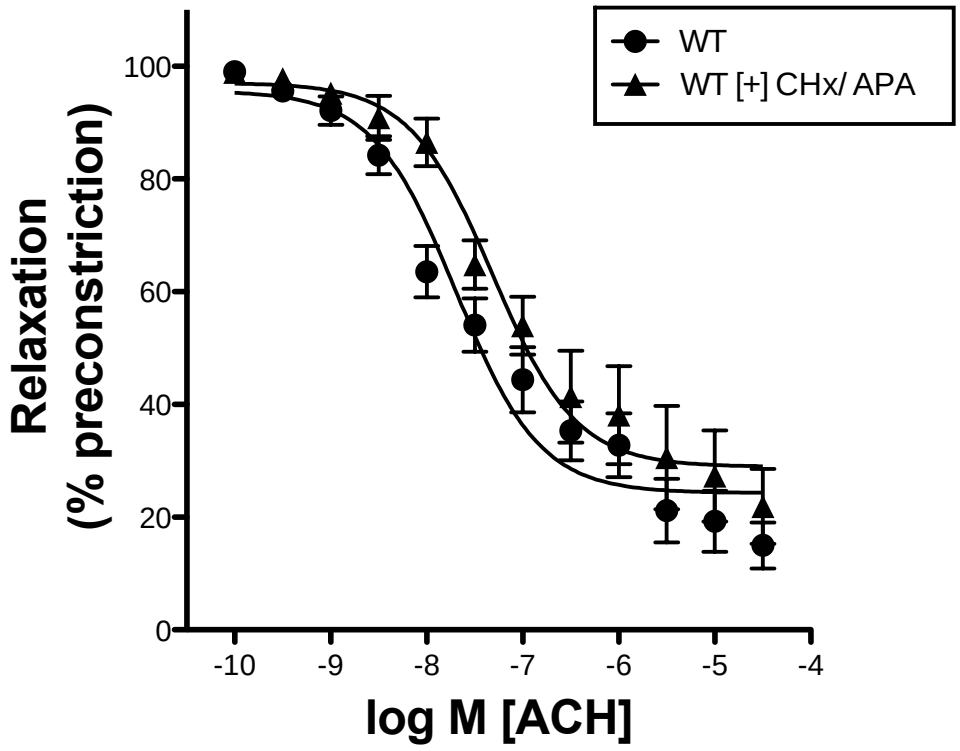

Cumulative concentration response to ACh in endothelial intact mesenteric rings of wild type mice when pre-treated with or without apamin (SK_{Ca} inhibitor) and charybdotoxin (IK_{Ca} inhibitor) (Non-treated; WT; n=7, WT [+] CHx/ APA; *Tst*$^{-/-}$; n=5). Vessel response to ACh was expressed as percentage of vessel pre-constriction. Values are mean±SEM, analysed by 2-way ANOVA. *Abbreviations; CHx, Charybdotoxin, APA; Apamin*.